REPUBLIQUE DU CAMEROUN
Paix – Travail – Patrie
****
UNIVERSITE DE YAOUNDE I
FACULTE DES SCIENCES
DEPARTEMENT DE DE BIOCHIMIE
****

REPUBLIC OF CAMEROUN
Peace – Work – Fatherland
****
UNIVERSITY OF YAOUNDE I
FACULTY OF SCIENCE
DEPARTMENT OF OF
BIOCHEMISTRY
****

Dynamics of Ion Acoustic Waves in Electronegative Plasmas

THESIS
Submitted for the award of PhD in Physics

Par : **PANGUETNA Chérif Souleman**
MSc in Physics

Sous la direction de
TABI Conrad Bertrand
Associate Professor
Bostwana Intenational University
of Science and Technology
KOFANE Timoléon Crépin
Professor
University of Yaoundé I

Année Académique : 2021

UNIVERSITE DE YAOUNDE I
FACULTE DES SCIENCES

THE UNIVERSITY OF YAOUNDE I
FACULTY OF SCIENCE

Département de Physique
Department of Physics

ATTESTATION DE CORRECTION DE LA THESE DE DOCTORAT/Ph.D.

Nous, KENFACK Jiotsa Aurélien, Professeur, et OWONO OWONO Luc Calvin, Professeur, respectivement Examinateur et Président du jury de soutenance de la thèse de Doctorat/Ph.D de M. **PANGUETNA Chérif Souleman** (Matricule N° : **99V212**) préparée sous la direction de TABI Conrad Bertrand, Associate Professor et KOFANE Timoléon-Crépin, Professeur, intitulée « **Dynamics of Ion Acoustic Waves in Electronegative Plasmas**», soutenue le 03 Mai 2021 en vue de l'obtention du grade de Docteur/Ph.D en Physique, option Mécanique et Systèmes complexes;

Attestons que toutes les corrections demandées par le jury de soutenance ont été effectuées.

En foi de quoi la présente attestation lui est délivrée pour servir et valoir ce que de droit.

Fait à Yaoundé, le 26 MAY 2021

Président du Jury	Examinateur	Le Chef de Département
OWONO OWONO Luc Calvin,	KENFACK Jiotsa Aurélien	NDJAKA Jean-Marie
Professeur	*Professeur*	*Professeur*

UNIVERSITE DE YAOUNDE I * FACULTE DES SCIENCES * Le Chef de Département DEPARTEMENT DE PHYSIQUE

"Better late than never."

Geoffrey Chaucer

Dedication

To my dear and beloved wife, PANGUETNA RACHIDETOU

Acknowledgements

Undertaking this Ph.D. has been a truly life-changing experience for me and it would not have been possible to do without the support and guidance that I received from many people.

Foremost, I am deeply grateful to all members of the jury for agreeing to read the manuscript and to participate in the defense of this thesis, these are: Prof. OWONO OWONO Luc Calvin, Prof. TCHAWOUA Clément, Prof. KENFACK JIOTSA Aurelien, Prof YAMAPI Réné and Prof. BOUETOU BOUETOU Thomas,

I would like to express my sincere gratitude to my co-directors, Prof. KOFANE Timoleon Crepin and Prof. TABI Conrad Bertrand, for the continuous support of my Ph.D. study and research, for their patience, motivation, enthusiasm, and immense knowledge. Their guidance helped me in all the time of research and writing of this thesis. I could not have imagined having a better advisor and mentor for my Ph.D. study.

I am also very grateful to all the teaching and research staff that have gaven me scientific knowledge during my academic training or taken some time to discuss and enrich my work. Here, I cordially thank the head of Physics Department Prof. NDJAKA Jean-Marie. Then, I would like to thank Prof. WOAFO Paul, Prof. PEMHA Elkana, Prof. BEN-Bolie Germain H., Prof. ZEKENG Serge, Prof. MANGUELE Dikoum Eléazer,

Prof. OWONO Ateba, Prof. BEGUIDE BONOMA and Prof. DJUIJE Germaine.

I also take this opportunity to thank all my academic elders who shared with me their experience on some mathematical approaches, the use of software essential for the research and interpretation of some complex phenomena. They are : Dr. MVOGO Alain, Dr. ADAMOU Dang Koko, Dr. ETEME Armand Sylvin. Additionally, I would like to thank my classmates who supported me with various actions throughout my academic career. I am thinking mainly of: Dr. OKALY Joseph Brizar, Dr. BANSI KAMDEM Delphin Christel, Dr. ISSA Sali and Dr. ONDOUA.

Some special words of gratitude go to my friends who have always been a major source of support when things would get a bit discouraging: NGOUMBE ZACHARIE, NDJOKE MOUTIT, FIFEN MOUNDOM, GHOMLIENJU, TAKENGNY FOMETIO, Dr. TSOBGNI FOZAP, KPOUMIE LINDOU, NTIECHE SIDIKOU, S-Ltn. FOSSI Ibrahim, Prof. KOL GUY, Dr. DAMFEU YEUDAM, KOUOTOU NJOYA, NSANGOU Arouna, Pr MOYOUWOU, MFOUAPON Alassa, NSANGOU J.C. and DJOKO DJUIKOUO. Thanks guys for always being there for me.

I am also very grateful to thank my family, for supporting me spiritually throughout the preparation of this thesis and my life in general: my parents and especially my late father Nji MBOUONGAPNA MEGNA Issa and my mother, MENAKOUE Zenabou; my uncles Nji CHINMOUN Issa Ousmane, MOULIOM Choibou and Prof. Mama FOUPOUAGNIGNI; my brothers and sisters, TEMFEMO Adija, MOLUH Mariatou, FOUPOUAPOUGNIGNI Rachidetou, POUNTOUGNIGNI Mariama, LIMI Issofa, NGAPNA Nouhou, PEMBOURA ZOULIHA and GHETYOU Ahmed, just to cite a few. Here, I address a special to my parents-in-law, Mr. Mefire Moussa and Mrs. Mefire Amsetou for all their support.

Finally, I have to thank my wife and love of my life, Rachidetou PANGUETNA, for keeping things going and for always showing how proud she is of me. This thesis is dedicated to her.

The last word goes for Raissa, Faiza, Dalila, Imane, Ziyad, Maryam and Adil, my beloved children, who has been the light of my life for the recent years and who has

given me the extra strength and motivation to get things done.

Contents

List of Figures

Abstract

The main purpose of the present study is to investigate how electronegative plasmas parameters namely, the negative ions concentration ratio (α) and the electron-to-negative ions temperature ratio (σ_n) modify the ion acoustic structures. We study the ion acoustic waves in an unmagnetized electronegative plasma made of Boltzmann electrons, Boltzmann negative ions and cold mobile positive ions. In one dimensional analysis, the reductive perturbation method is used to reduce the dynamics of the whole system to a cubic nonlinear Schrödinger equation, whose the nonlinear and dispersion coefficients, P and Q, are function of the negative ion parameters. The study of MI is used to show the correlation between the parametric analysis and the formation of modulated solitons obtained here as bright envelopes and kink-wave solitons. Furthermore, weakly relativistic ion acoustic waves are investigated in an electronegative plasma. Analytical solutions, in the form of rogue waves, are thereafter presented and their response to plasma parameters changes is discussed. In two dimensional investigation, the governing hydrodynamic equations are reduced to a Davey-Stewartson system, which is used to study the MI of ion acoustic waves along with the effect of plasma parameters. Numerically, parameters from the instability regions give rise to series of dromion solitons under the activation of modulational instability. The sensitivity of the numerical solutions to plasma parameters is discussed. Some exact solutions in the form of one- and two-dromion solutions are derived and their response to the effect of varying (α) and (σ_n) is discussed as well. In three-dimensional electronegative plasma model, modulated ion-acoustic waves are investigated via the activation of the modulational instability in the Davey-Stewartson equations. The contributions of the modulation angle and electronegative plasma parameters are discussed to that effect, including some particular cases such as the parallel and transverse modulations. Otherwise, the dynamics of coupled ion acoustic waves is introduced. Using the reductive perturbation technic, it is showed that the system can fully be described using a set of two coupled Schrödinger equations.

Keywords: Electronegative plasma; Ion-acoustic waves; Envelope solitons; Modulational insta1ibility; Rogue waves; Dromion; Relativistic plasma. Coupled excitation.

Résumé

Ce travail vise à examiner comment les paramètres électronégatifs du plasma telsque le taux de concentration des ions négatifs et le rapport de température électron-ions négatifs modifient les structures ioniques acoustiques. Nous avons étudié les ondes ioniques acoustiques dans un plasma électronégatif non magnétisé, constitué des électrons de Boltzman, des ions négatifs de Boltzman et des ions positifs froids et mobiles. La méthode de perturbation réductive est employée pour transformer les équations de base du modèle soit en une équation de Schrödinger Nonlinéaire Cubique à une dimension, soit au système de Davey-Stewartson à deux ou à trois dimensions. L'étude de l'instabilité modulationnelle est utilisée pour démontrer la corrélation entre les paramètres du milieu et la formation des solitons modulés obtenus telsque le bright et le kink en dimension un et les dromions en dimension deux. De plus, nous avons investigué sur les ondes ioniques acoustiques faiblement relativistes dans les plasmas électronégatifs. Des solutions analytiques sous forme de rogues waves (ondes scélérates ; vagues) sont alors présentées et leurs dépendances vis-à-vis des paramètres du système sont discutées. En dimension trois, les ondes ioniques acoustiques modulées sont étudiées à travers l'activation de l'instabilité modulationnelle dans l'équation de Davey-Stewartson. Dans ce cas, la contribution de l'angle de modulation (θ) et celle des paramètres électronégatifs ont été mises en exergue. Les cas particuliers comme la modulation transversale ou la modulation longitudinale ont été discutés. Par ailleurs, nous avons étudié la dynamique des ondes ioniques acoustiques couplées dans les plasmas électronégatifs. La technique de perturbation réductive a été employée pour montrer que la dynamique du système peut être pleinement décrite par un système couplé de deux équations de Schrödinger Nonlinéaires.

Mots clés: Plasma Electronégatif ; Ondes ioniques acoustiques; Solitons envelopes ; Instabilité modulationnelle; Ondes scélérates ; Dromion; Plasma relativiste. Excitation Couplée.

List of abbreviations

Initials	Meaning	**Initials**	Meaning
ENPs	Electronegative Plasmas	**KdV**	Korteweg-de Vries
IA	Ion Acoustic	**RPT**	Reductive Perturbation Technic
DIA	Dust Ion Acoustic	**mKdV**	Modified Korteweg-de Vries
NLS	Nonlinear Schrödinger	**MI**	Modulational Instability
IAWs	Ion Acoustic Waves	**ZK**	Zakarov-Kuznetsov
KP	Kadomtsev-Petviashvili	**DS**	Davey-Stewartson
DA	Dust-Acoustic	**GR**	Growth Rate
RWs	Rogue Waves	**AB**	Akhmediev Breather
KM	Kuznetsov-Ma	**RPM**	Reductive Perturbation Method

General introduction

Plasmas are usually composed of negative ions, positive ions and electrons. In the presence of a significant number of negative ions, they are qualified as ENPs. The presence of negative ions in a plasma modifies its basic nature and importantly affects wave propagation of various kinds as well as their characteristics. The charge neutrality condition gets modified in that context, leading to the increase in the negative ion density, while the number density of electrons decreases. This means that the shielding effect produced by the electrons decreases and the behavior of the plasma consequently changes.

0.1 Context of the thesis

Solitonic structures have long been an attractive topic in nonlinear physics, since they arise in nonlinear optics [1], Bose-Einstein condensates [2], biophysics [3–6] and plasma physics [7–9], just to cite a few. They are in general the result of the interplay between nonlinear and dispersive effects, and can propagate over long distance, keeping their shape and characteristics unchanged. In plasma physics, nonlinear excitations have been intensively investigated as solutions of the NLS and the KdV equations [7, 8, 10–12]. For example, it was reported by Mamun et al. [13, 14] that negative ions in a plasma modify the nonlinearity of the system and consequently affect the interplay between nonlinear and dispersive effects which are the main condition for the emergence of IAWs. Also, it was predicted that negative ions in such plasmas are in Boltzmann equilibrium [15, 16], and that was confirmed via some experiments by Ghim and Hershkowitz [17]. Latter, Mamun et al. [19] recently paid attention to the existence of IAWs and DIA waves in an ENP made of Boltzmann negative ions, Boltzmann electrons and cold mobile positive ions. This was followed by the investigation on other aspects and characteristics of such

plasmas waves, related to their response to external magnetic fields, in one or more dimension [13, 14], in the vicinity of the KdV equations obtained from the reductive perturbation approximation.

More recently, experimental observations of Peregrine solitons in nonlinear optical fibers [20, 21], water tank experiment [22, 23] and in plasmas [24, 25] have opened a new route to study their characteristics more deeply. Along the same line, IAWs are found to be modulationally unstable when the plasma contains a critical number of negative ions and described by the NLS equation. In fact, the MI of nonlinear excitations in plasmas is a well-known phenomenon leading to energy localization, the main consequence being the formation of bright envelope solitons. This means that, in the absence of instability, dark solitons are the most probable excitations to emerge in such systems. MI therefore originates from the fact that a small plane wave perturbation grows exponentially and the resulting sidebands get amplified, to finally display trains of oscillations. In general, the subsequent bright solitons are solutions of the NLS equation, which can be derived from generic hydrodynamic plasma equations using appropriate expansion methods such as the reductive perturbative method [26, 27], the derivative expansion method [28], the Kryslov-Bogoliubov method [29, 30], to name just a few. In more recent contributions, particular attention has been paid to the multi-dimensional versions of such methods, leading to more upgraded amplitude equations such as the DS equation and the multi-dimensional NLS equation, with at least two space variables. Periodic solutions and MI of the DS were proposed by Tajiri et al. [31]. Gill and co-workers [32] also studied 2D envelope electron acoustic waves in the presence of Cairns non-thermal distribution of hot electrons. Bedi and Gill [33] studied envelope electron acoustic waves subjected to transverse perturbations, in the presence of $\kappa-$distributed hot electrons. In three dimensions, Carbonaro [34] derived DS equations from a plasma system consisting of cold electrons, hot electrons and steady background of ions, and further supported the idea of Kourakis and Shukla [35] that in higher dimensions the MI phenomenon is mostly controlled by the modulation angle, leading to parallel, transverse and oblique modulations. The concept is also introduced in the present work and applied to ENPs. Some seminal works on two- and three-dimensional models include the ZK equation [36, 37], the KP equation [38, 39] and DS equations [40, 41]. Duha et al. [14] studied IAWs in magnetized dusty plasmas via the KP equation and showed that negative ion parameters may importantly affect the characteristics and stability of IAWs. Bedi and Gill [33] successfully derived the DS equation in a plasma in presence of kappa-distributed hot electrons and established the strong relationship between the NLS equation and the DS ones. They reinforced the idea of Nishinari et al. [26, 27] that the DS system is a higher-dimensional generalization of the NLS equation, since it includes transverse scale length and dynamics in the transverse direction. More importantly, the latter might bring

about additional nonlinear features compared to the NLS equation, and may support very rich behaviors under the activation of multi-dimensional MI and the subsequent plasma modes.

During the past thirty years, envelope solitons, generic solutions of the NLS equation, have been extensively studied. This because of their fundamental importance in nonlinear physics. Due to their localization properties, breather solitons have been used as models of RWs whose behaviors and characteristics are not yet fully unmasked, mainly because they may appear suddenly, propagate within short times, destroy everything on their way, and disappear without any trace [1, 2]. For instance, it has been well-established that they may appear in physical systems as the consequence of the interplay between nonlinear and dispersive effects, leading to the MI phenomenon [3−8]. Recently, interest in studying RWs has gone beyond oceanography and hydrodynamics [9, 10] to reach some other areas related to optics and photonics [11−14], Bose-Einstein condensation [15−17], biophysics [18−21], plasma physics [22, 23], just to name a few. Particularly, IA super RWs were found in an ultracold neutral plasma in the presence of ion-fluid and nonextensive electron distribution [24]. In the same direction, magnetosonic RWs, of first- and second-order, were investigated numerically in a magnetized plasma [25]. The occurrence of fundamental and second-order RWs was also investigated in a relativistically degenerate plasma using the NLS equation [23]. Comparison between experimental and theoretical occurrence of RWs was proposed recently and applied to multicomponent plasmas with negative ions [26]. A comprehensive analysis by El-Tantawy et al. [27] once more brought out the close relationship between the existence of ion-acoustic RWs and MI in ENPs in presence of Maxwellian negative ions, where the dynamical behaviors of the AB, KM breather and super-RWs were compared. Obviously, none of the above-cited works includes relativistic effects which should be considered in the emergence of IAWs when the speed of a plasma particle approaches that of light. IAWs in weakly relativistic plasmas were studied by Das et al. [39, 40], via the KdV equation, and applied to both nonisothermal and and isothermal plasmas. El-Labany [41] reported on the existence of modulated weakly relativistic IAWs in a collisionless, unmagnetized, warm plasma with nonthermal electrons using a NLS equation. The later was also derived recently by Abdikian [42], in three dimensions, to study the emergence of IAWs, under the activation of MI, in a magnetoplasma with pressure of relativistic electrons. Further confirmation was given on the effect of relativistic parameter to bring about new instability and dynamical regimes in the generation mechanism of modulated IAWs via MI.

0.2 Problematic and objectives of the thesis

A limited number of contributions have been devoted to nonlinear excitations in ENPs [86–90], and most of the works, to the best of our knowledge, have been limited to one-dimensional plasma systems. Some seminal works on two- and three-dimensional models include the ZK equation [36,37], the KP equation [38,39] and DS equations [40,41]. Duha et al. [14] studied IAWs in magnetized dusty plasmas via the KP equation and showed that negative ion parameters may importantly affect the characteristics and stability of IAWs. Moreover, none of the above-cited works includes relativistic effects which should be considered in the emergence of IAWs when the speed of a plasma particle approaches that of light. The nonlinear behaviors of plasma waves may be importantly modified by relativistic effects and lead to fascinating spectra of results, exploitable in the laboratory and in the space. Otherwise, the different studies conducted on the emergence and stability of solitary waves in electronegative plasmas, do not highlight the wave-wave interactions. And yet in any dispersive medium, several waves of the same or different nature, can spread and their interactions are inevitable. In this work, we mean to address comprehensively the response of such waves to the effects of the negative ion parameters, especially the negative ion concentration ratio and the electron-to negative ion temperature ratio in non-relativistic and relativistic ENPs as well as in one or multidimensional situations. We also analyze the impact of those parameters on the MI activation and the emergence and propagation of the wave-wave interaction in ENPs.

0.3 Outlines of the thesis

This thesis is divided into the following three chapters:

- In chapter one, we review some theoretical aspects of plasmas and ENPs. We also present, the historical background on plasmas and highlight some of their useful properties and characteristics. Finally, we present the plasmas fluid description that will be the starting-point for studying plasmas dynamics.

- In chapter two, we present the different mathematical models developed in this thesis to understand the ENPs dynamics. Specifically, we first show how to reduce the system to its amplitude equations using the reductive perturbation method. Then, we present some analysis methods like the general theory of MI and the Hirota bilinear scheme.

- Chapter three is dedicated to the presentation of the main results of this thesis. We mean to address comprehensively in one, two and three-dimensional cases, the response of IA waves to the effects of the negative ion parameters, especially

the negative ion concentration ratio and the electron-to -negative ion temperature ratio. We also show that under certain conditions, new classes of waves like bright and dark envelope soliton, one- and two-dromions solitons and rogue waves may emerge with complex profiles and characteristics.

The thesis ends with a general conclusion including the summary of the main results, some open problems and future orientations.

CHAPTER 1

Litterature review

1.1 Introduction

The three states of the matter solid, liquid and gas, are well known. However, plasma is increasingly being presented as a forth state of the matter. The nature and composition of plasma allow it to exhibit complex and interesting behaviors. The analysis of plasma properties not only helps to explain some natural phenomena, but also to set devices and some industrial processes. In this chapter, we stand out the literature reviews on plasmas theory. Some useful properties on plasmas like Debye length, temperature, and so on, are presented. Space plasma, plasma production and applications are also introduced here. Finally, we discuss the plasma fluid models with emphasis in ENPs.

1.2 Basics of plasmas

1.2.1 History of plasmas

The word plasma comes from Ancient Greek $\pi\lambda\alpha\sigma\mu\alpha$, meaning *moldable substance* [49], and describes the behavior of the ionized atomic nuclei and the electrons within the surrounding region of the plasma. Very simply, each of these nuclei is suspended in a movable sea of electrons. Plasma was first identified in a Crookes tube, and so described by Sir William Crookes in 1879. The nature of this matter was subsequently identified by British physicist Sir J.J. Thomson in 1897 [52]. The term *plasma* was coined by Irving Langmuir in 1928 [50]. Lewi Tonks and Harold Mott-Smith, both of whom worked with Irving Langmuir in the 1920s, recall that Langmuir first used the word *plasma* in

analogy with blood. Mott-Smith recalls, in particular, that the transport of electrons from thermionic filaments reminded Langmuir of the way blood plasma carries red and white corpuscles and germs [51]. Langmuir described the plasma he observed as follows: *Except near the electrodes, where there are sheaths containing very few electrons, the ionized gas contains ions and electrons in about equal numbers so that the resultant space charge is very small. We shall use the name plasma to describe this region containing balanced charges of ions and electrons [50].*

1.2.2 Plasma as the fourth state of the matter

It is common that matter appears in three states: solid, liquid, and gaseous. But in recent years more attention has been directed to the properties of matter in a fourth and unique state, which we call plasma. A plasma is consider as the fourth state of matter. Plasma is typically an ionized gas, but it is usually considered as a distinct state of matter in contrast to gases because of its particular properties. As we know that the gases are ionized mediums, so we can say that the plasma is the state having further ionisation than that of gases. A valuable definition is given by Chen 1984 as: *P*lasma is a quasineutral gas of charged and neutral particles which exhibits collective behavior [53]. It is the state of matter having one or both of positive and negative ions as well as electrons. The ions are obtained when atoms or molecules undergo ionization, while the overall charge on the species remains neutral. Plasma is so an overall neutral medium that is composed of ions. But the presence of charged ions in it shows that plasma is highly conducting in nature. The free electric charges make the plasma electrically conductive so that it responds strongly to electromagnetic fields. In fact, plasma is sometimes defined as a gas that is sufficiently ionized to exhibit plasma-like behavior. When even a small fraction of gas undergoes ionization, it exhibits the plasma-like behavior. Thus, fractionally ionized gases exhibit most of the interesting phenomena characteristic of fully ionized gases. Plasmas also made from the neutral gases by ionization process. In this case, it contains equal number of negative and positive charge particles. This situation implies that the oppositely charged fluids are strongly coupled, and tend to electrically neutralize one another on macroscopic length-scales. Such plasmas are termed quasi-neutral, because small deviations from exact neutrality have important dynamical consequences for certain types of plasma modes. The property called "collective effects" in plasmas, differentiates plasma from ordinary fluids and solids. This property, defined as that of the motion of charged ions, not only depends upon local conditions, but also upon the nature or state of plasma. Due to the long-range forces, each charged particle in the plasma interacts simultaneously with a considerable number of other charged particles, resulting in important collective effects.

1.2.3 Characteristics of plasmas

1.2.3.1 Quasi-neutrality and Debye length

When no external disturbance like an electron or ion is present, a plasma is macroscopically neutral. This means that under equilibrium conditions, with no external forces, in a volume of the plasma sufficiently large to contain a large number of particles and yet sufficiently small compared to the characteristic lengths for variation of macroscopic parameters such as density and temperature, the net resulting electric charge in a plasma is zero. Therefore, the equilibrium charge neutrality condition in the case of three species plasma reads

$$q_i n_{i0} + q_n n_{n0} - e n_{e0} = 0, \tag{1}$$

where n_{i0}, n_{n0} and n_{e0} are respectively, the unperturbed number densities of positive ions, negative ions and electrons. $q_i = Z_i e$ is the positive ions charge, $q_n = -Z_n e$ is the negative ions charge and e is the magnitude of the electron charge. If a local potential is imposed in the plasma, the opposite charged particles organize in order to confine the electric field from leaking in to the plasma. The Debye length is an important physical parameter for the description of a plasma [68]. It provides a measure of the distance over which the influence of the electric field of an individual charged particle is felt by the other charged particles inside the plasma. The charged particles arrange themselves in such a way as to effectively shield any electrostatic fields within a distance of the order of the Debye length. This shielding of electrostatic fields is a consequence of the collective effects of the plasma particles. A Debye sphere is a volume whose radius is the Debye length, in which there is a sphere of influence, and outside of which charges are screened. In most types of plasma, quasi-neutrality is not just an ideal equilibrium state, it is a state that the plasma actively tries to achieve by readjusting the local charge distribution in response to a disturbance. Consider a hypothetical experiment in which a positively charged ball is immersed in a plasma see Fig. 1 [53].

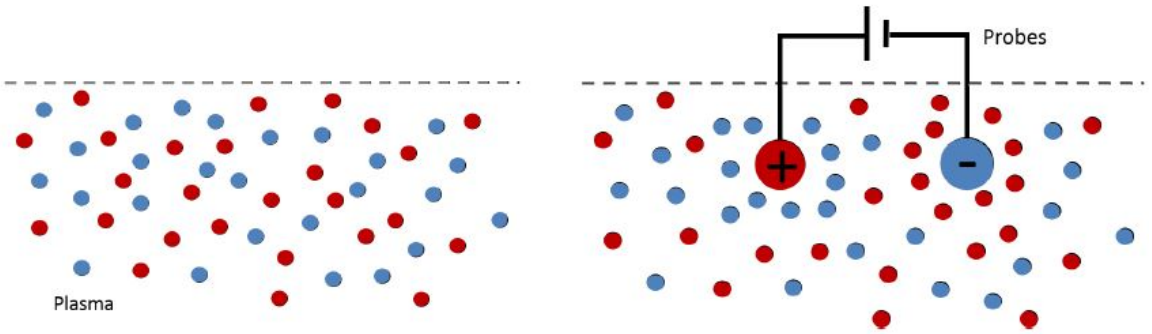

Figure 1: Debye shielding of charged spheres immersed in a plasma [53]

Plasma	Density n(m^3)	Electron temperature T(K)	Magnetic field B(T)	Debye length $\lambda_D(m)$
Gas discharge	10^{16}	10^4	-	10^{-4}
Tokamak	10^{20}	10^8	10	10^{-4}
Ionosphere	10^{12}	10^3	10^{-5}	10^{-3}
Magnetosphere	10^7	10^7	10^{-8}	10^2
Solar core	10^{32}	10^7	-	10^{-11}
Solar wind	10^6	10^5	10^{-9}	10
Interstellar medium	10^5	10^4	10^{-10}	10
Intergalactic medium	1	10^6	-	10^5

Table 1: The table shows the number density, the electron temperature, the magnetic field and the Debye length of some natural and artificial plasmas [55].

After some time, the ions in the ball's vicinity will be repelled and the electrons will be attracted, leading to an altered average charge density in this region. It turns out that, the potential $\phi(r)$ of this ball after such a readjustment has taken place, can be obtained from the solution of PoissonŠs equation.

$$\nabla^2\phi = -\frac{e}{\varepsilon_0}(n_i - n_e). \tag{2}$$

Assuming Boltzmann distribution for the electrons ($n_e = n_0 \exp(e\phi/kT_e)$) and for a small change in the sheath potential ($e\phi \ll kT_e$), such that the positive ion density is fixed ($n_i = n_0$), the equation (2) after TaylorŠs expansion of exponent term and neglecting all the higher order terms of ϕ gives

$$\frac{d^2\phi}{dx^2} = \frac{e^2 n_0}{\epsilon_0 k T_e}\phi, \tag{3}$$

Where n_0 is the plasma density far away from the charged conductor at potential ϕ_0 and ϕ is the potential at a distance x from the conductor. The solution to this equation can be written as

$$\phi = \phi_0 \exp\left(-\frac{|x|}{\lambda_D}\right), \tag{4}$$

Where the Debye length is defined as

$$\lambda_D = \left(\frac{\epsilon_0 k T_e}{e^2 n_e}\right)^{1/2}, \tag{5}$$

Thus quasineutrality, which is the basic criterion for an ionized gas to be plasma, will exist if the dimensions of the system are large compare to the Debye length. Also for Debye shielding to be statistically valid there must be a large number of particles N_D in a Debye sphere.

As mentioned before, the Debye length can also be regarded as a measure of the distance over which fluctuating electric potentials may appear in a plasma, corresponding to a conversion of the thermal particle kinetic energy into electrostatic potential energy. When a boundary surface is introduced in a plasma, the perturbation produced extends only up to a distance of the order of λ_D from the surface. In the neighborhood of any surface inside the plasma there is a layer of width of the order of λ_D, known as the plasma sheath, inside which the condition of macroscopic electrical neutrality may not be satisfied. Beyond the plasma sheath region there is the plasma region, where macroscopic neutrality is maintained. Generally, λ_D is very small. For example, in a gas discharge, where typical values for T and n_e are around 10^4K and $10^{16}m^{-3}$, respectively, we have $\lambda_D = 10^{-4}m$. For the Earth's ionosphere, typical values can be taken as $n_e = 10^{12}m^{-3}$ and $T = 10^3K$, yielding $\lambda_D = 10^{-4}m$. In the interstellar plasma, on the other hand, the Debye length can be several meters long as we can see in table 1. It is convenient to define a Debye sphere as a sphere inside the plasma of radius equal to λ_D. Any electrostatic fields originated outside a Debye sphere are effectively screened by the charged particles and do not contribute significantly to the electric field existing at its center. Consequently, each charge in the plasma interacts collectively only with the charges that lie inside its Debye sphere, its effect on the other charges being effectively negligible. The number of electrons N_D, inside a Debye sphere, is given by

$$N_D = \frac{4}{3}\pi\lambda_D^3 n_e = \frac{4}{3}\pi\left(\frac{\epsilon_0 kT}{n_e^{1/3}e^2}\right)^{3/2} \tag{6}$$

The Debye shielding effect is a characteristic of all plasmas, although it does not occur in every medium that contains charged particles. A necessary and obvious requirement for the existence of a plasma is that the physical dimensions of the system be large compared to λ_D. Otherwise there is just not sufficient space for the collective shielding effect to take place, and the collection of charged particles will not exhibit plasma behavior. If L is a characteristic dimension of the plasma, a first criterion for the definition of a plasma is therefore

$$L \gg \lambda_D \tag{7}$$

Since the shielding effect is the result of the collective particle behavior inside a Debye sphere, it is also necessary that the number of electrons inside a Debye sphere be very large. A second criterion for the definition of a plasma is therefore

$$n_e\lambda_D^3 \gg 1 \tag{8}$$

This means that the average distance between electrons, which is roughly given by $n_e^{-1/3}$, must be very small compared to λ_D. The quantity defined by

$$g = \frac{1}{n_e\lambda_D^3} \tag{9}$$

is known as the plasma parameter and the condition $g \ll$ is called the plasma approximation [53]. This parameter is also a measure of the ratio of the mean interparticle potential energy to the mean plasma kinetic energy. Note that the macroscopic neutrality is sometimes considered as a third criterion for the existence of a plasma.

1.2.3.2 Plasma temperature

Plasma is a collection of many bodies with range of velocities in three dimensional phase-space. When the density of particles in a velocity space is plotted against the velocity ranging from $-\infty$ to $+\infty$, we get a peak at the centre which falls away from the centre as described by a Maxwellian distribution [46]. The full width at half maximum of the distribution determines the temperature of the species and is associated with the mean velocity of the particles. The Maxwellian distribution of electrons is given by

$$f(v) = n\left(\frac{m}{2\pi kT}\right)^{3/2} \exp\left(-\frac{mv^2}{2kT}\right). \tag{10}$$

In the above expression, m denotes mass of electron and T denotes the temperature of the electron. The distribution function $f(v)$ describes the number of particles (dn) in a given velocity interval, $dn = f(v)dv$. This can be expressed in terms of energy and the electron energy distribution function, $f(E)$ is obtained from the velocity distribution function as

$$f(E) = n\left(\frac{4E}{\pi}\right)^{1/2} (kT)^{-3/2} \exp\left(-\frac{E}{kT}\right). \tag{11}$$

One can obtain the average particle velocity, $\bar{v}$ from the velocity distribution function as

$$\bar{v} = \left(\frac{8kT}{\pi m}\right)^{1/2} \tag{12}$$

T_e, T_i , T_- are generally used to denote the temperature of electrons, positive ions and negative ions. If plasma species fulfil the condition $T_g = T_i = T_e = T_{ex} = T_d = T_r$ where T_g, T_i, T_e, T_{ex}, T_d and T_r denote respectively to gas temperature, ion temperature, electron temperature, excitation temperature, dissociation temperature, and radiation temperature, then the plasma is said to be in thermal equilibrium. Complete thermal equilibrium is very difficult to observe, however, under certain laboratory conditions local thermal equilibrium can be achieved. If the ion temperature and gas temperature is comparable with the electron temperature, the plasma is said to be in local thermal equilibrium. Typically for low pressure plasmas, $T_e \gg T_i \approx T_g$ and therefore, the plasma is said to be in non-thermal equilibrium.

1.2.3.3 Plasma frequency

When the electrons in a quasineutral plasma are perturbed from their equilibrium positions, an electric field will be built in such a direction such that the resulting internal

space charge fields give rise to collective particle motions that tend to restore the original charge neutrality. As the ions are massive compared to the electrons, they form a uniform background. Due to inertia, the electrons will overshoot and oscillate about their equilibrium positions with a characteristic frequency, which is known as plasma frequency. Since these collective oscillations are high-frequency oscillations, the ions, because of their heavy mass, are, to a certain extent, unable to follow the motion of the electrons. On solving the basic fluid equations for a plasma with singly charged ions the electron-plasma frequency ω is [54]

$$\omega_p = \left(\frac{ne^2}{\varepsilon_0 m_e}\right)^2, \tag{13}$$

where m_e stands for the mass of an electron. For the properties of the plasma to be determined by electromagnetic rather than hydrodynamic collision, the plasma frequency must be large compared to the ordinary collision frequency.

1.2.3.4 Particle interactions and collective effects

The properties of a plasma are markedly dependent upon the particle interactions. The existence of collective effects is one of the basic features that distinguish the behavior of plasmas from that of ordinary fluids and solids. Due to the long range of electromagnetic forces, each charged particle in the plasma interacts simultaneously with a considerable number of other charged particles, resulting in important collective effects that are responsible for the wealth of physical phenomena that take place in a plasma [53]. The particle dynamics in a plasma is governed by the internal fields due to the nature and motion of the particles themselves, and by externally applied fields. The basic particle interactions are electromagnetic in character. Quantum effects are negligible, except for some cases of close collisions. In a plasma, we must distinguish between charge-charge and charge-neutral interactions. A charged particle is surrounded by an electric field and interacts with the other charged particles according to the coulomb force law, with its dependence on the inverse of the square of the separation distance. Furthermore, a magnetic field is associated with a moving charged particle, which also produces a force on other moving charges. The charged and neutral particles interact through electric polarization fields produced by distortion of the neutral particle's electronic cloud during a close passage of the charged particle. The field associated with neutral particles involves short-range forces, such that their interaction is effective only for interatomic distances sufficiently small to perturb the orbital electrons. It is appreciable when the distance between the centers of the interacting particles is of the order of their diameter, but nearly zero when they are farther apart. Its characteristics can be adequately described only by quantum-mechanical considerations. In many cases this interaction involves permanent or induced electric dipole moments. A distinction can be made between weakly ionized and strongly ionized plasmas in terms of the nature of the particle interactions.

In a weakly ionized plasma the charge-neutral interactions dominate over the multiple coulomb interactions. When the degree of ionization is such that the multiple coulomb interactions become dominant, the plasma is considered strongly ionized. As the degree of ionization increases, the coulomb interactions become increasingly important so that in a fully ionized plasma all particles are subjected to the multiple coulomb interactions.

1.2.3.5 Collisions in plasmas

Collisions between charged particles in a plasma differ fundamentally from those between molecules in a neutral gas because of the long-range character of the Coulomb force. In fact, binary collision processes can only be defined for weakly coupled plasmas. However, that binary collisions in weakly coupled plasmas are still modified by collective effects. Nevertheless, for large Λ, where Λ is the typical number of particles contained in a Debye sphere, we can speak of binary collisions, and therefore of a collision frequency, denoted by $\nu_{ss'}$ [54]. Here, $\nu_{ss'}$ measures the rate at which particles of species s are scattered by those of species s'. When specifying only a single subscript, one is generally referring to the total collision rate for that specie, including impacts with all other species. Very roughly,

$$\nu_s \simeq \sum_{s'} \nu_{ss'}. \tag{14}$$

The species designations are generally important. For instance, the relatively small electron mass implies that for unit ionic charge and comparable species temperatures, we have

$$\nu_e \sim \left(\frac{m_i}{m_e}\right)^{1/2} \nu_i. \tag{15}$$

Furthermore, the collision frequency ν measures the frequency with which a particle trajectory undergoes a major angular change due to Coulomb interactions with other particles. Coulomb collisions are, in fact, predominately small-angle scattering events, so the collision frequency is not the inverse of the typical time between collisions. Instead, it is the inverse of the typical time needed for enough collisions to occur that the particle trajectory is deviated through 90°. For this reason, the collision frequency is sometimes termed the 90°-*scattering rate*. It is conventional to define the mean-free-path

$$\lambda_{\text{mfp}} \equiv v_t/\nu. \tag{16}$$

Clearly, the mean-free-path measures the typical distance a particle travels between collisions (i.e., scattering events). A collision-dominated, or collisional plasma is one in which

$$\lambda_{\text{mfp}} \ll L, \tag{17}$$

where L is the observation length-scale. The opposite limit of large mean-free-path is said to correspond to a collisionless plasma. Collisions greatly simplify plasma behaviors by driving the system towards statistical equilibrium, characterized by Maxwell-Boltzmann distribution functions. Furthermore, short mean-free-paths generally ensure that plasma transport is local (i.e., diffusive) in nature, which is a considerable simplification. The typical magnitude of the collision frequency is

$$\nu \sim \frac{\ln \Lambda}{\Lambda}\,\omega_p. \tag{18}$$

Note that $\nu \ll \omega_p$ in a weakly coupled plasma. It follows that collisions do not seriously interfere with plasma oscillations in such systems. On the other hand, in a strongly coupled plasma, $\nu \gg \omega_p$, whine suggests that collisions effectively prevent plasma oscillations in such systems. This accords well with our basic picture of a strongly coupled plasma as a system dominated by Coulomb interactions which does not exhibit conventional plasma dynamics. It follows that

$$\nu \sim \frac{e^4\,\ln \Lambda}{4\pi {\epsilon_0}^2\, m^{1/2}}\frac{n}{T^{3/2}}. \tag{19}$$

Thus, diffuse, high temperature plasmas tend to be collisionless, whereas dense, low temperature plasmas are more likely to be collisional. Note that whilst collisions are crucial to the confinement and dynamics (e.g., sound waves) of neutral gases, they play a far less important role in plasmas. In fact, in many plasmas the magnetic field effectively plays the role that collisions play in a neutral gas. In such plasmas, charged particles are constrained from moving perpendicular to the field by their small Larmor orbits, rather than by collisions. Confinement along the field-lines is more difficult to achieve, unless the field-lines form closed loops or closed surfaces. Thus, it makes sense to talk about a collisionless plasma, whereas it makes little sense to talk about a collisionless neutral gas. Note that many plasmas are collisionless to a very good approximation, especially those encountered in astrophysics and space plasma physics contexts.

1.3 Types of plasmas

The production of an appropriate plasma in a laboratory usually needs the construction of a fairly large apparatus. If one goes outside the earth, however, the plasma state is the most abundant state of matter. Indeed, plasmic matter begins at about $50km$ above the earth's surface in the ionosphere. There are various types of plasmas in the universe, ranging from very high density ($n \sim 10^{36}/m^3$) inside a white dwarf to very low density ($n \sim 10^6/m^3$) in interstellar space. Fig.(2) shows various plasmas as a function of temperature and density. In this figure the various states are classified into four groups.

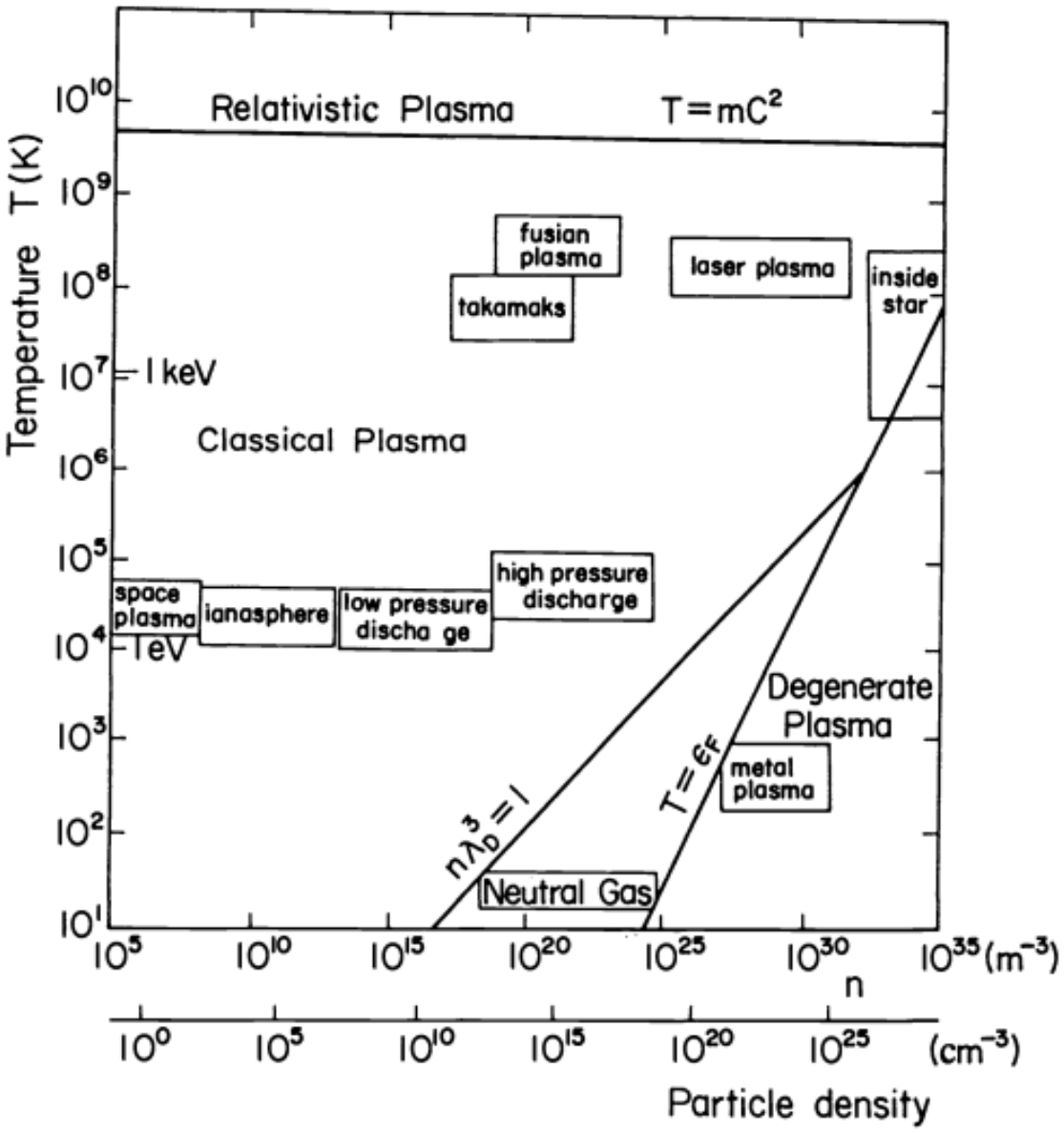

Figure 2: Types of plasmas in a logarithmic temperature-density parameter space [55]

The very high temperature state where the electrons must be treated relativistically is called relativistic plasma, whereas the very high density state where the electrons must be treated as a quantum-mechanical degenerate Fermi gas is called degenerate plasma. The remaining region is divided into classical plasma and neutral gas depending on whether the plasma condition is satisfied or not. As it can be seen from this figure, the neutral gas state is restricted to only a very narrow region. The classical plasma, specifically, have been studied in relation to thermonuclear fusion research. In this region, charged particle motion can be treated by nonrelativistic classical mechanics. However, the plasmas relevant to inertial confinement fusion research are often at very high density and the electrons have to be treated quantum mechanically as a degenerate Fermi gas [55]. Moreover, when a plasma is heated by an electromagnetic wave, for example,

by electron cyclotron resonance heating, a fraction of the electrons are selectively heated to a very high energy so that they do have to be treated relativistically. The relativistic effect is certainly important for special problems. A typical discharge plasma in a vacuum tube has an electron temperature which is much higher ($T_e \sim 1eV$) than the ion temperature ($T_j \sim 0.1eV$) and the degree of ionization in such a plasma is typically $10^3 - 10^5$, which is between the value predicted by the Saha formula of the electron temperature and that of the ion temperature [45]. A relatively highly ionized plasma at low temperature ($\sim 0.3eV$) and low density ($\sim 10^{16}/m^3$) can be produced by contact ionization of an alkali beam, by using a device called the Q-machine. Such a low density, low temperature plasma is useful for studying the basic properties of wave propagation in a plasma. Various methods for producing laboratory plasmas are described in [46]. In a low ionization plasma, various atomic processes, such as ionization and recombination, excitation and radiation, play important roles in determining its properties. These processes are also important in fusion plasmas, particularly in connection with spectroscopic diagnostics of plasmas. These problems are described in [47, 48].

1.4 Space plasmas

1.4.1 Solar corona and solar wind

The sun (Fig. 3.), as well as most stars, is made of plasma.

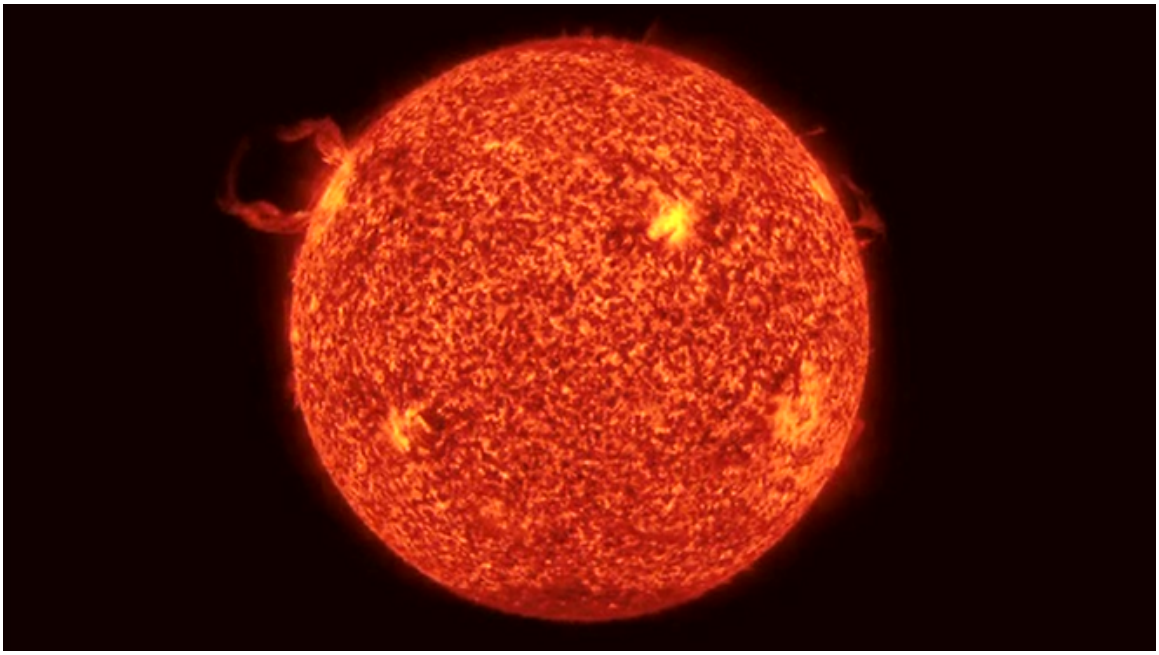

Figure 3: The Sun is a plasma

www.sciencelern.org.nz

In fact, space is dominated by plasma since 99 percent of matter in the universe is plasma. It consists mainly 71 percent (by mass) of hydrogen and 27 percent(by mass) of helium. Due to the very high temperatures found within the sun, these elements exist not in the gaseous state but as plasma. The sun emits a vast amounts of energy due to the thermonuclear fusion reactions occurring within the core that convert hydrogen nuclei into helium nuclei. The energy output from this reaction has been estimated to $3.86 \times 10^{23} kJ$ per second. Otherwise, the outer atmosphere of the Sun is known as the corona. Temperatures within this region are extremely high, giving some of the charged particles present sufficient energy to escape from the strong gravitational pull of the Sun. This stream of charged particles emanating from the Sun in all directions at speeds of about $400 km/s$ is called the solar wind (Fig. 4).

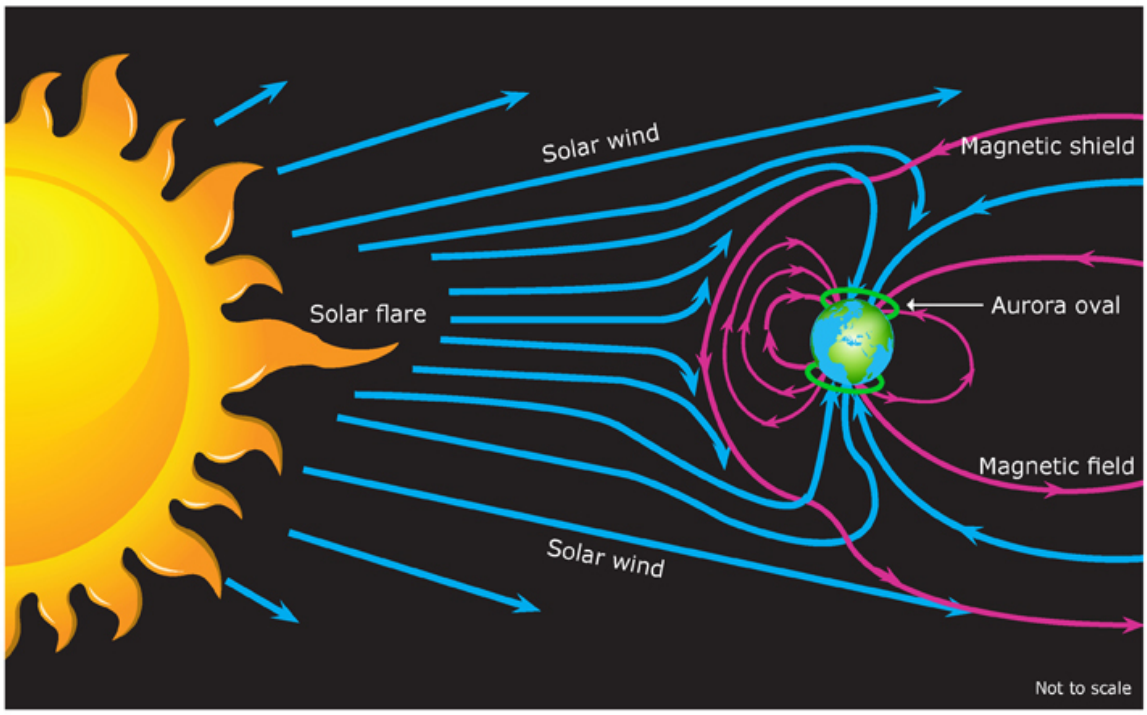

Figure 4: The solar wind plasma and magnetosphere

www.sciencelern.org.nz

It is a rapidly moving plasma that pushes out the edge of the solar system. The solar wind is not uniform. Although it is always directed away from the sun, its intensity and speed are dependent on the activity of the sun. For example, major solar eruptions known as coronal mass ejections (CMEs) can increase the plasma density and speed of the solar wind. This can impact on the Earth's magnetic field, causing increased auroral activity and, in extreme cases, geomagnetic storms that can disrupt communication systems and cause power surges on electrical transmission grids.

1.4.2 Ionosphere

In the uppermost region of the Earth's atmosphere, the intense incoming solar radiation causes the ionization of gaseous atoms. Ionization is the process in which neutral atoms or molecules gain or lose electrons to become electrically charged. This creates a mix of neutral atoms, electrons and ions called plasma.
The term ionosphere is used to describe this region of near-Earth space that extends mostly within the altitude range of $85 - 600km$. On descending through the ionosphere, the more energetic solar radiation is absorbed, resulting in a drop-off in the degree of ionization. In addition, the ratio of plasma/gas mix changes until, at an altitude of about $50km$, only gas exists.
Various regions within the ionosphere based on electron density have been described. As one can see in Fig. 5., these vary from daytime to night-time and play a key role in absorbing harmful radiation from the sun and outer space. In addition, the ionosphere influences radio wave propagation.

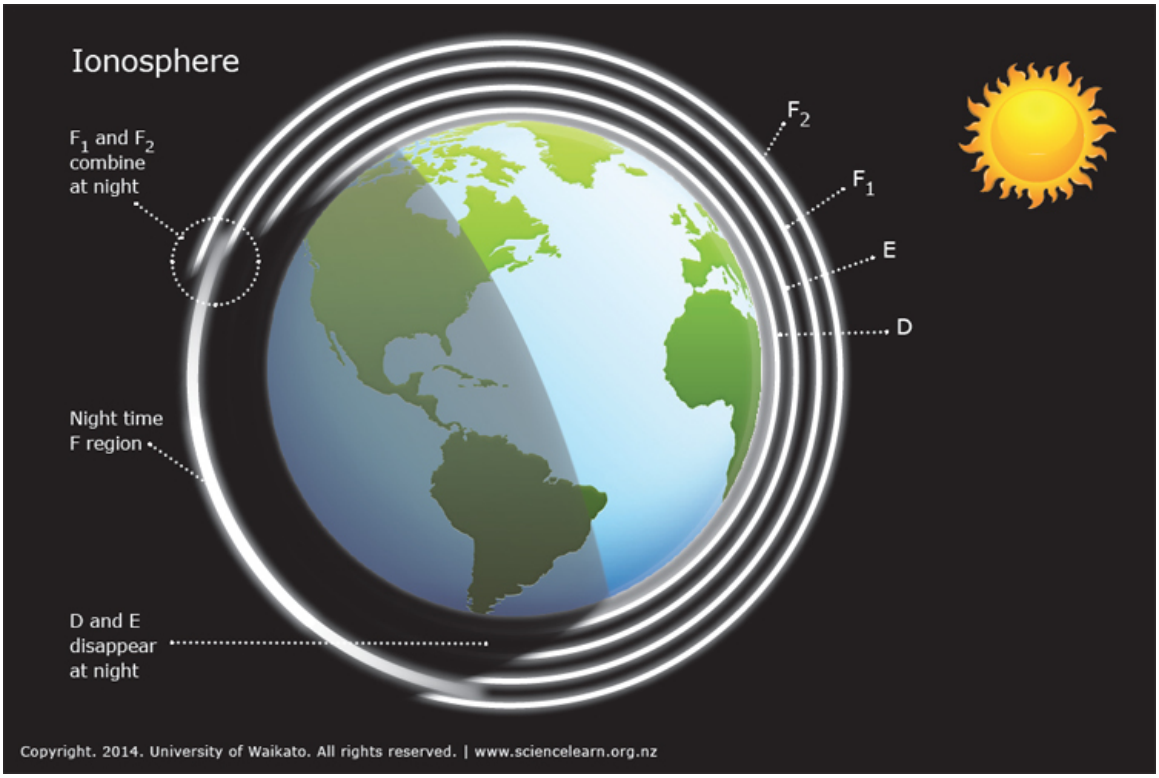

Figure 5: The layers of the ionosphere

www.sciencelern.org.nz

It can be used to bounce certain types of radio wave signals down to the ground, allowing for communication over very large distances.

1.4.3 Auroras

An aurora is a luminous glow in the E-region of the ionosphere seen mainly in high latitudes close to the poles. They are visual reminders of the solar wind: the more intense the solar wind, the more spectacular the aurora's display of colored lights.

Auroras are caused by high-energy charged particles from the solar wind becoming trapped in the Earth's magnetic field. As these particles spiral back and forth along the magnetic field lines, they come down into the ionosphere near the North and South Magnetic Poles, where the magnetic field lines disappear into the body of the Earth.

As these high-energy charged particles collide with oxygen and nitrogen atoms in the ionosphere, they excite them to higher energy levels. On returning to their normal resting levels, the atoms emit the energy gained in the form of visible light. It is this light in shades of green and red that we see in the aurora. In the northern hemisphere, we see the Aurora Borealis, and in the southern hemisphere, we see the Aurora Australis.

1.4.4 Magnetosphere

The magnetosphere is the region that surrounds a planet and the magnetic field of that planet, in which charged particles are trapped and controlled by that planet's magnetic field, rather than the solar magnetic field. More specifically, the Earth's magnetosphere is the region of space where the Earth's magnetic field is confined by the solar wind plasma, blowing outward from the sun. The magnetosphere prevents most of the particles from the sun, carried by solar wind, from hitting the Earth. This asymmetrical region surrounds Earth, extending from about one hundred to several thousand kilometers above the surface.

Because the Earth is made of magnetic elements such as Iron, Nickel, and Cobalt, the Earth acts as an extremely large magnet which attracts these charged particles among other things. In concurrence with that, as the Earth rotates, its hot core generates strong electric currents that produce the magnetic field. The sun and other planets have magnetospheres, but the Earth has the strongest one of all the rocky planets.

Like all magnets, the Earth also has both a North and South Poles. The Earth's north and south magnetic poles reverse at irregular intervals of hundreds of thousands of years. In addition, the poles wander over shorter periods of time (hundreds of years).

As the Sun's corona continuously emits plasma into the solar system, the solar wind that carries it distorts the shape of the magnetosphere by compressing it at the front and causing a long tail to form on the side away from the Sun; this long tail is called *the magnetotail*.

Although the magnetosphere blocks most of the plasma, some particles from the solar wind can enter the magnetosphere. The particles that enter from the magnetotail travel toward the Earth and create an aurora.

1.4.5 Plasmas outside the solar system

A great variety of natural plasmas exist beyond the solar system in stars, interstellar space, galaxies, intergalactic space, and far beyond to systems quite unknown before the start of astronomy from space vehicles. There is a variety of phenomena of great cosmological and astrophysical significance, including interstellar shock waves from remote supernova explosions, rapid variations of x-ray fluxes from neutron stars with densities like that of atomic nuclei, pulsating radio stars or pulsars (which are theoretically pictured as rapidly rotating neutron stars with plasmas emitting synchrotron radiation from the surface), and the plasma phenomena around the remarkable black holes (which are considered to be singular regions of space into which matter has collapsed, possessing such a powerful gravitational field that nothing, whether material objects or even light itself, can escape from them). The behavior of plasmas in the universe involves the interaction between plasmas and magnetic fields. The crab nebula, for example, is a rich source of plasma phenomena because it contains a magnetic field. The widespread existence of magnetic fields in the universe has been demonstrated by independent measurements, and a wide range of field magnitudes has been found, varying from $10^{-9} teslas$ in interstellar space to $1 tesla$ on the surface of magnetic variable stars.

1.5 Industrial Plasmas

1.5.1 Plasma Production

In order to convert a gas into a plasma state, it is necessary to tear away at least some of the electrons from the atoms, thereby converting these atoms into ions. This detachment of electrons from atoms is called ionization. A plasma is not usually made simply by heating up a container of gas. The problem is that for the most part, a container cannot be as hot as a plasma needs to be in order to be ionized, or the container itself would vaporize and become plasma as well. Plasmas can also be generated by ionization processes that raise the degree of ionization much above its thermal equilibrium value. There are many different methods of creating plasmas in the laboratory and, depending on the method, the plasma may have a high or low density, high or low temperature, it may be steady or transient, stable or unstable, and so on. In what follows, a brief description is presented of the most commonly known processes of photoionization and electric discharge in gases.

In nature and in the laboratory, ionization can occur in several ways: through collisions of fast particles with atoms; through photoionization by electromagnetic radiation; or via electrical breakdown in strong electric fields. The latter two are examples of field ionization, which is the mechanism most relevant to the plasma accelerator context. Typically, in the laboratory, a small amount of gas is heated and ionized by driving an electric current through it, or by shining radio waves into it. Either the thermal capac-

ity of the container is used to keep it from getting hot enough to melt during a short heating pulse, or the container is actively cooled for longer-pulse operation. Generally, these means of plasma formation give energy to free electrons in the plasma directly, and then electron-atom collisions liberate more electrons, and the process cascades until the desired degree of ionization is achieved.

Attempts to use radiation ionization in technology have not been very successful, because typical densities are such that the inverse process of recombination of electrons with ions proceeds very rapidly and leads to a condition of equilibrium. The most widely used method in the laboratory and in technology for obtaining a plasma is the electrical gas discharge. In nature, an example of this phenomenon is seen in lightning: In technology, typical examples would be electric sparks, electric arcs, gaseous flash lamps, and other gas discharge devices. Ionization is a discharge that depends on the production of an electron avalanche.

In addition to these basic methods for producing plasmas, there are many others of less importance. For example, in the search for ways to produce a thermonuclear plasma, work is being carried out on injection: ions acquire large velocities in an accelerator and are injected into a magnetic trap; electrons are attracted to the ions from the surrounding medium and together they form a hot plasma. An unusual method for separating electrons from atoms is the phenomenon of pressure ionization. At very high densities, all materials enter into the degenerate state in which the electrons are squeezed out of their high energy levels. If the energy of these levels (the so-called Fermi energy) exceeds the ionization energy, then the electron shells are broken and the electrons are detached from the atoms. This phenomenon can occur in ultra-dense stars, white dwarfs, and the interior of large hydrogen planets and, according to some authorities, even in the core of the earth. In experiments on compression of matter by converging shock waves an electrical conductivity is observed which can be explained by pressure ionization. However, the necessary densities are so high that the material becomes more like a metal than a plasma.

1.5.2 Some applications of plasmas

There are all sorts of uses for plasmas. To give one example, if we want to make a short-wavelength laser, we need to generate a population inversion in highly excited atomic states. Generally, gas lasers are pumped into their lasing states by driving an electric current through the gas, and using electron-atom collisions to excite the atoms. X-ray lasers depend on collisional excitations of more energetic states of partially ionized atoms in a plasma. Sometimes a magnetic field is used to hold the plasma particles together long enough to create the highly ionized states. A whole field of plasma chemistry exists where the chemical processes that can be accessed through highly excited atomic states are exploited. Plasma etching and deposition in semiconductor technology is a very important related enterprise. Plasmas used for these purposes are sometimes called

process plasmas. Perhaps the most exciting application of plasmas is the production of power from thermonuclear fusion. Nuclear fusion is the process of recombining nuclei to form different nuclei and release vast amounts of energy. This is the process that powers the sun. If we can harness it, nuclear fusion has the potential to provide us with nearly limitless amounts of clean energy. There are three conditions necessary for nuclear fusion: high temperatures (to about $10^7 K$), high density, and prolonged stability. The high temperature requirement places us in the regime of plasmas. While experiments have attained these high temperatures, the primary difficulty is in achieving a sufficiently high combination of density and stability. A deuterium ion and a tritium ion which collide with energy in the range of tens of keV have a significant probability of fusing, and producing an alpha particle and a neutron, with $17.6 MeV$ of excess energy [56]. A promising way to access this energy is to produce a plasma with a density in the range $10^{20}/m^{-3}$ and average particle energies of tens of keV. This is not a simple requirement to meet, since electrons within a fusion plasma travel at velocities of $\sim 108\ m.s^{-1}$, while a fusion device must have a characteristic size of $\sim$ 2 m, in order to be an economic power source.

Plasma medicine is an emerging field that combines plasma physics, life sciences and clinical medicine. It is being studied in disinfection, healing, and cancer [72]. Most of the research is in vitro and in animal models. It uses ionized gas (physical plasma) for medical uses or dental applications [57]. The plasma sources used for plasma medicine are generally low temperature plasmas, and they generate ions, chemically reactive atoms and molecules, and UV-photons. These plasma-generated active species are useful for several bio-medical applications such as sterilization of implants and surgical instruments as well as modifying biomaterial surface properties. Sensitive applications of plasma, like subjecting human body or internal organs to plasma treatment for medical purposes, are also possible. This possibility is being heavily investigated by research groups worldwide under the highly-interdisciplinary research field called plasma medicine.

Plasma is also being used in many high technology industries. It is used in making many microelectronic or electronic devices such as semiconductors. It can help make features on chips for computers. Plasma is also used in making transmitters for microwaves or high temperature films. It can even be used in work with minerals such as diamond, and in extracting economically valuable metals from rock.

1.6 Electronegative plasma concept

1.6.1 Electronegative plasmas description

Electronegative plasmas can be define as those formed in electron attaching gases and having such a density of negative ions that they must be taken into account. By contrast the properties of conventional electropositive plasmas owe much to the large mass

difference between the positive and negative charge carriers.

The self-consistent electric field acting in a plasma retards the most mobile charged particles, which usually leads to a Boltzmann distribution of electrons. If negative ions cross the discharge volume several times during their lifetime in the volume processes, these particles also obey the Boltzmann distribution. It is demonstrated that this condition is usually satisfied when the characteristic time of electron attachment is small as compared to the time of ambipolar diffusion of the negative ions (ion diffusion at an electron temperature). In the opposite case, the profiles of electrons and negative ions are similar. An assumption that is frequently made in plasma physics is that when the plasma is contained in a potential well that confines the negative particles, it accelerates the positive ones so that the fluxes of particles of opposite sign are equal throughout the volume all the way to the boundary wall. In the absence of negative ions, this gives rise to the concept of ambipolar diffusion at higher pressure [58]. In situations where there are a significant number of negative ions and the plasma is essentially collisionless, it is permissible to set

$$n_e = n_{e0} \exp(\phi), \tag{20}$$

where n_e is the electron density, n_{e0} the unperturbed density of electron and $\phi = \frac{eV}{kT_e}$ (where V is the electrostatic potential and T_e the electron temperature) measured relative to the potential at the center (k is Boltzmann's constant and e the electronic charge) and to set

$$n_n = n_{n0} \exp(\sigma_n \phi), \tag{21}$$

where n_n is the negative ion density and en $\sigma_n = T_e/T_n$ (where T_n is the negative-ion temperature). This follows from their respective equations of motion to the walls under the potential gradient.

1.6.2 The technological interest of electronegative plasmas

Electronegative plasmas have been used for decades in fundamental plasma physics studies and for various applications, including etching for micro-electronics, thermonuclear fusion and more recently, spacecraft propulsion [59, 60]. These plasmas can be formed using many different types of electrical discharges fed with electronegative gases (such as H2, O2, CF4, SF6, Cl2, I2) [60, 67]. For example Cl_2 based discharges are found to be a good source of etchant for platinum and aluminium [61]. The active chlorine atoms are produced in the plasma by electron impact dissociation of chlorine molecule according to the reaction $2e^- + Cl_2 \rightarrow 2Cl^-$. Along with the formation of reactive species the electronegative gases also produces negative ions mainly through dissociative attachment. The role of negative ions in plasmas is important as their presence in the discharge can modify the Bohm speed that affects the positive ion flux at the substrate. With an abundance of negative ions, the electron population may reduce significantly in the plasma.

On the other hand, the effective temperature of the plasma may increase as low energy electrons are lost via attachments with neutrals to form negative ions. The discharge impedance also increases with the increase of negative ions. Very electronegative, or ionŰion (also called pair-ion), plasmas where the ratio between the negative ion and electron densities (referred to as the electronegativity) reaches values of a few thousand or more, have potential use in the majority of the above-mentioned applications because of the reduced impact of electrons on wall sheath formation, and similar responses of the plasma to positive or negative voltage biases.

1.7 Waves in plasma

Plasma contains a wide variety of waves because of its fluid like behaviour and also because of its long range interaction between the particles in it. Waves in plasmas can be classified as electromagnetic or electrostatic according to whether or not there is an oscillating magnetic field. Applying Faraday's law of induction to plane waves, we find $\vec{k} \wedge \vec{B} = \vec{E}$ equation implying that an electrostatic wave must be purely longitudinal. An electromagnetic wave, in contrast, must have a transverse component, but may also be partially longitudinal [62, 63]. It is well known that plasma is a dispersive media. Again from the study of plasma oscillation it is obvious that plasma waves can propagate in a dispersive media. So in plasma medium, plasma particles and waves can coexist and they can interact with each other and the oscillation can occur. It is also used in the communication technology. As the information between the human beings is exchanged by the radio waves, so plasma has great applications in this field. Waves are also important for large-scale processes in nature. These waves helped in the propagation of light from sun to earth. The light waves present in the solar radiation heat the earth, but effect of this heating is balanced by cooling due to emission of long wavelength thermal wave radiation from the earth. Plasma waves are accelerating the ionized particles to speeds above the escape velocity. In space plasma, the study of plasma is dealing with the reorganization of basic properties of the plasma like effect of magnetic field and density etc. It also involves the measurement of the characteristic frequencies of the plasma to understand these basic properties. Strong interactions can occur between these plasma waves because the charged in plasma respond to static and oscillatory electromagnetic fields. These strong interactions are often referred as instabilities. Langmuir waves named after the scientist Irving Langmuir are an example of these plasma oscillations. These are the rapid oscillations of the electron density in conducting media such as plasmas or metals. These plasma waves and instabilities are sometimes important to study the energy evolution and flux of plasma in its magnetized phase. These are also beneficial to predict the state of plasma and can also apply to other plasma related phenomenon. The strong whistler mode waves in the magnetosphere of a planet are one of the greater examples in this case. These waves have a deep effect

on the motion of the electrons because these waves have phase velocities which nearly match the motion of electrons around the magnetic field. In this case, the result can be a scattering process which would dump electrons otherwise trapped in the Earth.s Van Allen radiation belts into the atmosphere causing the aurora or northern lights.

1.7.1 Electromagnetic electron waves

In plasma physics, an electromagnetic electron wave is a wave in a plasma which has a magnetic field component and electrons are the main particles that oscillate. In an unmagnetized plasma, an electromagnetic electron wave is simply a light wave modified by the plasma. In a magnetized plasma, there are two modes perpendicular to the field, the O and X modes, and two modes parallel to the field, the R and L waves. These are transverse in nature. In these waves the electric and magnetic field vectors are perpendicular to each other and also perpendicular to the direction of propagation of wave.

1.7.2 Electrostatic waves

Electrostatic waves are longitudinal waves produced in plasma. They occur due to local perturbations of the electric neutrality, which accelerate charged particles in the plasma's neighbourhood, resulting in charge oscillations. These plasma oscillations can be produced by a local pulse [64] due to a probe or a grid launcher excitation [65, 66]. Electrostatic waves are longitudinal waves produced in plasma. They occur due to local perturbations of the electric neutrality, which accelerate charged particles in the plasmaŠs neighbourhood, resulting in charge oscillations. These plasma oscillations can be produced by a local pulse [64] due to a probe or a grid launcher excitation [65, 66]. Electrostatic waves are longitudinal and have no electric field component perpendicular to the direction of propagation ($\vec{k} \wedge \vec{E} = 0$). Since, $\vec{k}$ is in direction of propagation, $\vec{E}$ and $\vec{k}$ are parallel. Thus, the magnetic field of the wave is zero.

1.7.3 Ion acoustic wave

In plasma physics, an ion acoustic wave is one type of longitudinal oscillation of the ions and electrons in a plasma, much like acoustic waves traveling in neutral gas. However, because the waves propagate through positively charged ions, ion acoustic waves can interact with their electromagnetic fields, as well as simple collisions. In plasmas, ion acoustic waves are frequently referred to as acoustic waves or even just sound waves. These waves can propagate through collisionless medium while sound waves do not do the same. This is the main difference between these two types of waves. A second difference is that plasma also contains electrons which have their effect on the wave dispersion equation. Electrons are very mobile due to their small size and mass so they

quickly follow the ion motion trying to maintain the charge neutrality in the medium. Motion of these electrons is due to a small electric field that are generated by the plasma as a result of variations in the local ion density. Ion acoustic wave is the low frequency plasma wave. Here, the electron and ion fluids must be considered together. According to [65], the ordinary acoustic waves and ion acoustic waves can differentiate on the basis of The electric field induced by a slight charge separation. The electron component of the ion acoustic wave tends to propagate faster than the ion component. The electric field retards the electron motion, forcing the two species to propagate together. They commonly govern the evolution of number density, for instance due to pressure gradients, on time scales longer than the frequency corresponding to the relevant length scale. Ion acoustic waves can occur in an unmagnetized plasma or in a magnetized plasma parallel to the magnetic field. For a single ion species plasma and in the long wavelength limit, the waves are dispersionless ($\omega = v_s k$) with a speed given by

$$v_s = \sqrt{\frac{\gamma_e Z k_B T_e + \gamma_i k_B T_i}{m}} \tag{22}$$

where k_B is Boltzmann's constant, M is the mass of the ion, Z is its charge, T_e is the temperature of the electrons and T_i is the temperature of the ions. Normally γ_e is taken to be unity, on the grounds that the thermal conductivity of electrons is large enough to keep them isothermal on the time scale of ion acoustic waves, and γ_i is taken to be 3, corresponding to one-dimensional motion. In collisionless plasmas, the electrons are often much hotter than the ions, in which case the second term in the numerator can be ignored.

1.7.4 Nonlinearity and waves structure

Nonlinear science is believed by many to be the most deeply important frontier for understanding nature since they are of great importance in the physical world. Nonlinear waves are present in a large quantity around us. These involve the disasters like tidal waves, explosions and sonic blasts. These problems are occurring due to the disturbances in our natural environment as well as with human activities. Due to which they respond beyond their linear regions or limits. Inspite of these disadvantages, they are very popular in many phenomena of physics. They have many applications in different regions of physics like these waves are responsible for describing the plasma behaviour and also help in energy transport in biological molecules. Nonlinear waves are also used in art technology, communication technology and femtosecond pulsed lasers. Nonlinearities cannot be ignored, when the amplitudes of the waves are sufficiently large. There are many factors due to which the nonlinearities come into play. These comes from the harmonic generation involving fluid advection, the nonlinear Lorentz force, trapping of particles in the wave potential, ponderomotive force, solitary structures, shock waves, vortices, double layers, etc. are the examples of nonlinearities in plasmas. These com-

posed of the localized waves in plasma medium that leads to above structures. Study of these structures is very important from both theoretical and experimental points of view. The nonlinear structures take away the plasma from the thermodynamic equilibrium. These structures are either impulsively produced in laboratory and space plasmas because of free energy sources or superficially launched in laboratory plasmas under controlled conditions.

1.7.5 Solitary waves and solitons

Much type of nonlinear waves is seen in the space plasmas. A solitary wave is a hump or dip shaped nonlinear wave of permanent profile. It forms due to the balance between nonlinearity and the dispersion. Where they cancel the effect of each other and balanced one another. The same has been done only in the case when the effect of dissipation is negligible compared to those of the effects of nonlinearity and dispersion. While when the dissipative effect is greater than or comparable to the dispersive effect then these shock structures are encountered. Solitons are a specific type of solitary waves with the remarkable feature that, when two (or more) of them collide, they do not scatter but emerge with the same shape and velocity. The word soliton was coined by Zabusky and Kruskal [158] to emphasize that a soliton is a localized entity which may keep its identity after an interaction. In the absence of nonlinearity, dispersion can destroy a solitary wave as the various components of the wave propagate at different velocities. Introducing nonlinearity without dispersion again rules out the possibility of solitary waves because the pulse energy is continuously injected into high frequency modes. But with both dispersion and nonlinearity, solitary waves can again form. The history of solitons is an interesting one [36], with solitons first being seen as water waves in canals in England [69]. By studying the nature of waves, Russell claimed that the propagation of isolated wave was a consequence of the property of the medium rather than the circumstances of the wave generation. Since then, it took rather a long time to establish that some special nonlinear wave equations admit solutions consisting of isolated wave that can propagate and undergo collisions without losing their respective identities. The first theoretical work describing solitons was done by Rayleigh in 1879, and in 1895, Korteweg and de Vries [70] found the first equation describing a solitary wave [70](the KdV equation). Special solution of the KdV equation leads to the solitary wave. It means that the soliton wave becomes an important tool in the mathematical examination of KdV equation. The concept of soliton has had a significant effect and consequences in various branches of mathematics, physics, and engineering. This becomes possible only after the discovery of the inverse scattering transform [71]. This discovery contributes to exact solutions of nonlinear partial differential equations. In the last stage of the 20th century, soliton theory made its impact in industry also. When the term soliton is mentioned in the history of science, numerical simulations played an important role. Along with the inverse scattering transform, numerical simulations have been powerful

tools to reveal the mysterious characteristics of solitons. Zabusky and Kruskal [158] investigated a numerical study of KdV equation. They observed that a single solitary wave behaves like a particle in its interaction with another one. They also observed that under certain conditions any initial pulse can break up into a number of solitons which can move in plasma with different phase velocities. Also the solitons interact with each other and after the interaction they emerge out without any change in their shape and velocity. Some important nonlinear equations which give rise to solitary waves in plasma are KdV equation, modified KdV equation, Gardner equation, nonlinear Schrodinger equation etc.

1.8 Theoretical description of plasma phenomena

For the theoretical description of plasma phenomena, there are basically four principal approaches with several different choices of approximations, each of which applies to different circumstances. One useful approximation, known as particle orbit theory, consists in studying the motion of each charged particle in the presence of specified electric and magnetic fields. This approach is not really plasma theory, but rather the dynamics of a charged particle in given fields. Nevertheless it is important, since it provides some physical insight for a better understanding of the dynamic processes in plasmas. It has proven to be useful for predicting the behavior of very low density plasmas, which is determined primarily by the interaction of the particles with external fields. This is the case, for example, of the highly rarefied plasmas of the Van Allen radiation belts and the solar corona, as well as of cosmic rays, high energy accelerators, and cathode ray tubes. Since a plasma consists of a very large number of interacting particles, in order to provide a macroscopic description of plasma phenomena it is appropriate to adopt a statistical approach. This implies a great reduction in the amount of information to be handled. In the kinetic theory statistical description it is necessary to know only the distribution function for the system of particles under consideration. The problem consists in solving the appropriate kinetic equations that govern the evolution of the distribution function in phase space. One example of differential kinetic equation is the Vlasov equation, in which the interaction between the charged particles is described by smeared out internal electromagnetic fields consistent with the distributions of electric charge density and current density inside the plasma, and the effects of short-range correlations (close collisions) are neglected. When collisions between the plasma particles are very frequent, so that each species is able to maintain a local equilibrium distribution function, then each species can be treated as a fluid described by a local density, local macroscopic velocity and local temperature. In this case the plasma is treated as a mixture of two or more interpenetrating fluids. This theory is called two-fluid or many-fluid theory, depending on the number of different species considered. In addition to the usual electrodynamic equations, there is a set of hydrodynamic equations expressing conservation of mass, of

momentum, and of energy for each particle species in the plasma. Another approach consists in treating the whole plasma as a single conducting fluid using lumped macroscopic variables and their corresponding hydrodynamic conservation equations. This theory is usually referred to as the one-fluid theory. An appropriately simplified form of this theory, applicable to the study of very low frequency phenomena in highly conducting fluids immersed in magnetic fields, is usually referred to as the magnetohydrodynamic (MHD) approximation.

1.9 Fluid description of plasmas

The single particle approach gets to be horribly complicated to describe plasmas. Basically, one needs a more statistical approach because each particle cannot be followed separately. Fortunately, this is not usually necessary because, surprisingly, most of plasma phenomena observed in real experiments can be explained by a rather crude fluid model, in which the identity of the individual particle is neglected, and only the motion of fluid elements is taken into account. Of course, in the case of plasmas, the fluid contains electrical charges.

1.9.1 The Concept of a Fluid Description

There is one essential difference between hydrodynamics and plasma fluid models. In hydrodynamics, the molecules of the liquid are strongly coupled. This means that the molecules are continuously colliding with their neighbors. A pair of particles will only slowly drift apart by diffusion. Hence, it is meaningful to partition the liquid into macroscopic fluid elements, which contain many molecules that stay close together for a long time. These fluid elements move along streamlines of the flow pattern. In an ideal plasma, however, the electrons and ions do not experience their nearest neighbors. This means that Coulomb collisions are rare. Rather, the electrons and ions follow the forces from the average electric and magnetic fields that are produced by many other particles. Therefore, we can partition the plasma into small cells but this does not imply that the particles will stay inside their cells for an extended time. The electrons and ions will typically leave a cell of size l after a transit time $T_t \approx l/v_{th}$ while particles from neighboring cells enter this volume. Therefore, we can use these cells as a kind of bank account to keep a gain and loss record of the total number of particles in such a cell, or the total momentum, or the heat content. This approach gives us a kind of hydrodynamic description, but the analogy to real liquids has its limitations. Depending on the situation, we can arbitrarily choose a description with cells that are fixed in a resting frame of reference, or we can transform to a moving frame of reference that follows the mean flow velocity of the plasma.

1.9.2 Continuity equation

The particle conservation equation is also called the continuity equation. In fact, the motion of a fluid is described by a vector velocity field $\overrightarrow{v}(\overrightarrow{r})$, the mean velocity of all the individual particles which make up the fluid at $\overrightarrow{r}$. In addition, the particle density $n(r)$ is required. We are here discussing the motion of fluid of a single type of particle of mass m and charge q, so the charge and mass density are qn and mn, respectively. The conservation equation of a one type particle thus reads:

$$\frac{\partial n}{\partial t} + div(n\overrightarrow{v}) = 0. \tag{23}$$

1.9.3 momentum conservation equation

Several forces interact in plasmas, but three of these forces strongly determine their behavior. It is the Lorentz force, the pressure gradient force and the collision effects. First, each of the particles charged reacts to electric and magnetic fields by the Lorentz force as:

$$qn(\overrightarrow{E} + \overrightarrow{v} \times \overrightarrow{B}), \tag{24}$$

where $\overrightarrow{E}$ and $\overrightarrow{B}$ are respectively the electric and magnetic fields.
Next, in a gas, $p = nkT$ is the force per unit area arising from thermal motions. The surrounding fluid exerts this force on the element. The pressure gradient force is given by

$$\overrightarrow{F}_p = -\frac{\overrightarrow{grad}p}{n} = -\frac{\overrightarrow{grad}(nkT)}{n}. \tag{25}$$

Finally, collisions between unlike particles do exchange momentum between the species. Therefore, once we realize that any quasi-neutral plasma consists of at least two different species (electrons and ions) and hence two different interpenetrating fluids, we may need to account for another momentum loss (gain) term. The force due to collisions is

$$\overrightarrow{F}_c = -m\sum_{k,l}\nu_{kl}(\overrightarrow{v}_k - \overrightarrow{v}_l), \tag{26}$$

where ν_{kl} denote to the collision frequency between species k and species l.
Hence, we can immediately generalize the momentum equation for species k to

$$m_k n_k \frac{dv_k}{dt} = m_k n_k \left[\frac{\partial v_k}{\partial t} + (\overrightarrow{v}.\overrightarrow{grad})\overrightarrow{v}\right] = q_k n_k(\overrightarrow{E} + \overrightarrow{v} \times \overrightarrow{B}) - \overrightarrow{grad}p - m_k n_k \nu_{kl}(\overrightarrow{v}_k - \overrightarrow{v}_l) \tag{27}$$

1.9.4 Poisson equation

The poisson equation brings out the conservation of the electric charges in the plasma. Lets consider for example a three-species ENP made by of positive ions, negative ions and electrons. The electric field that exist in this plasma may obey Maxwell equations. In this condition, one can write

$$div\overrightarrow{E} = \frac{\rho}{\varepsilon_0}, \tag{28}$$

where $\overrightarrow{E} = -\overrightarrow{grad}\phi$ and $\rho = \sum_s q_s n_s = e(Z_+ n_+ + Z_- n_- - n_e)$. Here, Z_- and Z_+ are, respectively, the atomic numbers of negative and positive species, n_+ and n_- are the number densities of positive and negative species, e is the magnitude of the electron charge and ϕ is the electric potential. Finally, the poisson equation reads

$$\Delta\phi = -\frac{e}{\varepsilon_0}(Z_+ n_+ + Z_- n_- - n_e). \tag{29}$$

1.10 Conclusion

In this chapter, we have reviewed some theoretical aspects of plasmas and ENPs. We have also presented the historical background on plasmas. We have highlighted some properties and characteristics of plasma which will be useful in this work. Finally, we have presented, in a succinct but detailed way, the plasma fluid description that will be the starting-point for studying plasmas dynamics. We intend to use this fluid model in the next chapter to present different methods that we use in this work in the particular case of cold ENPs.

CHAPTER 2

Methodology

2.1 Introduction

During the last two decades, ion acoustic waves has long been intensively studied both theoretically and experimentally. Several perturbation techniques are used to reduce the fluid model equations to the amplitude equation in one or more dimensions. Depending on the excitation modes, the problem of nonlinear waves propagating in plasmas can be described by NLS, DS, KP, KdV, coupled NLSE equations etc., leading to envelope or non-envelope soliton wave structures. These cited equations are derived from model equations by techniques such as the multiple scale expansion method, the reductive perturbation method and others asymptotic expansion [26, 27]. They have a central importance in quantum mechanics. In addition, they arise in many physical problems, including nonlinear water waves, ocean waves, plasma waves, and are of great importance in development of soliton and inverse scatting transform theory [1-4]. Generally, these equations are put into real forms, to obtain exact solutions, using some methods such as Jacobi elliptic expantion, tanh-function, inverse scatting method, Hirota bilinear method and so on. Direct methods as complex thanh-function method, complex-hyperbolic function method, complex ansatz method, complex Jacobi elliptic method and others [1,2, 20-30]. Otherwise, for envelope solitons, they have been found greatly interesting in studying the MI of different wave modes in plasma, due to its importance in stable wave propagation. In ENPs as we mentioned above, the presence of negative ions drastically changes the response of such waves to disturbances. Our aims in this work is to analyse the effects of negative ions parameters, especially the electrons-to-negative ion temperature ratio (σ_n) and the negative ion concentration ratio (α), in the formation, propagation and stability of the solitary waves in electronegative plasmas. To achieve these objectives, we should firstly employ some adapted methods among those indicated

above, to reduce fluid equations into the amplitude equation. On the other hand, solutions of amplitude equations and their stability analysis should be investigated by others methods. In so doing, we present in the next section of this chapter the equations of the model under our study. In the third section, we present the reductive perturbation methods for one-, two- and three-dimensional analysis. The fourth section is devoted to the multiple scale expansion technique. The method used for linear stability analysis is presented in the fifth section for both one- and multidimensional analysis. Finally, in section six, the hirota bilinear method, for finding one and two soliton solutions, is exposed

2.2 Governing equations

We consider a three-species unmagnetized electronegative plasma system composed of Maxwellian electrons and negative ions in addition to cold mobile positive ions [19,151, 157]. So, the usual ion-fluid equations governing the IAWs in 3D geometry is

$$\frac{\partial n_i}{\partial t} + div(n_i \overrightarrow{v}) = 0, \tag{30a}$$

$$\frac{\partial \overrightarrow{v}}{\partial t} + (\overrightarrow{v}.\overrightarrow{grad})\overrightarrow{v} = -\overrightarrow{grad}\phi, \tag{30b}$$

$$\Delta\phi = \mu_e \exp\phi + \mu_n \exp\sigma_n\phi - n_i, \tag{30c}$$

where n_i is the number-density of positive ions, normalized by the unperturbed value n_{i0}. $\overrightarrow{v} = u\overrightarrow{e_x} + v\overrightarrow{e_y} + w\overrightarrow{e_z}$ with u, v and w, the velocity of charged dusts (with mass m_i) in x, y and z directions, respectively. Overall charge neutrality at equilibrium is $n_i^{(0)} = n_e^{(0)} + n_n^{(0)}$. The variables appearing in Eqs.(30a)−(30c) have been appropriately normalized. Thus, n_i is normalized by the unperturbed ion density n_{i0}. $\overrightarrow{v}$ is normalized by the dust-acoustic (DA) speed $c = \sqrt{Zk_BT_e/m_i}$ with T_e denoting the electron temperature, k_B the Boltzmann constant and Z the charged dust state, i.e., the number of electrons per ions residing on the dust-grain surface. Also, ϕ is the electrostatic wave potential normalized by k_BT_e/e, where e is the magnitude of the electron charge. The time and space variables are normalized by the ion Debye length $\lambda_D = (k_BTe/4\pi e^2 n_i)^{1/2}$ and the ion plasma period $\omega^{-1} = (4\pi e^2 n_{i0}/m_i)^{-1/2}$, respectively. Here, $\sigma_n = T_e/T_n$ is the electrons-to-negative ion temperature ratio, $\mu_e = n_{e0}/n_{i0}$ and $\mu_n = n_{n0}/n_{i0}$, where n_{i0} , n_{n0} , and n_{e0}, are the unperturbed densities of the positive ions, negative ions and electrons, respectively. At equilibrium, the neutrality condition of the plasma reads $\mu_e + \mu_n = 1$, where $\mu_e = n_{e0}/n_{i0} = 1/(1+\alpha)$, with $\alpha = n_{n0}/n_{e0}$ being the negative ion concentration ratio. Using the power series expansion of the exponential function around zero, the Eq.(30c) above becomes:

$$\frac{\partial^2\phi}{\partial x^2} + \frac{\partial^2\phi}{\partial y^2} + \frac{\partial^2\phi}{\partial z^2} = 1 + a_1\phi + a_2\phi^2 + a_3\phi^3 - n_i, \tag{31}$$

where,

$$a_1 = \mu_e + \mu_n \sigma_n, \quad a_2 = \frac{\mu_e + \mu_n \sigma_n^2}{2}, \quad a_3 = \frac{\mu_e + \mu_n \sigma_n^3}{6}. \tag{32}$$

Eqs.(30a), (30b) and (31) include nonlinear and dispersive terms whose effects can be preserved by using the reductive perturbation expansion technique. To understand how this technique applies to our system, we will successively conduct a one-dimensional, then two-dimensional and finally three-dimensional study, with the aim of recovering the equations governing the dynamics of modulated waves in ENPs.

2.3 The reductive perturbation method

2.3.1 One-dimensional analysis in non-relativistic plasma: derivation of the NLS equation

In the case of a one-dimensional plasma system, the Eqs.(30) above become:

$$\frac{\partial n_i}{\partial t} + \frac{\partial n_i u_i}{\partial x} = 0, \tag{33a}$$

$$\frac{\partial u_i}{\partial t} + u_i \frac{\partial u_i}{\partial x} + \frac{\partial \phi}{\partial x} = 0, \tag{33b}$$

$$\frac{\partial^2 \phi}{\partial^2 x} = 1 + a_1 \phi + a_2 \phi^2 + a_3 \phi^3 - n_i, \tag{33c}$$

with u_i being the velocity of charged dusts (with mass m_i) in the x-direction. The reductive perturbation method implies the introduction of the spatial and temporal stretched variables $\xi = \epsilon(x - v_g t)$ and $\tau = \epsilon^2 t$, where v_g is the group velocity and ϵ, a small parameter (about 10^{-3}) that measures the strength of nonlinearity. To simplify the reasoning, we choose the equilibrium position for which the potential is zero. The dependent physical variables around their equilibrium values are expanded as

$$\begin{pmatrix} n_i(x,t) \\ u_i(x,t) \\ \phi(x,t) \end{pmatrix} = \begin{pmatrix} 1 \\ 0 \\ 0 \end{pmatrix} + \sum_{p=1}^{\infty} \epsilon^p \sum_{l=-\infty}^{+\infty} \begin{pmatrix} n_l^{(p)}(\xi,\tau) \\ u_l^{(p)}(\xi,\tau) \\ \phi_l^{(p)}(\xi,\tau) \end{pmatrix} A^l(n,t). \tag{34}$$

It is obvious that the above series contains all overtones $A^l(n,t) = \exp[il(kx - \Omega t)]$ up to order p. These are due to nonlinear terms with the corresponding coefficients being of maximum order ϵ^p, along with the relations $\left(n_l^{(p)}\right)^* = n_{-l}^{(p)}$, $\left(u_l^{(p)}\right)^* = u_{-l}^{(p)}$, and $\left(\phi_l^{(p)}\right)^* = \phi_{-l}^{(p)}$, where $()^*$ denotes the complex conjugate of the corresponding quantity. Substituting (34) into (33a), (33b) and (33c), the first-order harmonics (ϵ^1) are obtained in the form

$$n_1^{(1)} = (k^2 + a_1)\phi_1^{(1)}, \text{ and } u_1^{(1)} = \frac{\omega}{k}(k^2 + a_1)\phi_1^{(1)}, \tag{35}$$

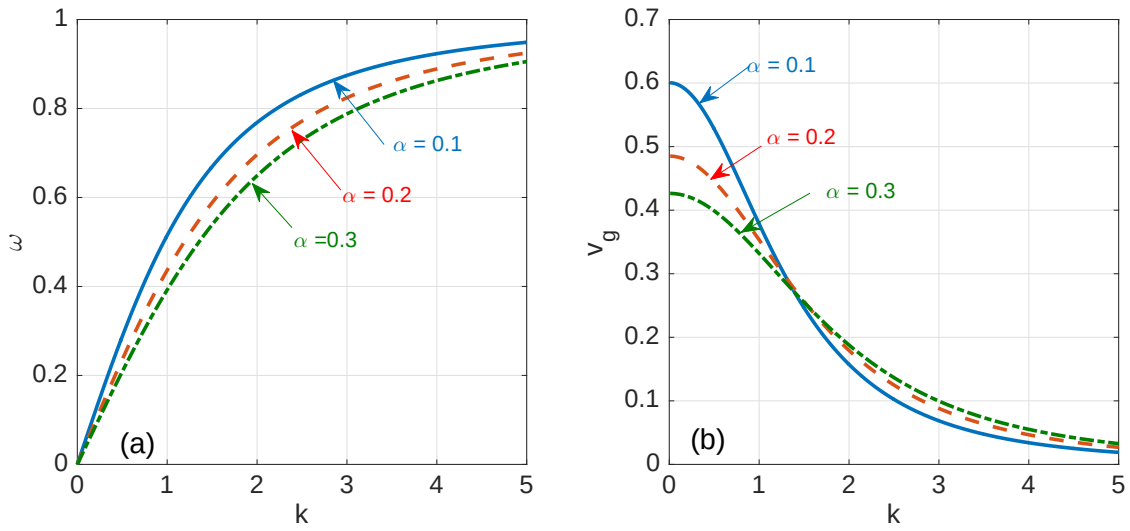

Figure 6: The angular wave frequency ω and the group velocity v_g are plotted against the wavenumber k in panels (a) and (b), respectively. The influence of the negative ion concentration ratio α is studied in both cases for σ_n=17.5.

given that the dispersion relation

$$\omega^2 = \frac{k^2}{k^2 + a_1} \tag{36}$$

is satisfied. The later obviously depends on plasma parameters as shown in Fig. 6(a), where it is plotted versus the wavenumber k for different values of the negative ion concentration ratio α. The frequency here is found to be an increasing function of the later. For the second order (ϵ^2), with $n = 2$ and $l = 0$, we obtain

$$\phi_0^{(2)} = \beta_\phi |\phi_1^{(1)}|^2, \quad n_0^{(2)} = \beta_n |\phi_1^{(1)}|^2, \quad \text{and} \quad u_0^{(2)} = \beta_u |\phi_1^{(1)}|^2, \tag{37}$$

with $\beta_\phi = \frac{-2a_2 v_g^2 + (k^2 - 3a_1)}{a_1 v_g^2 - 1}$, $\beta_n = a_1\beta_\phi + 2a_2$, and $\beta_u = \frac{-2\omega}{(k^2+a_1)^2} + v_g\beta_n$. At the same order, for $l = 1$, solutions $\phi_1^{(2)}$, $n_1^{(2)}$ and $u_1^{(2)}$ exist under the compatibility condition

$$v_g = a_1 \frac{\omega^3}{k^3} = \frac{a_1}{(k^2 + a_1)^{3/2}}, \tag{38}$$

which is in fact the group velocity of the IAWs. As ω, v_g is shown in Fig. 6(b) to strongly depend on plasma parameters, especially α. Indeed, the presence of negative ions in plasmas media reinforces the group volocity for small values the wave number k. For $l = 2$, the components of the second harmonic mode are obtained as

$$\phi_2^{(2)} = \alpha_\phi (\phi_1^{(1)})^2, \quad n_2^{(2)} = \alpha_n (\phi_1^{(1)})^2, \quad u_2^{(2)} = \alpha_u (\phi_1^{(1)})^2, \tag{39}$$

where

$$\alpha_\phi = \frac{(k^2+a_1)^2}{2k^2} - \frac{a_2}{3k^2}, \quad \alpha_n = (a_1+4k^2)\alpha_\phi + a_2, \quad \alpha_u = \frac{\omega}{k}(\alpha_n - (k^2+a_1)^2).$$

By making use of all the previous steps, canceling the third-order equations, with $n = 3$ and $l = 1$, and letting $\phi_1^{(1)} = \psi$, we finally get the NLS equation for IA envelope waves in the form

$$j\frac{\partial\psi}{\partial\tau} + P\frac{\partial^2\psi}{\partial\xi^2} + Q|\psi|^2\psi = 0, \tag{40}$$

where the coefficients P and Q are given by:

$$\begin{aligned} Q &= \frac{\omega^3}{2k^2}\left[-\frac{2k}{\omega}(k^2+a_1)(\alpha_u+\beta_u) - (k^2+a_1)(\alpha_n+\beta_n) + 2a_2(\alpha_\phi+\beta_\phi) - 3a_3\right], \\ P &= -\frac{3a_1\omega^5}{2k^4}. \end{aligned} \tag{41}$$

and $j^2 = -1$.

P and Q are the dispersion and the nonlinear coefficients, respectively. In Figs. 7(a1) and (a2), they are plotted versus k and α. In general P is negative, but Q is negative in some intervals of k and the negative ion concentration ration α. This is explicitly shown in Figs. 7(b1) and (b2), where the negative intervals of Q (versus k) depend on the value of α. For small values of the later, there are two regions where $Q < 0$, i.e., $k < k_{cr,1}$ and $k > k_{cr,2}$, and one region where $Q > 0$, $k_{cr,1} < k < k_{cr,2}$. The same calculations are repeated in Figs. 8(a1)-(a2) and (b1)-(b2), where the effect of the electron-to-negative ion temperature ratio σ_n is studied. Its effect is contrary to what is observed for α, i.e., increasing its value rather gives rise to two intervals where $Q < 0$ (see Fig. 8(b2)). It is also obvious that Q is 10^3 times higher than P, which suggests that the appearance of nonlinear waves will mostly depend on the sign of Q.

2.3.2 One-dimensional analysis in relativistic plasma

In its original formulation, the model for ENPs is composed of Maxwellian electrons and negative ions, in addition to cold mobile positive ions [19, 157]. In the presence of weak relativistic effects, the dynamics of IAWs is governed by the following set of normalized fluid equations:

$$\frac{\partial n_i}{\partial t} + \frac{\partial n_i u_i}{\partial x} = 0, \tag{42a}$$

$$\frac{\partial(\gamma u_i)}{\partial t} + u_i\frac{\partial(\gamma u_i)}{\partial x} + \frac{\partial\phi}{\partial x} = 0, \tag{42b}$$

$$\frac{\partial^2\phi}{\partial x^2} = \mu_n \exp\sigma_n\phi + \mu_e \exp\phi - n_i. \tag{42c}$$

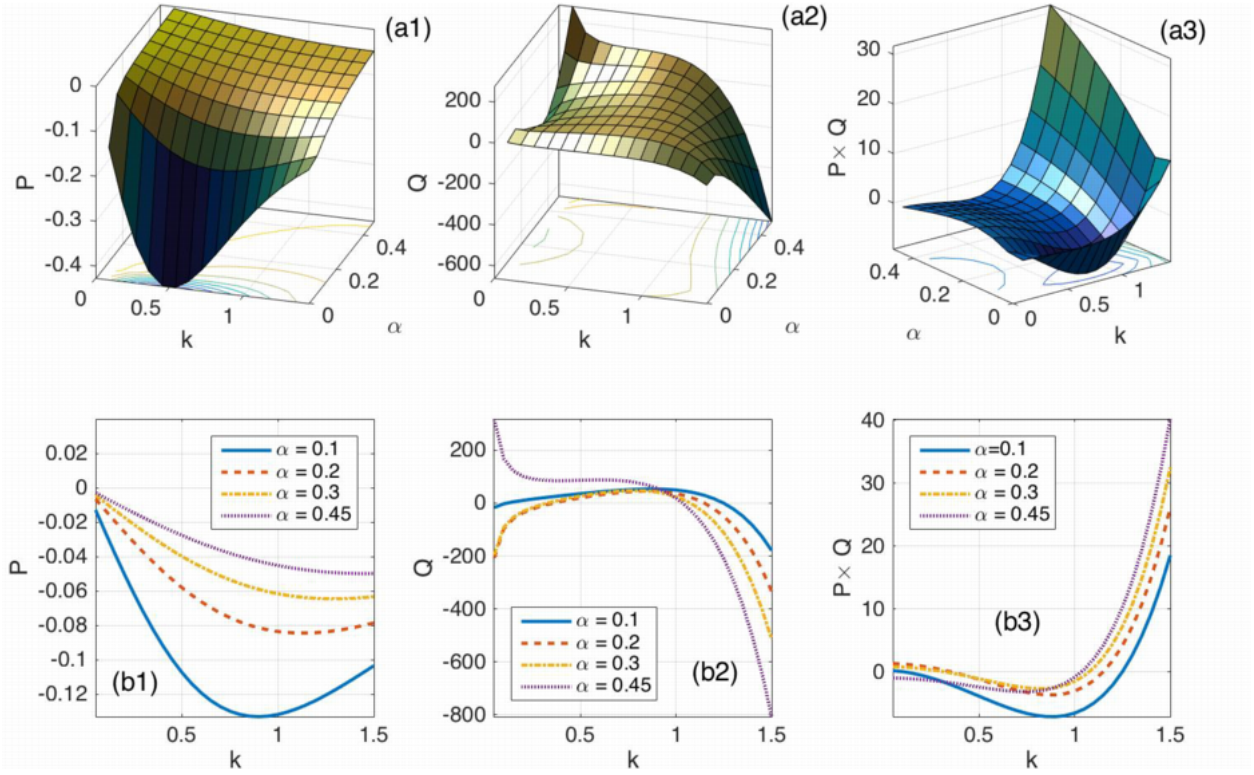

Figure 7: Panels $(\mathrm{aj})_{j=1,2}$ show plots of the parameters P and Q, along with their product $P \times Q$, versus the wavenumber k and the negative ion density ratio α. The dispersion coefficient P is as a whole negative and the nonlinearity coefficient is positive in some intervals, and higher than P. This gives interesting features from their product which, depending on the value of alpha, admits one or two positive intervals. This is clearly illustrated in panels $(\mathrm{bj})_{j=1,2,3}$, where the parameters and their product are plotted versus the wavenumber k. For $\alpha = 0.1$, 0.2 and 0.3, Q has two negative intervals and remains positive for $k_{cr,1} < k < k_{cr,2}$. For higher values of α, Q is positive the interval $0 < k < k_{cr,2}$. In panels (b3) then, one observes two regions where $P \times Q$ is positive, and one region where it is negative, corresponding to regions where $Q > 0$. We have fixed $\sigma_n = 17.5$.

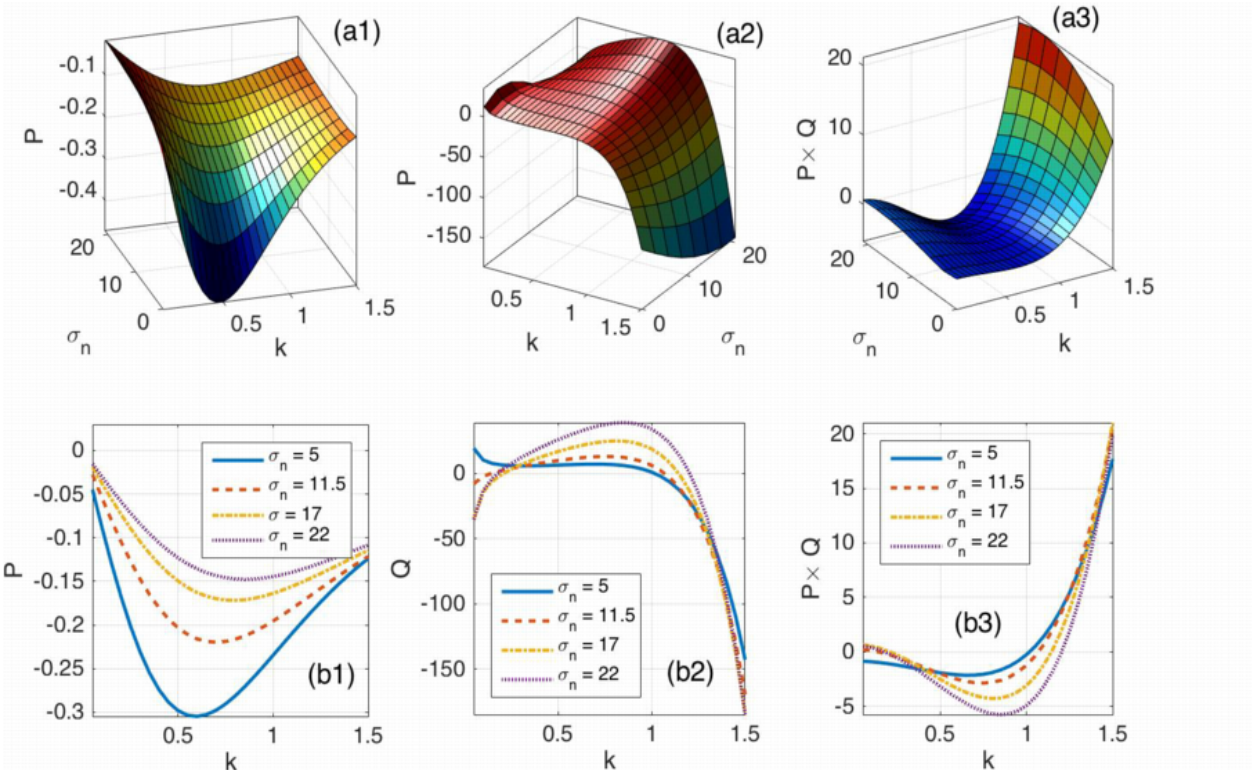

Figure 8: Panels $(\text{aj})_{j=1,2}$ show plots of the parameters P and Q, along with their product $P \times Q$, versus the wavenumber k and the electron-to-negative ion temperature ratio σ. The dispersion coefficient P remains negative for any k and σ_n. However, for small values of σ_n, there is only one region where Q is negative. With increasing σ_n, there are two intervals like in Fig.2. Equally, the product $P \times Q$, for small values of σ_n has one positive interval for k, while two positive regions appear for $\sigma_n \geq 11.5$. All the panels have been plotted for $\alpha = 0.1$.

The relativistic character of the studied plasma system relies on the factor

$$\gamma = \frac{1}{\sqrt{1-\alpha_1 u_i^2}} \simeq 1 + \frac{\alpha_1}{2} u_i^2, \tag{43}$$

which is the result of Lorentz transformations. The parameter α_1 incorporates the relativistic effect, here manifested in terms of the plasma density, by the relationship $\alpha_1 = c_s^2/c^2$. All the other parameters remain as described in Sec.(2.1). Using the power series expansion of the exponential function around zero, Eq.(42c) above becomes

$$\frac{\partial^2 \phi}{\partial x^2} = 1 + a_1\phi + a_2\phi^2 + a_3\phi^3 - n_i, \tag{44}$$

where $a_1 = \mu_e + \mu_n\sigma_n$, $a_2 = \frac{\mu_e+\mu_n\sigma_n^2}{2}$, and $a_3 = \frac{\mu_e+\mu_n\sigma_n^3}{6}$. Modulated IAWs appear in physical systems as the consequence of the interplay between nonlinearity and dispersion. The procedure employed in Sec.(2.3.1) remains validhere, along with the trial solution of Eq.(34) for the dependant variables n_i, u_i and ϕ. Therefore, at $(\epsilon^1)-$order, we have the set of equations

$$-j\omega n_1^{(1)} + jku_1^{(1)} = 0, \;\; -j\omega u_1^{(1)} + jk\phi_1^{(1)} = 0, \;\; (k^2 + a_1)\phi_1^{(1)} - n_1^1 = 0, \tag{45}$$

which is solvable under the condition that the dispersion relation $\omega^2 = \frac{k^2}{k^2+a_1}$ be verified, leading to the first harmonic of perturbation

$$n_1^{(1)} = \frac{k^2}{\omega^2}\phi_1^{(1)}, \;\; \text{and} \;\; v_1^{(1)} = \frac{k}{\omega}\phi_1^{(1)}. \tag{46}$$

We process the same way to obtain the second-order terms, namely the amplitudes of the second harmonics and constant terms as well as the non-vanishing contribution to the first harmonics. We obtain the following equation for $p = 2$ and $l = 0$:

$$a_1\phi_0^{(2)} - n_0^{(2)} + 2a_2|\phi_1^{(1)}|^2 = 0. \tag{47}$$

The $(p = 2,\, l = 1)$-order provides the compatibility condition in term of group velocity, $v_g = a_1\frac{\omega^3}{k^3}$.

For $l = 2$, the components of the second harmonic mode $n_2^{(2)}$, $v_2^{(2)}$, and $\phi_2^{(2)}$ are obtained in term of $\phi_1^{(1)}$ as

$$\phi_2^{(2)} = \alpha_\phi(\phi_1^{(1)})^2, \;\; n_2^{(2)} = \alpha_n(\phi_1^{(1)})^2, \;\; v_2^{(2)} = \alpha_v(\phi_1^{(1)})^2, \tag{48}$$

with

$$\alpha_\phi = \frac{k^2}{2\omega^2} - \frac{a_2}{3k^2}, \;\; \alpha_n = (a_1 + 4k^2)\alpha_\phi + a_2, \;\; \alpha_u = \frac{\omega}{k}\alpha_n - \frac{k^3}{\omega^3}.$$

The zeroth harmonic mode also appears due to the self-interaction of the modulated

carrier wave. Its expression cannot be completely found using the second-order. We will have to consider the third-order equations. Therefore, the set of equations given by the $(l = 0)$-components of the third-order part are given by

$$-v_g n_0^{(2)} + v_0^{(2)} = -\frac{2k^3}{\omega^3}|\phi_1^{(1)}|^2, \quad -v_g u_0^{(2)} + \phi_0^{(2)} = -\frac{k^2}{\omega^2}|\phi_1^{(1)}|^2, \tag{49}$$

to which we have added Eq.(47) from $(n = 2, l = 0)$. Along the same line, the following second-order quantities in the zeroth harmonic are found

$$\phi_0^{(2)} = \beta_\phi|\phi_1^{(1)}|^2, \;\; n_0^{(2)} = \beta_n|\phi_1^{(1)}|^2, \;\; v_0^{(2)} = \beta_v|\phi_1^{(1)}|^2, \tag{50}$$

with

$$\beta_\phi = \frac{-2a_2v_g^2 + (k^2 - 3a_1)}{a_1v_g^2 - 1}, \;\; \beta_n = a_1\beta_\phi + 2a_2, \;\; \beta_v = \frac{-2\omega}{(k^2 + a_1)^2} + v_g\beta_n.$$

Finally, substituting the above derived expressions into the $(n = 3, l = 1)$-components, we obtain the NLS equation

$$j\frac{\partial\psi}{\partial\tau} + P\frac{\partial^2\psi}{\partial\xi^2} + Q|\psi|^2\psi = 0 \tag{51}$$

for the slow evolution of the first-order amplitude of the plasma perturbation potential $\phi_1^{(1)} = \psi$. P and Q are the dispersion and nonlinearity coefficients, respectively, whose expressions are

$$\begin{aligned} Q &= \frac{\omega^3}{2k^2}\left[\frac{3\alpha_1k^4}{2\omega^2} - \frac{2k}{\omega}(k^2 + a_1)(\alpha_u + \beta_u) - (k^2 + a_1)(\alpha_n + \beta_n) + 2a_2(\alpha_\phi + \beta_\phi) - 3a_3\right], \\ P &= -\frac{3a_1\omega^5}{2k^4}. \end{aligned} \tag{52}$$

The NLS equation is one of the most important equation which models nonlinear waves in many physical situations. Despite the NLS equation support for spatially localized envelope soliton such as the bright and dark-type solitons, there is a hierarchy of freak (rational) solutions to the self-focusing NLS equation. These solutions represent excitations due to the MI of plasma and known as the RWs [83, 150]. They have been described as waves which appear from nowhere and disappear without a trace. There is also an extensive literature studying various types of solitons on finite background (SFB) consisting of a localized nonlinear structure evolving upon a nonzero background plane wave. A general SFB solution of the NLS equation has been explicitly proposed

in the form [81, 97, 112, 139, 155]

$$\psi(\xi,\tau)=\sqrt{\frac{2P}{Q}}\left\{\frac{(1-4a)\cosh(2bP\tau)+\sqrt{2a}\cos(c\xi)+i\sinh(2bP\tau)}{\sqrt{2a}\cos(c\xi)-\cosh(2bP\tau)}\right\}\exp(2iP\tau). \quad (53)$$

Here, the single governing parameter a determines the physical behaviour of the solution through the function arguments $b=\sqrt{8a(1-2a)}$ and $c=\frac{2\pi}{L}=2\sqrt{1-2a}$, with L being the periodicity length of the solution [97, 112]. We should stress that the above solution (185) can describe three different kinds of breather solutions, depending on the value of a. The super RW solutions of the focusing NLS equation (51) are localized both in time and space. There are, in fact, two such solutions, the Peregrine soliton and the second-order rogue wave soliton. Although the Peregrine RW is derived as a limiting case of the KM breather, especially when $a \to 1/2$, the two types of solutions can be obtained using the generalized expression [146]

$$\psi_k(\xi,\tau)=\sqrt{\frac{2P}{Q}}\left\{(-1)^k+\frac{G_k(\xi,\bar{\tau})+2jP\tau H_k(\xi,\bar{\tau})}{F_k(\xi,\bar{\tau})}\right\}\exp(2jP\tau), \quad (54)$$

where k is the order of the solution and $\bar{\tau}=2P\tau$. The functions $G_k(\xi,\bar{\tau})$, $H_k(\xi,\bar{\tau})$ and $F_k(\xi,\bar{\tau})$ are polynomials in variables of $\bar{\tau}$ and ξ, with $F_k(\xi,\bar{\tau})$ not having no real zero. In order to get the two solutions, we will restrict our study to the cases $k \leq 2$.

2.3.3 Two-dimensional analysis: derivation of the DS equation

The formulation of the model, remain the same in Eqs.(30) in witch $\overrightarrow{V}=u\overrightarrow{e_x}+v\overrightarrow{e_y}$ with u and v being the velocity of charged dusts (with mass m_i) in x and y directions, respectively. Using the power series expansion of the exponential terms in (30c) around zero, it becomes

$$\frac{\partial^2\phi}{\partial^2 x}+\frac{\partial^2\phi}{\partial^2 y}=1+a_1\phi+a_2\phi^2+a_3\phi^3-n_i, \quad (55)$$

where, $a_1=\mu_e+\mu_n\sigma_n$, $a_2=\frac{\mu_e+\mu_n\sigma_n^2}{2}$ and $a_3=\frac{\mu_e+\mu_n\sigma_n^3}{6}$.

In order to investigate the propagation of IAWs and derive the set of DS equations, we employ the standard reductive perturbation expansion. The stretched variables in space and time may be introduced as $\xi=\epsilon(x-v_g t)$, $\eta=\epsilon y$ and $\tau=\epsilon^2 t$, where v_g is the group velocity that will be found later by the solvability condition of equations (55). The dependent physical variables around their equilibrium values are expanded as follows:

$$\begin{pmatrix} n_i(x,y,t)\\ u_i(x,y,t)\\ v_i(x,y,t)\\ \phi(x,y,t)\end{pmatrix}=\begin{pmatrix}1\\0\\0\\0\end{pmatrix}+\sum_{p=1}^{\infty}\epsilon^p\sum_{l=-\infty}^{+\infty}\begin{pmatrix} n_l^{(p)}(\xi,\eta,\tau)\\ u_l^{(p)}(\xi,\eta,\tau)\\ v_l^{(p)}(\xi,\eta,\tau)\\ \phi_l^{(p)}(\xi,\eta,\tau)\end{pmatrix}A^l(n,t). \quad (56)$$

As done previously, we substitute solutions (56) into equations (33a), (33b) and (55), and we equate each coefficient in powers of ϵ to zero. We obtain, at order (ϵ^1), for $l = 1$, the solutions

$$\phi_1^{(1)} = \frac{1}{k^2 + a_1} n_{i1}^{(1)}, \quad u_1^{(1)} = \frac{\omega}{k} n_{i1}^{(1)}, \quad v_1^1 = 0, \tag{57}$$

which exist under the dispersion relation

$$\omega^2 = \frac{k^2}{k^2 + a_1}. \tag{58}$$

At the same order, but for $l = 0$, we obtain $n_{i0}^{(1)} = u_0^{(1)} = v_0^{(1)} = \phi_0^{(1)} = 0$. The coefficients of the second harmonic, at order (ϵ^2), may be found using the same procedure. This leads for example to the equation

$$a_1 \phi_0^{(2)} - n_{i0}^{(2)} - 2a_2 |\phi_1^{(1)}|^2 = 0, \tag{59}$$

for $l = 0$, and the set of equations

$$\begin{aligned} &- v_g \frac{\partial n_{i1}^{(1)}}{\partial \xi} - j\omega n_{i1}^{(2)} + jk u_1^{(2)} + \frac{\partial u_1^{(1)}}{\partial \xi} = 0, \quad -j\omega v_1^{(2)} = -\frac{\partial \phi_1^{(1)}}{\partial \eta} \\ &- v_g \frac{\partial u_1^{(1)}}{\partial \xi} - j\omega u_1^{(2)} + jk\phi_1^{(2)} = -\frac{\partial \phi_1^{(1)}}{\partial \xi}, \quad (k^2 + a_1)\phi_1^{(2)} - n_{i1}^{(2)} = 2jk \frac{\partial \phi_1^{(1)}}{\partial \xi}, \end{aligned} \tag{60}$$

for $l = 1$, from which the solvability condition

$$v_g = a_1 \frac{\omega^3}{k^3} \tag{61}$$

is obtained, along with the solutions

$$\begin{aligned} v_1^{(2)} &= \frac{-j}{\omega(k^2 + a_1)} \frac{\partial n_1^{(1)}}{\partial \eta}, \quad \phi_1^{(2)} = \frac{n_1^{(2)}}{(k^2 + a_1)} + \frac{2jk}{(k^2 + a_1)^2} \frac{\partial n_1^{(1)}}{\partial \xi}, \\ u_1^{(2)} &= \frac{jk}{(k^2 + a_1)^{3/2}} \frac{\partial n_1^{(1)}}{\partial \xi} + \frac{\omega}{k} n_1^{(2)}. \end{aligned} \tag{62}$$

For $l = 2$, we extract the set of equations

$$\begin{aligned} &- 2j\omega n_{i2}^{(2)} + 2jk u_2^{(2)} + 2jk n_{i1}^{(1)} u_1^{(1)} = 0, \quad -2j\omega u_2^{(2)} + jk(u_1^{(1)})^2 + 2jk n_{i1}^{(1)} u_1^{(1)} = 0, \\ &(4k^2 + a_1)\phi_2^{(2)} - n_{i2}^{(2)} + a_2(\phi_1^{(1)})^2 = 0 \ \text{ and } \ - 2j\omega v_2^{(2)} = 0, \end{aligned} \tag{63}$$

which admits the solutions

$$\phi_2^{(2)} = \alpha_\phi (n_{i1}^{(1)})^2, \quad n_{i2}^{(2)} = \alpha_n (n_{i1}^{(1)})^2, \quad u_2^{(2)} = \alpha_u (n_{i1}^{(1)})^2, \quad v_2^{(2)} = 0, \tag{64}$$

with

$$\alpha_\phi = \frac{1}{2k^2} - \frac{a_2}{3k^2(k^2+a_1)^2},\quad \alpha_n = (a_1+4k^2)\alpha_\phi + \frac{a_2}{(k^2+a_1)^2},\quad \alpha_u = \frac{\omega}{k}(\alpha_n - 1). \quad (65)$$

The zeroth-harmonic mode also appears due to the self-interaction of the modulated carrier wave. Its expression cannot be determined completely within the second order and we will have to consider the third-order equations. Thus, the set of equations corresponding to the $(l=0)-$components of the third-order part of the reduced equations is given by

$$\begin{aligned} &- v_g\frac{\partial n_{i0}^{(2)}}{\partial\xi} + \frac{\partial u_0^{(2)}}{\partial\xi} + \frac{\partial v_0^{(2)}}{\partial\eta} + \frac{2}{(k^2+a_1)^{1/2}}\frac{\partial|n_{i1}^{(1)}|^2}{\partial\xi} = 0,\\ &- v_g\frac{\partial u_0^{(2)}}{\partial\xi} + \frac{\partial\phi_0^{(2)}}{\partial\xi} + \frac{1}{k^2+a_1}\frac{\partial|n_{i1}^{(1)}|^2}{\partial\xi} = 0,\quad -v_g\frac{\partial v_0^{(2)}}{\partial\xi} + \frac{\partial\phi_0^{(2)}}{\partial\eta} + \frac{1}{k^2+a_1}\frac{\partial|n_{i1}^{(1)}|^2}{\partial\eta} = 0, \end{aligned} \quad (66)$$

to which we have added Eq. (59) from the order $(\epsilon^2,\, l=0)$. This leads to

$$\delta_1\frac{\partial^2\phi_0^2}{\partial\xi^2} - \frac{\partial^2\phi_0^2}{\partial\eta^2} - \delta_2\frac{\partial^2|n_{i1}^{(1)}|^2}{\partial\xi^2} - \delta_3\frac{\partial^2|n_{i1}^{(1)}|^2}{\partial\eta^2} = 0, \quad (67)$$

with

$$\delta_1 = v_g^2a_1 - 1,\quad \delta_2 = \frac{2v_g}{(k^2+a_1)^{1/2}} + \frac{1}{k^2+a_1} - \frac{2a_2v_g^2}{(k^2+a_1)^2},\quad \delta_3 = \frac{1}{k^2+a_1}. \quad (68)$$

The various expressions found in the above calculations are then introduced into the $(l=1)$-component of the third-order part of the equations. One finds the following amplitude equation

$$j\frac{\partial n_{i1}^{(1)}}{\partial\tau} + \gamma_1\frac{\partial^2 n_{i1}^{(1)}}{\partial\xi^2} + \gamma_2\frac{\partial^2 n_{i1}^{(1)}}{\partial\eta^2} + \gamma_3|n_{i1}^{(1)}|^2 n_{i1}^{(1)} + \gamma_4\phi_0^{(2)}n_{i1}^{(1)} = 0, \quad (69)$$

with the coefficients

$$\begin{aligned} \gamma_1 &= \frac{3ka_1}{2(k^2+a_1)^{5/2}},\quad \gamma_2 = \frac{a_1}{2k(k^2+a_1)^{3/2}},\\ \gamma_3 &= -\frac{k}{2(k^2+a_1)^{1/2}}\left[6 + \frac{2k^2}{a_1} + \frac{3a_1}{2k^2} - \frac{4a_2}{3k^2(k^2+1)} - \frac{2a_2}{3k^2}\right.\\ &\quad \left. + \frac{2a_2}{(k^2+a_1)^2} + \frac{2a_2^2}{3k^2(k^2+a_1)^3} - \frac{3a_3}{(k^2+a_1)^3}\right]\\ \gamma_4 &= -\frac{k(k^2+a_1)^{3/2}}{a_1} - \frac{ka_1}{2(k^2+a_1)^{1/2}} + \frac{ka_2}{(k^2+a_1)^{3/2}}. \end{aligned} \quad (70)$$

Further introducing the notations $F = n_{i1}^{(1)}$ and $G = \phi_0^{(2)}$, Eqs. (69) and (67) become

$$j\frac{\partial F}{\partial \tau} + \gamma_1 \frac{\partial^2 F}{\partial \xi^2} + \gamma_2 \frac{\partial^2 F}{\partial \eta^2} + \gamma_3 |F|^2 F + \gamma_4 GF = 0, \tag{71a}$$

$$\delta_1 \frac{\partial^2 G}{\partial \xi^2} - \frac{\partial^2 G}{\partial \eta^2} - \delta_2 \frac{\partial^2 |F|^2}{\partial \xi^2} - \delta_3 \frac{\partial^2 |F|^2}{\partial \eta^2} = 0. \tag{71b}$$

Eqs.(71) are the well-known DS equations in two-space directions that was initially derived by Davey and Stewartson to describe modulated waves packets in water of finite depth [147].

2.3.4 Three-dimensional analysis

In this section, we consider the full three-dimensional description of the model in Eqs. (30) in witch $\overrightarrow{V} = u\overrightarrow{e_x} + v\overrightarrow{e_y} + w\overrightarrow{e_z}$, where u, v and w are the velocities of charged particles (with mass m_i) in x, y and z directions, respectively. In order to investigate the propagation of IAWs and derive the amplitude equations in three dimensions, we introduce the stretched variables in space and time as, $\xi = \epsilon(x - v_g t)$, $\eta = \epsilon y$, $\zeta = \epsilon z$ and $\tau = \epsilon^2 t$. Trial solutions are taken as

$$n = 1 + \sum_{p=1}^{\infty} \epsilon^p \sum_{l=-\infty}^{+\infty} n_{il}^{(p)}(\xi, \eta, \zeta, \tau) A^l(x, t), \tag{72a}$$

$$\phi = \sum_{p=1}^{\infty} \epsilon^p \sum_{l=-\infty}^{+\infty} \phi_l^{(p)}(\xi, \eta, \zeta, \tau) A^l(x, t), \tag{72b}$$

$$\overrightarrow{V} = \sum_{p=1}^{\infty} \epsilon^p \sum_{l=-\infty}^{+\infty} \begin{pmatrix} u_l^{(p)}(\xi, \eta, \zeta, \tau) \\ v_l^{(p)}(\xi, \eta, \zeta, \tau) \\ w_l^{(p)}(\xi, \eta, \zeta, \tau) \end{pmatrix} A^l(x, t). \tag{72c}$$

We obtain at ϵ^1 order, for $l = 1$, the following solutions corresponding to the first harmonic of perturbation

$$\phi_1^{(1)} = \frac{1}{k^2 + a_1} n_{i1}^{(1)},\ u_1^{(1)} = \frac{\omega}{k} n_{i1}^{(1)},\ v_1^1 = 0,\ w_1^1 = 0, \tag{73}$$

that satisfy the dispersion relation

$$\omega^2 = \frac{k^2}{k^2 + a_1}. \tag{74}$$

At $(\epsilon^2)-$order, for $l = 0$, we get

$$a_1 \phi_0^{(2)} - n_{i0}^{(2)} - 2a_2 |\phi_1^{(1)}|^2 = 0, \tag{75}$$

and

$$
\begin{aligned}
&-v_g\frac{\partial n_{i1}^{(1)}}{\partial\xi}-j\omega n_{i1}^{(2)}+jku_1^{(2)}+\frac{\partial u_1^{(1)}}{\partial\xi}=0,\quad -v_g\frac{\partial u_1^{(1)}}{\partial\xi}-j\omega u_1^{(2)}+jk\phi_1^{(2)}=-\frac{\partial\phi_1^{(1)}}{\partial\xi}=0,\\
&-j\omega v_1^{(2)}=-\frac{\partial\phi_1^{(1)}}{\partial\eta},\quad -j\omega w_1^{(2)}=-\frac{\partial\phi_1^{(1)}}{\partial\zeta},\quad (k^2+a_1)\phi_1^{(2)}-n_{i1}^{(2)}=2jk\frac{\partial\phi_1^{(1)}}{\partial\xi},
\end{aligned}
\tag{76}
$$

for $l=1$. For $l=2$, the system reduces to

$$
\begin{aligned}
&-2j\omega n_{i2}^{(2)}+2jku_2^{(2)}+2jkn_{j1}^{(1)}u_1^{(1)}=0,\quad -2j\omega u_2^{(2)}+jk(u_1^{(1)})^2+2jkn_{i1}^{(1)}u_1^{(1)}=0,\\
&(4k^2+a_1)\phi_2^{(2)}-n_{i2}^{(2)}+a_2(\phi_1^{(1)})^2=0,\quad -2j\omega v_2^{(2)}=0,\quad -2j\omega w_2^{(2)}=0,
\end{aligned}
\tag{77}
$$

which provides the compatibility condition

$$
v_g=a_1\frac{\omega^3}{k^3}. \tag{78}
$$

By solving equation (77), we find the second-harmonic quantities $n_{2i}^{(2)}$, $u_2^{(2)}$ and $\phi_2^{(2)}$ in term of $\phi_1^{(1)}$ in the form

$$
\phi_2^{(2)}=\alpha_\phi\left(n_{i1}^{(1)}\right)^2,\quad n_{i2}^{(2)}=\alpha_n\left(n_{i1}^{(1)}\right)^2,\quad u_2^{(2)}=\alpha_u\left(n_{i1}^{(1)}\right)^2,\quad v_2^{(2)}=w_2^{(2)}=0, \tag{79}
$$

with

$$
\alpha_\phi=\frac{1}{2k^2}-\frac{a_2}{3k^2(k^2+a_1)^2},\quad \alpha_n=(a_1+4k^2)\alpha_\phi+\frac{a_2}{(k^2+a_1)^2},\quad \alpha_u=\frac{\omega}{k}(\alpha_n-1). \tag{80}
$$

The set of equations in the $(l=0)-$components of the third-order part of the reduced equations is given by

$$
\begin{aligned}
&-v_g\frac{\partial n_{i0}^{(2)}}{\partial\xi}+\frac{\partial u_0^{(2)}}{\partial\xi}+\frac{\partial v_0^{(2)}}{\partial\eta}+\frac{\partial w_0^{(2)}}{\partial\zeta}+\frac{2\omega}{k}\frac{\partial|n_{i1}^{(1)}|^2}{\partial\xi}=0;\quad -v_g\frac{\partial v_0^{(2)}}{\partial\xi}+\frac{\partial\phi_0^{(2)}}{\partial\zeta}+\frac{\omega^2}{k^2}\frac{\partial|n_{i1}^{(1)}|^2}{\partial\zeta}=0;\\
&-v_g\frac{\partial u_0^{(2)}}{\partial\xi}+\frac{\partial\phi_0^{(2)}}{\partial\xi}+\frac{\omega^2}{k^2}\frac{\partial|n_{i1}^{(1)}|^2}{\partial\xi}=0;\quad -v_g\frac{\partial v_0^{(2)}}{\partial\xi}+\frac{\partial\phi_0^{(2)}}{\partial\eta}+\frac{\omega^2}{k^2}\frac{\partial|n_{i1}^{(1)}|^2}{\partial\eta}=0,
\end{aligned}
\tag{81}
$$

to which we add Eq. (75), from (ϵ^2), for $l=0$. From Eqs. (81), we get

$$
\delta_1\frac{\partial^2\phi_0^2}{\partial\xi^2}-\left(\frac{\partial^2\phi_0^2}{\partial\eta^2}+\frac{\partial^2\phi_0^2}{\partial\zeta^2}\right)-\delta_2\frac{\partial^2|n_{i1}^{(1)}|^2}{\partial\xi^2}-\delta_3\left(\frac{\partial^2|n_{i1}^{(1)}|^2}{\partial\eta^2}-\frac{\partial^2|n_{i1}^{(1)}|^2}{\partial\zeta^2}\right)=0, \tag{82}
$$

with

$$\delta_1 = v_g^2 a_1 - 1, \delta_2 = \frac{2v_g\omega}{k} + \frac{\omega^2}{k^2} - \frac{2a_2 v_g^2 \omega^4}{k^4}, \delta_3 = \frac{\omega^2}{k^2}. \tag{83}$$

The various expressions found in the above calculations are then introduced into the $(l = 1)-$component of the third-order part of the equations. This leads to the following amplitude equation

$$j\frac{\partial n_{i1}^{(1)}}{\partial \tau} + \gamma_1 \frac{\partial^2 n_{i1}^{(1)}}{\partial \xi^2} + \gamma_2 \left(\frac{\partial^2 n_{i1}^{(1)}}{\partial \eta^2} + \frac{\partial^2 n_{i1}^{(1)}}{\partial \zeta^2} \right) + \gamma_3 |n_{i1}^{(1)}|^2 n_{i1}^{(1)} + \gamma_4 \phi_0^{(2)} n_{i1}^{(1)} = 0, \tag{84}$$

where

$$\begin{aligned} \gamma_1 &= \frac{-3ka_1}{2(k^2+a_1)^5/2}, \quad \gamma_2 = \frac{a_1}{2k(k^2+a_1)^3/2}, \\ \gamma_3 &= -\frac{k}{2(k^2+a_1)^{1/2}} \left[6 + \frac{2k^2}{a_1} + \frac{3a_1}{2k^2} - \frac{4a_2}{3k^2(k^2+1)} - \right. \\ &\left. \frac{2a_2}{3k^2} + \frac{2a_2}{(k^2+a_1)^2} + \frac{2a_2^2}{3k^2(k^2+a_1)^3} - \frac{3a_3}{(k^2+a_1)^3} \right], \\ \gamma_4 &= -\frac{k(k^2+a_1)^{3/2}}{a_1} - \frac{ka_1}{2(k^2+a_1)^{1/2}} + \frac{ka_2}{(k^2+a_1)^{3/2}}. \end{aligned} \tag{85}$$

Further introducing the notations $F = n_{i1}^{(1)}$ and $G = \phi_0^{(2)}$, the coupled equations (82) and (84) become

$$j\frac{\partial F}{\partial \tau} + \gamma_1 \frac{\partial^2 F}{\partial \xi^2} + \gamma_2 \left(\frac{\partial^2 F}{\partial \eta^2} + \frac{\partial^2 F}{\partial \zeta^2} \right) + \gamma_3 |F|^2 F + \gamma_4 GF = 0, \tag{86a}$$

$$\delta_1 \frac{\partial^2 G}{\partial \xi^2} - \left(\frac{\partial^2 G}{\partial \eta^2} + \frac{\partial^2 G}{\partial \zeta^2} \right) - \delta_2 \frac{\partial^2 |F|^2}{\partial \xi^2} - \delta_3 \left(\frac{\partial^2 |F|^2}{\partial \eta^2} + \frac{\partial^2 |F|^2}{\partial \zeta^2} \right) = 0. \tag{86b}$$

The above system (86) represents the DS equations in three space dimensions.

2.4 The multiple-scale expansion technique: derivation of the coupled NLS equations: Derivation of the coupled NLS equations

We introduce the stretched variables in space and time as $x_n = \epsilon^n x$ and $t_n = \epsilon^n t$. This gives the differential relations $\frac{\partial}{\partial x} = \sum_{n=0}^{N} \epsilon^n \frac{\partial}{\partial x_n}$ and $\frac{\partial}{\partial t} = \sum_{n=0}^{N} \epsilon^n \frac{\partial}{\partial t_n}$. The dependent

physical variables around their equilibrium values are such that

$$\begin{pmatrix} n_i(x,t) \\ u_i(x,t) \\ \phi(x,t) \end{pmatrix} = \begin{pmatrix} 1 \\ 0 \\ 0 \end{pmatrix} + \sum_{p=1}^{\infty} \epsilon^p \begin{pmatrix} n_p(x_0, x_1, x_2, ...;\ t_0, t_1, t_2, ...) \\ u_p(x_0, x_1, x_2, ...;\ t_0, t_1, t_2, ...) \\ \phi_p(x_0, x_1, x_2, ...;\ t_0, t_1, t_2, ...) \end{pmatrix}. \tag{87}$$

Substituting Eqs.(87) into the basic Eqs.(30) and equating the quantities with equal power of ϵ and keeping up to the cubic-order terms in the perturbation expansion, we obtain the sets of differential equations at different orders of ϵ.
In (ϵ^1) order,

$$\frac{\partial n_1}{\partial t_0} + \frac{\partial u_1}{\partial x_0} = 0, \quad \frac{\partial u_1}{\partial t_0} + \frac{\partial \phi_1}{\partial x_0} = 0, \quad \frac{\partial^2 \phi_1}{\partial x_0^2} = a_1\phi_1 - n_1. \tag{88}$$

At (ϵ^2)-order,

$$\begin{aligned} &\frac{\partial n_2}{\partial t_0} + \frac{\partial n_1}{\partial t_1} + \frac{\partial u_2}{\partial x_0} + \frac{\partial u_1}{\partial x_1} + n_1\frac{\partial u_1}{\partial x_0} + u_1\frac{\partial n_1}{\partial x_0} = 0, \\ &\frac{\partial u_2}{\partial t_0} + \frac{\partial u_1}{\partial t_1} + u_1\frac{\partial u_1}{\partial x_0} + \frac{\partial \phi_2}{\partial x_0} + \frac{\partial \phi_1}{\partial x_1} = 0, \\ &\frac{\partial^2 \phi_2}{\partial x_0^2} + 2\frac{\partial^2 \phi_1}{\partial x_0 x_1} = a_1\phi_2 + a_2(\phi_1)^2 - n_2. \end{aligned} \tag{89}$$

At (ϵ^3)-order,

$$\begin{aligned} &\frac{\partial n_3}{\partial t_0} + \frac{\partial n_2}{\partial t_1} + \frac{\partial n_1}{\partial t_2} + \frac{\partial u_3}{\partial x_0} + \frac{\partial u_2}{\partial x_1} + \frac{\partial u_1}{\partial x_2} + n_2\frac{\partial u_1}{\partial x_0} + n_1\frac{\partial u_2}{\partial x_0} + n_1\frac{\partial u_1}{\partial x_1} + u_2\frac{\partial n_1}{\partial x_0} + u_1\frac{\partial n_2}{\partial x_0} + u_1\frac{\partial n_1}{\partial x_1} = 0, \\ &\frac{\partial u_3}{\partial t_0} + \frac{\partial u_2}{\partial t_1} + \frac{\partial u_1}{\partial t_2} + u_2\frac{\partial u_1}{\partial x_0} + u_1\frac{\partial u_1}{\partial x_1} + \frac{\partial \phi_3}{\partial x_0} + \frac{\partial \phi_2}{\partial x_1} + \frac{\partial \phi_1}{\partial x_2} = 0, \\ &\frac{\partial^2 \phi_3}{\partial x_0^2} + \frac{\partial^2 \phi_1}{\partial x_1^2} + 2\frac{\partial^2 \phi_1}{\partial x_0 x_2} + 2\frac{\partial^2 \phi_2}{\partial x_0 x_1} = a_1\phi_3 + 2a_2\phi_1\phi_2 + a_3(\phi_1)^3 - n_3, \end{aligned} \tag{90}$$

In this section, we look for the solution of the field equations governing various order terms in the perturbation expansion.
For (ϵ^1) order equation, the set of Eqs. (87) are linear and should have solutions of the following forms:

$$\begin{aligned} n_1 &= N\exp(j\theta) + N'\exp(j\theta') + c.c., \\ u_1 &= u_1^{(1)}\exp(j\theta) + u'^{(1)}_1\exp(j\theta') + c.c., \\ \phi_1 &= \phi_1^{(1)}\exp(j\theta) + \phi'^{(1)}_1\exp(j\theta') + c.c., \end{aligned} \tag{91}$$

where N, N', u_1^1, u'^1_1, ϕ_1^1 and ϕ'^1_1 are unknown complex amplitudes to be found from the solution of the field equation, θ and θ' are the phases defined by $\theta = \omega t_0 - kx_0$ and $\theta' = \omega' t_0 - k' x_0$. Here ($\omega$,$k$) are, respectively, the angular frequency and the wave number

of the progressive wave, while (ω', k') are those of the regressive wave. Introducing Eqs. (91) into Eqs. (88), the following relations are obtained

$$\begin{aligned} u_1^{(1)} &= \frac{\omega}{k}N, \quad \phi_1^{(1)} = \frac{\omega^2}{k^2}N = \frac{1}{k^2+a_1}N, \\ u'^{(1)}_1 &= -\frac{\omega'}{k'}N', \quad \phi'^{(1)}_1 = \frac{\omega'^2}{k'^2}N' = \frac{1}{k'^2+a_1}N', \end{aligned} \tag{92}$$

which provide the dispersion relations

$$\omega^2 = \frac{k^2}{k^2+a_1}, \;\; \omega'^2 = \frac{k'^2}{k'^2+a_1}. \tag{93}$$

For (ϵ^2)-order equation, we first introduce Eqs. (91) and (92) into (89) and obtain

$$\begin{aligned} \frac{\partial n_2}{\partial t_0} + \frac{\partial u_2}{\partial x_0} = &-\left(\frac{\partial N}{\partial t_1} + \frac{\omega}{k}\frac{\partial N}{\partial x_1}\right)e^{j\theta} + \left(\frac{\partial N'}{\partial t_1} - \frac{\omega'}{k'}\frac{\partial N'}{\partial x_1}\right)e^{j\theta'} + 2i\omega N^2 e^{2j\theta} \\ &+ 2i\omega' N'^2 e^{2j\theta'} + j\left((\omega+\omega') + \frac{k'\omega}{k} + \frac{k\omega'}{k'}\right)NN'e^{j(\theta+\theta')} \\ &+ j\left((\omega-\omega') + \frac{k'\omega}{k} - \frac{k\omega'}{k'}\right)NN'^* e^{j(\theta-\theta')} + cc, \end{aligned} \tag{94a}$$

$$\begin{aligned} \frac{\partial u_2}{\partial t_0} + \frac{\partial \phi_2}{\partial x_0} = &-\left(\frac{\omega}{k}\frac{\partial N}{\partial t_1} + \frac{\omega^2}{k^2}\frac{\partial N}{\partial x_1}\right)e^{j\theta} + \left(\frac{\omega'}{k'}\frac{\partial N'}{\partial t_1} + \frac{\omega'^2}{k'^2}\frac{\partial N'}{\partial x_1}\right)e^{j\theta'} \\ &+ i\frac{\omega^2}{k}N^2 e^{2j\theta} + j\frac{\omega'^2}{k'}N'^2\exp(2j\theta') + j\omega\omega'\left(\frac{1}{k}+\frac{1}{k'}\right)NN'e^{j(\theta+\theta')} \\ &+ j\omega\omega'\left(\frac{1}{k'}-\frac{1}{k'}\right)NN'^* e^{j(\theta-\theta')} + cc, \end{aligned} \tag{94b}$$

$$\begin{aligned} \frac{\partial^2\phi_2}{\partial x_0^2} + n_2 - a_1\phi_2 = &+2j\frac{\omega^2}{k}\frac{\partial N}{\partial x_1}e^{j\theta} - 2j\frac{\omega'^2}{k'}\frac{\partial N'}{\partial x_1}e^{j\theta'} + a_2\frac{\omega^4}{k^4}N^2e^{2j\theta} \\ &+ a_2\frac{\omega'^4}{k'^4}N'^2\exp(2j\theta') + 2a_2\frac{\omega^2\omega'^2}{k^2k'^2}NN'e^{j(\theta+\theta')} + 2a_2\frac{\omega^2\omega'^2}{k^2k'^2}NN'e^{j(\theta-\theta')} \\ &+ a_2\frac{\omega^4}{k^4}|N|^2 + a_2\frac{\omega'^4}{k'^4}|N'|^2 + cc. \end{aligned} \tag{94c}$$

Here, N^* is the complex conjugate of N. From Eqs. (94), one can easily suggests n_2, u_2 and ϕ_2 to be given by

$$\begin{aligned} n_2 &= \hat{N}_2^{(0)} + N_2^{(1)}e^{j\theta} + N'^{(1)}_2 e^{j\theta'} + N_2^{(2)}e^{2j\theta} + N'^{(2)}_2 e^{2j\theta'} + N_2^{(+)}e^{j(\theta+\theta')} + N_2^{(-)}e^{j(\theta-\theta')} + c.c., \\ u_2 &= \hat{u}_2^{(0)} + u_2^{(1)}e^{j\theta} + u'^{(1)}_2 e^{j\theta'} + u_2^{(2)}e^{2j\theta} + u'^{(2)}_2 e^{2j\theta'} + u_2^{(+)}e^{j(\theta+\theta')} + u_2^{(-)}e^{j(\theta-\theta')} + c.c., \\ \phi_2 &= \hat{\phi}_2^{(0)} + \phi_2^{(1)}e^{j\theta} + \phi'^{(1)}_2 e^{j\theta'} + \phi_2^{(1)}e^{2j\theta} + \phi'^{(1)}_2 e^{2j\theta'} + \phi_2^{(+)}e^{j(\theta+\theta')} + \phi_2^{(-)}e^{j(\theta-\theta')} + c.c., \end{aligned} \tag{95}$$

where $\hat{N}_2^{(0)}$, $u_2^{(1)}$... $p_2^{(0)}$ are some functions of slow variables. Introducing these solutions into Eqs. (94) leads to the set of equations

$$\hat{N}_2^{(0)} = a_1\hat{\phi}_2^{(0)} + a_2\frac{\omega^4}{k^4}|N|^2 + a_2\frac{\omega^4}{k^4}|N'|^2, \tag{96}$$

$$\begin{aligned}
j\omega N_2^{(1)} - jku_2^{(1)} &= -\left(\frac{\partial N}{\partial t_1} + \frac{\omega}{k}\frac{\partial N}{\partial x_1}\right), \quad j\omega u_2^{(1)} - jk\phi_2^{(1)} = -\left(\frac{\omega}{k}\frac{\partial N}{\partial t_1} + \frac{\omega^2}{k^2}\frac{\partial N}{\partial x_1}\right), \\
N_2^{(1)} &= \left(a_1 + k^2\right)\phi_2^{(1)} + 2j\frac{\omega^2}{k}\frac{\partial N}{\partial x_1}, \\
j\omega N'^{(1)}_2 - jk'u'^{(1)}_2 &= -\left(\frac{\partial N'}{\partial t_1} + \frac{\omega'}{k'}\frac{\partial N'}{\partial x_1}\right), \quad j\omega u'^{(1)}_2 - jk'\phi'^{(1)}_2 = -\left(\frac{\omega'}{k'}\frac{\partial N'}{\partial t_1} + \frac{\omega'^2}{k'^2}\frac{\partial N'}{\partial x_1}\right), \\
N'^{(1)}_2 &= (a_1 + k'^2)\phi'^{(1)}_2 + 2j\frac{\omega'^2}{k'}\frac{\partial N'}{\partial x_1},
\end{aligned} \tag{97}$$

$$\begin{aligned}
\omega N_2^{(2)} - ku_2^{(2)} &= \omega N^2, \quad 2\omega u_2^{(2)} - 2k\phi_2^{(2)} = \frac{\omega^2}{k}N^2, \\
N_2^{(2)} &= (4k^2 + a_1)\phi_2^{(2)} + a_2\frac{\omega^4}{k^4}N^2, \quad \omega N'^{(2)}_2 - k'u'^{(2)}_2 = \omega' N'^2, \\
2\omega' u'^{(2)}_2 - 2k'\phi'^{(2)}_2 &= \frac{\omega'^2}{k'}N'^2, \quad N'^{(2)}_2 = (4k'^2 + a_1)\phi'^{(2)}_2 + a_2\frac{\omega'^4}{k'^4}N'^2.
\end{aligned} \tag{98}$$

The expressions of the following variables are also carrying-out:

$$\begin{aligned}
n_2^{(-)} = A_n^{(-)}NN', \quad u_2^{(-)} = A_u^{(-)}NN', \quad \phi_2^{(-)} = A_\phi^{(-)}NN', \\
n_2^{(+)} = A_n^{(+)}NN'^*, \quad u_2^{(+)} = A_u^{(+)}NN'^*, \quad \phi_2^{(+)} = A_\phi^{(+)}NN'^*,
\end{aligned} \tag{99}$$

with

$$\begin{aligned}
A_n^{(\pm)} &= \frac{\alpha^{(\pm)}}{\beta^{(\pm)}}, \quad A_\phi^{(\pm)} = \frac{(\omega \pm \omega')^2}{(k \pm k')^2}A_n^{(\pm)} - \delta^\pm, \quad A_u^{(\pm)} = \frac{\omega \pm \omega'}{k \pm k'}A_n^{(\pm)} - \left\{\frac{\omega}{k} + \frac{\omega'}{k'}\right\}, \\
\alpha^{(\pm)} &= 1 - \frac{(\omega \pm \omega')^2}{(k \pm k')^2}\left\{(k \pm k')^2 + a_1\right\}, \quad \beta^{(\pm)} = 2a_2\frac{\omega^2\omega'^2}{k^2k'^2} - \delta^\pm\left\{(k \pm k')^2 + a_1\right\}, \\
\delta^{(\pm)} &= \frac{2\omega\omega'}{kk'} + \frac{\omega^2k' \pm \omega'^2k}{kk'(k \pm k')}.
\end{aligned}$$

Solving Eqs. (97) for $u_2^{(1)}$ and $\phi_2^{(1)}$, we find

$$u_2^{(1)} = \frac{\omega}{k}N_2^{(1)} - \frac{i}{k}\left\{\frac{\partial N}{\partial t_1} + \frac{\omega}{k}\frac{\partial N}{\partial x_1}\right\}, \quad \phi_2^{(1)} = \frac{\omega^2}{k^2}N_2^{(1)} - \frac{2j\omega}{k^2}\left\{\frac{\partial N}{\partial t_1} + \frac{\omega}{k}\frac{\partial N}{\partial x_1}\right\}. \tag{100}$$

Comparing Eqs. (100) to Eqs. (97) and taking into account the dispersion relation, we obtain

$$a_1\frac{\omega^3}{k^3}\frac{\partial N}{\partial x_1} + \frac{\partial N}{\partial t_1} = 0. \tag{101}$$

From Eqs. (101), the nonzero solution for N must be in the form $N = N(\xi, t_2, ..., x_2, ...)$, where $\xi = x_1 - \lambda t_1$, with λ being the group velocity of the first wave and given by

$$\lambda = a_1 \frac{\omega^3}{k^3}. \tag{102}$$

Thus, the solutions for $u_2^{(1)}$ and $\phi_2^{(1)}$ from Eqs. (100) become

$$\begin{aligned} u_2^{(1)} &= \frac{\omega}{k} N_2^{(1)} - \frac{i}{k}\left(\frac{\omega}{k} - \lambda\right)\frac{\partial N}{\partial \xi}, \quad \phi_2^{(1)} = \frac{\omega^2}{k^2} N_2^{(1)} - \frac{2j\omega}{k^2}\left(\frac{\omega}{k} - \lambda\right)\frac{\partial N}{\partial \xi}, \\ {u'}_2^{(1)} &= \frac{\omega'}{k'} {N'}_2^{(1)} - \frac{i}{k'}\left(\frac{\omega'}{k'} - \lambda'\right)\frac{\partial N'}{\partial \xi'}, \quad {\phi'}_2^{(1)} = \frac{\omega'^2}{k'^2} {N'}_2^{(1)} - \frac{2j\omega'}{k'^2}\left(\frac{\omega'}{k'} - \lambda'\right)\frac{\partial N'}{\partial \xi'}. \end{aligned} \tag{103}$$

Here, one can note that $N' = N'(\xi', t_2, ..., x_2, ...)$ and $\xi' = x_1 - \lambda' t_1$. These suggest that the group velocity λ' of the second wave is given by

$$\lambda' = a_1 \frac{\omega'^3}{k'^3}. \tag{104}$$

The set given in Eqs. (98) leads to the following solutions:

$$\begin{aligned} N_2^{(2)} &= \alpha_n N^2, \quad u_2^{(2)} = \alpha_u N^2, \quad \phi_2^{(2)} = \alpha_\phi N^2. \\ {N'}_2^{(2)} &= \alpha'_n N'^2, \quad {u'}_2^{(2)} = \alpha'_u N'^2, \quad {\phi'}_2^{(2)} = \alpha'_\phi N'^2, \end{aligned} \tag{105}$$

where

$$\begin{aligned} \alpha_n &= \frac{4k^2 + a_1}{2k^2} - \frac{a_2\omega^2}{3k^4}, \quad \alpha_u = \frac{\omega}{k}(\alpha_n - 1), \quad \alpha_\phi = \frac{\omega^2}{k^2}\left(\alpha_n - \frac{3}{2}\right), \\ \alpha'_n &= \frac{4k'^2 + a_1}{2k'^2} - \frac{a_2\omega'^2}{3k'^4}, \quad \alpha'_u = \frac{\omega'}{k'}(\alpha'_n - 1), \quad \alpha'_\phi = \frac{\omega'^2}{k'^2}\left(\alpha'_n - \frac{3}{2}\right). \end{aligned}$$

the solution cannot be determined completely within the second-order equation. Therefore, we need the equations governing $\hat{N}_2^{(0)}$, $\hat{n}_2^{(0)}$, $\hat{\phi}_2^{(0)}$, $N_3^{(1)}$, ${N'}_3^{(1)}$, $u_3^{(1)}$, ${u'}_3^{(1)}$, $\phi_3^{(1)}$, ${\phi'}_3^{(1)}$. Introducing Eqs. (95) into the third-order Eqs. (94), we have

$$\begin{aligned} \frac{\partial \hat{N}_2^{(0)}}{\partial t_1} + \frac{\partial \hat{u}_2^{(0)}}{\partial x_1} + \frac{\omega}{k}\frac{\partial |N|^2}{\partial x_1} + \frac{\omega'}{k'}\frac{\partial |N'|^2}{\partial x_1} = 0, \\ \frac{\partial \hat{u}_2^{(0)}}{\partial t_1} + \frac{\partial \hat{\phi}_2^{(0)}}{\partial x_1} + \frac{\omega^2}{2k^2}\frac{\partial |N|^2}{\partial x_1} + \frac{\omega'^2}{2k'^2}\frac{\partial |N'|^2}{\partial x_1} = 0, \end{aligned} \tag{106}$$

on which we add Eq. (96). Recalling that N and N' depend, respectively, on ξ and ξ', these equations suggest that $\hat{N}_2^{(0)}$, $\hat{n}_2^{(0)}$ and $\hat{\phi}_2^{(0)}$ can be decomposed in the following form:

$$\begin{aligned} \hat{N}_2^{(0)} &= N_2^{(0)}(\xi, ...) + {N'}_2^{(0)}(\xi', ...), \quad \hat{u}_2^{(0)} = u_2^{(0)}(\xi, ...) + {u'}_2^{(0)}(\xi', ...), \\ \hat{\phi}_2^{(0)} &= \phi_2^{(0)}(\xi, ...) + {\phi'}_2^{(0)}(\xi', ...). \end{aligned} \tag{107}$$

Then, Eqs. (106) become

$$\begin{aligned} &-\lambda\frac{\partial N_2^{(0)}}{\partial\xi}+\frac{\partial\hat{u}_2^{(0)}}{\partial\xi}+\frac{\omega}{k}\frac{\partial|N|^2}{\partial\xi}=0,\quad -\lambda\frac{\partial u_2^{(0)}}{\partial\xi}+\frac{\partial\phi_2^{(0)}}{\partial\xi}+\frac{\omega^2}{2k^2}\frac{\partial|N|^2}{\partial\xi}=0,\\ &\hat{N}_2^{(0)}=a_1\hat{\phi}_2^{(0)}+a_2\frac{\omega^4}{k^4}|N|^2. \end{aligned} \tag{108}$$

The solution of Eqs. (108) yields the following results:

$$N_2^{(0)}=\beta_n|N|^2,\quad u_2^{(0)}=\beta_u|N|^2,\quad \phi_2^{(0)}=\beta_\phi|N|^2, \tag{109}$$

with

$$\beta_\phi=\frac{2\lambda^2a_2\omega^4-2k^3\lambda\omega-k^2\omega^2}{2k^4(1-\lambda^2a_1)},\quad \beta_u=\lambda a_1\beta_\phi+\lambda a_2\frac{\omega^4}{k^4}-\frac{\omega}{k},\quad \beta_n=a_1\beta_\phi+a_2\frac{\omega^4}{k^4}.$$

From Eqs. (103) and (106), similar expressions are obtained for $N'^{(0)}_2$, $u'^{(0)}_2$ and $\phi'^{(0)}_2$, provided that the unprimed quantities are replaced by primed quantities. In order to complete the solution, we need the equations governing $N_3^{(1)}$, $N'^{(1)}_3$, $u_3^{(1)}$, $u'^{(1)}_3$, $\phi_3^{(1)}$ and $\phi'^{(1)}_3$. By equating the terms in $\exp\theta$ on one hand, and those in $\exp\theta'$ on the other, we obtain

$$\begin{aligned} j\omega N_3^{(1)}-jku_3^{(1)}&=-\frac{\partial N_2^{(1)}}{\partial t_1}-\frac{\partial N}{\partial t_2}-\frac{\partial u_2^{(1)}}{\partial x_1}-\frac{\omega}{k}\frac{\partial N}{\partial x_2}-2j(k\hat{u}_2^{(0)}+\omega\hat{n}_2^{(0)})N\\ &\quad+j(ku_2^{(2)}+\omega n_2^{(2)})N^*+j\frac{k}{k'}(k'u_2^{(+)}+\omega' n_2^{(+)})N'^*+j\frac{k}{k'}(k'u_2^{(-)}+\omega' n_2^{(-)})N',\\ j\omega u_3^{(1)}-jk\phi_3^{(1)}&=-\frac{\partial u_2^{(1)}}{\partial t_1}-\frac{\omega}{k}\frac{\partial N}{\partial t_2}-\frac{\partial\phi_2^{(1)}}{\partial x_1}-\frac{\omega^2}{k^2}\frac{\partial N}{\partial x_2}+2j\omega\hat{u}_2^{(0)}N+j\omega u_2^{(2)}N^*\\ &\quad+j\omega'\frac{k}{k'}u_2^{(+)}N'^*+j\omega'\frac{k}{k'}u_2^{(-)}N',\\ n_3^{(1)}-(k^2+a_1)\phi_3^{(1)}&=2jk\frac{\partial\phi_2^{(1)}}{\partial x_1}+2j\frac{\omega^2}{k}\frac{\partial N}{\partial x_2}-\frac{\omega^2}{k^2}\frac{\partial^2N}{\partial x_1^2}+4a_2\frac{\omega^2}{k^2}\hat{\phi}_2^{(0)}N+2a_2\frac{\omega^2}{k^2}\phi_2^{(2)}N^*\\ &\quad+2a_2\frac{\omega'^2}{k'^2}\phi_2^{(+)}N'^*+2a_2\frac{\omega'^2}{k'^2}\phi_2^{(-)}N'+2a_3\frac{\omega^6}{k^6}|N|^2N+2a_3\frac{\omega^2\omega'^4}{k^2k'^4}|N'|^2N. \end{aligned} \tag{110}$$

and

$$
\begin{aligned}
j\omega' N_3^{'(1)} - jk' u_3^{'(1)} &= -\frac{\partial N_2^{'(1)}}{\partial t_1} - \frac{\partial N'}{\partial t_2} - \frac{\partial u_2^{'(1)}}{\partial x_1} - \frac{\omega'}{k'}\frac{\partial N'}{\partial x_2} - 2j(k'\hat{u}_2^{(0)} + \omega'\hat{n}_2^{(0)})N' + j(k' u_2^{'(2)} \\
&\quad + \omega' n_2^{'(2)})N'^* + j\frac{k}{k'}(k' u_2^{(+)} + \omega' n_2^{(+)})N'^* + j\frac{k}{k'}(k' u_2^{(-)} + \omega' n_2^{(-)})N', \\
j\omega' u_3^{'(1)} - jk' \phi_3^{'(1)} &= -\frac{\partial u_2^{'(1)}}{\partial t_1} - \frac{\omega'}{k'}\frac{\partial N'}{\partial t_2} - \frac{\partial \phi_2^{'(1)}}{\partial x_1} - \frac{\omega'^2}{k'^2}\frac{\partial N'}{\partial x_2} + 2j\omega'\hat{u}_2^{(0)}N' + j\omega' u_2^{'(2)}N'^* \\
&\quad + j\omega\frac{k'}{k}u_2^{(+)}N^* + j\omega\frac{k'}{k}u_2^{(-)}N, \\
n_3^{'(1)} - (k'^2 + a_1)\phi_3^{'(1)} &= 2jk'\frac{\partial \phi_2^{'(1)}}{\partial x_1} + 2j\frac{\omega'^2}{k'}\frac{\partial N'}{\partial x_2} - \frac{\omega'^2}{k'^2}\frac{\partial^2 N'}{\partial x_1^2} + 4a_2\frac{\omega'^2}{k'^2}\hat{\phi}_2^{(0)}N' + 2a_2\frac{\omega'^2}{k'^2}\phi_2^{'(2)}N'^* \\
&\quad + 2a_2\frac{\omega^2}{k^2}\phi_2^{(+)}N^* + 2a_2\frac{\omega^2}{k^2}\phi_2^{(-)}N + 2a_3\frac{\omega'^6}{k'^6}|N'|^2N' + 2a_3\frac{\omega'^2\omega^4}{k'^2k^4}|N|^2N'.
\end{aligned}
\tag{111}
$$

Eliminating $N_3^{(1)}$, $u_3^{(1)}$ and $\phi_3^{(1)}$ from Eqs. (110) , we get

$$
\begin{aligned}
&2j\omega\left(\frac{\partial N_2^{(1)}}{\partial t_1} + \lambda\frac{\partial N_2^{(1)}}{\partial x_1}\right) + 2j\omega\left(\frac{\partial N}{\partial t_2} + \lambda\frac{\partial N}{\partial x_2}\right) + \left(\lambda^2 - 4\frac{\omega\lambda}{k} + \frac{2\omega^2}{k^2} - 4\frac{\omega^4}{k^2} + \frac{4\lambda\omega^3}{k}\right)\frac{\partial^2 N}{\partial \xi^2} \\
&+ \left(-\frac{4a_2\omega^4}{k^2}\beta_\phi + 2\omega^2\beta_n + \omega^2\alpha_n + 4k\omega\beta_u + 2k\omega\alpha_u - 2a_3\frac{\omega^8}{k^6}\right)|N|^2N \\
&+ \left(-\frac{4a_2\omega^4}{k^2}\beta'_\phi + 2\omega^2\beta'_n + \omega\omega'\frac{k}{k'}\left(A_n^{(+)} + A_n^{(-)}\right) + k^2\left(\frac{\omega}{k} + \frac{\omega'}{k'}\right)(A_u^{(+)} + A_u^{(-)}) \right. \\
&\left. + 4k\omega B'_u - 2a_2\frac{\omega^4}{k^2}\alpha_\phi - 2a_2\frac{\omega^2\omega'^2}{k'^2}(A_\phi^{(+)} + A_\phi^{(-)})\right)|N'|^2N = 0.
\end{aligned}
\tag{112}
$$

By introducing a new variable τ as $t_2 = \tau$ and $x_2 = \epsilon\xi + \lambda\tau$, we obtain the following NLS equation:

$$
j\frac{\partial N}{\partial \tau} + \alpha_1\frac{\partial^2 N}{\partial \xi^2} + \alpha_2|N|^2N + \alpha_3|N'|^2N = 0, \tag{113}
$$

where the coefficients α_1, α_2 and α_3 are given by

$$
\begin{aligned}
\alpha_1 &= \frac{\lambda^2}{2\omega} - \frac{2\lambda}{k} - 2\frac{\omega^3}{k^2} + \frac{2\lambda\omega^2}{k}, \quad \alpha_2 = \frac{\omega}{2}(\alpha_n + 2\beta_n) + k(\alpha_u + 2\beta_u) - \frac{2a_2\omega^3}{k^2}\beta_\phi - a_3\frac{\omega^7}{k^6}, \\
\alpha_3 &= \omega\beta'_n + 2k\beta'_u - \frac{2a_2\omega^3}{k^2}\beta'_\phi - \frac{a_2\omega^3}{k^2}\alpha_\phi + \frac{\omega' k}{2k'}\left(A_n^{(+)} + A_n^{(-)}\right) \\
&\quad + \frac{k^2}{2\omega}\left(\frac{\omega}{k} + \frac{\omega'}{k'}\right)\left(A_u^{(+)} + A_u^{(-)}\right) - \frac{a_2\omega\omega'^2}{k'^2}\left(A_\phi^{(+)} + A_\phi^{(-)}\right).
\end{aligned}
\tag{114}
$$

Performing a similar reasoning form Eqs. (110), the counterpart of Eq. (113) is obtained

in the form

$$j\frac{\partial N'}{\partial \tau} + \alpha_1' \frac{\partial^2 N'}{\partial \xi'^2} + \alpha_2' |N'|^2 N' + \alpha_3' |N|^2 N' = 0, \tag{115}$$

where α_1', α_2' and α_3' are respectively obtained from α_1, α_2 and α_3 by replacing (ω, k) by (ω', k'). Further introducing the change of variables $\xi' = x_1 - \lambda' t_1 = \xi - (\lambda - \lambda')t_1$, Eqs. (113) and (111)can then be rewritten in terms of ξ and τ as

$$j\frac{\partial N}{\partial \tau} + \alpha_1 \frac{\partial^2 N}{\partial \xi^2} + \alpha_2 |N|^2 N + \alpha_3 |N'|^2 N = 0, \tag{116a}$$

$$j\frac{\partial N'}{\partial \tau} + j\left(\frac{\lambda' - \lambda}{\epsilon}\right)\frac{\partial N'}{\partial \xi} + \alpha_1' \frac{\partial^2 N'}{\partial \xi^2} + \alpha_2' |N'|^2 N' + \alpha_3' |N|^2 N' = 0. \tag{116b}$$

Here, we are interested in the particular case $k' = -k$, i.e., $\omega' = \omega$ and $\lambda' = -\lambda$. In addition, we perform the dependent-variable transformation $N' = N' \exp -j\left(\frac{\lambda}{\epsilon}\xi + \frac{\lambda^2}{\mu_1}\tau\right)$ to get ride of the terms in $\frac{\partial N'}{\partial \xi}$ from Eq. (116b). One finally obtains the following nonlinearly coupled NLS equations:

$$j\frac{\partial N}{\partial \tau} + \mu_1 \frac{\partial^2 N}{\partial \xi^2} + \left(\mu_2 |N|^2 + \mu_3 |N'|^2\right) N = 0, \tag{117a}$$

$$j\frac{\partial N'}{\partial \tau} + \mu_1 \frac{\partial^2 N'}{\partial \xi^2} + \left(\mu_2 |N'|^2 + \mu_3 |N|^2\right) N' = 0, \tag{117b}$$

where

$$\mu_1 = \alpha_1, \quad \mu_2 = \alpha_2, \quad \mu_3 = \alpha_3 = \omega\beta_n - 2k\beta_u - \frac{2a_2\omega^3}{k^2}\beta_\phi - \frac{\omega^3}{2k^2}\left(4k^2 + a_1\right) - \frac{2a_2^2\omega^7}{k^6}. \tag{118}$$

2.5 Linear stability analysis and modulational instability

MI is related to the apparition of solitons in system where there are competitive effects between nonlinearity and dispersion. In general, nonlinear modulated waves share the same regions of parameter with solitons solutions. Nonlinear equations admit plane wave solutions that may be stable or unstable, depending on the system parameters.

2.5.1 One-dimensional plasmas

Solutions for Eq.(41) can be assumed in the form $\psi = \psi_0(\xi)\exp(jQ\psi^2\tau)$, where ψ_0 is a real constant amplitude of the pump carrier wave. The stability of any solution is investigated under small perturbations in phase, in amplitude or in both. Since

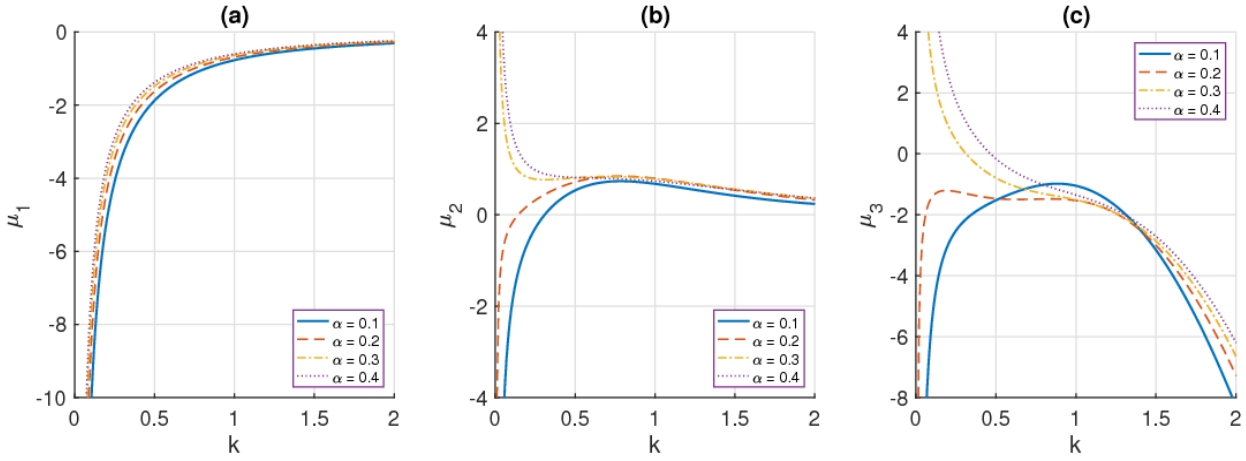

Figure 9: Panels (a), (b) and (c) show plots of the parameters μ_1, μ_2 and μ_3, versus the wave number k and different values of the negative ion density ratio α. The dispersion coefficient μ_1 is always negative while the nonlinearity coefficient μ_2 and the coupling coefficient μ_3 can change signs according to intervals. For $\alpha = 0.1$ and 0.2, μ_2 is negative for $k < k_{cr,1}$ and becomes positive for $k > k_{cr,1}$, while μ_3 is always negative. Conversely, For hight value of α, μ_3 is positive for $k < k_{cr,2}$ and becomes negative for $k > k_{cr,2}$, while μ_2 is always positive. We have fixed $\sigma_n = 17$.

we are interested in amplitude modulation, the corresponding perturbed solution then writes $\psi = (\psi_0 + \delta\psi)\exp(jQ\psi^2\tau)$, where $\xi = (K\zeta - \Omega\tau)$ is the modulation phase with $K \ll k$ and $\Omega \ll \omega$ are respectively the wave number and the frequency of the modulation; $\delta\psi \ll \psi_0$ is the small amplitude of perturbation, which is introduced in the form $\delta\psi = U + jV$, where $U = U_0\exp[j(K\zeta - \Omega\tau)]$ and $V = V_0\exp[j(K\zeta - \Omega\tau)]$. After substituting all these into Eq. (41) and linearizing around the unperturbed plane wave solution, one finally obtains the nonlinear dispersion relation

$$\Omega^2 = (PK^2)^2\left(1 - \frac{2Q\psi_0^2}{PK^2}\right). \tag{119}$$

For the plane wave solution to be unstable, the frequency Ω should be complex, i.e., $\Omega^2 < 0$. Obviously, this highly depends on the sign of Q/P. When Q/P is negative, it is clear that Ω will be real and for $Q/P > 0$, it is likely that the perturbation frequency be negative. In general, the instability is a purely growing mode for $Q/P > 0$, which is materialized by the MI growth rate.

2.5.2 Multi-dimensional Plasmas

The DS equations

$$j\frac{\partial F}{\partial \tau} + \gamma_1\frac{\partial^2 F}{\partial \xi^2} + \gamma_2\frac{\partial^2 F}{\partial \eta^2} + \gamma_3|F|^2F + \gamma_4 GF = 0, \tag{120a}$$

$$\delta_1 \frac{\partial^2 G}{\partial \xi^2} - \frac{\partial^2 G}{\partial \eta^2} - \delta_2 \frac{\partial^2 |F|^2}{\partial \xi^2} - \delta_3 \frac{\partial^2 |F|^2}{\partial \eta^2} = 0, \tag{120b}$$

govern the MI of 2D IAWs and we look for the stability/instability conditions for the emergence of modulated waves in ENPs. Similar procedure was adopted in Refs. [26, 27, 40] on a simplified 2D model, i.e., by considering only one ion type. Homogeneous solutions for the DS system are usually considered in the form $F = F_0 \exp j(\alpha_1 \xi + \alpha_2 \eta - \Omega\tau + \varphi)$, $G = G_0$, where $F_0, G_0, \alpha_1, \alpha_2$ and ϕ are real constants. The above trial solutions may propagate in the system under the condition that the dispersion relation $\Omega = \gamma_1 \alpha_1^2 + \gamma_2 \alpha_2^2 - \gamma_3 F_0^2 - \gamma_4 G_0$ be satisfied. Small perturbations are usually introduced into such solutions in order to test their stability and robustness. We therefore consider the perturbed solutions

$$F = (F_0 + \Delta F) e^{j(\alpha_1 \xi + \alpha_2 \eta - \Omega\tau + \varphi + \Delta\varphi)}, \;\; G = G_0 + \Delta G, \tag{121}$$

where the perturbations ΔF, ΔG and $\Delta\varphi$ are assumed to be

$$\begin{pmatrix} \Delta F \\ \Delta G \\ \Delta \varphi \end{pmatrix} = \begin{pmatrix} \delta F \\ \delta G \\ \delta \varphi \end{pmatrix} \mathrm{Re}\left\{ e^{j(\mu_1 \xi + \mu_2 \eta - \nu\tau)} \right\}. \tag{122}$$

Making use of this and linearizing around the unperturbed plane waves lead to a homogeneous system in δF, δG and $\delta\varphi$, which admits non-trivial solutions if its determinant is zero. This yields the nonlinear dispersion relation

$$\nu_1^2 = (\mu_1^2 \gamma_1 + \mu_2^2 \gamma_2) \left(\mu_1^2 \gamma_1 + \mu_2^2 \gamma_2 - 2\gamma_3 F_0^2 + 2\gamma_4 F_0^2 \frac{\mu_1^2 \delta_2 + \mu_2^2 \delta_3}{\mu_2^2 - \mu_1^2 \beta_1} \right), \tag{123}$$

where $\nu_1 = (\nu - 2\gamma_1 \mu_1 \alpha_1 - 2\gamma_2 \mu_2 \alpha_2)$. The plane wave will then be said to be unstable under modulation if $\nu_1^2 < 0$, i.e.,

$$\left(\mu_1^2 \gamma_1 + \mu_2^2 \gamma_2\right)^2 \left\{ 1 - 2F_0^2 \left(\frac{\gamma_3(\mu_2^2 - \mu_1^2 \beta_1) - \gamma_4(\mu_1^2 \delta_2 + \mu_2^2 \delta_3)}{(\mu_2^2 - \mu_1^2 \beta_1)(\mu_1^2 \gamma_1 + \mu_2^2 \gamma_2)} \right) \right\} < 0. \tag{124}$$

Obviously, the stability/instability condition only depends on the term in brackets, which also give the threshold amplitude

$$F_{0,cr}^2 = \frac{1}{2} \frac{(\mu_2^2 - \mu_1^2 \beta_1)(\mu_1^2 \gamma_1 + \mu_2^2 \gamma_2)}{\gamma_3(\mu_2^2 - \mu_1^2 \beta_1) - \gamma_4(\mu_1^2 \delta_2 + \mu_2^2 \delta_3)} \tag{125}$$

above which modulated IAWs may be observed.
Similarly, the 3D-DS equations

$$j \frac{\partial F}{\partial \tau} + \gamma_1 \frac{\partial^2 F}{\partial \xi^2} + \gamma_2 \left(\frac{\partial^2 F}{\partial \eta^2} + \frac{\partial^2 F}{\partial \zeta^2} \right) + \gamma_3 |F|^2 F + \gamma_4 G F = 0, \tag{126a}$$

$$\delta_1\frac{\partial^2 G}{\partial\xi^2}-\left(\frac{\partial^2 G}{\partial\eta^2}+\frac{\partial^2 G}{\partial\zeta^2}\right)-\delta_2\frac{\partial^2|F|^2}{\partial\xi^2}-\delta_3\left(\frac{\partial^2|F|^2}{\partial\eta^2}+\frac{\partial^2|F|^2}{\partial\zeta^2}\right)=0 \tag{126b}$$

admit the trivial homogeneous solutions $F=F_0e^{j\gamma_3F_0^2\tau}$ and $G=0$, where F_0 is a real constant that represents the amplitude of carrier wave. MI of IAWs is investigated under small perturbations in phase, in amplitude or in both. For amplitude modulation, the corresponding perturbed solutions then write $F=(F_0+\delta F(\xi,\eta,\zeta,\tau))e^{j\gamma_3F_0^2\tau}$ and $G=\delta G(\xi,\eta,\zeta,\tau))$, with $\delta F\ll F_0$. After linearizing Eqs. (126) around the unperturbed plane wave solutions, we obtain the governing equations for the small perturbations δF and δG in the form

$$j\frac{\partial\delta F}{\partial\tau}+\gamma_1\frac{\partial^2\delta F}{\partial\xi^2}+\gamma_2\left(\frac{\partial^2\delta F}{\partial\eta^2}+\frac{\partial^2\delta F}{\partial\zeta^2}\right)+\gamma_3F_0^2(\delta F+\delta F^*)+\gamma_4\delta GF_0=0, \tag{127a}$$

$$\begin{aligned}\delta_1\frac{\partial^2\delta G}{\partial\xi^2}-\left(\frac{\partial^2\delta G}{\partial\eta^2}+\frac{\partial^2\delta G}{\partial\zeta^2}\right)-\delta_2F_0\frac{\partial^2(\delta F+\delta F^*)}{\partial\xi^2}\\ -\delta_3F_0\left(\frac{\partial^2(\delta F+\delta F^*)}{\partial\eta^2}+\frac{\partial^2(\delta F+\delta F^*)}{\partial\zeta^2}\right)=0.\end{aligned} \tag{127b}$$

We make use of the transformation $\delta F=a+ib$ and $\delta G=c+id$, with

$$(a,b,c,d)=(a_0,b_0,c_0,d_0)e^{j(\mu_1\xi+\mu_2\eta+\mu_3\zeta-\Omega\tau)},$$

and obtain the nonlinear dispersion relation

$$\Omega^2=\left[\gamma_1\mu_1^2+\gamma_2(\mu_2^2+\mu_3^2)\right]^2\left[1+\frac{2F_0^2}{(\gamma_1\mu_1^2+\gamma_2(\mu_2^2+\mu_3^2))}\left(\frac{\delta_2\gamma_4\mu_1^2+\delta_3\gamma_4(\mu_2^2+\mu_3^2)}{-\delta_1\mu_1^2+\mu_2^2+\mu_3^2}-\gamma_3\right)\right]. \tag{128}$$

The perturbation wavenumber vector can be expressed using spherical coordinates, i.e., $(\mu_1,\mu_2,\mu_3)=(K\cos\theta,K\sin\theta\cos\varphi,K\sin\theta\sin\varphi)$. Eq. (128) then reduces to

$$\Omega^2=K^2P^2\left(K^2-2F_0^2\frac{Q}{P}\right), \tag{129}$$

where

$$P=\gamma_1\cos^2\theta+\gamma_2\sin^2\theta\quad\text{and}\quad Q=\gamma_3+\gamma_4\frac{\delta_2\cos^2\theta+\delta_3\sin^2\theta}{\delta_1\cos^2\theta-\sin^2\theta}. \tag{130}$$

There will be instability if the frequency Ω is complex, i.e., $\Omega^2<0$.

2.6 The Hirota Bilinear method

Single soliton solutions can be found easily, from the NLS, KdV, mKdV and DS equations, by using the travelling wave ansatz $f=f(x-vt)$. However, a question remains: what about multisoliton solutions? First of all it must be stated that explicit N-soliton

solutions can only be found for integrable equations. If one is only interested in finding multisoliton solutions the best tool is Hirota's bilinear method [82], although many other methods can also be used. It is important to realize that PDEs appearing in a given physical problem are not usually in the best form for the subsequent mathematical analysis. Hirota noticed that the best dependent variables for constructing soliton solutions are those in which the solution appears as a finite sum of exponentials. In that purpose, lets consider de following KdV equation.

$$\frac{\partial u}{\partial t} + 6u\frac{\partial u}{\partial x} + \frac{\partial^3 u}{\partial x^3}. \tag{131}$$

Hirota was based his reasoning on the observation that the solutions of Eq. (131), as obtained from the inverse scattering method, were in the form $u = 2\partial_x^2 \ln(detM)$, where M is a matrix exhibiting the (x, t) dependency, detM was a polynomial of exponentials. Hirota then made the logical step of introducing a new dependent variable F by $u = 2\partial_x^2 \ln(F)$. If this is substituted into Eq. (131), it can be written as

$$\partial_x(F_{xxxx}F - 4F_{xxx}F + 3F_{xx}^2 + FF_{xt} - F_xFt = 0). \tag{132}$$

This equation is fifth order in derivatives, but one overall derivative can be extracted. In order to apply Hirota's method, it is necessary that the equation be quadratic and that the derivatives only appear in combinations that can be expressed using Hirota's D-operator defined by

$$D_x^n g \cdot F = (\partial_{x_1} - \partial_{x_2})^n F(x_1)G(x_2)|_{x_2=x_1=x}. \tag{133}$$

For example,

$$D_xF \cdot G = F_xG - FG_x, \tag{134a}$$

$$D_xD_tF \cdot G = F_{xt}G - F_xG_t - F_tG_x + -FG_{xt}. \tag{134b}$$

Thus D-operates on a product of two functions like the Leibniz rule, except that it is antisymmetric,

$$D_x^nF \cdot G = (-1)^n D_x^nG \cdot F, \tag{135}$$

Using the D-operator we can write Eq. 132 in the following condensed form

$$(D_x^4 + D_xD_t)F \cdot F = 0. \tag{136}$$

Now, let P be a polynomial in Hirota D-operator. A generalized bilinear differential equation writes

$$P(D)F \cdot F = 0. \tag{137}$$

Here are some useful properties of polynomial P:

$$P(D)F \cdot G = P(-D)G \cdot F, \tag{138a}$$

$$P(D)1 \cdot F = P(-\partial)F, \tag{138b}$$

$$P(D)F \cdot 1 = P(\partial)F. \tag{138c}$$

$$P(D) \exp ax \cdot \exp bx = P(a-b) \exp (a+b)x, \tag{138d}$$

$$P(D) \exp ax \cdot \exp bx = P(a-b) \exp (a+b)x. \tag{138e}$$

The multisoliton solutions are obtained by finite perturbation expansions around the vacuum $F = 1$:

$$F = 1 + \delta f_1 + \delta^2 f_2 + \delta^3 f_3 + ... \tag{139}$$

Here δ is a formal expansion parameter, and for an N-soliton solution of Eq. (139), the expansion stops at δ^N. If the bilinear form contains several functions, similar expansions should be written for all of them. For the one-soliton solution (1SS), only one term is needed. If we substitute

$$F = 1 + \delta f_1 \tag{140}$$

into Eq. (136), we obtain

$$P(D)\{1 \cdot 1 + \delta 1 \cdot f_1 + \delta f_1 \cdot 1 + \delta^2 f_1 \cdot f_1\} = 0. \tag{141}$$

It is clear that the term of order δ^0 vanishes. We use properties Eqs. (138b) and (138c) for the terms of order δ^0 so that we get

$$P(\partial) f_1 = 0. \tag{142}$$

The soliton solutions correspond to the exponential solutions of Eq. (142). For a 1SS, f_1 is taken with just one exponential as

$$f_1 = \exp \eta_1, \quad \eta_1 = k_1 x + \omega_1 t + a_1. \tag{143}$$

Replacing Eq. (143) into Eq. (142), one obtains the following dispersion relation

$$P(r_1) = 0, \quad r_1 = (k_1, \omega_1). \tag{144}$$

Finally, the δ^2-order term vanishes because

$$P(D) \exp \eta_1 \cdot \exp \eta_1 = \exp 2\eta_1 P(r_1 - r_1) = 0. \tag{145}$$

Thus, the 1SS is given by Eqs.(143) and (144), where the parameters are constrained by the dispersion relation. For KdV, the dispersion relation is $\omega^3 = k$.

To construct two-solitons solution of KdV PDE, we take $F = 1 + \delta f_1 + \delta^2 f_2$, where $f_1 = \exp\eta_1 + \exp\eta_2$ for $\eta_i = k_i x + \omega_i t + a_i$, $i = 1, 2$. After inserting F into the Eq. (136), we make the coefficients of $\delta^n, (n = 1, 2, 3, 4)$ to vanish. The coefficient of δ^0 is

$$P(D)1 \cdot 1 = 0. \tag{146}$$

The coefficient of δ^1 gives

$$P(D)\{1 \cdot f_1 + f_1 \cdot 1\} = 2P(\partial)\{\exp\eta_1 + \exp\eta_2\}, \tag{147}$$

which implies $P(r_i) = k_i^4 + k_j\omega_i = 0$ i.e. $\omega_i = k_i^3$ for $i = 1, 2$. The coefficient of δ^2 is given by

$$\begin{aligned} P(D)\{1 \cdot f_2 + f_2 \cdot 1\} + P(D)\{f_1 \cdot f_1\} &= 2P(\partial)f_2 + P(D)\{(\exp\eta_1 + \exp\eta_2) \cdot (\exp\eta_1 + \exp\eta_2)\}, \\ &= 2\left[P(\partial)f_2 + P(D)\{\exp\eta_1 \cdot \exp\eta_2\}\right], \\ &= 2\left[P(\partial)f_2 + P(r_1 - r_2)\{\exp(\eta_1 + \eta_2)\}\right] = 0. \end{aligned} \tag{148}$$

This makes f_2 to have the form $f_2 = A_{12}\exp(\eta_1 + \eta_2)$. If we put f_2 in the above equation, we obtain A_{12} as

$$A_{12} = -\frac{P(r_1 - r_2)}{P(r_1 + r_2)} = \frac{(k_1 - k_2)^2}{(k_1 + k_2)^2}. \tag{149}$$

Finally, we set $\delta = 1$, thus $F = 1 + \exp\eta_1 + \exp\eta_2 + A_{12}\exp(\eta_1 + \eta_2)$.

2.7 Conclusion

This chapter was devoted to the presentation of the fluid model equations governing the dynamic of ENP system composed of Maxwellian electrons and negative ions in addition to cold mobile positive ions. We have also presented analytical methods used in this thesis. Asymptotic expansion techniques, like the reductive perturbation and the multiple-scale expansion methods, have been presented. Using these methods, we were able to derive the amplitude equations like NLS, DS or coupled NLS equation which is also called Manakov system. We note that, coefficients of these equations depend on electronegative parameters of the plasma. Stability conditions have been discussed, using the MI analysis of the plane wave solution for the amplitude equations. Also, we have explored the Hirota bilinear scheme to show how to derive one- and two- solitons solutions. This last method will allow us to solve the DS-Equation and obtain the one- and two- dromions structures.

CHAPTER 3

Results and discussion

3.1 Introduction

During the last twenty years, more evidence and interest have been brought to the existence of solitons in various domains of physics, mainly due to their importance in nonlinear optics [1,77,102], in Biophysics [3–6] and, more recently, in Bose-Einstein condensates [2, 80, 93]. In ENPs, the nonlinearity of the system is considerably affect and consequently the characteristics of IAWs [18, 117, 118]. In this chapter, we mean to address comprehensively in one, two and three-dimensional cases, the response of IAWs to the effects of the negative ion parameters, especially the negative ion concentration ratio and the electron-to -negative ion temperature ratio. We also show that under certain conditions, new classes of waves like bright and dark envelope soliton, one- and two-dromions solitons and rogue waves may emerge. One of the direct mechanisms leading to the formation of modulated IA waves is MI, a consequence of the interplay between nonlinear and dispersive effects [5,107,126,130]. In the one-dimensional analysis, among others, we examine the special case of the wave-wave interaction and finally, we find the great interest to investigate on the weakly relativistic ENPs. These investigations will allow us to have a precise idea of how plasma electronegative parameters impact the emergence, the propagation and the stability of solitary waves in such media.

3.2 One dimensional mode excitations

3.2.1 Single mode analysis

3.2.1.1 Envelope excitations

The NLS equation has solutions, which include envelope solitons, breather-type localized structures. In this work, we are interested in envelope solitons whose importance has been discussed in a broad range of areas including biophysics [127–129, 131], plasma physics [7], nonlinear optics and metamaterials [109], just to name a few. As a whole, finding some kinds of solutions for Eq. (40) requires the study of the sign of the product $P \times Q$, which, when positive leads to the bright-envelope IA solitons. For a complete analysis in this regard, we have represented PQ versus k and α in Fig. 7(a3), and only versus k in Fig. 7(b3), with changing α. From the parametric analysis of the previous chapter on the signs of P and Q, one can predict the occurrence of the two positive intervals of the product PQ with increasing α.This is indeed obvious in Fig. 7(b3), where the two regions $k < k_{cr,1}$ and $k > k_{cr,2}$ clearly appear. Moreover, with in mind the results of Figs. 8(a1), (a2), (b1) and (b2), it would be more interesting to also explore the effect of σ_n on the formation of modulated IAWs. This is performed in panels (a3) and (b3) of Fig. 8, where PQ is respectively plotted in the plane (k, σ_n) and versus k, respectively. In the later, the change in σ_n importantly affects the positive region of PQ, but the effect is contrary to that observed for α. The two positive zones exist and get reduced with increasing σ_n. Also, in the two cases, depending on negative parameter values, there exists one region where PQ is positive, i.e., $k > k_{cr,2}$. Although we are not quite sure of their values, one may also state that there are two critical values of k, $k_{cr,1}$ and $k_{cr,2}$ so that bright envelope solitons may be found for $k < k_{cr,1}$ and $k > k_{cr,2}$. Otherwise, when parameters are picked from intervals where $PQ < 0$, solutions for Eq.(40) will be of envelope dark-type [7,143,144]. The general envelope-type solution is written in the form

$$\psi(\xi, \tau) = \psi_0(\xi, \tau) e^{j\Theta(\xi,\tau)} + c.c., \tag{150}$$

where the slowly varying amplitude ψ_0 and the phase correction Θ are real quantities, obtained by plugging solution Eq.(150) into Eq.(40). In this section, we study two cases based on the previous discussion on the sign of the product $P \times Q$.

(i) The bright-type envelope solutions

These solutions arise in regions of parameters where $PQ > 0$. Making use of trial solution Eq.(150), the bright soliton solutions for Eq.(40) are given by [143, 144]

$$\psi_0 = \rho_0 sech\left(\frac{\xi - v_e\tau}{L}\right), \text{ and } \Theta = \frac{1}{2P}\left\{v_e\xi - \left(PQ\rho_0^2 + \frac{1}{2}v_e^2\right)\tau\right\}, \tag{151}$$

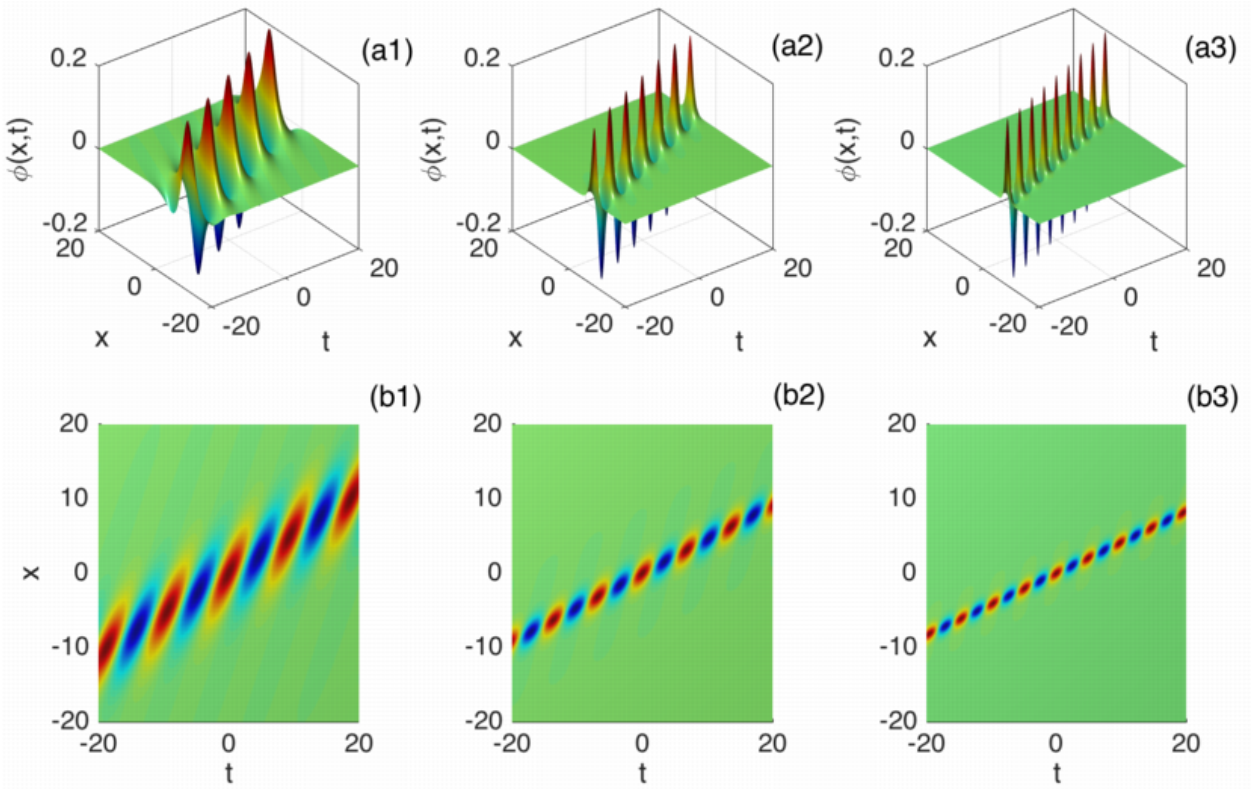

Figure 10: Spatiotemporal evolution of solutions Eq.(151), with their corresponding density plots, for different values of the wavenumber k: (a1)-(b1) $k = 1.2$, (a2)-(b2) $k = 1.3$ and (a3)-(b3) $k = 1.8$, with $\alpha = 0.3$ and $\sigma_n = 17.5$.

where v_e is the velocity of the envelope and L, the envelope spatial width related to the amplitude ρ_0 by $L\rho_0 = \sqrt{2P/Q}$. The global solution $\phi(x,t)$ describing the electric potential may be obtained by considering the different steps of Section 2. The corresponding solutions are shown in Fig. 10 for different values of the wavenumber k. For any value of k, the bright soliton profile remains constant as it propagates, but the phase, which slowly depends on space and time, experiences small deformation of the wave packet internal structure during propagation. Equally, the plasma negative ion parameters such as α and σ_n are also supposed to influence their structures. This is for example summarized in Fig. 11, where the effect of the negative ion concentration ratio α is to reduce the spatial expansion of the obtained solution. For $\alpha = 0.3$, for example, one indeed gets more spatially localized structures. The parameter α indeed gives an idea on the suitable concentration of the negative ions and its consequences on the formation of bright-envelope IAWs. For instance, localized modulated IAW packets have been observed in the earth's magnetosphere, where they are related to localized field and density variations [78, 115].

(ii) The dark-type envelope solutions

Such solutions are usually obtained in regions of parameters where $P \times Q < 0$ and may

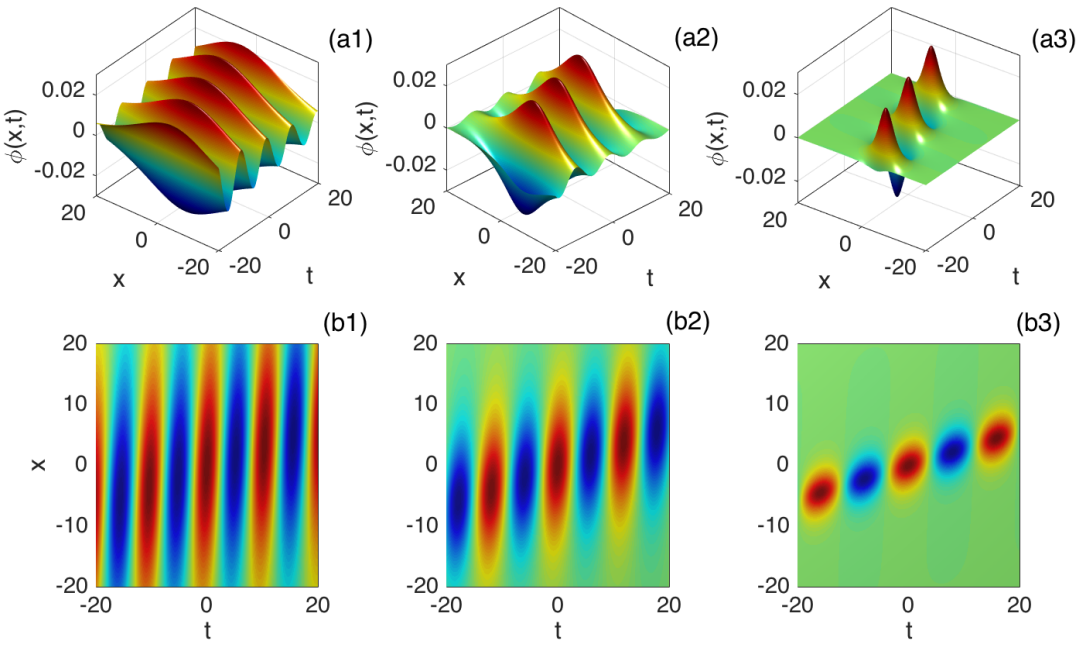

Figure 11: Space-time evolution of solutions Eq.(151), along with their corresponding density plots, under the effect of the negative ion concentration ratio α: $\alpha = 0.1$, $\alpha = 0.2$ and $\alpha = 0.3$, with $\sigma_n = 17.5$ and $k = 0.22$.

propagate as dark envelope wavepackets. Their general expression writes [143, 144]

$$\psi_0 = \rho_0 \left| \tanh\left(\frac{\xi - v_e\tau}{L'}\right)\right|, \quad \text{and} \quad \Theta = \frac{1}{2P}\left\{v_e\xi - \left(PQ\rho_0^2 + \frac{v_e^2}{2}\right)\tau\right\}, \tag{152}$$

where $L'\rho_0 = \sqrt{2|P/Q|}$. The corresponding solutions are represented in Fig. 12 for different values of α. In particular, the localized part is enclosed between temporally oscillating structures, but spatially, there are jumps between the dark breathers which characterize the kink-antikink origin of these structures. Such effects are more ostensible in Fig. 12 (a3)-(b3), where $\alpha = 0.3$. Also, one clearly remarks that the number of oscillating structures between kink profiles reduces with increasing α, which still confirms the important effect of negative ions on the electric potential in the plasma. This introduces a new class of soliton which we call here the "kink-wave" soliton. In order to better picture some specific features of the kink-wave soliton, it has been plotted in space for different values of α (see Fig. 13). In panels $(\text{aj})_{j=1,2,3}$, we have imposed $\alpha = 0.1$ and $\phi(x,t)$ has been plotted at different instant to picture the time frame. One clearly sees the oscillating features inside the two states of the kink, main characteristic of the kink-wave IA soliton. With increasing α, we obtain the features of Fig $13(\text{bj})_{j=1,2,3}$, where the frequency of oscillations drops, leading to some multi-humped features of the solution. Finally, for $\alpha = 0.3$, the signature of the electric potential is displayed in Fig. $13(\text{cj})_{j=1,2,3}$. Once again, the frequency of the oscillating part has dropped. To get

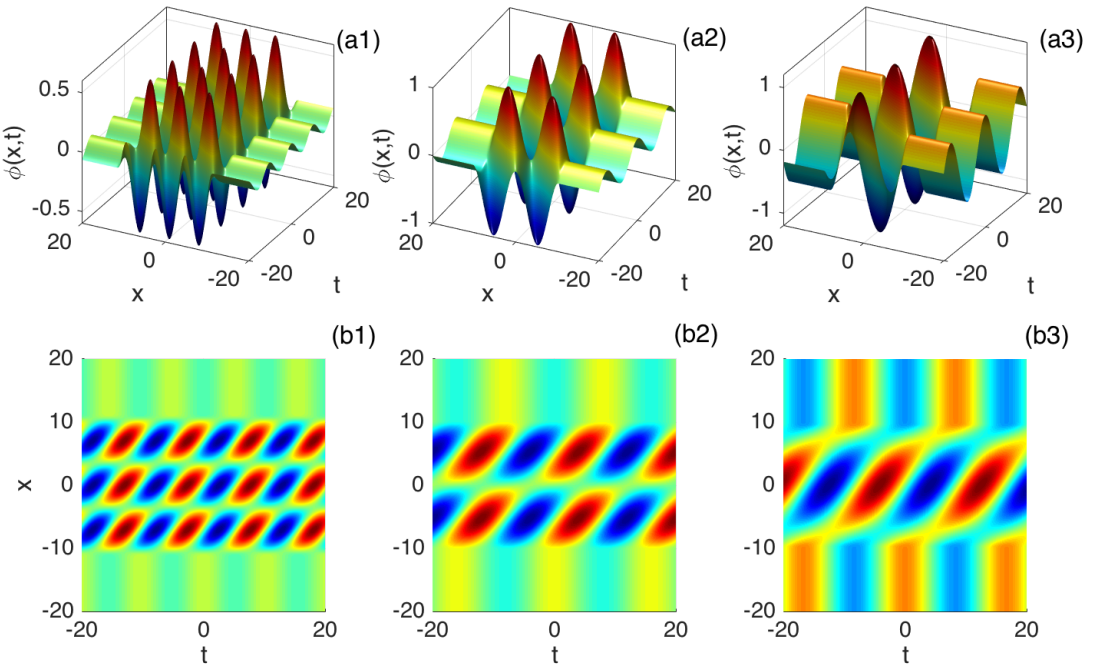

Figure 12: Panels show space-time evolution of the dark envelope solutions (151), with their corresponding density plots, for different values of the negative ion concentration ratio α: $\alpha = 0.1$, $\alpha = 0.2$ and $\alpha = 0.3$, with $\sigma_n = 17.5$ and $k = 0.65$.

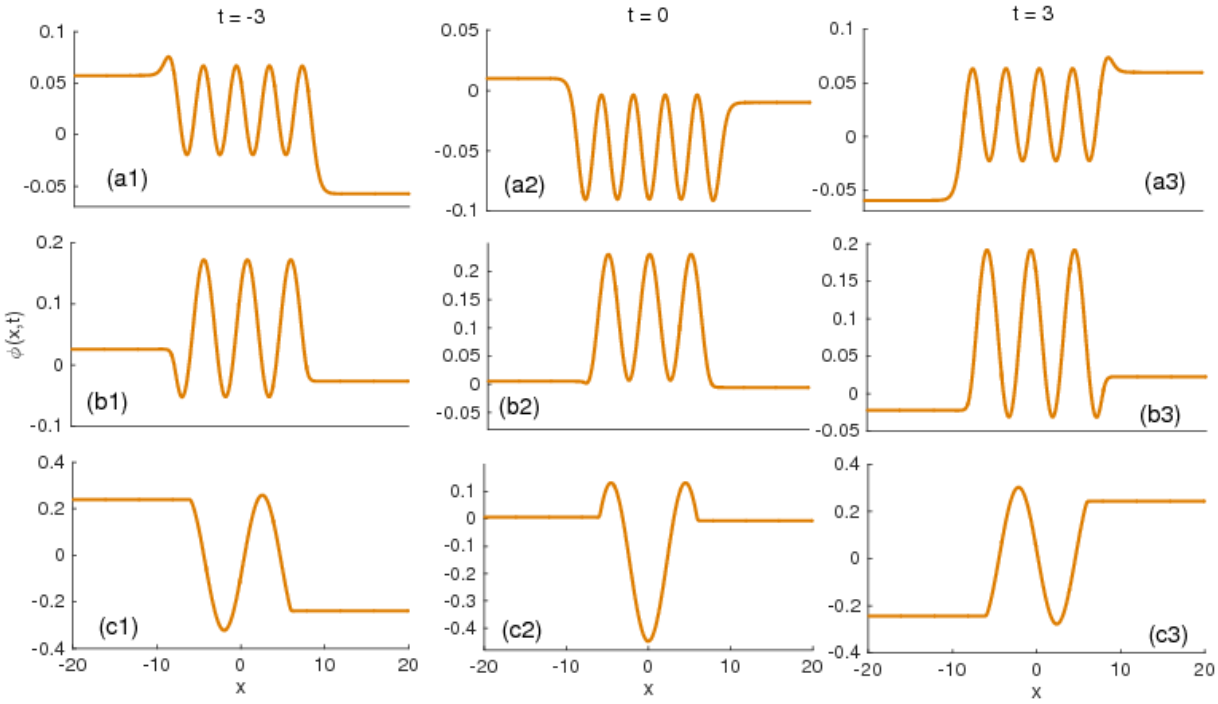

Figure 13: Panels show spacial features of the dark envelope solutions (152), under the effect of the negative ion concentration ratio α. Panels $(\mathrm{aj})_{j=1,2,3}$ are plotted for $\alpha = 0.1$, $(\mathrm{bj})_{j=1,2,3}$ for $\alpha = 0.2$ and $(\mathrm{cj})_{j=1,2,3}$ for $\alpha = 0.3$, with $\sigma_n = 17.5$.

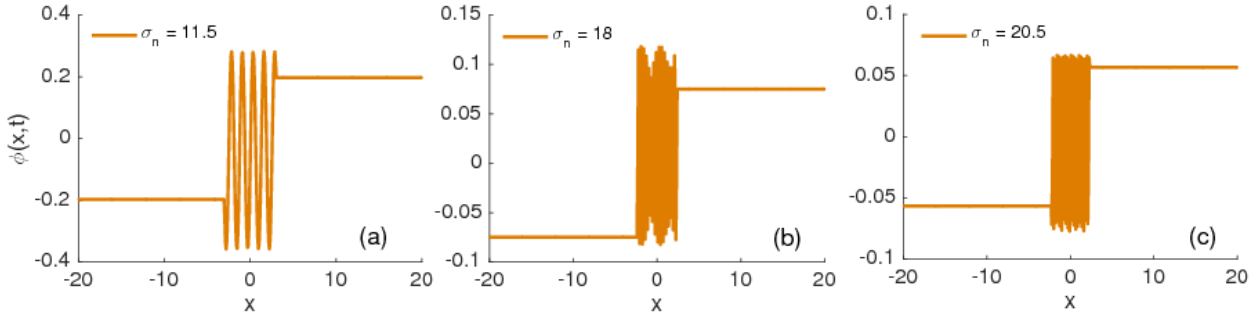

Figure 14: Panels show spacial evolution of the dark envelope solutions (152) for different values of the electron-to-negative ion temperature ratio σ_n, where panel(a) corresponds to $\sigma_n = 20$, (b) to $\sigma_n = 21$ and (c) to $\sigma_n = 22.5$, with $\alpha = 0.1$.

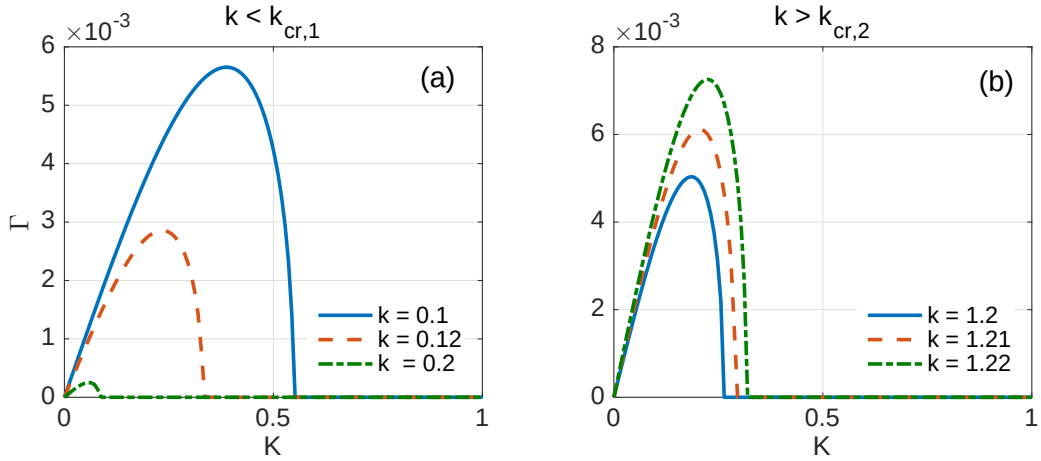

Figure 15: Panels show the growth rate of instability versus the perturbation wavenumber K. In panel (a), small values of the initial wavenumber k are considered, while in panel (b) high values of k introduced. Below $k_{cr,1}$, Γ is a decreasing function of k, and above $k_{cr,2}$, it increases with increasing k. We have considered $\alpha = 0.1$ and $\sigma = 11.5$.

these results, we have considered $\sigma_n = 17.5$. With increasing α, the concentration of negative ions increases and this affects the electron-to-negative ion temperature whose effects may be seen by changing the value of σ_n as depicted in Fig. 14. It is clear from there that the frequency of the oscillating part of the solution increases with σ_n, leading to more obvious features of the kink form. This straightforwardly corroborates what was already predicted in Figs. 7 and 8, where the effect of σ_n on the coefficients was contrary to that of α.

3.2.1.2 Modulational instability of a single mode

In the previous chapter, we detected regions of positive PQ, depending on the value of α and σ_n. In general, the instability is a purely growing mode for $Q/P > 0$, which is materialized by the MI growth rate. In Fig. 15, where the growth rate is represented versus the perturbation wavenumber K, we have for example consider the case where there are two regions, i.e., $k < k_{cr,1}$ and $k > k_{cr,2}$, respectively. In the first case, Γ is

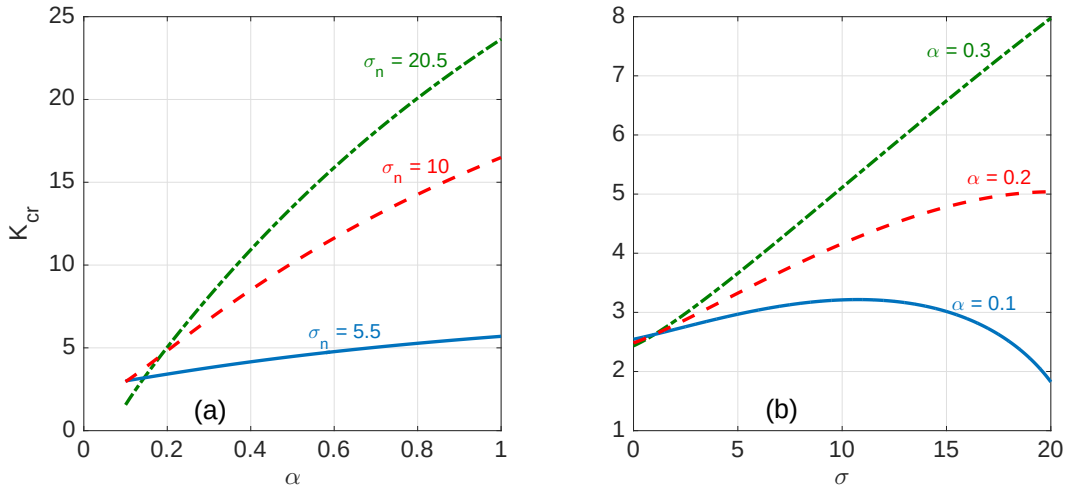

Figure 16: Panels show the critical wavenumber K_c versus (a) the negative ion concentration ratio, α, and (b) the electro-to-negative ion temperature ratio, σ_n. In each of the case one respectively changes σ_n and α, with $k = 0.2$ and $\psi_0 = 0.2$.

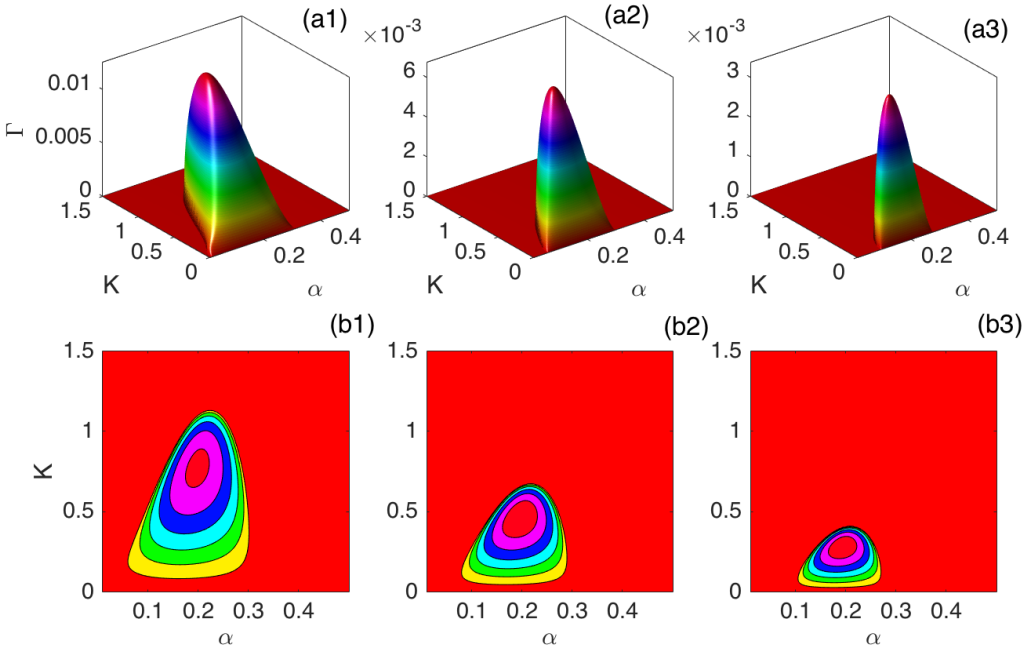

Figure 17: The GR of MI is plotted versus the wavenumber K and the negative ion concentration ratio. The small $k-$regime has been considered and different values of the initial wavenumber are taken to be: (a1)-(b1) $k = 0.1$, (a2)-(b2) $k = 0.15$ and (a3)-(b3) $k = 0.2$, with $\sigma_n = 17.5$ and $\psi_0 = 0.2$.

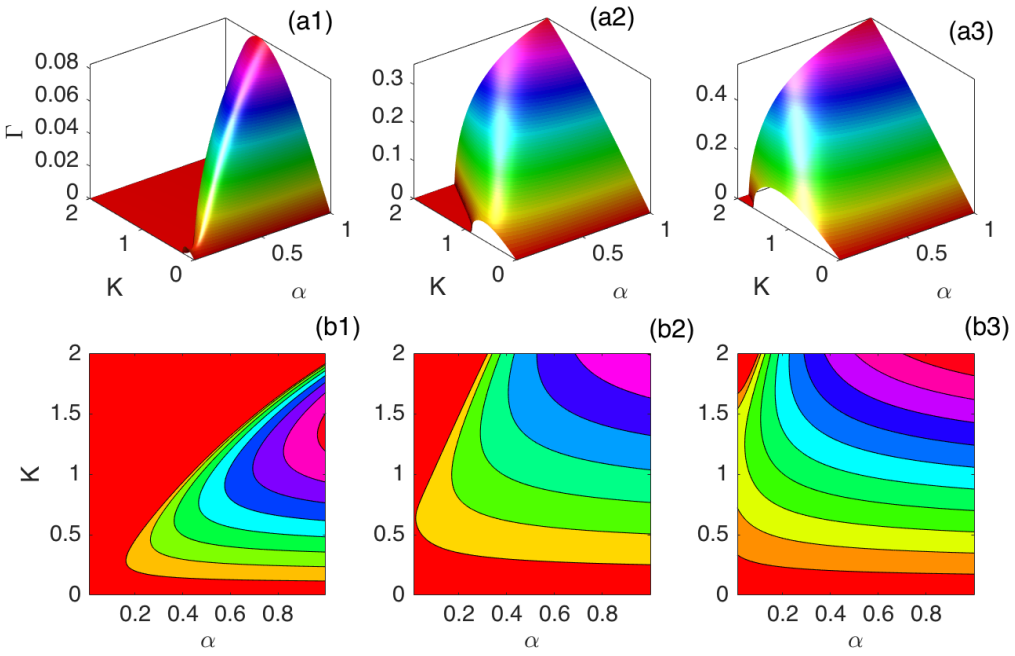

Figure 18: The GR of MI is plotted versus the wavenumber K and the negative ion concentration ratio. The high $k-$regime has been considered and different values of the initial wavenumber are taken to be: (a1)-(b1) $k = 1.2$, (a2)-(b2) $k = 1.25$ and (a3)-(b3) $k = 1.5$, with $\sigma_n = 17.5$ and $\psi_0 = 0.2$.

a decreasing function of k (see Fig. 15(a)), while in the second case, Γ increases with k. We should however stress that we have fixed the value of α to 0.2, which to some extend might not give all the information related to the onset of instability. In fact, two parameters, α and σ_n, are considered to have strong impact on the emergence of nonlinear patterns of the electric potential ϕ. This is also confirmed by the plots of Fig. 16, where the critical wavenumber $K_c = \psi_0\sqrt{|2Q/P|}$ is strongly modified by the negative ion parameters. In Fig. 16(a), K_c is plotted versus the negative ion concentration ratio α and its dependence on the electron-to-negative ion temperature ratio σ_n is illustrated. Inversely, in Fig. 16(b), K_c is shown versus σ_n and different values of α are used. It then appears that K_c is an increasing function of both α and σ_n, and therefore may affect importantly the instability growth rate Γ, along with the formation of modulated IAWs. It might then be of importance to study the behaviors of such parameters when one considers small and high regions of the unperturbed wavenumber k. In Fig. 17, for example, we have plotted the growth rate versus K and α (Figs. 17(aj)$_{j=1,2,3}$), and its corresponding stability/instability diagrams (Figs. 17(bj)$_{j=1,2,3}$), for different values of $k < k_{cr,1}$. The features of MI are described by a breast of instability, which gets reduced with increasing k. On the other side, in Fig. 18, the same calculations are performed for $k > k_{cr,2}$, and Γ is an increasing function of k. The results of Figs. 17 and 18 therefore confirm our prediction from Fig. 15. Beyond the effects of the unperturbed wavenumber k, one may also notice that for $k < k_{cr,1}$, only values of α between 0.1 and 0.3 are

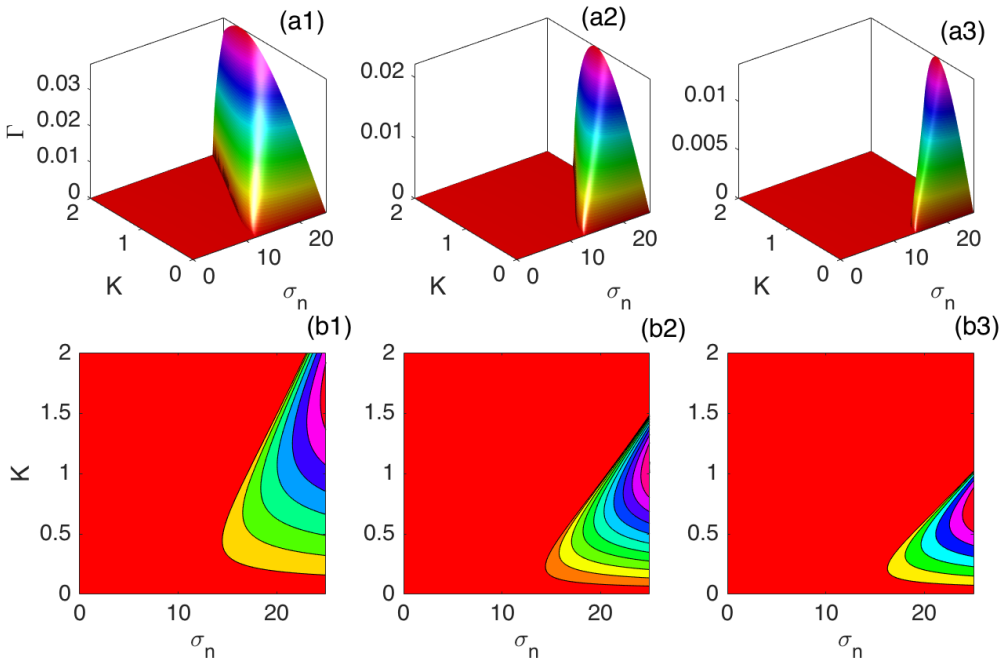

Figure 19: Growth rate of MI is plotted versus the wavenumber K and the electron-to-negative ion temperature ratio σ_n. The case $k < k_{1,cr}$ has been considered and different values of the initial wavenumber are taken to be: (a1)-(b1) $k = 0.1$, (a2)-(b2) $k = 0.15$ and (a3)-(b3) $k = 0.2$, with $\alpha_n = 0.3$ and $\psi_0 = 0.2$.

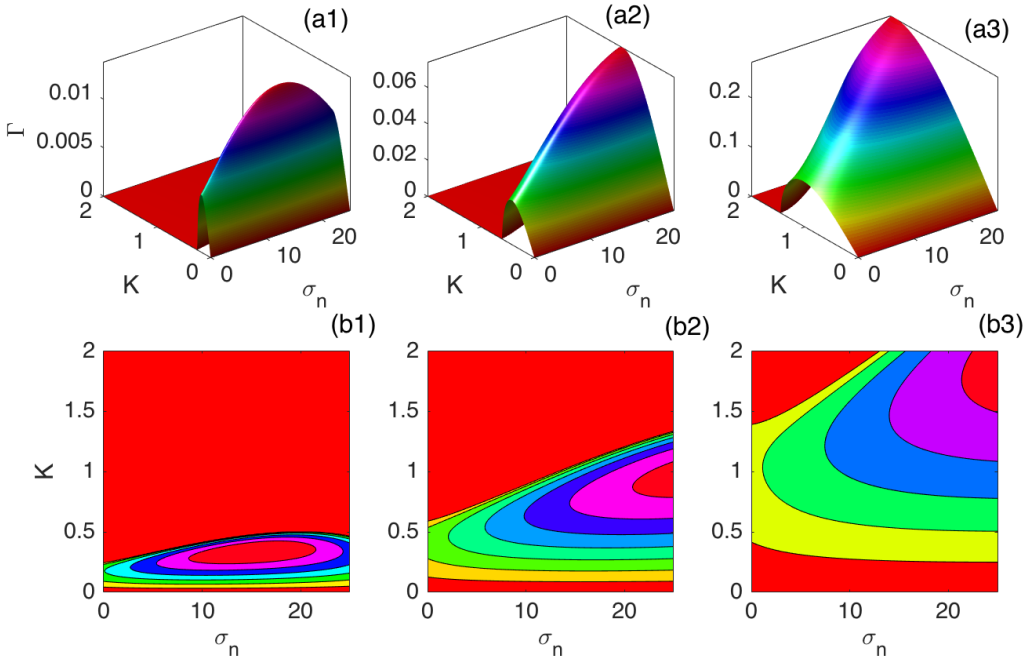

Figure 20: Grow rate of MI is plotted versus the wavenumber K and the electron-to-negative ion temperature ratio. The case $k > k_{2,cr}$ has been considered and different values of the initial wavenumber are taken to be: (a1)-(b1) $k = 1.2$, (a2)-(b2) $k = 1.25$ and (a3)-(b3) $k = 1.5$, with $\alpha = 0.3$ and $\psi_0 = 0.2$.

supposed to give rise to localized structures. Intervals for K also get reduced and for $k = 0.2$, the instability region is well inside small K and small α (see Fig. 17(b3)). The contrary is observed in Fig. 18, where high values of both α and K are expected to give rise to trains of modulated waves. To complete our analysis, we have also plotted the MI growth rate versus the ratio σ_n, still for the two different intervals of positive PQ. For $k < k_{1,cr}$, results are summarized in Fig. 19, where unstable wave patterns are expected for values of σ_n higher than 15. However, with increasing k in that interval, the instability region gets reduced as previously. Interestingly, the region of instability gets expanded with increasing k within the interval $k > k_{cr,2}$. Here, unstable wave patterns are expected for all σ_n, but the corresponding interval of K gets expanded with increasing k as shown in Fig. 20. To be more explicit, the two regions of k display different behaviors and the increase, or decrease, of the growth rate Γ, both in the $(K, \alpha)-$ and $(K, \sigma_n)-$planes is strongly affected by the wavenumber k. This also gives an idea on the concentration of negative ions that may leads to the formation of modulated IAWs under the activation of MI. In, the process, the nonlinearity of the plasma system is importantly modified, and this conditions the formation and emergence of any kind of envelope trains of wave, given that parameters are picked from regions of instability, while the initial plane wave may propagate unperturbedly where such regions disappear.

3.2.2 Coupled mode analysis

3.2.2.1 Stability of plane wave solutions

In order to study the emergence of nonlinear IAWs in system Eqs.(117) via the activation of MI, we consider its plane wave solutions in the forms $N = a_0 e^{j\Omega_n \tau}$ and $N' = a'_0 e^{j\Omega'_n \tau}$, given that the real amplitudes a_0 and a'_0, and the frequencies Ω_n and Ω'_n satisfy the linear dispersion relation $\Omega_n = \Omega'_n = \mu_2 a_0^2 + \mu_3 a'^2_0$. Small perturbations, $\delta a(\xi, \tau)$ and $\delta a'(\xi, \tau)$, around the above unperturbed states can be introduced so that $N = (a_0 + \delta a)e^{j\Omega_n \tau}$ and $N' = (a'_0 + \delta a')e^{j\Omega_n \tau}$, leading to the linearized equations

$$\begin{aligned} j\frac{\partial \delta a}{\partial \tau} + \mu_1 \frac{\partial^2 \delta a}{\partial \xi^2} + \mu_2 a_0^2(\delta a + \delta a^*) + \mu_3 a_0 a'_0(\delta a' + \delta a'^*) = 0, \\ j\frac{\partial \delta a'}{\partial \tau} + \mu'_1 \frac{\partial^2 \delta a'}{\partial \xi^2} + \mu_2 a'^2_0(\delta a' + \delta a'^*) + \mu_3 a'_0 a_0(\delta a + \delta a^*) = 0. \end{aligned} \tag{153}$$

Moreover, assuming solutions for Eqs. (153) to be $\delta a = U e^{j(K\xi - \Omega\tau)} + V e^{-j(K\xi - \Omega^*\tau)}$ and $\delta a' = U' e^{j(K\xi - \Omega\tau)} + V' e^{-j(K\xi - \Omega^*\tau)}$, where K and Ω are respectively the wave number and an arbitrary frequency of the perturbation, we find the following homogeneous system

of equations for U, V, U' and V':

$$\begin{pmatrix} M_{11}+\Omega & M_{12} & M_{13} & M_{13} \\ M_{12} & M_{11}-\Omega & M_{13} & M_{13} \\ M_{13} & M_{13} & M_{11}+\Omega & M_{12} \\ M_{13} & M_{13} & M_{12} & M_{11}-\Omega \end{pmatrix} \begin{pmatrix} U \\ V \\ U' \\ V' \end{pmatrix} = \begin{pmatrix} 0 \\ 0 \\ 0 \\ 0 \end{pmatrix}, \tag{154}$$

with the matrix elements being $M_{11} = \mu_2 a_0^2 - \mu_1 K^2, M_{12} = \mu_2 a_0^2$ and $M_{13} = \mu_3 a_0^2$. Eqs. (154) will admit non-trivial solutions if its determinant is zero, which leads to the nonlinear dispersion relation

$$\Omega^4 - A\Omega^2 + B = 0, \tag{155}$$

with

$$A = 2(\mu_2 a_0^2 - \mu_1 K^2)^2 + 2\mu_3^2 a_0^4 \Omega^4 - A\Omega^2 = 0, \tag{156a}$$

and

$$B = (\mu_2 a_0^2 - \mu_1 K^2)^4 + 2\mu_3^2 a_0^4 \left(\mu_2^2 a_0^4 - (\mu_2 a_0^2 - \mu_1 K^2)^2\right). \tag{156b}$$

The plane waves, solutions of system (117), will then be stable if

$$A > 0, \quad B > 0, \text{ and } \Delta = A^2 - 4B > 0. \tag{157}$$

In order to verify the above conditions, we have plotted in Fig. 21 the parameters A, B and Δ versus the perturbation wavenumber K. For the whole analysis, we have fixed $\alpha = 0.3$ and considered $\sigma_n = 16$ for Fig. 21(aj)$_{j=1,2,3}$ and $\sigma_n = 22$ for Fig. 21(bj)$_{j=1,2,3}$. Obviously, in all the cases, the parameter A and the discriminant Δ are exclusively positive. The stability of the plane wave solutions just depends on the sign of the parameter B, which for some values of plasma parameters and the wavenumber k presents both negative and positive intervals. To remind, solutions for Eq. (155) are in general given by

$$\Omega_{\pm}^2 = \frac{1}{2}\left(A \pm \sqrt{A^2 - 4B}\right). \tag{158}$$

We note in Fig. 21(a) and Fig. 21(c) that the conditions $A \geq 0$ and $\Delta \geq 0$ are systematically verified and therefore, the stability of the wave depends only on the sign of B. In fact, if $B < 0$, the solutions Ω_+ of Eq. (155) are reals, while solutions Ω_- are complex. In this second case, the gain of instability is determined by the absolute value of the imaginary part of Ω_-^2 as followed:

$$\Gamma = \text{Imag}\left\{\left|\sqrt{\Omega_-^2}\right|\right\}. \tag{159}$$

Moreover, the equation $B = 0$ has two non-zero solutions in perturbation wavenumber values K, that we can name K_{cr1} and K_{cr2}. Consequently, we can predict the waves to be unstable for K being in the regions $K_{cr1} < K < K_{cr2}$. To confirm this observation,

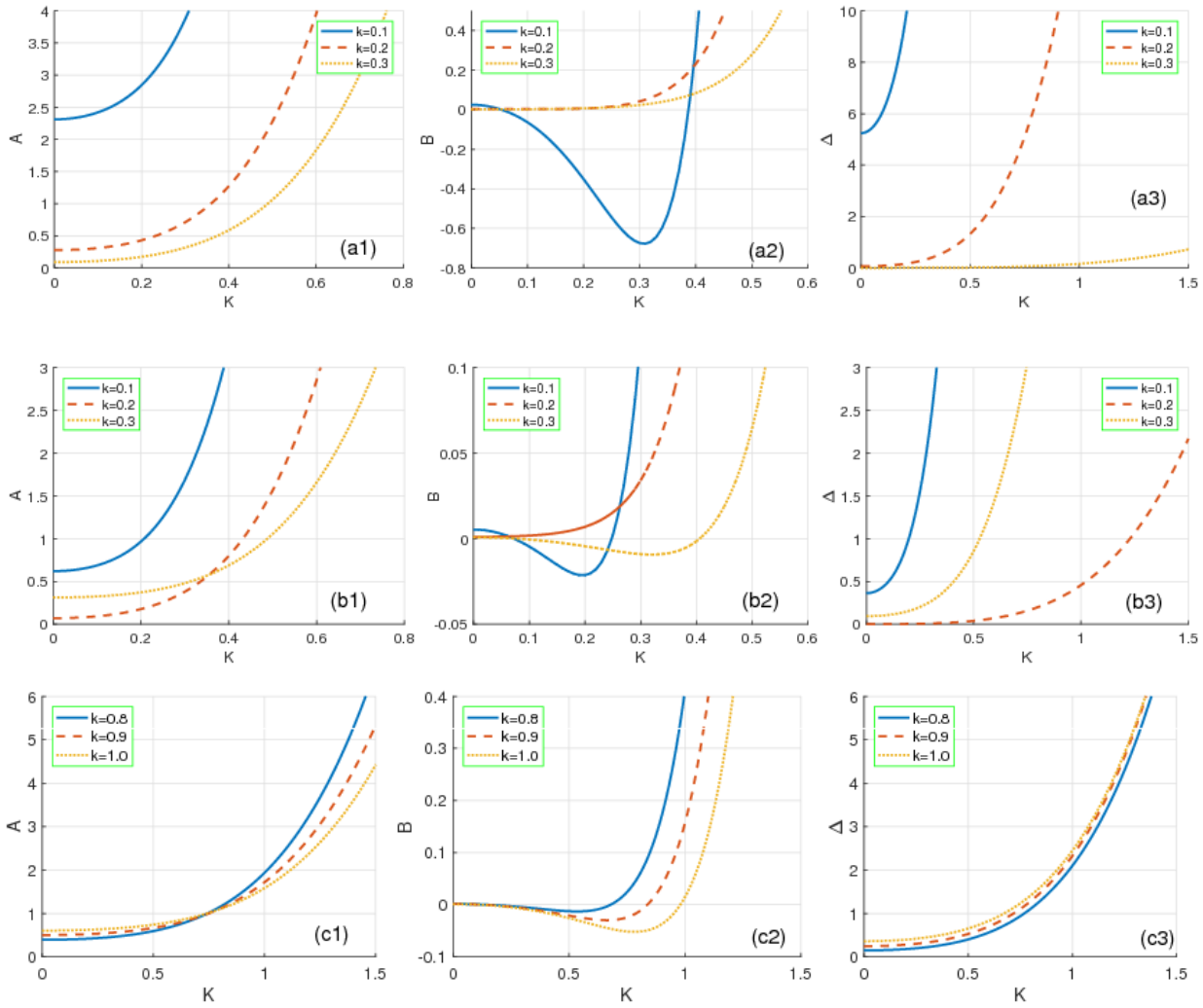

Figure 21: Panels show plots of the parameters A and B of Eqs. (156a), (156b) and the discriminant $\Delta = A^2 - 4B$, versus the perturbation wavenumber K. For panels $(\text{aj})_{j=1,2,3}$ and $(\text{bj})_{j=1,2,3}$, the wavenumber k takes the values 0.1,0.2 and 0.3. For the upper panels, $\sigma_n = 16$, while for panels $(\text{bj})_{j=1,2,3}$, $\sigma_n = 22$. Panels $(\text{cj})_{j=1,2,3}$ are plotted for different k with values 0.8, 0.9 and 1, with $\sigma_n = 16$. All the curves are obtained for $\alpha = 0.3$ and $a_0 = a_0' = 0.05$.

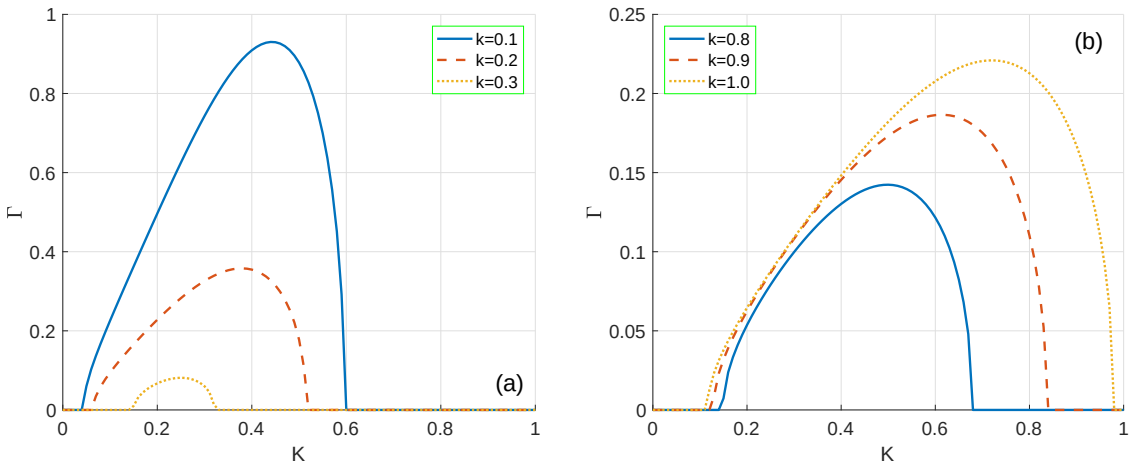

Figure 22: Instability growth rate Γ versus the perturbation wavenumber K. Panel (a) shows the instability intervals of K for small values of k and corresponds to the stability/instability features discussed in Fig. 21(bj)$_{j=1,2,3}$, while panel (b) displays the growth rate of instability for big K, and corresponds to the results of Fig. 21(cj)$_{j=1,2,3}$.

we plot in Figs. 22, the instability growth rate Γ as a function of K and for different values of k. We note the existence of a critical value of the main wavenumber k that we call here k_{cr}. Thus, for $k < k_{cr}$, Γ is a decreasing function of k , whereas, for $k > k_{cr}$, Γ increases with k as shown respectively in Fig. 22(a) and Fig. (22b). These observations are nonetheless valid only for the fixed values of plasma electronegative parameters such as $\alpha = 0.5$ and $\sigma_n = 15$. The impact of these two parameters on the stability can be demonstrated by making a 3D representation of the instability growth rate, taking into account the regions of small and large values of k, that were detected previously. In Figs. 23 for example, we have represented the growth rate Γ and the corresponding densitiy plots, for $k < k_{cr}$ and identified two zones of instabilities where amplitudes decrease when k increases. Although this conclusion confirms the decrease of the growth rate amplitude as k increases, the existence of two regions of instabilities, in this case, could not be predicted by the observations in Fig. (22). On the other hand, in Fig. (23), for $k > k_{cr}$, the instability growth rate, is described by a breast of instability, as in the case of the propagation of a single wave. In this case, the increase of k decreases the growth rate of the instability, thus confirming the predictions of Fig. 22. The study of the σ_n effect allowed us to complete our analysis. In Fig. 24(aj)$_{j=1,2,3}$, we have represented Γ as a function of σ_n and K, for $k < k_{cr}$. We observe one zones of instability where amplitude decreases with k. while that of the other increases as k increases. In Fig. 24(bj)$_{j=1,2,3}$, where we represent Γ for three values of $k > k_{cr}$, we notice the existence of two regions of instability. In this case, the first zone of instability disappears progressively, while the second zone expands as k increases.

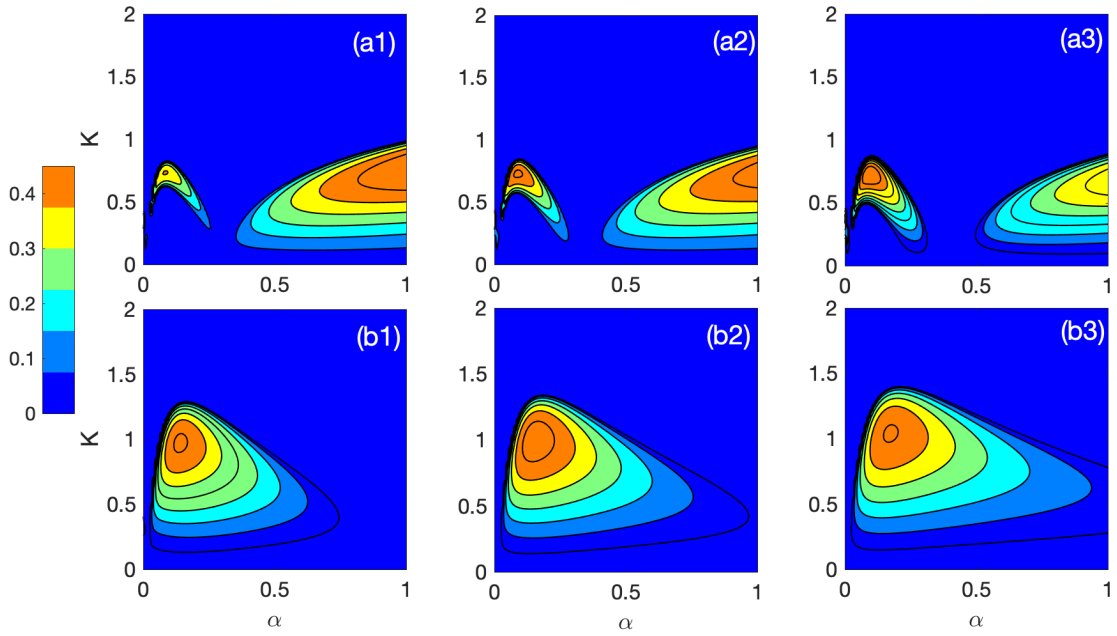

Figure 23: MI growth rate is represented in the $(\alpha, K)-$plane in agreement with the predictions in Fig. 22. Panels $(\mathrm{aj})_{j=1,2,3}$ display results for $k = 0.1$, $k = 0.2$ and $k = 0.3$, while panels $(\mathrm{bj})_{j=1,2,3}$ show the stability/instability features for $k = 0.8$, $k = 0.9$ and $k = 1.0$, with $\sigma_n = 17$ and $a_0 = a_0' = 0.05$.

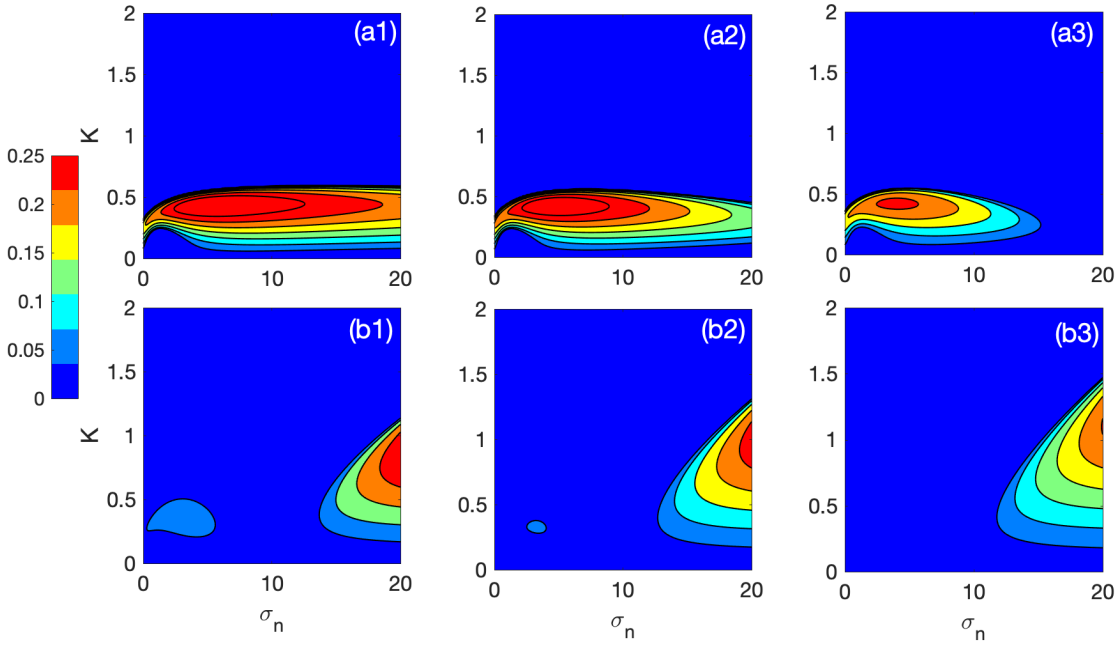

Figure 24: MI growth rate is represented in the $(\sigma_n, K)-$plane in agreement with the predictions in Fig. 22. Panels $(\mathrm{aj})_{j=1,2,3}$ display results for $k = 0.1$, $k = 0.2$ and $k = 0.3$, while panels $(\mathrm{bj})_{j=1,2,3}$ show the stability/instability features for $k = 0.8$, $k = 0.9$ and $k = 1.0$, with $\alpha = 0.1$ and $a_0 = a_0' = 0.05$.

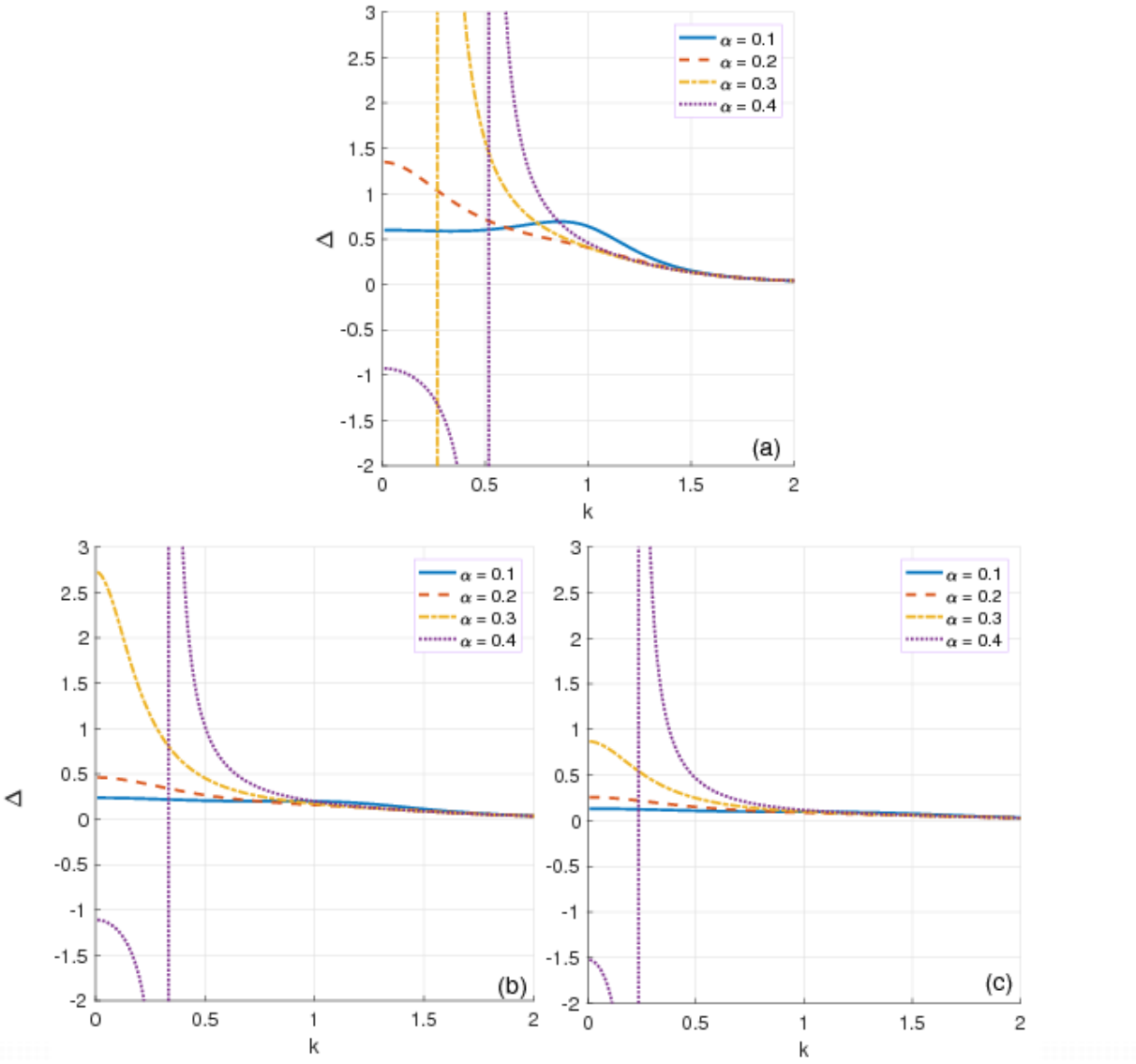

Figure 25: Panels show plots of the quantity $\Delta = \frac{\mu_1\mu_2 - \mu_1\mu_3}{\mu_2^2 - \mu_3^2}$ versus the wavenumber k. Each panel contains results for different values of the negative ion concentration ratio α, and panel (a) corresponds to $\sigma_n = 12$, panel (b) corresponds to $\sigma_n = 17$ and $\sigma_n = 22$.

3.2.2.2 Coupled mode solutions

In the case of coupled solutions, the two components N and N' are considered to be different from zero. However, the type of solution will depend on the sign of the coefficient

$$\Delta = \frac{\mu_1\mu_2 - \mu_1\mu_3}{\mu_2^2 - \mu_3^2} \tag{160}$$

so that when $\Delta > 0$, Eqs. (117) will admit bright envelope solutions. On the contrary, when $\Delta < 0$, dark-envelope solitons will be obtained as solutions. In doing so, we have represented Δ in Fig. 25, where each panel corresponds to a different value of the electron-to-negative ion temperature ratio σ_n, Solutions for individual equations

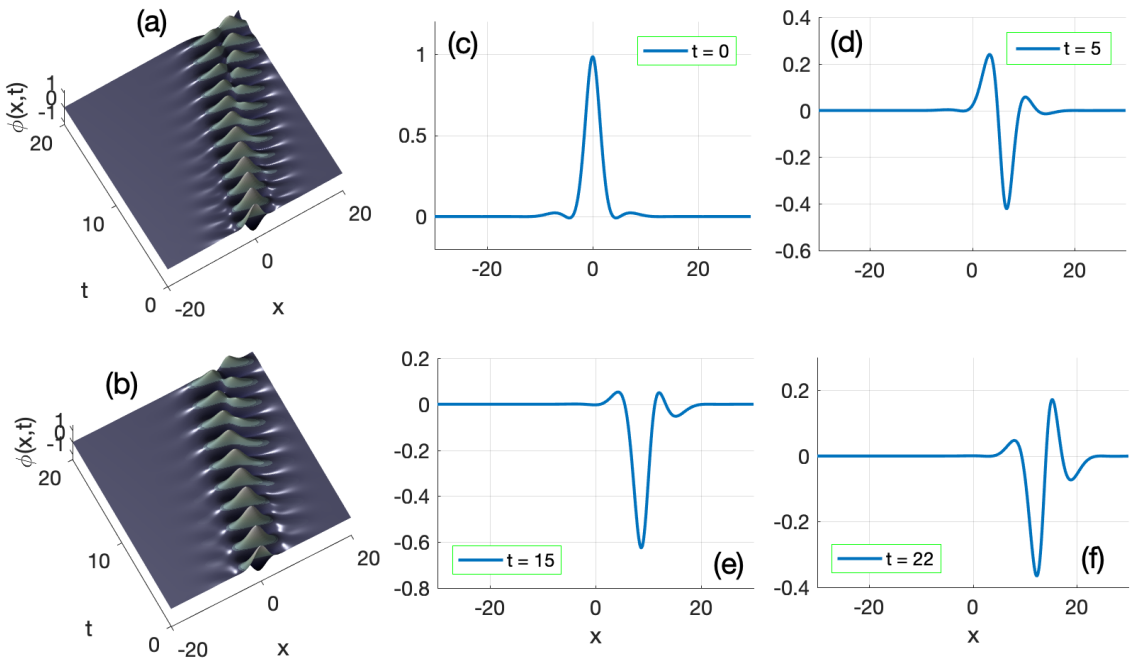

Figure 26: Panels show plots of the coupled solution (43). (a) and (b) show the spatiotemporal behaviors of the coupled soliton solution for the respective values $\alpha = 0.1$ and $\alpha = 0.2$ of the negative-ion concentration ratio. (c)-(d) display the time effect on the solution for $\alpha = 0.1$. All the calculations have been made using the parameter values $\sigma_n = 22$, $n_0 = n_0' = 0.8$, $K_1 = K_2 = 0.05$, $\epsilon = 0.02$, $k = 0.1$ and $k' = -k$.

Eqs. (117) are given by

$$N(\xi,\tau) = N_0 sech(n_0\xi + 2\mu_1 n_0 K_1 \tau) e^{j(K_1\xi - \Omega_1\tau)}, \tag{161a}$$

$$N'(\xi,\tau) = N_0' sech(n_0'\xi + 2\mu_1 n_0' K_2 \tau) e^{j(K_2\xi - \Omega_2\tau)} \times e^{-j\left(\frac{\lambda}{\epsilon}\xi + \frac{\lambda^2}{\mu_1}\tau\right)}, \tag{161b}$$

where

$$N_0^2 = \frac{2n_0^2\mu_1}{\mu_2+\mu_3}, \quad N_0'^2 = \frac{2n_0'^2\mu_1}{\mu_2+\mu_3}, \quad \Omega_1 = -\mu_1(n_0^2 - K_1^2), \quad \Omega_2 = -\mu_1(n_0'^2 - K_2^2), \quad K_2 = K_1.$$

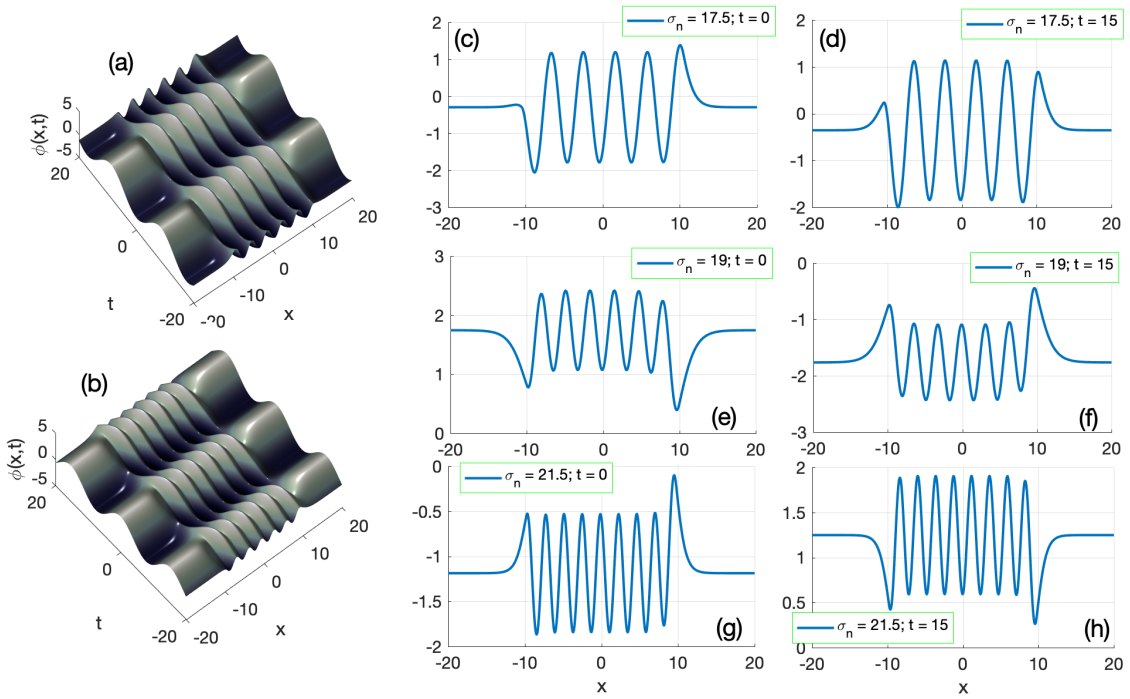

Figure 27: Panels (a) and (b) show the space-time plots of the coupled solution (45) for the respective values $\sigma_n = 17.5$ and $\sigma_n = 19$ of the electron-to-negative ions temperature ratio. Panels (c)-(d) display the time effect on the coupled solution for different cases of σ_n. The other parameter values have been taken as $\alpha = 0.33$, $n_0 = n_0' = 0.1$, $k = 0.02$, $k' = -k$, $\epsilon = 0.02$ and $K_1 = K_2 = 0.01$.

This leads to the coupled solution

$$\begin{aligned}\phi(x,t) = {} & \frac{2\epsilon N_0}{k^2 + a_1} sech(\epsilon n_0 x + \epsilon n_0(2\epsilon\mu_1 K_1 - \lambda)t) \\ & \times \cos\{(\epsilon K_1 - k)x + (\omega - \epsilon K_1 - \epsilon^2\Omega_1)t\} + \frac{2\epsilon N_0'}{k'^2 + a_1} sech(\epsilon n_0' x + \epsilon n_0'(2\epsilon\mu_1 K_2 - \lambda)t) \\ & \times \cos\left\{(\lambda + \epsilon K_2 - k')x + \left[\omega' - \lambda^2 + \epsilon\left(\frac{\epsilon\lambda^2}{\mu_1} - \lambda K_2 - \epsilon\Omega_2\right)\right]t\right\} + O(\epsilon^2).\end{aligned} \tag{162}$$

Plots of the above coupled solution are given in Fig. 26, where the effect of the negative-ion concentration ratio α has been considered. In the case $\Delta < 0$, solutions for system Eqs. (117) are such that

$$N(\xi,\tau) = N_0 \tanh(n_0\xi + 2\mu_1 n_0 K_1\tau)e^{j(K_1\xi - \Omega_1\tau)}, \tag{163a}$$

$$N'(\xi,\tau) = N_0' \tanh(n_0'\xi + 2\mu_1 n_0' K_2\tau)e^{j(K_2\xi - \Omega_2\tau)} \times e^{-j\left(\frac{\lambda}{\epsilon}\xi + \frac{\lambda^2}{\mu_1}\tau\right)}, \tag{163b}$$

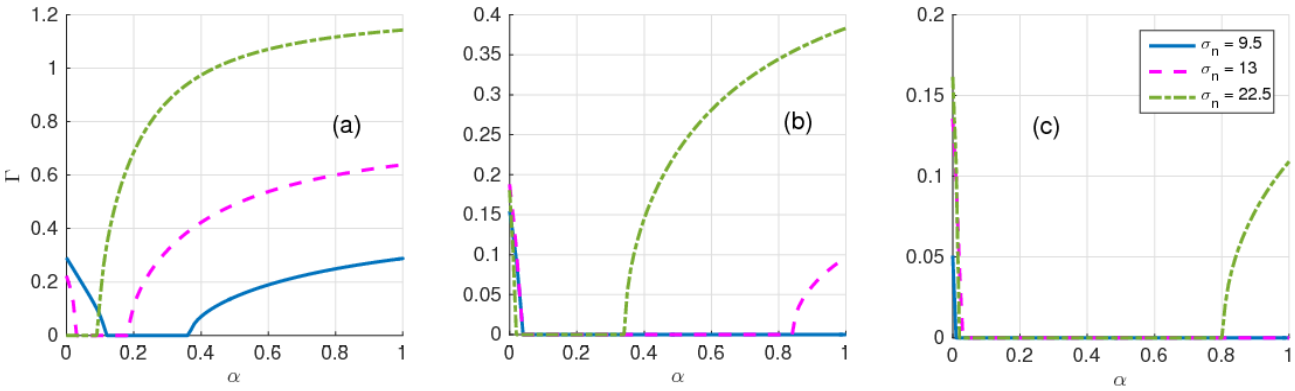

Figure 28: Instability growth rate versus α, the negative ion concentration ratio. Instability features are obtained for different values of σ_n. Panel (a) corresponds to $k = 0.8$, panels (b) and (c) to $k = 1.2$ and 1.5, respectively. The intervals of α that may lead to unstable IAWs are those corresponding to $\Gamma > 0$. The rest of parameter values are: $\alpha_1 = \alpha_2 = 1.8$, $F_0 = 0.25$, $G_0 = 0.03$ and $\mu_1 = \mu_2 = 1.25$.

with

$$N_0^2 = -\frac{2n_0^2\mu_1}{\mu_2+\mu_3}, \quad N_0'^2 = -\frac{2n_0'^2\mu_1}{\mu_2+\mu_3}, \quad \Omega_1 = -\mu_1(2n_0^2 + K_1^2) - \mu_3 N_0'^2,$$
$$\Omega_2 = \mu_1(2n_0'^2 + K_2^2) - \mu_3 N_0^2, \quad K_2 = K_1.$$

The general solution of the system from the above set of solutions is obtained in the form

$$\begin{aligned}\phi(x,t) = {} & \frac{2\epsilon N_0}{k^2+a_1}\tanh(\epsilon n_0 x + \epsilon n_0(2\epsilon\mu_1 K_1 - \lambda)t) \\ & \times \cos\{(\epsilon K_1 - k)x + (\omega - \epsilon K_1 - \epsilon^2\Omega_1)t\} + \frac{2\epsilon N_0'}{k'^2+a_1}\tanh(\epsilon n_0' x + \epsilon n_0'(2\epsilon\mu_1 K_2 - \lambda)t) \\ & \times \cos\left\{(\lambda + \epsilon K_2 - k')x + \left[\omega' - \lambda^2 + \epsilon\left(\frac{\epsilon\lambda^2}{\mu_1} - \lambda K_2 - \epsilon\Omega_2\right)\right]t\right\} + O(\epsilon^2).\end{aligned} \tag{164}$$

Fig. 26 exhibits the dependency of the coupled solutions on the electron-to-negative ions temperature ratio σ_n. This panels show that the frequency of the oscillating modes increases as σ_n becomes large.

3.3 Two-dimensional mode excitations

3.3.1 Modulational instability of the 2D mode

It was shown in Refs. [19, 138], it was shown that some values of α and σ_n do not support the formation of nonlinear waves in ENPs. In order to verify this for the rest of the calculations, we have first plotted the growth rate of MI versus the negative ion concentration ratio α, for different values of σ_n, with fixed perturbation wavenumbers μ_1 and μ_2. The growth rate plotted in Fig. 28 is given by $\Gamma = \sqrt{-\nu_1^2}$, and should be positive for instable patterns to emerge. Indeed, the results presented in Fig. 28 confirm the fact that not all the values of the plasma parameters will lead to solitonic structures in this plasma system. In the first case, for $k = 0.8$, there are clearly two regions where $\Gamma > 0$, with one belonging to the interval $\alpha < 0.16$ and the other appearing in the interval $\alpha > 0.38$. The second interval expands with increasing σ_n, while the first reduces and even becomes inexistent for high values the temperature ratio σ_n. Fixing $k = 1.2$, the same behavior persists, except that for $\sigma_n = 9.5$, only the interval of the small α appears, while the interval for high α latter appears when σ_n increases. One may also notice the behavior in Fig. 28(c) of Γ, where additional unstable regions appear for higher σ_n and $k = 1.5$. Using these intervals of α, we have illustrated some features of the instability spectrum in Fig. 29 in the $(\sigma_n, \mu_2)-$plane for α picked respectively from small and high regions of Fig. 28, for different values of k and $\mu_1 = 1.25$. Note that regions with contour lines indicate where unstable wave patterns are expected to emerge, while the plane wave is supposed to remain stable in the remaining blue regions. In Fig. 29 $(\text{aj})_{j=1,2,3}$, we have for example fixed $k = 0.8$, when α takes the respective values 0.01 (see Fig. 29(a1)), 0.015 (see Fig. 29(a2)) and 0.02 (see Fig. 29(a3)). Obviously, with increasing the negative ion concentration ratio, the region of instability gets more and more reduced and the highest value of the growth rate delocalizes. To plot Fig. $29(\text{bj})_{j=1,2,3}$, we have considered $k = 1.2$, α keeping the respective values as previously. Interestingly, the single region of instability observed here progressively splits into two regions with increasing α. Also, the left region of instability tends to disappear in favor of the right one, therefore leading almost to the case of Fig. 29(a1). The last case, i.e., Fig. $29(\text{cj})_{j=1,2,3}$, has been obtained for $k = 1.2$, but with α taking high values, i.e., 0.5 (see Fig. 29(c1)), 0.7 (see Fig. 29(c2)) and 0.8 (see Fig. 29(c3)). The features of instability are different in this case and the instability region delocalizes as α increases. Also, for the particular case of Fig. 29(c2), the region where IAWs are expected is quite large compared to the other two cases. We also confirm that the case of Fig. 29(c3) is included in Fig. 29(c2). To remind, when parameters are picked from regions of instability, nonlinear modulated IAWs are expected to evolve in the system. This is confirmed to be fully sensitive to the electronegative character of the plasma studied here, which implies that the criterion (124) gives more exotic behaviors of the instability of IAWs than the one-dimensional case, and particularly the case that does not specifically include the presence of negative ions among other species. Nevertheless, the linear stability analysis gives only information about regions of

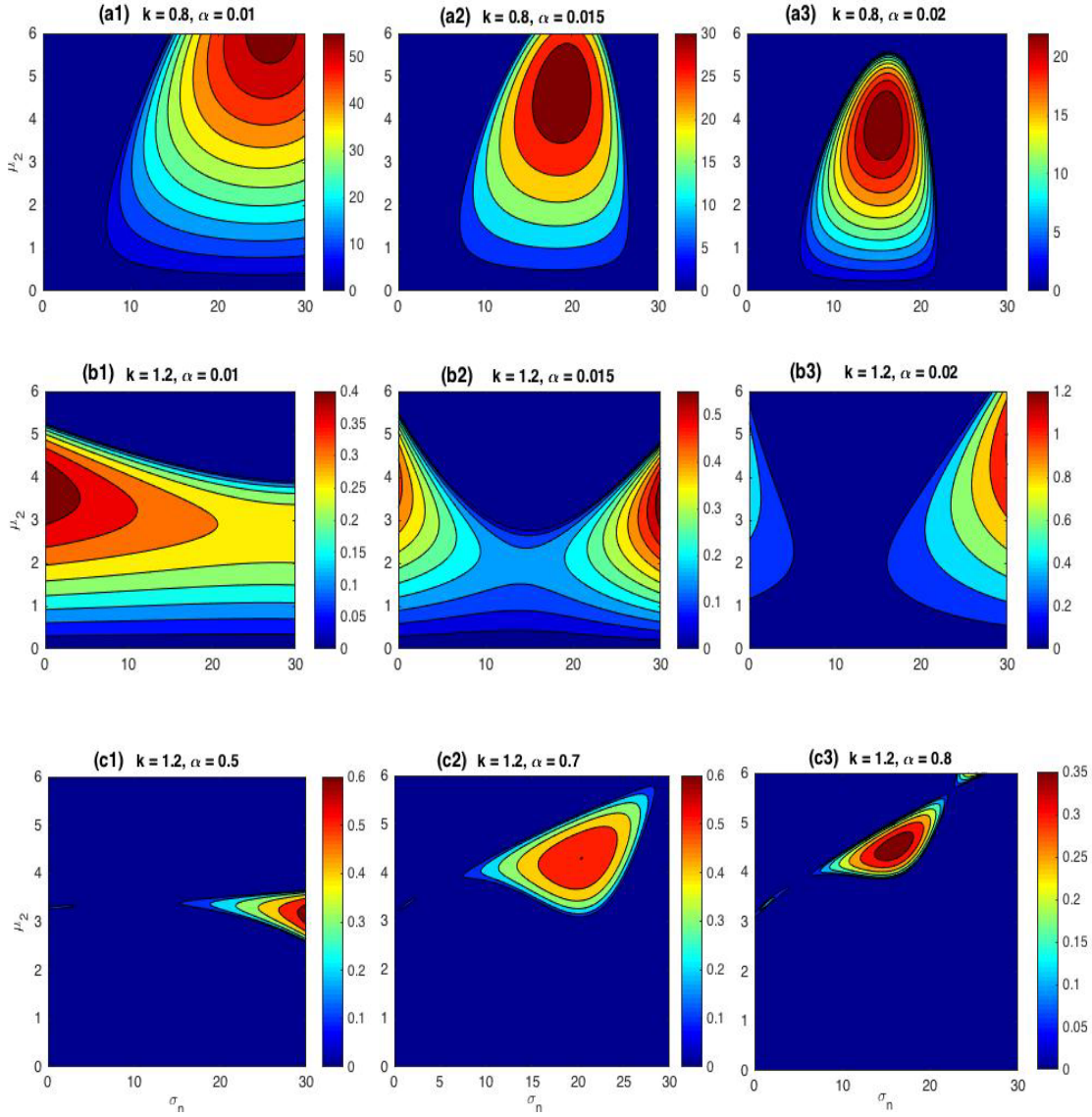

Figure 29: The instability growth rate is plotted in the $(\sigma_n, \mu_2)-$plane in agreement with the intervals of α found in Fig. 28. In panels $(\text{aj})_{j=1,2,3}$, we have fixed $k = 0.8$ and: (a1) $\alpha = 0.01$, (a2) $\alpha = 0.015$ and (a3) $\alpha = 0.02$. In panels $(\text{bj})_{j=1,2,3}$, we consider $k = 1.2$, while α takes the respective values as in panels (aj). Panels $(\text{bj})_{j=1,2,3}$ are plotted for $k = 1.2$, but α takes the respective values 0.5, 0.7 and 0.8, which corresponds to the respective panels (c1), (c2) and (c3). We have also fixed $\alpha_1 = \alpha_2 = 1.8$, $F_0 = 0.25$, $G_0 = 0.03$ and $\mu_1 = 1.25$.

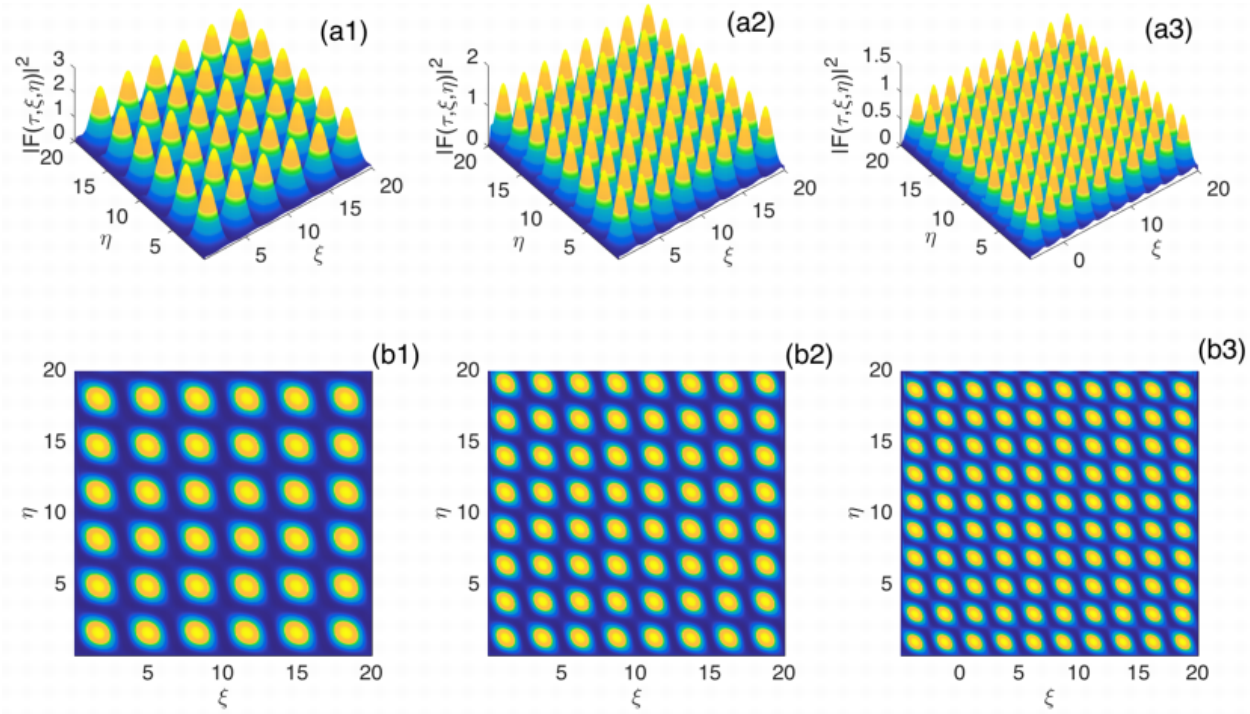

Figure 30: Panels show wave patterns due to MI in the DS model (31), using Eqs. (32) as initial conditions. Numerical solutions are obtained at time $\tau = 200$. Panels (a1)-(b1) have been plotted for $(\alpha = 0.01; \sigma_n = 12.5)$, panels (a2)-(b2) for $(\alpha = 0.02; \sigma_n = 12.5)$ and panels (a3)-(b3) $(\alpha = 0.9; \sigma_n = 22.5)$, with the other parameter values being: $\alpha_1 = \alpha_2 = 1.8$, $F_0 = 0.25$, $G_0 = 0.03$, $\mu_1 = \mu_2 = 1.25$ and $k = 1.2$.

parameters where the trains of waves and soliton-like structures may be expected. It does not say anything about the long-time evolution of the investigated waves. Appropriate numerical results, via direct numerical simulation of the DS Eqs. (120), using Eqs.(121) as initial conditions, are consequently depicted in Fig. 30. Parameters have mainly been picked from the theoretically predicted instability regions of Figs. 29, which confirms the accuracy of our stability analysis of the plane wave solution. We should stress that unstable regions of parameters are those where the plane wave solution breaks into solitonic trains as the result of the competition between nonlinearity and dispersion. Here obviously, we spontaneously get dromion-lattice structures, significant excitations that are localized in all directions of the plasma with constant period. Figs. 30(aj)$_{j=1,2,3}$ show the amplitude of $F(\tau, \xi, \eta)$ and Figs. 30(bj)$_{j=1,2,3}$ show their corresponding density plots at time $\tau = 200$. Most importantly, it is clearly visible that the frequency of the obtained patterns is very sensitive to the variation of the electronegative parameters α and σ_n. For the case of Figs. 30 (a1)-(b1) and (a2)-(b2), for example, we have respectively fixed $(\alpha = 0.02; \sigma_n = 12.5)$ and $(\alpha = 0.08; \sigma_n = 12.5)$. With increasing the value of α, leaving σ_n constant, there is an increase in the frequency of the dromion-lattices. This was already pointed out by El-Tantawy et al. [137] in the case of the breather solutions of the one-dimensional model. We should stress that values for α and σ_n, to illustrate these two cases, were picked from Fig. 29(a3). In Figs. 30(a3)-(b3), we have rather considered

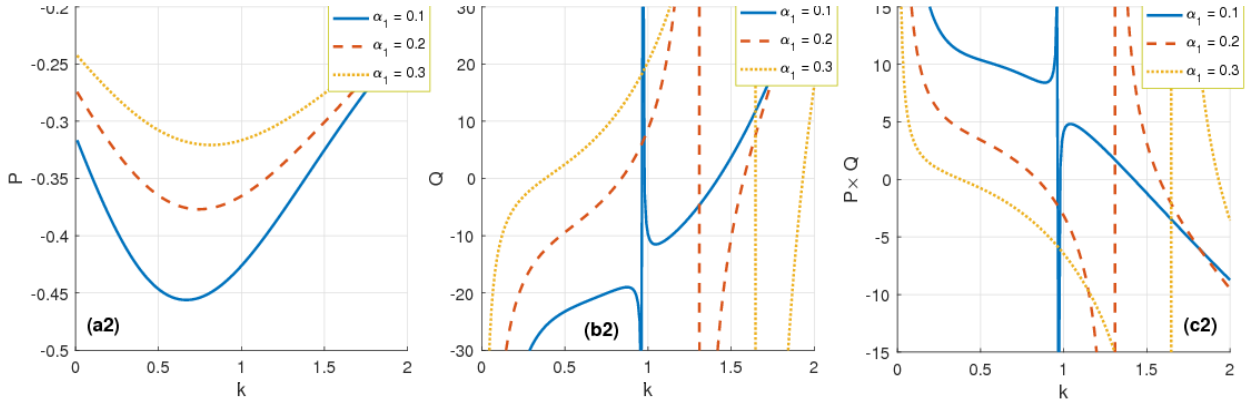

Figure 31: (a)γ_1/γ_2 is plotted versus the wave number k for $\sigma_n = 12.5$, with different values of α_n picked from the diagrams of Fig. 28. (b) γ_3 is plotted versus k under the same conditions, using the same values of parameters. For any $k > 0$, γ_1/γ_2 is positive, while γ_3 presents positive and negative regions.

the couple of parameters ($\alpha = 0.9; \sigma_n = 22.5$), which corresponds to the region of instability detected in Fig. 29(c2). For these regions, one notices a significant increase in the frequency of the dromions, which shows that α and σ_n cause the explosion of unstable wave patterns. Moreover, one might notice the decrease in the wave amplitude when α and σ_n increase. In the recent years, dromion solitons have been found to be exact solutions for the DS-I equation. The fact that they are obtained here under the activation of MI is a clear sign that when values of parameters are suitably chosen, the set of Eqs. (120) may adopt the DS-I equation comportment and exact dromion solutions may therefore be derived as proposed in the next section.

3.3.2 One- and two-dromion structures

The DS equations are divided into two types, the DS-I and DS-II equations, depending on the sign and values of parameters, and the physical systems studied [75, 140]. Here, obviously, from the previous section, one may obtain the two types of systems. However, the dromion soliton solutions obtained numerically in Figs. 30 are solutions of the DS-I system. It has been shown that the system of Eqs.(120) may display DS-I behaviors if the conditions [42]

$$\gamma_1/\gamma_2 > 0 \quad \text{and} \quad \gamma_3 > 0 \tag{165}$$

are satisfied. These might then be the necessary conditions to find dromion solutions. The regions of parameters where this is possible are displayed in Fig. 31, where γ_1/γ_2 and γ_3 are plotted versus the wavenumber k, for different values of the negative ion concentration ratio α. In Fig. 31(a), the first condition is exclusively fulfilled, given that γ_1/γ_2 is always positive for any $k > 0$. Obviously, the condition on γ_3 is the only one that influences the form of Eqs.(120) (see Fig. 31(b)). It should be noticed that the intervals of k, where $\gamma_3 > 0$, change with α and there, Eqs.(31) will take the DS-I form.

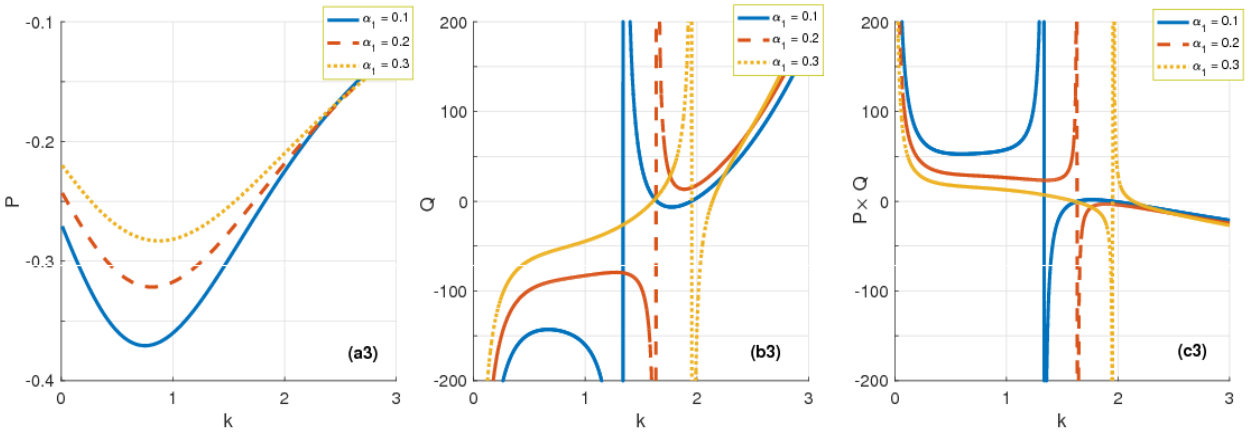

Figure 32: γ_3 is plotted versus the wavenumber k for $\sigma_n = 22.5$, with α taking different values as predicted in the diagrams of Fig. 28. For any $k > 0$, γ_3 presents positive and negative regions, which correspond to the DS-I domain.

Otherwise, when $\gamma_3 < 0$, Eqs.(120) will turn into the DS-II form. In the particular case of Fig. 31, the region where $\gamma_3 > 0$ gets expanded with increasing α. Here, we have fixed $\sigma_n = 12.5$. In order to complete this analysis, we have increased σ_n to 22.5 to plot γ_3 as given by Fig. 32. Contrarily to what is observed in Fig. 31, the region where $\gamma_3>0$ gets reduced when α increases. It i important to precise that together with the wavenumber k, the plasma parameters α and σ_n have been shown to importantly influence the occurence of MI and in turn, some of the regions where γ_3 is positive are those detected in the study of MI, principally in Fig. 28. Using this, finding solutions for Eqs.(30) might require the dependent and independent variables to be rescaled so that

$$Q = \gamma_3|F|^2 + \gamma_4 G, \quad \xi' = \frac{1}{\sqrt{\delta_1\gamma_3 + \delta_2\gamma_4}}\xi, \quad \eta' = \frac{1}{\sqrt{\gamma_3 - \delta_3\gamma_4}}\eta. \tag{166}$$

We also rotate the coordinate axes by 45 degrees and we introduce the following new independent variables

$$X = \frac{1}{\sqrt{2}}(\xi' + \eta'), \quad Y = \frac{1}{\sqrt{2}}(\xi' - \eta'). \tag{167}$$

Substituting the above into Eqs.(120) leads to the following idealized form of the DS-I system

$$iF_\tau + a(F_{XX} + F_{YY}) + bF_{XY} + FQ = 0, \tag{168a}$$

$$a'(Q_{XX} + Q_{YY}) + b'Q_{XY} + 2(|F|)^2_{XY} = 0, \tag{168b}$$

where a, a', b and b' are constants given by

$$\begin{aligned} a &= \frac{\gamma_1}{2(\delta_1\gamma_3 + \delta_2\gamma_4)} + \frac{\gamma_2}{2(\gamma_2 - \delta_3\gamma_4)}, \quad b = \frac{\gamma_1}{2(\delta_1\gamma_3 + \delta_2\gamma_4)} - \frac{\gamma_2}{2(\gamma_2 - \delta_3\gamma_4)}, \\ a' &= \frac{\delta_1}{2(\delta_1\gamma_3 + \delta_2\gamma_4)} - \frac{1}{2(\gamma_2 - \delta_3\gamma_4)}, \quad b' = \frac{\delta_1}{2(\delta_1\gamma_3 + \delta_2\gamma_4)} + \frac{1}{2(\gamma_2 - \delta_3\gamma_4)}. \end{aligned} \tag{169}$$

It is obvious that even after the different transformations, the above set of equations still depends on the plasma parameters, especially α and σ_n. In order to solve Eqs.(168), they can be transform into the bilinear forms

$$D_{XY} f.f = m\,(g \cdot g^*) \quad \text{and} \quad (iD_\tau + a(D_{XX} + D_{YY}) + bD_{XY})g \cdot f = 0, \tag{170}$$

through the variable transformation

$$F = \frac{g}{f} \quad \text{and} \quad Q = c(\ln f)_{XY}, \tag{171}$$

where the Hirota bilinear $D-$operator is defined by

$$D_x^n g \cdot f = (\partial_{x_1} - \partial_{x_2})^n f(x_1) g(x_2)|_{x_2 = x_1 = x}. \tag{172}$$

The functions f and g can be expanded in the form of power series as $f = 1 + \delta^2 f_2 + \delta^4 f_4$ and $g = \delta g_1 + \delta^3 g_3$, where δ is an arbitrary parameter. The different solutions are found by replacing f and g into Eq.(170) and collecting terms with the same power in δ. The remaining calculations are made to find g_1, g_3, f_2 and f_4. However, a general expression for g_1 is given by

$$g_1 = \sum_{j=1}^{N} \exp\theta_j, \quad \text{with} \quad \theta_j = k_j X + l_j Y - j\omega_j t + \alpha_j, \tag{173}$$

where k_j, l_j and α_j are complex constants. For the rest, the Hirota method as been presented in chapter two. The one- and two-dromion solutions have been proposed in [42]. In what follows, we exploit those results in order to discuss the features of such waves in ENPs.

3.3.2.1 The one-dromiom soliton

The generalized form of the one-soliton solution is given by

$$F_{1D} = \frac{g_{1D}}{f_{1D}} = \frac{\rho \exp(\theta_1 + \theta_2)}{1 + \alpha \exp(\theta_1 + \theta_1^*) + \beta \exp(\theta_2 + \theta_2^*) + \gamma \exp(\theta_1 + \theta_1^* + \theta_2 + \theta_2^*)}, \tag{174}$$

where $|\rho|^2 = (p_1 + p_1^*)(p_2 + p_2^*)(\gamma - \zeta\beta)$, $\theta_1 = p_1 X + \omega_1 t + \alpha_1$ and $\theta_2 = p_2 Y + \omega_2 t + \alpha_2$, with ζ, β, and γ being real positive constants, $\omega_1 = iap_1^2$ and $\omega_2 = iap_2^2$. It should be noticed that the relative sign of the real parts of p_1 and p_2 determines whether γ should be larger or smaller than $\zeta\beta$. Using suitable values of parameters, especially the couple (α, k), we obtain the one-dromion solition shown in Figs. 33(a)-(d), where upper panels display plots of the the dromion solution and the lower panels display their density plots. From solution (174), $\phi_1^{(1)}(X, Y, t) = (k^2 + a1)F_{1D}$ has been represented at different instants, and one clearly sees how its shape and amplitude are conserved. However, these

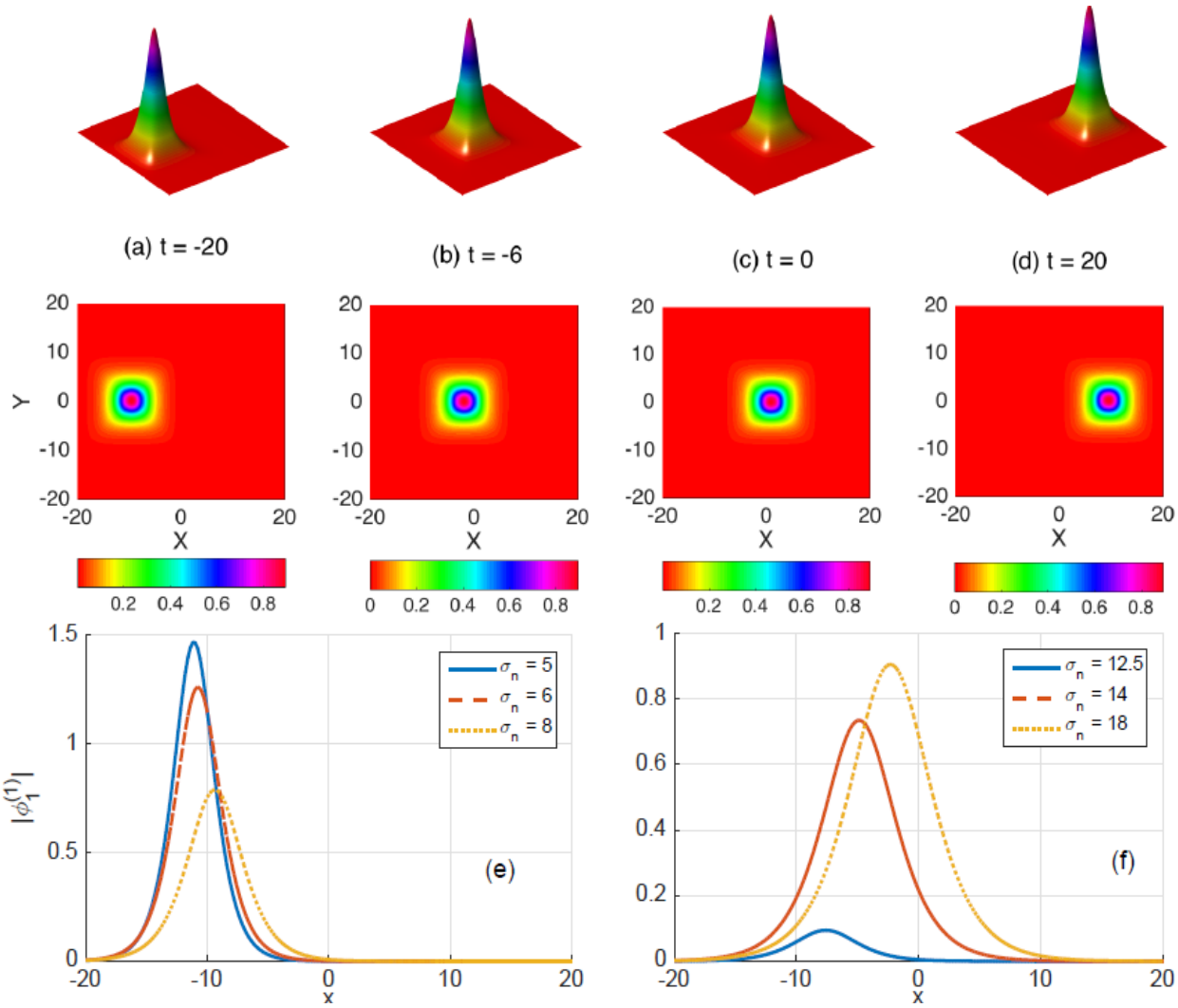

Figure 33: Panels (a)-(d)show the surface and corresponding density plots of the one-dromion solution (174) in the $(X, Y)-$space at different instants. (e) and (f) show the effect of the ENP parameters, α and σ_n, on the amplitude and width of the one-dromion solution. For (a)-(d) parameters are fixed as: $k = 0.15$, $\alpha = 0.2$ and $\sigma_n = 5.5$. For (e) and (f) we have used the values for α and k with changing σ_n.

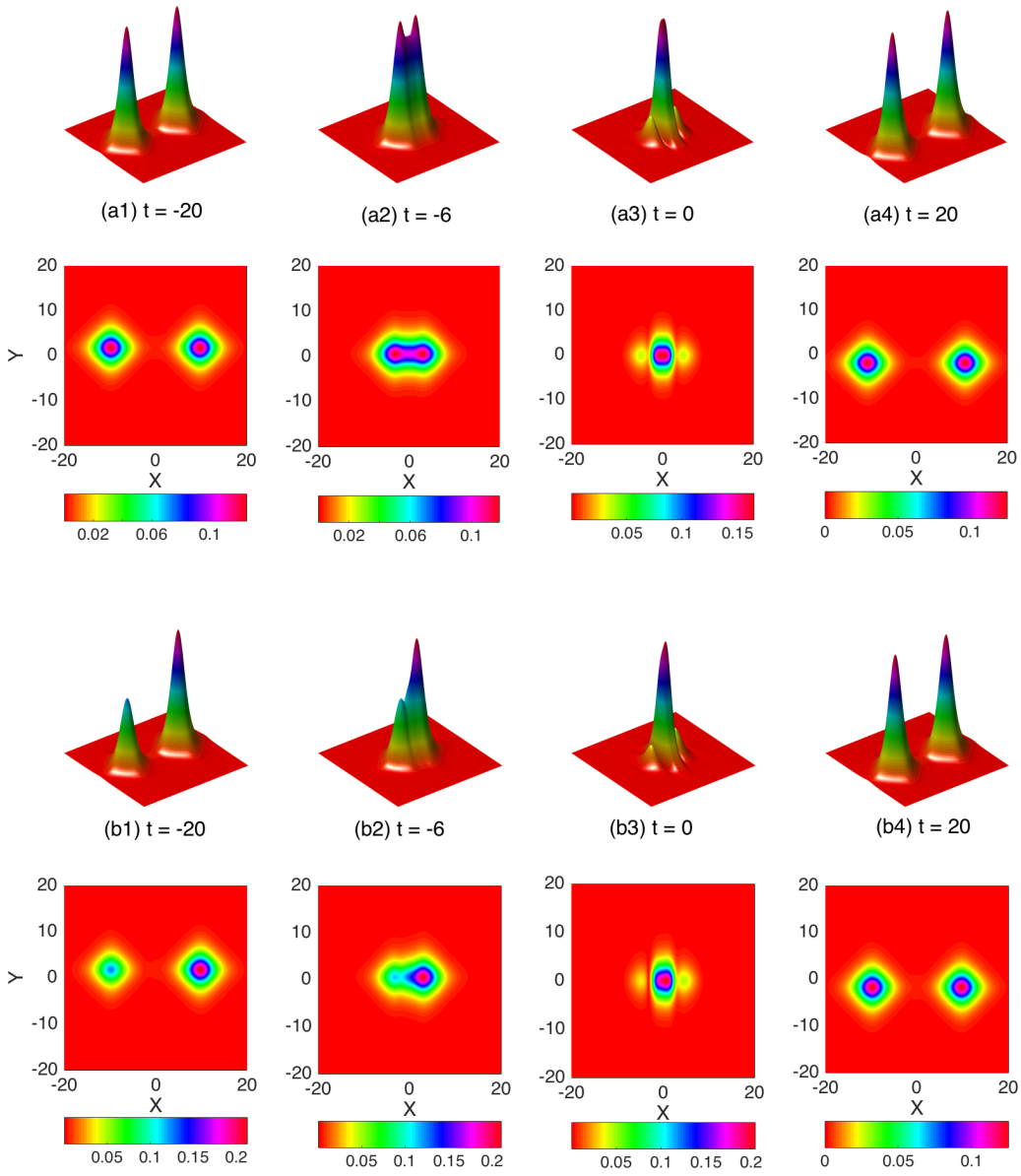

Figure 34: Panels show the elastic collision of the two-dromion solution (175) in the $(X, Y)-$space at different instants. In $(\mathrm{aj})_{j=1,2,3}$, two dromions of the same amplitude interact and keep their individual characteristics after collision. In panels $(\mathrm{bj})_{j=1,2,3}$, a small dromion and a highly localized one interact and there is an equipartition of energy after collision, leading to two identical waves, with the same characteristics. Parameters are $k = 0.15$, $\alpha = 0.2$ and $\sigma_n = 5.5$.

characteristics are sensitive to the plasma parameters as shown in Figs. 33 (e) and (f). We have fixed $\alpha = 0.25$ and, as a whole, for $\sigma_n < 10$, the amplitude is a decreasing function of σ_n as shown in Fig. 33(e). Contrarily, Fig. 33(f) shows that the amplitude of the dromion increases with $\sigma_n > 10$. Importantly, the width of the solution gets expanded when σ_n increases in both cases.

3.3.2.2 The two-dromion soliton

One can proceed in a similar way and find the two-dromion solution in the form

$$F_{2D} = \frac{\left\{\begin{array}{l} \rho_{11}\exp(\theta_1+\theta_3)+\rho_{12}\exp(\theta_2+\theta_3) \\ +\rho_{21}\exp(\theta_1+\theta_1^*+\theta_2+\theta_3)+\rho_{22}\exp(\theta_1+\theta_2+\theta_2^*+\theta_3)\end{array}\right\}}{\left\{\begin{array}{l} 1+A\exp(\theta_1+\theta_1^*)+B\exp(\theta_2+\theta_2^*)+C\exp(\theta_3+\theta_3^*)+D(\exp(\theta_1+\theta_2^*) \\ +\exp(\theta_2+\theta_1^*))+E(\exp(\theta_1+\theta_2^*+\theta_3+\theta_3^*)+(\exp(\theta_2+\theta_1^*+\theta_3+\theta_3^*)) \\ +F\exp(\theta_1+\theta_1^*+\theta_2+\theta_2^*)+G\exp(\theta_2+\theta_2^*+\theta_3+\theta_3^*) \\ +G\exp(\theta_1+\theta_1^*+\theta_3+\theta_3^*)+I\exp(\theta_1+\theta_1^*+\theta_2+\theta_2^*+\theta_3+\theta_3^*)\end{array}\right\}}, \tag{175}$$

where A, B, C, D, E, F, G, H, I are real positive constants. θ_1, θ_2 and θ_3 are assumed as $\theta_1 = p_1X + \omega_1 t + \beta_1$, $\theta_2 = p_2X + \omega_2 t + \beta_2$, $\theta_3 = p_3Y + \omega_3 t + \beta_3$, with the conditions $\omega_1 = iap_1^2$, $\omega_2 = iap_2^2$ and $\omega_3 = iap_3^2$. Commonly, solitonic structures undergo elastic and inelastic collisions where they exchange or share energy [108]. During elastic collisions the two waves conserve their respective characteristics before and after interacting as shown in Fig. 34(aj)$_{j=1,2,3,4}$ at different instants. Another scenario, which may arise during elastic collisions is energy equipartition. This is for example depicted in Fig. 34(bj)$_{j=1,2,3,4}$. When two dromions with different amplitudes and width interact, the one with the highest amplitude may transfer some energy to the small one, the whole process leading to two identical dromions of equal amplitude and width. In Fig. 35, a different spectrum of behaviors is obtained, where the two dromions initially having the same amplitude, interact and merge into one. This is not surprising, as the phenomenon of inelastic collision is inherent to multi-component plasmas, which may include electrons, positive and negative ions [96,154]. This is one of the main mechanism leading to the production of plasma particles, via energy recombination among the available dynamical modes [96, 154]. Experiments on plasmas have shown the existence of interacting solitons, as it was the case in a monolayer strongly coupled complex (dusty) plasma [119]. One may also notice the contribution by Mandal and Sharma [103, 104] who reported interacting solitons in the electron-acoustic regime of collisionless plasmas. Using a one-dimensional ENP model, interaction between positive and negative solitons was studied with emphasis on the coupled effects of α and σ_n [138]. However, in the latest context, dromion solutions have not been reported in the literature, including their response to strong concentration of negative ions and the subsequent plasma temperature.

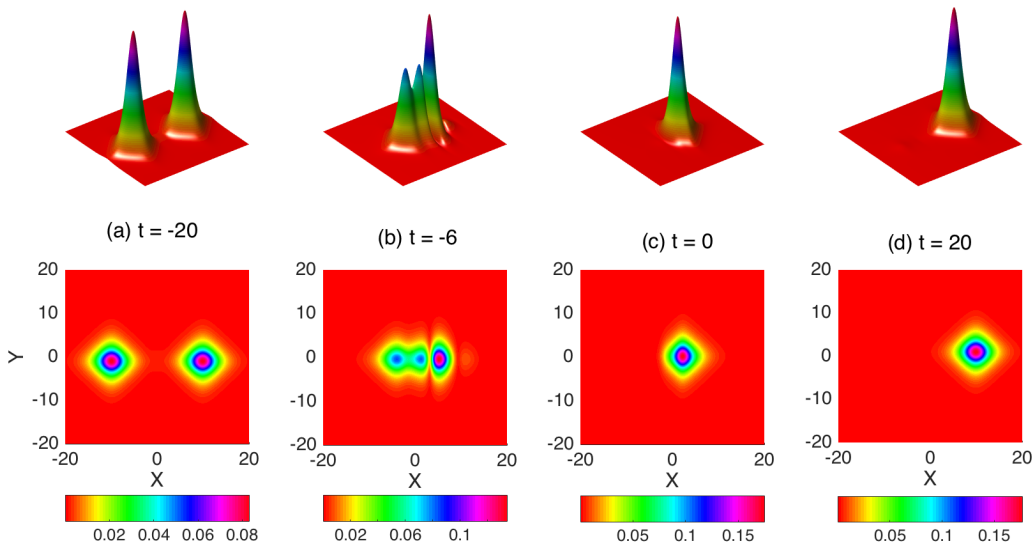

Figure 35: Panels show inelastic collision time frame of two identical dromions in the $(X, Y)-$space at different instants. After collision, the two waves merge into one, which carries the sum of the energies brought by each of the dromions. Parameters are: $k = 0.15$, $\alpha = 0.2$ and $\sigma_n = 5.5$.

3.4 Electronegative (3+1)-dimensional modulated excitations

Relying on the linear stability analysis performed in chapter 2 for (3+1)-dimensional DS-equations, there will be instability if the frequency Ω is complex, i.e., $\Omega^2 < 0$. According to expression (129), this mainly depends on the product $P \times Q$ and the value of the perturbation wavenumber which is such that $K < K_{cr} = F_0\sqrt{\frac{2Q}{P}}$. There will be instability if the frequency Ω is complex, i.e., $\Omega^2 < 0$. Although we obtain a result similar to the one in Ref. [35], we remark here that the instability condition depends of the angle θ which may lead to different instability scenarios as shown in Fig. 36, where $P \times Q$ is plotted versus the modulation angle θ, additionally to the effects of the plasma parameters. In Fig. 36(a), for example, $\sigma_n = 5.5$ and one observes two lateral regions of instability for $\alpha = 0.01$, especially in the intervals $0.1\pi \leq \theta \leq 0.23\pi$ and $0.75\pi \leq \theta \leq 0.88\pi$. However, with $\alpha = 0.08$ and 0.2, one observes a central region of instability which excludes the lateral ones observed previously. This later behavior persists for $\sigma_n = 16$ as the central instability interval of θ gets expanded when α increases (see Fig. 36(b)). More interestingly, lateral regions of instability appear once more for $\sigma_n = 22.5$, with $\alpha = 0.01$, in the intervals $0 < \theta \leq 0.22\pi$ and $0.78\pi \leq \theta \leq \pi$ (see Fig. 36(c)). With increasing α, the previous central region, where $P \times Q > 0$, appears again, and tends to expand. In general, MI is characterized by its growth rate given by

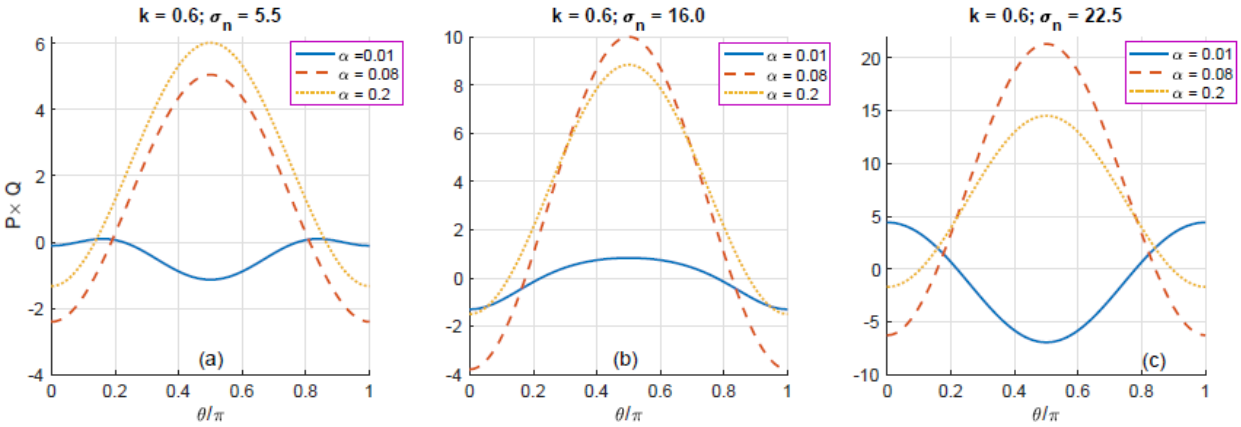

Figure 36: Panels show the plots of the product $P \times Q$ versus the modulation angle θ, under the influence of the plasma parameters σ_n and α. Each panel corresponds to a value of σ_n submitted to the increasing effect of α.

the expression

$$\Gamma = \sqrt{-\Omega^2} = |PK|\sqrt{2\frac{QF_0^2}{P} - K^2}. \tag{176}$$

Fig. 37 is a good illustration of the above growth rate of instability which has been plotted versus the perturbation wavenumber K and the electron-to-negative ion temperature ratio σ_n. We have in fact considered different values of the modulation angle θ to clearly illustrate what is discussed in Fig. 36. Panels $(\text{aj})_{j=1,2,3}$ have been plotted for $\theta = \pi/10$, a value that gives rise to instability domains. Especially, for $k = 0.70$, one notices the coexistence of two regions of instability, both for very small and high σ_n, that disappear with increasing θ as shown in Fig. 37(b3). For the rest, θ and k have the effect of reducing the instability domain expansion. Those regions are where modulated IAWs are expected, depending on the right choice of both the wave and plasma parameters. In what follows, depending on the value of θ, we address two main cases known as the parallel and the transverse modulations [35].

3.4.1 Parallel modulation

Parallel modulation is obtained for $\theta = 0$, which reduces the coefficients P and Q to the simplified expressions

$$P = \gamma_1 \quad \text{and} \quad Q = \gamma_3 + \frac{\gamma_4\delta_2}{\delta_1}. \tag{177}$$

Interestingly, the above two coefficients still depend of the wavenumber k as clearly depicted by Fig. 38 (a1) and (a2). In this case, the sign of P remains negative with changing the value of the electron-to-negative ion temperature ratio σ_n. However, due to the later, there are regions of k where the nonlinearity coefficient Q is positive or negative. This brings about some instability regions as shown in Fig. 38(a3), where

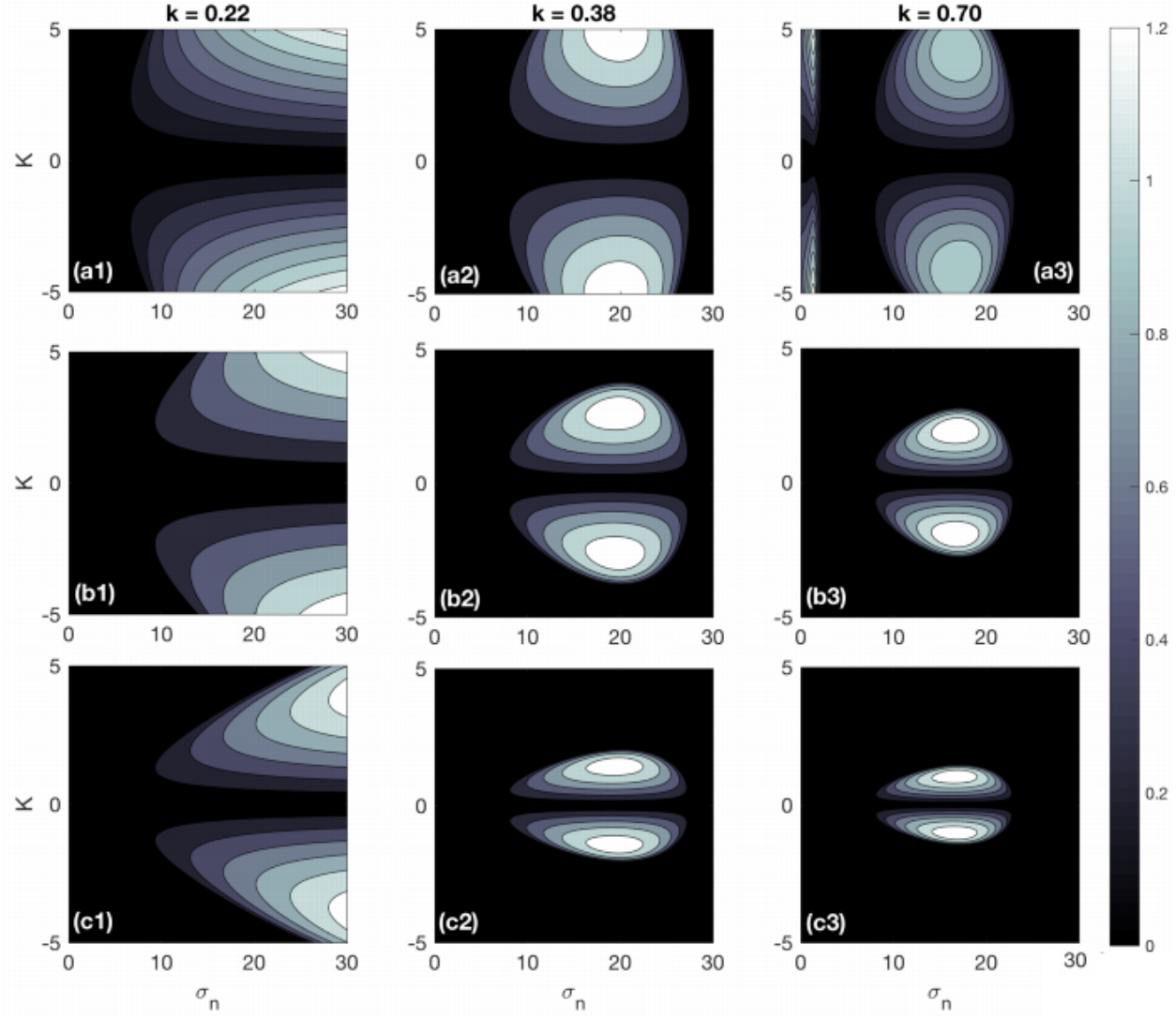

Figure 37: The growth rate of MI is plotted versus the wavenumber K and the electron-to-negative ion temperature ratio σ_n in the generalized case, i.e., $\theta \neq 0$. Panels $(\mathrm{aj})_{j=1,2,3}$ corresponds to to $\theta = \pi/10$, panels $(\mathrm{bj})_{j=1,2,3}$, gives results for $\theta = \pi/5$ and panels $(\mathrm{cj})_{j=1,2,3}$ have been recorded for $\theta = \pi/3$. The three columns correspond to different values of the wavenumber k, with $\alpha = 0.8$.

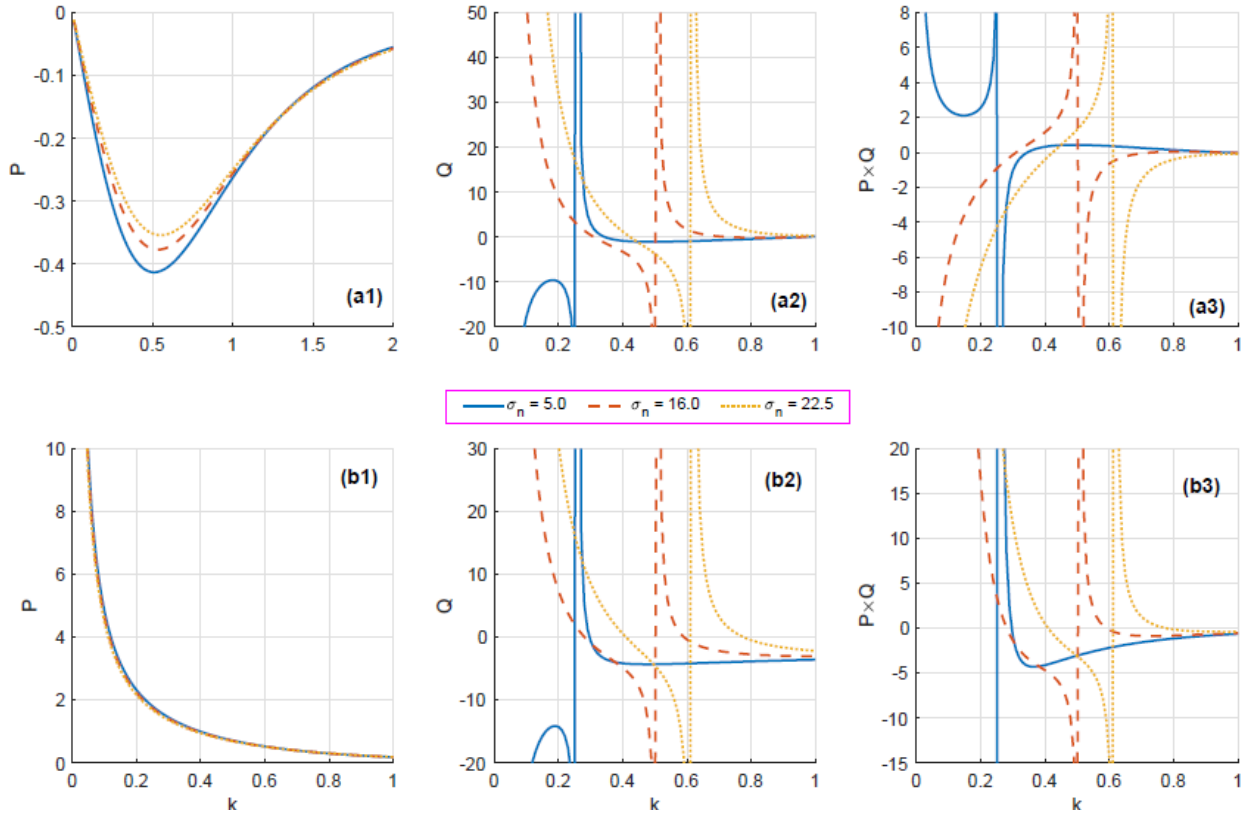

Figure 38: The dispersion coefficient P, the nonlinearity coefficient Q and the product $P \times Q$ are depicted versus the wavenumber k for different values of the electron-to-negative ion temperature ratio σ_n. Panels $(\mathrm{aj})_{j=1,2,3}$ correspond to the parallel modulation, i.e., $\theta = 0$, while panels $(\mathrm{bj})_{j=1,2,3}$ stand for the perpendicular modulation, i.e., $\theta = \pi/2$. The solid blue line corresponds to $\sigma_n = 5$, the dashed-red line corresponds to $\sigma_n = 16.0$ and the dotted-yellow line corresponds to $\sigma_n = 22.5$, with $\alpha = 0$.

we have plotted the product $P \times Q$. Specifically, for $\sigma_n = 5$, $P \times Q$ presents two positive regions, i.e., $0 < k < 0.25$ and $0.32 < k < 0.85$. For the rest, only one region of instability exists for $\sigma_n = 16$ and 22.5, which are respectively $0.3 < k < 0.5$ and $0.42 < k < 0.6$. Using these values of the wavenumber k, we have also plotted the MI growth rate in Fig. 39 versus the perturbation wavenumber K and σ_n. While the different panels $(\mathrm{aj})_{j=1,2,3}$ correspond to different values of the wavenumber k, they have been plotted when the negative ion concentration ratio takes the value $\alpha = 0.1$. There, regions of instability are detected and one sees how sensitive they are to the values of k. Along the same line, still considering the previous values of k, the MI growth rate has been plotted for $\alpha = 0.5$ and the corresponding results are recorded in Fig. $39(\mathrm{bj})_{j=1,2,3}$. Compared to the case in panels $(\mathrm{aj})_{j=1,2,3}$, regions of instability are restricted to small values of the electron-to-negative ion temperature ratio σ_n.

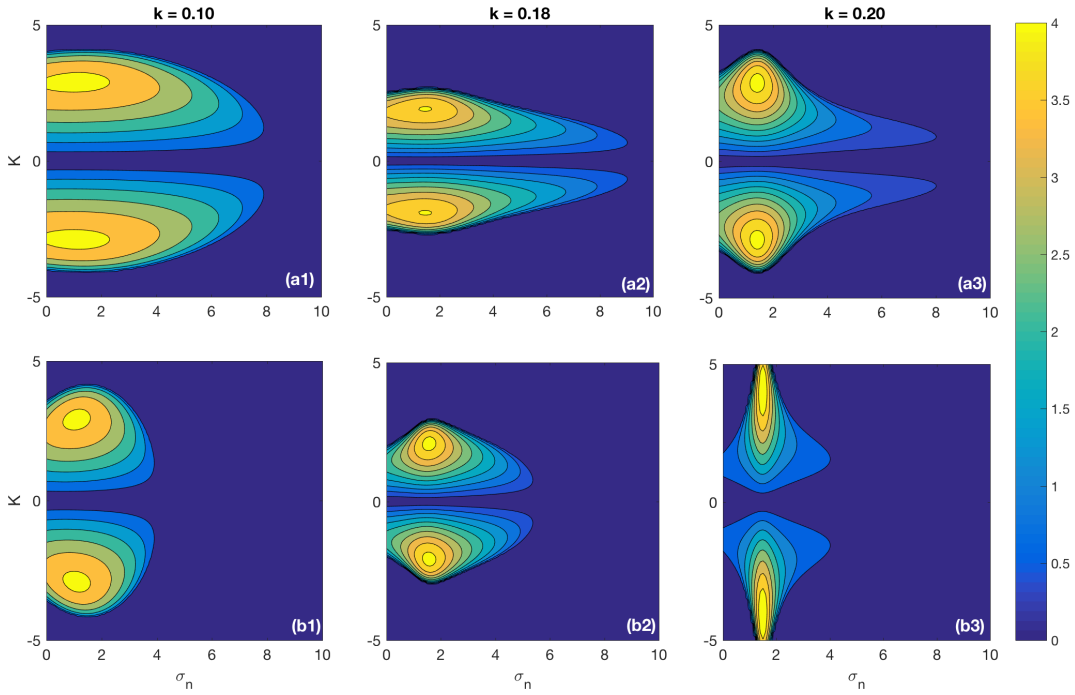

Figure 39: The growth rate of MI is plotted versus the wavenumber K and the electron-to-negative ion temperature ratio σ_n for the parallel modulation ($\theta = 0$). The columns, from left to right correspond respectively to $k = 0.1$, 0.18 and 0.20. The upper line, i.e., panels $(\text{aj})_{j=1,2,3}$ corresponds to to $\alpha = 0.1$ and the lower line, made of panels $(\text{bj})_{j=1,2,3}$, gives results for $\alpha = 0.5$.

3.4.2 Transverse modulation

The transverse modulation is obtained for $\theta = \pi/2$, which reduces P and Q to

$$P = \gamma_2 \quad \text{and} \quad Q = \gamma_3 - \gamma_4\delta_3. \tag{178}$$

They are plotted in Figs. 38 (b1) and (b2). Contrarily to the case $\theta = 0$, the dispersion parameter P remains positive with changing σ_n, while the value of Q is very sensitive to such a change. Also in this case, there are regions of instability, i.e., where $P \times Q > 0$, as shown in Fig. 38(b3). Obviously, regions of k where MI is expected are the opposite of what has been obtained in Fig. 38(a3). If only very limited values of k can give rise to instability for $\sigma_n = 5$, regions of instability are more obvious for $\sigma_n = 16$ and 22.5. For each of the later cases, there are two regions of instability $0.23 < k < 0.5$ and $0.5 < k < 0.55$ for $\sigma_n = 16$; $0.45 < k < 0.6$ and $0.6 < k < 0.75$ for $\sigma_n = 22.5$. The detected regions of k may indeed give rise to unstable patterns as shown in contour plot of the MI growth rate of Fig. 40. In Figs. $40(\text{aj})_{j=1,2,3}$, we have considered $\alpha = 0.1$ as in Fig. 39, except that here, one notices a delocalization of the instability domain in the $(\sigma_n, K)-$plane. To remind, for the case of the parallel modulation, instability has been

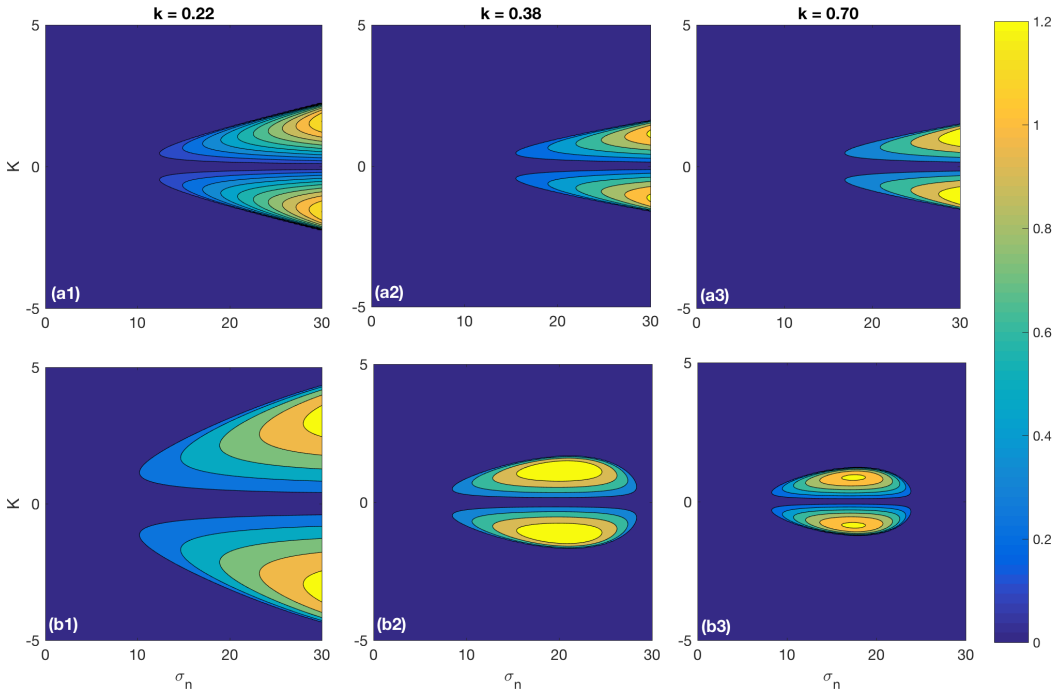

Figure 40: The growth rate of MI is plotted versus the wavenumber K and the electron-to-negative ion temperature ratio σ_n for the perpendicular modulation ($\theta = \pi/2$). The columns, from left to right correspond respectively to $k = 0.22$, 0.38 and 0.70. The upper line, i.e., panels $(\text{aj})_{j=1,2,3}$ corresponds to to $\alpha = 0.1$ and the lower line, made of panels $(\text{bj})_{j=1,2,3}$, gives results for $\alpha = 0.5$.

detected in regions of small σ_n, i.e., values that belong to the interval $0 < \sigma_n < 10$. For the transverse modulation, modulated IAWs may mainly be found in regions belonging to the interval $10 \leq \sigma_n \leq 30$. In Fig. $40(\text{bj})_{j=1,2,3}$, we have fixed $\alpha = 0.5$. Compared to Fig. 39(a1), the regions of K giving rise to instability are larger in Fig. 40(b1). There is indeed instability delocalization for $k = 0.38$, where regions of instability belong to the interval $9.8 \leq \sigma_n \leq 28.5$ (see Fig. 40(b2)). The detected region gets more reduced both in the $K-$ and σ_n- directions, when $k = 0.70$, as depicted in Fig. 40(b3).

3.5 Low relativistic ENPs: modulational instability and rogue waves

The procedure presented in Sec. 2.5.1. is followed here, leading to a dispertion relation having the form of Eq.(119), with the critical wavenumber of the perturbation being $K_{cr} = \psi_0\sqrt{\frac{2Q}{P}}$. For the plane wave to be unstable under modulation the condition

$\Omega^2 < 0$ should be satisfied, i.e.,

$$K < K_{cr} = \psi_0 \sqrt{\frac{2Q}{P}}, \tag{179}$$

which clearly shows that for $PQ > 0$, the amplitude modulated envelope is unstable. This includes several factors related to the ENP system, including the electron-to-negative ion temperature ratio, the negative ion concentration ratio and the newly introduced relativistic parameter α_1. The relativistic character of the studied plasma system clearly appears in the expression of the nonlinearity coefficient Q, which can be rewritten in the form

$$Q = Q_{rel} + Q_0, \tag{180}$$

Q_0 being the non-relativistic expression that was obtained previously in Eq.(41), which was found to be negative, so that the analysis of MI was found to be controlled by the expression of Q that was positive or negative for some values of the wavenumber k. We should stress that the coefficient of dispersion in the present study keeps the same expression, and therefore keeps the same features as in non-relativistic model. For its part, the relativistic contribution in the expression of Q is such that

$$Q_{rel} = \frac{3k^2\omega}{4}\alpha_1, \tag{181}$$

and the MI criterion $PQ > 0$ is given by $(Q_{rel} + Q_0) \times P > 0$. Indeed, this criterion can be expanded to get

$$Q_0 P > \frac{9\alpha_1 \omega^6 a_1}{8k^2}, \tag{182}$$

where the right-hand side is what was obtained for the non-relativistic ENP. Therefore, the relativistic contribution is a perturbation to the case of non-relativistic model, which to the best of our knowledge has not been discussed extensively. In the meantime, knowing $Q_0 P$, it is possible to find the range of α_1 that gives rise to MI through the inequality

$$\alpha_1 < \frac{8k^2}{9\omega^6 a_1} Q_0 P = \alpha_{1,cr}. \tag{183}$$

Obviously, the critical value of the relativistic parameter depends on the plasma parameter, and its value is sensitive to the change of the negative-ion concentration ratio, for example, as shown in Fig. 41. We note that in any of the cases, α_1 should remain positive for MI to occur. Fig. 41(a) has been plotted for $\sigma_n = 11.5$ and displays the response of α_1 to the absence of negative ions ($\alpha = 0$) and its comportment when the plasma contains negative ions ($\alpha = 0.1$). In the first case, there are two regions where α_1 is positive, and such regions, labelled MI, are likely to support the formation of envelope

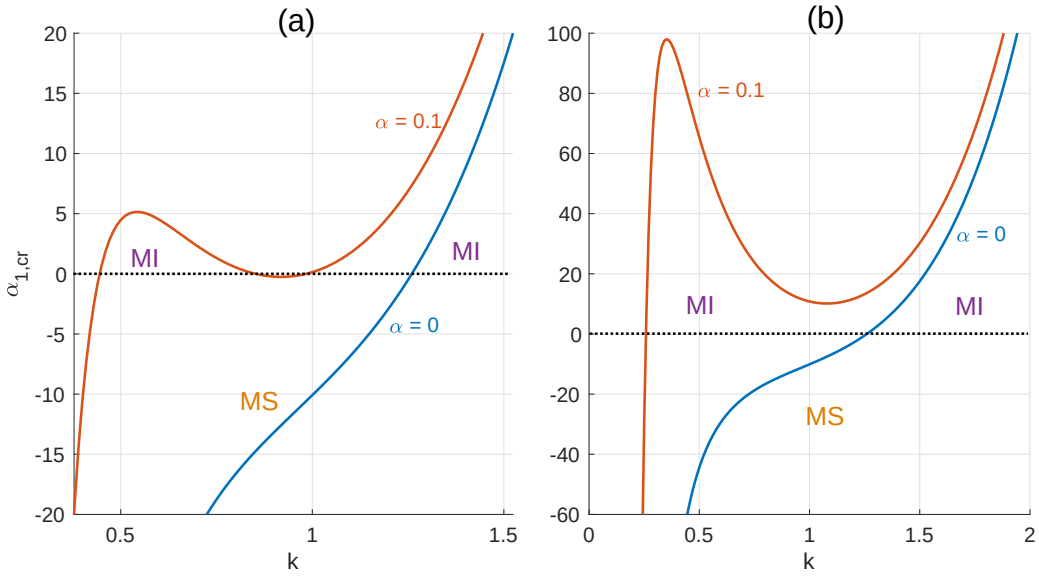

Figure 41: Panels show plots of the critical value of the relativistic parameter α_1, versus the wavenumber k, for different values of the electron-to-negative ion temperature ratio. The blue corresponds to $\alpha = 0$ and the red line corresponds to $\alpha = 0.1$, with: (a) $\sigma_n = 11.5$ and (b) $\sigma_n = 21$. Regions of modulational instability are denoted by MI, while regions of modulational stability are indicated as MS.

bright solitons, this in presence of negative ions. However, the absence of negative ions is characterized by only one region where α_1 is positive or region of MI. In Fig. 41(b), the value of the electron-to-negative ion ratio is increased to 21. One observes that in absence of negative ions, there is still one region where α_1 is positive, but the two regions brought by the presence of negative ions in Fig. 41(a) merge to form only one large region. Therefore, the electron-to-negative ion temperature ratio enlarges the domain of k and α_1 that may lead to the formation of bright, or NLS, envelope solitons as the consequence of MI. One should remember that for intervals of k where $\alpha_1 < 0$, no MI should be expected. Such regions in Fig. 41 are indicated by the label (MS). Some of the values of α_1 appearing in those areas have been chosen to plot the product PQ in Fig. 42. Fig. 42(a) has been obtained for the value $\sigma_n = 5$ of the electron-to-negative ion temperature ratio. There, the instability domain is very sensitive to the change in α_1, and there exists only one region of instability for a value $k > k_{cr}$ of the wavenumber. However, the region of stability expands with increasing α_1. In Fig. 42(b), there is only one interval of instability for the non-relativistic case, while for $\alpha_1 = 5$, two regions of instability appear. However, when $\sigma_n = 10$, the emerging small region of instability disappears. This behavior becomes more obvious in Fig. 42(c), where $\sigma_n = 21$. For $\alpha_1 = 0$, the non-relativistic system presents one large region of instability, which breaks into two regions under relativistic effects. Based on all the above calculations, it is clear that critical wavenumber of perturbation given by Eq.(179) can also be rewritten in a

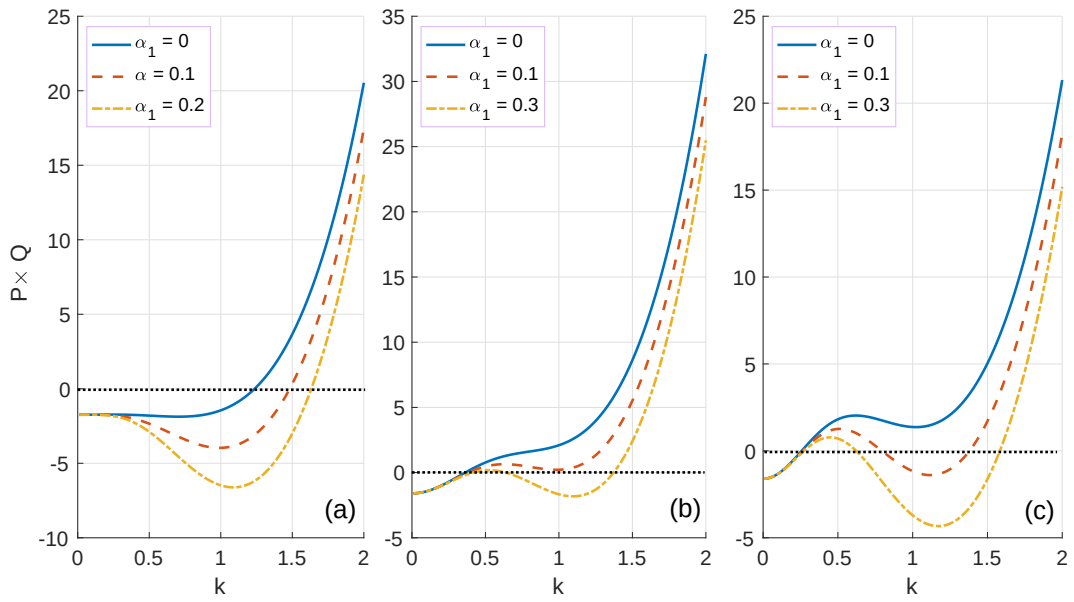

Figure 42: Panels show how the product PQ responds to the change in α_1. (a) corresponds to $\sigma_n = 5$, (b) to $\sigma_n = 11.5$ and (c) to $\sigma_n = 21$. The blue line corresponds to the non-relativistic case, while the red and color lines picture the correction brought by the relativistic parameter α_1, with $\alpha = 0.3$.

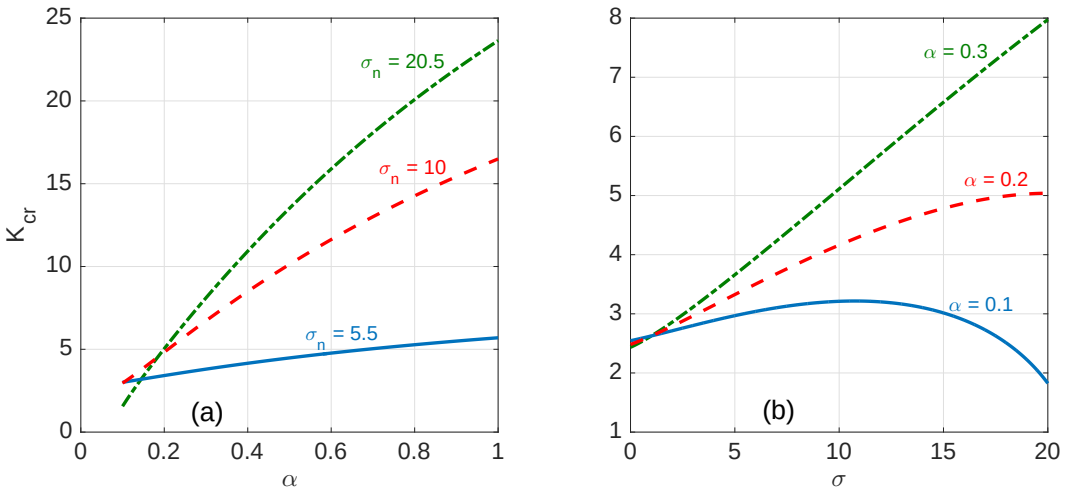

Figure 43: Panel shows plots of the critical K_{cr} versus the relativistic parameter α_1, in the absence ($\alpha = 0$) and presence ($\alpha = 0.1$) of negative ions, with $\sigma_n = 21$.

way we perceive clearly the relativistic contribution in the form

$$K_{cr} = \frac{K_{cr,0}}{\sqrt{1+\frac{Q_{rel}}{Q_0}}}, \tag{184}$$

where $K_{cr,0} = \psi_0\sqrt{2Q/P}$ is the critical value of K obtained for the non-relativistic case. Eq.(189) suggests that if $Q_0 \to \infty$, the non-relativistic problem will be retried. Otherwise, relativistic effects will be present in the system and influence the features of K_{cr} as shown in Fig. 43, where the two curves give information both in absence and presence of negative ions. In general, K_{cr} is an increasing function of α_1, but the range for instability to occur is larger than when negative ions are absent. In such intervals, one may expect the appearance of RWs. Despite the NLS equation support for spatially localized envelope soliton such as the bright and dark-type solitons, there is a hierarchy of freak (rational) solutions to the self-focusing NLS equation. These solutions represent excitations due to the MI of plasma and known as the RWs [83, 150]. They have been described as waves which appear from nowhere and disappear without a trace. There is also an extensive literature studying various types of solitons on finite background (SFB) consisting of a localized nonlinear structure evolving upon a nonzero background plane wave. A general SFB solution of the NLS equation has been explicitly proposed in the form [81, 97, 112, 139, 155]

$$\psi(\xi,\tau) = \sqrt{\frac{2P}{Q}}\left\{\frac{(1-4a)\cosh(2bP\tau)+\sqrt{2a}\cos(c\xi)+j\sinh(2bP\tau)}{\sqrt{2a}\cos(c\xi)-\cosh(2bP\tau)}\right\}\exp(2iP\tau). \tag{185}$$

Here, the single governing parameter a determines the physical behaviour of the solution through the function arguments $b = \sqrt{8a(1-2a)}$ and $c = \frac{2\pi}{L} = 2\sqrt{1-2a}$, with L being the periodicity length of the solution [97, 112]. We should stress that the above solution (185) can describe three different kinds of breather solutions, depending on the value of a. The super RW solutions of the focusing NLS equation (51) are localized both in time and space. There are, in fact, two such solutions, the Peregrine soliton and the second-order rogue wave soliton. Although the Peregrine RW is derived as a limiting case of the KM breather, especially when $a \to 1/2$, the two types of solutions can be obtained using the generalized expression [146]

$$\psi_k(\xi,\tau) = \sqrt{\frac{2P}{Q}}\left\{(-1)^k + \frac{G_k(\xi,\bar{\tau})+2jP\tau H_k(\xi,\bar{\tau})}{F_k(\xi,\bar{\tau})}\right\}\exp(2jP\tau), \tag{186}$$

where k is the order of the solution and $\bar{\tau} = 2P\tau$. The functions $G_k(\xi,\bar{\tau})$, $H_k(\xi,\bar{\tau})$ and $F_k(\xi,\bar{\tau})$ are polynomials in variables of $\bar{\tau}$ and ξ, with $F_k(\xi,\bar{\tau})$ not having no real zero. In order to get the two solutions, we will restrict our study to the cases $k \leq 2$.

The growth of periodic perturbations on a plane wave background arising in many

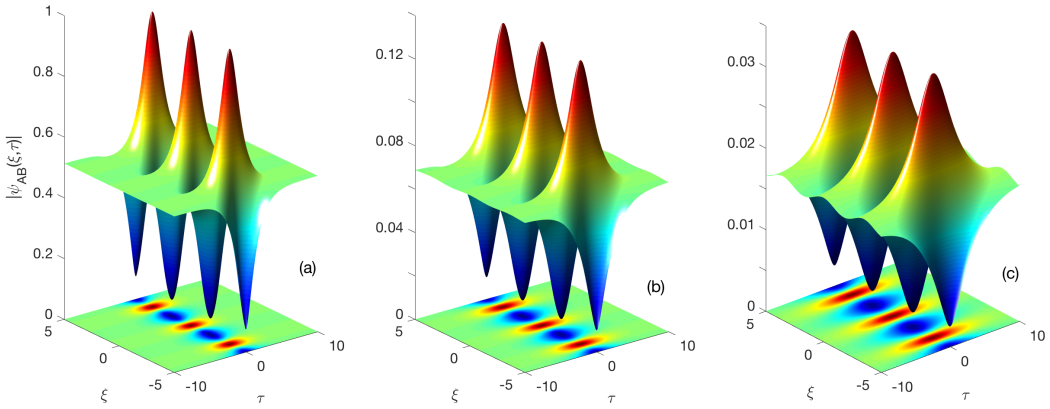

Figure 44: Panels show the surface and contour plots of the Akhmediev Breather, with their corresponding density plots, for different values of the relativistic parameter: (a) $\alpha_1 = 0.1$, (b) $\alpha_1 = 0.2$ and (c) $\alpha_1 = 0.3$. Values for the rest of parameters are $\alpha = 0.1$, $\sigma_n = 11.5$ and $k = 1.8$.

nonlinear dispersive systems is the consequence of the fundamental property of MI, this in the narrow band approximation. Beyond this context, the nonlinear stage of MI is described by the exact breather solution of the NLS, which has been considered as prototypes of RWs [133–136], that can be analytically studied under the conditions that allow MI to emerge in the NLS equation. For example, Figs. 44 and 45 give plots of

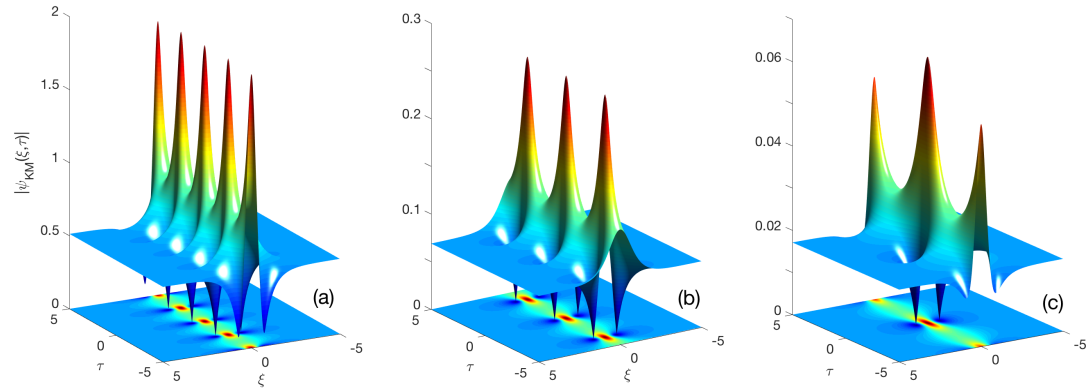

Figure 45: Panels show the evolution and contour plots of the Kuznetsov-Ma Breathers, for different values of the relativistic parameter: (a) $\alpha_1 = 0.1$, (b) $\alpha_1 = 0.2$ and (c) $\alpha_1 = 0.3$. Values for the rest of parameters are $\alpha = 0.1$, $\sigma_n = 11.5$ and $k = 1$.

the Akhmediev breather (AB) [112] and the KM breather [9, 99], respectively. The AB, from solution (185) is obtained for $0 < a < 1/2$, and the largest modulation occurs for $\tau = 0$, with the maximum of the envelope at $\xi = 0$. For its part, the KM breather is

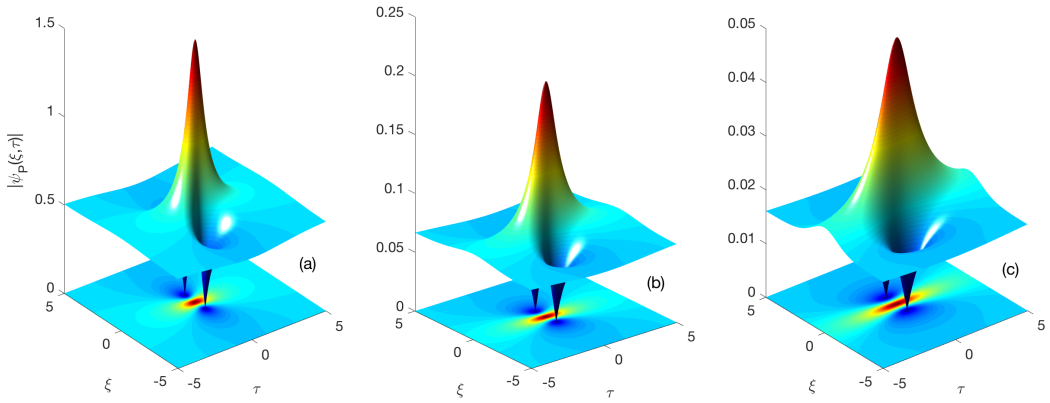

Figure 46: Panels show the evolution and the corresponding contour plots of the fundamental/Peregrine soliton for different values of the relativistic parameter: (a) $\alpha_1 = 0.1$, (b) $\alpha_1 = 0.2$ and (c) $\alpha_1 = 0.3$. Values for the rest of parameters are $\alpha = 0.1$, $\sigma_n = 10$ and $k = 1.2$.

obtained for $1/2 < a < \infty$. Its explicit expression has been proposed in the form [9, 99]

$$\psi_{KM}(\xi,\tau) = \sqrt{\frac{2P}{Q}}\left\{1 + \frac{2(1-2a)\cos(2b_1 P\tau) - jb_1\sin(2b_1 P\tau)}{\sqrt{2a}\cosh(c_1\xi) - \cos(2b_1 P\tau)}\right\}\exp(2jP\tau), \quad (187)$$

where $b_1 = -jb = \sqrt{8a(2a-1)}$ and $c_1 = -jc = \sqrt{4(2a-1)}$. This waveform is localized in space, but periodic in time. Interestingly, one can recover the Peregrine solution in the limit of infinite temporal period. It was reported recently by El-Tantawy et al. [139] that these breather solutions are very sensitive to the change in ENP parameters such as α and σ_n. However, the MI in the improved model has also shown big changes in the features of MI due the presence of the relativistic parameter α_1. This is also ostensible in the panels of Fig. 44, where the time and spatial expansion of the breather get modified with increasing α_1, this because it appears in the exponential growth-rate of the MI through $Q = Q_0 + Q_{rel}$. For the KM breather, the relativistic parameter has the effect of increasing the temporal separation between the adjoining solitonic objects and decreasing their amplitude, which implies reduction nonlinear effects, causing energy loss and wave amplitude drop. From Eq.(186), the Peregrine soliton is obtained for $k = 1$, with the polynomials H_1, G_1 and F_1 being such that $H_1(\xi,\bar{\tau}) = 2G_1(\xi,\bar{\tau}) = 8$ and $F_1(\xi,\bar{\tau}) = 1 + 4\xi^2 + 16(P\tau)^2$. The corresponding solution is written in the form [114, 146, 152]

$$\psi_P(\xi,\tau) = \sqrt{\frac{2P}{Q}}\left\{1 - \frac{4(1+4jP\tau)}{1+4\xi^2+16(P\tau)^2}\right\}\exp(2jP\tau). \quad (188)$$

It should be noted that it is also the limiting case of the Akhmediev solution when the

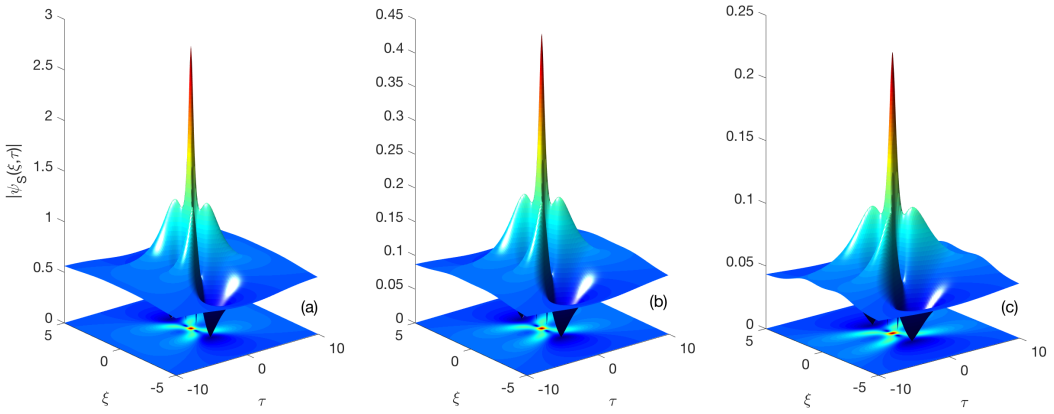

Figure 47: Panels show the evolution of the second order super rogue waves for different values of the relativistic parameter: (a) $\alpha_1 = 0.1$, (b) $\alpha_1 = 0.2$ and (c) $\alpha_1 = 0.3$. Values for the rest of parameters are $\alpha = 0.1$, $\sigma_n = 10$ and $k = 1.2$.

spatial period tends to infinity. This solution has the form of a single-peaked structure that decays to a plane wave asymptotic background at either large ξ or τ, but exhibits non-trivial behaviors over a small region in (ξ, τ) as shown in Fig. 46. The second-order/super RW is obtained from Eq.(186) if $k = 2$, and the polynomials that build the corresponding solution are given by

$$\begin{aligned} G &= \frac{3}{8} - 3\xi^2 - 2\xi^4 - 9\hat{\tau}^2 - 10\hat{\tau}^4 - 12\xi^2\hat{\tau}^2, \\ H &= \frac{15}{4} + 6\xi^2 - 4\xi^4 - 2\hat{\tau}^2 - 4\hat{\tau}^4 - 8\xi^2\hat{\tau}^2, \\ D &= \frac{3}{24} + \frac{9}{8}\xi^2 + \frac{1}{2}\xi^4 + \frac{2}{3}\xi^6 + \frac{33}{8}\hat{\tau}^2 + \frac{9}{2}\hat{\tau}^4 + \frac{2}{3}\hat{\tau}^6 - 3\xi^2\hat{\tau}^2 + 2\xi^4\hat{\tau}^2 + 2\xi^2\hat{\tau}^4, \end{aligned} \tag{189}$$

with $\hat{\tau} = 2P\tau$. This leads to the simplified expression

$$\psi_2(\xi,\tau) = \sqrt{\frac{2P}{Q}}\left\{1 + \frac{G + 2jP\tau H}{D}\right\}\exp(2j|P|\tau), \tag{190}$$

which is in fact a nonlinear superposition of simple solutions. This implies that two or more Peregrine solitons can be combined into a more complicated doubly-localized structures with a higher amplitude. One of the interesting features of such solutions is that the higher-order excitations are of higher amplitudes and more focused ones compared to the principal solution, i.e., their maximum amplitude can reach many times that of the background level. The corresponding solutions are shown in Fig. 47. The two solutions are very sensitive to the change in the relativistic parameter α_1. Their amplitude decreases with increasing the later, as already seen in the previous cases, i.e., for the breather solutions.

Experimental observation of second-order RWs has been reported recently by Pathak

et al. [113] in a multicomponent plasma containing negative ions, where it was shown that super RWs were more possible to observe experimentally than ordinary RWs. They considered different cases, including plasmas in presence and absence of negative ions. As already discussed here, the presence of negative ions can indeed modify the instability features and disturb the appearance of coherent structures in plasma. Coupled to relativistic effects, new behaviors may appear, either in the amplitude or the width, or in both, of the emerging RWs. More interestingly, such waves appear in regions

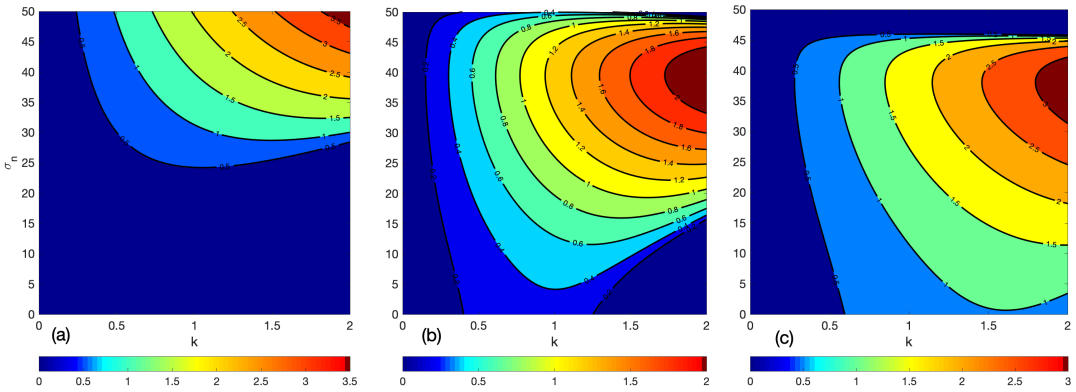

Figure 48: Panels show the maximum RW amplitude $|\psi_{S,max}|$, versus k and σ_n, for $\alpha_1 = 0.1$ and (a) $\alpha = 0$, (b) $\alpha = 0.5$ and (c) $\alpha = 0.85$. The lines delimitate areas of parameters where $P/Q > 0$, while the dark-blue region are where $P/Q < 0$.

of parameters where modulated IAWs are expected as the result of the interplay between nonlinear and dispersive effects, this because they have in common the term $\sqrt{\frac{2P}{Q}}$ which should be positive. It is for example supported in Fig. 48 that the negative ion concentration ratio α has influence on the RW amplitude, where the different panels

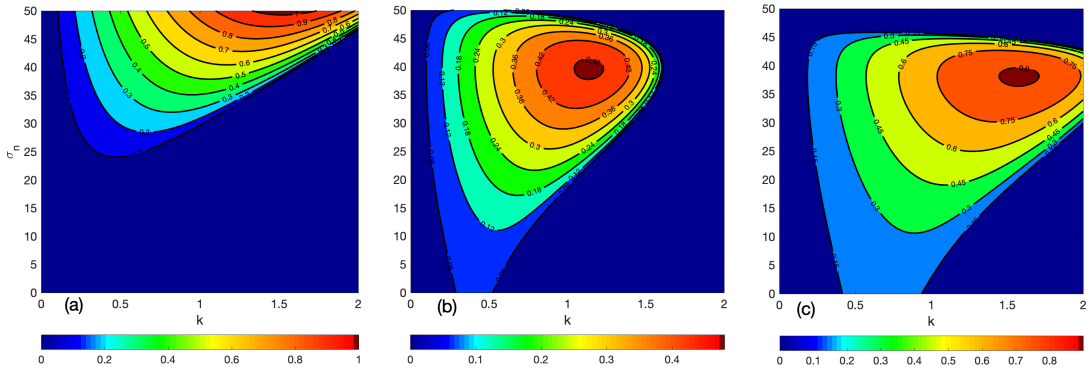

Figure 49: Panels show the maximum RW amplitude $|\psi_{S,max}|$, versus k and σ_n, for $\alpha_1 = 0.3$ and (a) $\alpha = 0$, (b) $\alpha = 0.5$ and (c) $\alpha = 0.85$. The lines delimitate areas of parameters where $P/Q > 0$, while the dark-blue region are where $P/Q < 0$.

correspond respectively to $\alpha = 0.1$, 0.5 and 0.85. Depending on such values, the regions of instability, related to the RW appearance, display different features. For $\alpha = 0$, it is obvious from Fig. 48(a), the RW solutions exist in regions of high σ_n, i.e., $25 \leq \sigma_n \leq 50$, where the highest $|\psi_{S,max}| = |\psi_S(0,0)| = 4\sqrt{\frac{2P}{Q}}$ belongs to $k = 2$, while high amplitude RW are expected for $k = 1.8$ in the case $\alpha = 0.5$ depicted in Fig. 48(b). Of course, $\alpha = 0$ corresponds to the case where there are no negative ions. The result is therefore not surprising because Fig. 41 revealed the appearence of modulated waves even in absence of negative ions, where $0 < \alpha_1 < \alpha_{1,cr}$. Comparing these two cases, one clearly sees that the wave amplitude in Fig. 48(b) has decreased and the zone of instability gets delocalized, with the highest MI growth rate appearing in the interval $30 \leq \sigma_n \leq 45$. For $\alpha = 0.85$, $|\psi_{S,max}|$ is shown in Fig. 48(c). Obviously, $|\psi_{S,max}|$ has increased and regions of instability are expanded, compared to what is observed in Fig. 48(b). It should be noted that the calculations of Fig. 48 have been made for a relativistic parameter $\alpha_1 = 0.1$. The same calculations are repeated in Fig. 49, but for $\alpha_1 = 0.3$, with α keeping the same values as previously. Although the detected regions of instability display the same behaviors as in Fig. 48, it is nevertheless obvious that the wave amplitude is lower, which shows that against α_1, α can influence the appearance and formation of RWs in the studied weakly relativistic plasma system. The dynamical behaviors of RWs was discussed in the non-relativistic model of ENPs and a critical value for α was proposed [142], below which the wave amplitude decreases or increases, depending on the other plasma parameter values. However, in our context, it is highly ostensible that the relativistic character of the studied system contributes to change such behaviors, therefore leading to much richer comportments.

3.6 Conclusion

In this chapter, we have addressed the formation of modulated IAWs in an ENP composed of Boltzmann negative ions, Boltzmann electrons and cold mobile positive ions. In one-dimensional analysis, exact solutions have been found in the form of bright and kink-wave envelopes, and their response to the negative ion concentration ratio (α) and the electron-to-negative ion temperature ratio (σ_n) has been discussed. Mainly, we have observed that α and σ_n had divergent effects on the kink-wave solution. The same feature have also been observed in the study of MI, where the occurrence of of modulated waves has been discussed with respect to some two detected positive intervals of the product PQ. Indeed, negative ions modify the features of the found plasma waves because of their strong effect on the nonlinearity of the system.

In the two-dimensional analysis, we have studied the propagation of modulated IAWs and some subsequent exact solutions. The MI of planar waves has been addressed based on α and σ_n, which were found to importantly affect the features of instability. A parametric analysis of MI has been performed to that effect, where some values of α

and σ_n have been found to be against the emergence of modulated IAWs. Analytical investigations of MI have been confirmed numerically, where the activation of MI in the DS equations has led to series of dromion-like structures, very sensitive to plasma parameters. The impact of the plasma parameters on their shape and characteristics has also been discussed, along with some collision scenarios. We have shown that when parameters are suitably fixed, such dromion solutions may undergo elastic and inelastic interactions.

In the three-dimensional analysis, a comprehensive parametric study of wave instability has been conducted, where regions of instability/stability have been revealed to be very sensitive not only to the modulation angle θ, but also to σ_n and α. Two main cases have finally been addressed, the longitudinal ($\theta = 0$) and the transverse ($\theta = \pi/2$) modulations. It has, in general, been found that the two regimes do not belong to the same intervals of the electron-to-negative ion temperature ratio (σ_n) and the wavenumber k. This indeed shows that they have different dynamical features mainly under the activation of MI. Moreover, a weakly relativistic model of ENP has been proposed in this work, and we have addressed the dynamics of IAWs. In fact, we have studied the MI, through its growth rate, and its response to plasma parameters such as α, σ_n and α_1. The results show that there are regions of parameters where the MI is very sensitive to the relativistic parameter, via the representation of the MI growth rate. The regions where the plane wave is unstable support the occurrence of RWs, and, based on that straightforward relationship, some RW solutions have been presented. In that context, the Ackmediev and KM breathers have been found to respond to the variations of α_1. Super RWs of first- and second-orders have also been presented, and their particular case has been adopted to perform some parametric analysis of MI and RW amplitude. We have confronted the effects of α, the negative-ion concentration ratio, and α_1. In general, the maximum amplitude of the second-order RW has been found to decrease with increasing α_1, showing that relativistic effects may cause energy dispersion.

General conclusion and open questions

Summary and Contributions

In this thesis, we have addressed in one and multidimensional studies the formation of modulated IA waves in an ENP composed of Boltzmann negative ions, Boltzmann electrons and cold mobile positive ions both in relativistic and non-relativistic situations. In chapter one, we have presented the generalities on plasmas and some of their useful properties. We have also discussed the plasma fluid models with emphasis on ENPs. The second chapter was devoted to the presentation of the analytical methods used in this thesis. Chapter three has been devoted to the presentation and discussion of the results reported in this work. In one dimensional analysis, the reductive perturbation method has been employed to reduce the whole dynamics to a NLS equation, with coefficients depending on the negative ions parameters of the plasma. Exact solutions have been found in the form of bright and "kink-wave" envelopes, and their response to the negative ion concentration ratio (α), and the electron-to-negative ion temperature ratio (σ_n), has been discussed. The occurrence of modulated IA waves has been discussed with respect to some two detected positive intervals of the product PQ. Furthermore, we have considered two- and three-dimensional ENPs models to study the propagation of modulated IAWs and some subsequent exact solutions. Using the reductive perturbation method, we have shown that IAWs may be described using the DS equations. In the two-dimensional case, the MI of planar waves has been addressed based on system parameters, which were found to importantly affect the features of instability. Analytical investigations of MI have been confirmed numerically, where the activation of MI in the DS equations has led to series of dromion-like structures. In the three-dimensional context, the activation of MI has reveled various dynamical modes, this because of the presence of the modulation angle θ. In that respect, a comprehensive parametric analysis of wave instability has been conducted, where regions of instability/stability have been revealed to be very sensitive to θ, σ_n and α. When the used parameters fall well inside the instability regions, ion acoustic solitons may be expected to emerge and display

coherent spatiotemporal behaviors. In the proposed model, finding such exact solutions remains an opened problem which is actually under investigation, especially in the presence of magnetic and relativistic effects. We have also proposed in this work, a weakly relativistic model of ENPs. In fact, after reducing the the proposed model to a NLS equation, we have studied the MI, through its growth rate, and its response to plasma parameters such as α, σ_n and α_1. The results show that there are regions of parameters where the MI is very sensitive to the relativistic parameter. The regions where the plane wave is unstable support the occurrence of RWs, and, based on that straightforward relationship, some RW solutions have been presented. The effects of α, the negative-ion concentration ratio, and α_1, the relativistic parameter have been confronted.

Open problems and future directions

Although very important results on the impact of ENP parameters have been obtained in this work, many points remain to be explored in future research:

- More suitable plasma environments with more than one negative ion speciy, both in the non-relativistic and the relativistic context should be studied.
- Since the ion or electron acoustic waves in Plasmas are strongly influenced by the magnetic field, it is interesting to analyze the behavior of these waves in magnetized plasmas.
- In this work, we considered in the case of the one-dimensional analysis, that the positive ions were weakly relativistic. However, we believe that the extension of this analysis to two- or three-dimensional space will make it possible to better appreciate the impact of the electronegative parameters on the emergence and propagation of waves.
- Future research should be devote to the development of a discrete electronegative plasmas model, in the case of dusty ENPs.

Bibliography

[1] A. Mohamadou, B. E. Ayissi and T. C. Kofané, Phys. Rev. E **74** (2006) 046604.

[2] E. Wamba, A. Mohamadou and T. C. Kofané, Phys. Rev. E **77** (2008) 046216.

[3] A. S. Etémé, C. B. Tabi and A. Mohamadou, Commun. Nonl. Sci. Num. Simul. **43** (2017) 211.

[4] I. Maïna, C. B. Tabi, A. Mohamadou, H. P. F. Ekobena and T. C. Kofané, Chaos **25** (2015) 043118.

[5] G. R. Y. Mefire, C. B. Tabi, A. Mohamadou, H. P. F. Ekobena and T. C. Kofané, Chaos **23** (2013) 033128.

[6] C. B. Tabi, R.Y. Ondoua, H. P. Ekobena, A. Mohamadou and T. C. Kofané, Phys. Lett. A **380** (2016) 2374.

[7] I. Kourakis and P. K. Shukla, Nonl. Proc. Geophys. **12** (2005) 407.

[8] J. Borhanian, I. Kourakis and S. Sobhanian, Phys. Lett. A **373** (2009) 3667.

[9] E. A. Kuznetsov, Sov. Phys. Dokl. **22** (1977) 507.

[10] H. Ikezi, R. Taylor and D. Baker, Phys. Rev. Lett. **25** (1970) 11.

[11] A-u.-Rahman, M. McKerr, W. F. El-Taibany, I. Kourakis and A. Qamar, Phys. Plasmas **22** (2015) 022305.

[12] H. Washimi and T. Taniuti, Phys. Rev. Lett. **17** (1966) 996.

[13] M. G. Anowar, K. S. Ashrafi and A. A. Mamun, J. Plasma Phys. **77** (2011) 133.

[14] S. S. Duha, M. S. Rahman, A. A. Mamun and G. M. Anowar, J. Plasma Phys. **78** (2012) 279.

[15] R. N. Franklin and J. Snell, J. Plasma Phys. **64** (2000) 131.

[16] A. J. Lichtenberg, I. J. Kouznetsov, Y. T. Lee, M. A. Lieberman, I. D. Kaganovich and L. D. Tsendin, Plasma Sour. Sci. Technol. **6** (1997) 437.

[17] Y. K. Ghim and N. Hershkowitz, Appl. Phys. Lett. **94** (2009) 151503.

[18] G. C. Das and A. Nag, Assam Univ. J. Sci. Technol. **5** (2010) 169.

[19] A. A. Mamun, P. K. Shukla and B. Eliasson, Phys. Rev. E **80** (2009) 046406.

[20] J. M. Dudley, G. Genty and B. J. Eggleton, Optics Exp. **16** (2008) 3644.

[21] B. Kibler, J. Fatome, C. Finot, G. Millot, F. Dias, G. Genty, N. Akhmediev and J. M. Dudley, Nat. Phys. **6** (2010) 790.

[22] A. Chabchoub, N. Hoffmann, M. Onorato and N. Akhmediev, Phys. Rev. X **2** (2012) 011015.

[23] A. Chabchoub, N. Hoffmann, M. Onorato, A. Slunyaev, A. Sergeeva, E. Pelinovsky and N. Akhmediev, Phys. Rev. E **86** (2012) 056601.

[24] H. Bailung, S. K. Sharma and Y. Nakamura, Phys. Rev. Lett. **107** (2011) 255005.

[25] S. K. Sharma and H. Bailung, J. Geophys. Res. Space Phys. **118** (2013) 919.

[26] K. Nishinari, K. Abe and J. Satsuma, J. Phys. Soc. Jpn. **62** (1993) 2021.

[27] K. Nishinari, K. Abe and J. Satsuma, Phys. Plasmas. **1** (1994) 2559.

[28] R. Sabry, W. M. Moslem and P. K. Shukla, Astrophys. Space Sci. **333** (2011) 203.

[29] N. Jehan, M. Salahuddin, H. Saleem and A. M. Mirza, Phys. Plasmas. **15** (2008) 092301.

[30] N. Jehan, M. Salahuddin and A. M. Mirza, Phys. Plasmas. **16** (2009) 062305.

[31] M. Tajiri, H. Miura and T. Arai, Phys. Rev. E **66** (2002) 067601.

[32] T. S. Gill, C. Bedi and A. S. Bains, Phys. Plasmas **16** (2009) 032111.

[33] C. Bedi and T. S. Gill, Phys. Plasmas **19** (2012) 062109.

[34] P. Carbonaro, Chaos Solit. Fract. **45** (2012) 959.

[35] I. Kourakis and P. K. Shukla, Phys. Rev. E **69** (2004) 036411.

[36] M. A. Allen and G. Rowlands, J. Plasma Phys. **50** (1993) 413.

[37] S. Munro and E. J. Parkes, J. Plasma Phys. **62** (1999) 305.

[38] W. S. Duan, Chaos Solit. Fract. **14** (2002) 503.

[39] X. N. Chen and S. D. Sharma, J. Fluid Mech. **291** (1995) 263.

[40] J.-K. Xue, Phys. Lett. A **330** (2004) 390.

[41] W. S. Duan, Phys. Plasmas **10** (2003) 3022.

[42] S. S. Ghosh, A. Sen and G. S. Lakhina, Nonl. Proces. Geophys. **9** (2002) 463.

[43] R. A. Gottscho and C. E. Gaebe, IEEE Trans. Plasma Sci. **14** (1986) 92.

[44] J. M. Dudley, G. Genty, F. Dias , B. Kibler and N. Akhmediev, Opt. Express **17** (2009) 21497.

[45] M.N. Saha Proc. Roy. Soc. A **99** (1921) 135.

[46] N.A. Krall, A.W. Trivelpiece, *Principles of Plasma Physics*, (McGraw-Hill, New York 1973).

[47] H. Griem, *Spectral Line Broadening by Plasmas* (Academic, New York 1974)

[48] G.Y. Marr, *Plasma Spectroscopy* (Elsevier, Amsterdam, 1968)

[49] F. F. Chen, *Introduction to Plasma Physics and Controlled Fusion (Second Edition)*, (Plenum Press, New York, 1984).

[50] I. Langmuir, Proc. Nat. Acad. Sci. US. **14** (1928) 628.

[51] T. Lewi, Am. J. of Phys. **35** (1967) 857.

[52] J. J. Thomson, Phyl. Mag. **44** (1897) 263.

[53] F. F. Chen, *Introduction to Plasma Physics and controlled fusion*, (Springer International Publishing, 1984).

[54] A. S. Eddington, *The Internal Constitution of the Stars*,(Cambridge University Press, 1926).

[55] K. Nishikawa and M. Wakatani, *Plasma Physics: Basic Theory with Fusion Applications*,(Springer-Verlag Berlin Heidelberg, New York, 1990).

[56] R. J. Goldston and P. H. Rutherford, *Introduction to Plasma Physics*,(Institute of Physics Publishing, Bristol and Philadelphia, 1938).

[57] R. E. J. Sladek, *Plasma needle : non-thermal atmospheric plasmas in dentistry* (PhD thesis, 2006). doi:10.6100/IR613009

[58] W. Schottky, Phys. Z. **25** (1924) 635.

[59] M. H. Corbett, Proc. 31st Int. Electr. Propuls. Conf. (2009) 151.

[60] D. J. Economou, Appl. Surf. Sci. **253** (2007) 6672.

[61] D. L. Flamm, Pure and Appl. Chem. **62** (1990) 170.

[62] T. H. Stix, *Waves in Plasmas*, (Springer-Verlag New York, 1992)

[63] D. G. Swanson, *Plasma Waves, Second Edition*, (Institute of Physics Bristol, 2003).

[64] F. Anderegg, C. F. Driscoll, D. H. E. Dubin, T. M. OŠNeil and F. Valentini, Phys. Plasmas **16** (2009) 055705.

[65] N. S. Suryanarayana, J. Kaur and V. Dubey, J. Mod. Phys. **1** (2010) 281.

[66] L. Oksuz, D. Lee and N. Hershkowitz, **17** (2008) 015012.

[67] U. Fantz, Nucl. Fusion **49** (2009) 125007.

[68] P. Debye and E. Hückel, Phys. Z. **24** (1923) 183.

[69] J. S. Russel, *Report on Waves*,(Report of the Fourteenth Meeting of the British Association for the Advancement of Science, John Murray, Londres, 1844).

[70] D. J. Korteweg and G. de Vries, *On the change of form of long waves advancing in a rectangular canal and on a new type of long stationary waves*, (Philosophical Magazine 5^{th} Series, 36, 1895).

[71] C. S. Gardner, J. M. Greene, M. D. Kruskal and R. M. Miura, Phys. Rev. Lett. **19** (1967) 1095.

[72] Gay-Mimbrera, J.García, M.C. Isla-Tejera, B. Rodero-Serrano, A. García-Nieto, A.V. Ruano, J. Adv. in Ther. **33** (2016) 894.

[73] R. Ichiki, S. Yoshimura, T. Watanabe, Y. Nakamura and Y. Kawai, Phys. Plasmas **9** (2002) 4481.

[74] A. Abdikian, Phys. Plasmas **24** (2017) 052123.

[75] M. J. Ablowitz and H. Segur, "Solitons and the Inverse Scattering Transform", (SIAM, Philadelphia, 1981).

[76] J. Jacquinot, B. D. McVey and J. E. Scharer, Phys. Rev. Lett. **39** (1977) 88.

[77] V. V. Afanasjev, Opt. Lett. **18** (1993) 790.43

[78] Y. Alpert, Phys. Rep. **339** (2001) 323.

[79] H.-X. Jia, Y-J. Liu and Y-N. Wang, Z. Naturforsch **71** (2016) 27.

[80] P. A. Andreev and L. S. Kuzmenkov, Phys. Rev. A **78** (2008) 053624.

[81] B. Kibler, J. Fatome, C. Finot, G. Millot, G. Genty, B. Wetzel, N. Akhmediev, F. Dias and J. M. Dudley, Sci. Rep. **2** (2012) 463.

[82] R. Hirota, Phys. Rev. Lett. **27** (1971) 1192 .

[83] W. R. Sun and L. Wang, Eur. Phys. J. Plus **133** (2018) 495

[84] H. Bailung, S. K. Sharma and Y. Nakamura, Phys. Rev. Lett. **107** (2011) 255005.

[85] B. Frisquet, B. Kibler and G. Millot, Phys. Rev. X **3** (2013) 041032.

[86] A. S. Bains, B. Li and M. Tribeche, Phys. Plasma **20** (2013) 092119.

[87] S. A. El-Tantawy and W. M. Moslem, Astrophys. Space Sci. **337** (2012) 209.

[88] S. Guo, L. Mei and Z. Zhang, Phys. Plasma **22** (2015) 052306.

[89] S. K. El-Labany, W. M. Moslem, Kh. A. Shnishin, S. A. El-Tantawy and P. K. Shukla, Phys. Plasma **18** (2011) 042306.

[90] A. Mannan, A. A. Mamun and P. K. Shukla, Phys. Scr. **85** (2012) 065501.

[91] G. C. Das and S. N. Paul, Phys. Fluids **28** (1985) 823.

[92] T. Kimura, K. Imagaki and K. Ohe, J. Phys. D **31** (1998) 2295.

[93] C. Becker, S. Stellmer, P. Soltan-Panahi1, S. Dörscher, M. Baumert, E.-M. Richter, J. Kronjäger, K. Bongs and K. Sengstock, Nat. Phys. **4** (2008) 496.

[94] E. A. Kuznetsov and A. M. Rubenchik and V. E. Zakharov, Phys. Rep. **142** (1986) 103.

[95] S. El-Labany, M. A. Krim, S. El-Warraki, and W. El-Taibany, Chin. Phys. **12** (2003) 759.

[96] H. P. Le and J.-L. Cambier, Phys. Plasmas **23** (2016) 063505.

[97] L. H. Wang, K. Porsezian and J. S. He, Phys. Rev. E **87** (2013) 053202.

[98] L. Li and F. Yu, Sci. Rep. **7** (2017) 10638.

[99] Y. C. Ma, Stud. Appl. Math. **60** (1979) 43.

[100] S. E. Madiba, C. B. Tabi, H. P. F. Ekobena and T. C. Kofané, Physica A **514** (2019) 298.

[101] C. B. Tabi, I. Maïna, A. Mohamadou, H. P. F. Ekobena and T. C. Kofané, Physica A **435** (2015) 1

[102] Y. Kodama and A. Hasegawa, Opt. Lett. **17** (1992) 31.

[103] D. Mandal and D. Sharma, Phys. Plasma **21** (2014) 102107.

[104] D. Mandal and D. Sharma, Phys. Plasma **23** (2016) 022108.

[105] M. Mehdipoor, Astrophys. Space Sci. **348** (2013) 115 .

[106] D. Mihalache, D. Mazilu, F. Lederer, Y. V. Kartashov, L-C. Crasovan, L. Torner, and B. A. Malomed, Phys. Rev. Lett. **97** (2006) 073904

[107] J. C. F. Mimshe, C.B. Tabi, H. Edongue, H. P. F. Ekobena and T.C. Kofané, Phys. Scr. **87** (2013) 025801.

[108] M. A.-Moghanjoughi, Phys. Plasma **17** (2010) 092304.

[109] A. Mohamadou, P.H. Tatsing, C.G. T. Latchio, C. B. Tabi and T. C. Kofané, J. Mod. Opt. **61** (2014) 1670.

[110] A. E. Mowafy and W. M. Moslem, J. King Saud Univ.Sci. **24** (2012) 343.

[111] Y. Nakamura and I. Tsukabayashi, Phys. Rev. Lett. **52** (1984) 2356 .

[112] N. Akhmediev and V. I. Korneev, Theor. Math. Phys. **69** (1986) 1089.

[113] P. Pathak, S. K. Sharma, Y. Nakamura, and H. Bailung, Phys. Plasmas **23** (2016) 022107.

[114] D.H. Peregrine, J. Aust. Math. Soc. Ser. B: Appl. Math **25** (1983) 16.

[115] R. Pottelette, R. E. Ergun, R. A. Treumann, M. Berthomier, C. W. Carlson, J. P. McFadden and I. Roth, Geophys. Res. Lett. **26** (1999) 2629.

[116] O. Rahman, A. A. Mamun and K. S. Ashrafi, Astrophys. Space Sci. **335** (2001) 425.

[117] S. Hussain, S.A. Shan, N. Akhtar and M.M. Masud, Astrophys. Space Sci. **352** (2014) 605.

[118] S.A. Shan and N. Akhtar, Astrophys. Space Sci. **346** (2013) 367.

[119] S. K. Sharma, A. Boruah and H. Bailung, Phys. Rev. E **89** (2014) 013110.

[120] P. K. Shukla and A. A. Mamun, New J. Phys. **5** (2003) 17.

[121] S. K. Sharma and H. Bailung, J. Geophys. Res.: Space Phys. **118** (2013) 919.

[122] S. Li, B. Prinari and G. Biondini, Phys. Rev. E **97** (2018) 022221.

[123] C. Sulem and P. L. Sulem, *The nonlinear Schrödinger equation*, (Springer-Verlag, 1999)

[124] W. Craig, U. Schanz and C. Sulem, Annales I. H. P. Sec. C **14** (1977) 615.

[125] S. Sultana, S. Islam, A. A. Mamun, and R. Schlickeiser, Phys. Plasmas **25** (2018) 012113.

[126] C.B. Tabi, I. Maïna, A. Mohamadou H. P. F. Ekobena and T.C. Kofané, EPL **106** (2014) 18005.

[127] C.B. Tabi, A. Mohamadou and T.C. Kofané, Eur. Phys. J. D **50** (2008) 307.

[128] C.B. Tabi, A. Mohamadou and T.C. Kofané, Int. J. Biomath. **2** (2009) 405.

[129] C.B. Tabi, A. K. Dang, R. D. Oumarou, H. P. F. Ekobena and T.C. Kofané, Physica A **442** (2016) 498.

[130] C.B. Tabi, A. S. Etémé and A. Mohamdou, Physica A **474** (2017) 186.

[131] C.B. Tabi, H. P. F. Ekobena, A. Mohamadou and T.C. Kofané, Phys. Scr. **83** (2011) 035802.

[132] N. Akhmediev, A. Ankiewicz and M. Taki, Phys. Lett. A **373** (2009) 675.

[133] N. Akhmediev, V. Eleonskii and N. Kulagin, Theor. Math. Phys. **72** (1987) 809.

[134] E. Kuznetsov, Solitons in a parametrically unstable plasma, in: Akademiia Nauk SSSR Doklady, 236, 1977, pp. 575-577.

[135] K.B. Dysthe and K. Trulsen, Phys. Scr. **T82** (1999) 48.

[136] A. Osborne, M. Onorato and M. Serio, Phys. Lett. A **275** (2000) 386.

[137] S. A. El-Tantawy, A. M. Wazwaz and S. A. Shan, Phys. Plasmas **24** (2017) 022105.

[138] S. A. El-Tantawy, Chaos Solit. Fract. **93** (2016) 162.

[139] S. A. El-Tantawy, A. M. Wazwaz and S. Ali Shan, Phys. Plasmas **24** (2017) 022105.

[140] R. Radha and M. Lakshmanan, J. Phys. A **30** (1997) 3229.

[141] S. A. El-Tantawy, N. A. El-Bedwehy and W. M. Moslem, J. Plasma Phys. **79** (2013) 1049.

[142] S. A. El-Tantawy, N. A. El-Bedwehy and S. K. El-Labany, Phys. Plasmas **20** (2013) 072102.

[143] R. Fedele, Phys. Scr. **65** (2002) 502.

[144] R. Fedele and H. Schamel, Eur. Phys. J. B. **27** (2002) 313.

[145] R. Taylor, K.R. MacKenzie and H. Ikezi, Rev. Sci. Instrum. **43** (1972) 1675.

[146] A. Ankiewicz, P. A. Clarkson and N. Akhmediev, J. Phys. A: Math. Theor. **43** (2010) 122002.

[147] A. Davey and K. Stewartson, Proc. R. Soc. London Ser. A **338** (1974) 101.

[148] J. D. T. Tchinang, A.B. M. Togueu and C. Tchawoua, Phys. Lett. A **380** (2016) 3057.

[149] D. D. E. Temgoua and T. C. Kofané, Phys. Rev. E **93** (2016) 062223.

[150] S. Toenger, T. Godin, C. Billet, F. Dias, M. Erkintalo, G. Genty and J. M. Dudley, Sci. Rep. **5** (2015) 10380.

[151] V. N. Tsytovich, S. V. Vladimirov, G. E. Morfill and J. Goree, Phys. Rev. E **63** (2001) 056609.

[152] A. Ankiewicz, N. Devine and N. Akhmediev, Phys. Lett. A **373** (2009) 3997.

[153] S. V. Vladimirov, K. Ostrikov and G. E. Morfill, Phys. Rev. E **67** (2003) 036406.

[154] J. Vranjes, M. Kono, D. Petrovic, S. Poedts, A. Okamoto, S. Yoshimura and M. Y. Tanaka, Plasma Sour. Sci. Technol. **15** (2006) S1

[155] W.-R. Sun, B. Tian, Y. Sun, J. Chai and Y. Jiang, Laser Phys. **26** (2016) 035402.

[156] A.-X. Zhang and J.-K. Xue, Phys. Rev. A **75** (2007) 013624.

[157] X. Zheng, Y. Chen, H. Hu, G. Wang, F. Huang, C. Dong and M. Y. Yu, Phys. Plasmas **16** (2009) 023701.

[158] N. J. Zabusky and M. D. Kruskal, Phys. Rev. Lett. **15** (1965) 240.

List of publications

1. **C.S. Panguetna**, C.B. Tabi and T.C. Kofané, *Two-dimensional Modulated Ion-Acoustic Excitations in Electronegative Plasmas*, Physics of Plasmas 24 (2017) 9,

2. **C.S. Panguetna**, C.B. Tabi and T.C. Kofané, *Electronegative Nonlinear Oscillating Modes in Plasmas*, Communications in Nonlinear Science and Numerical Simulation 55 (2018) 326.

3. C.B. Tabi, **C.S. Panguetna** and T.C. Kofané, Electronegative *(3+1)-Dimensional Modulated Excitations in Plasmas*, Physica B: Condensed Matter 545 (2018) 370.

4. **C.S. Panguetna**, C.B. Tabi and T.C. Kofané, Low Relativistic Effects on the Modulational Instability of Rogue Waves in Electronegative Plasmas, Journal of Theoretical and applied Physics. 13 (2019) 237.

5. C.B. Tabi, **C.S. Panguetna** and T.C. Kofané, *Modulational Instability of Coupled Waves in Electronegative Plasmas*, Physica Scripta. 95 (2020) 075211.

Commun Nonlinear Sci Numer Simulat 55 (2018) 326–337

Contents lists available at ScienceDirect

Commun Nonlinear Sci Numer Simulat

journal homepage: www.elsevier.com/locate/cnsns

Research paper

Electronegative nonlinear oscillating modes in plasmas

Chérif Souleman Panguetna[a], Conrad Bertrand Tabi[b,c,*], Timoléon Crépin Kofané[a]

[a] Laboratoire de Mécanique, Département de Physique, Faculté des Sciences, Université de Yaoundé I, B.P. 812 Yaoundé, Cameroun
[b] Laboratoire de Biophysique, Département de Physique, Faculté des Sciences, Université de Yaoundé I, B.P. 812 Yaoundé, Cameroun
[c] Botswana International University of Science and Technology, Private Bag 16 Palapye, Botswana

ARTICLE INFO

Article history:
Received 25 January 2017
Accepted 18 July 2017
Available online 22 July 2017

Keywords:
Electronegative plasma
Ion-acoustic waves
Envelope solitons
Modulational instability

ABSTRACT

The emergence of nonlinear modulated waves is addressed in an unmagnetized electronegative plasma made of Boltzmann electrons, Boltzmann negative ions and cold mobile positive ions. The reductive perturbation method is used to reduce the dynamics of the whole system to a cubic nonlinear Schrödinger equation, whose the nonlinear and dispersion coefficients, P and Q, are function of the negative ion parameters, namely the negative ion concentration ratio (α) and the electron-to-negative ion temperature ratio (σ_n). It is observed that these parameters importantly affect the formation of modulated ion-acoustic waves, either as exact solutions or via the activation of modulational instability. Especially, the theory of modulational instability is used to show the correlation between the parametric analysis and the formation of modulated solitons, obtained here as bright envelopes and kink-wave solitons.

1. Introduction

During the last twenty years, more evidence and interest have been brought to the existence of solitons in various domains of physics, mainly due to their importance in nonlinear optics [1–3], in Biophysics [4–7] and, more recently, in Bose-Einstein condensates [8–10]. They are in general solutions of equations, continuum or discrete, which include nonlinear and dispersive terms, and can travel over long distance keeping their shape even during mutual collisions. Based on their theoretical prediction in Plasmas by Zabusky and Kruskal [11], and their experimental confirmation thereafter [12,13], the study of ion-acoustic (IA) waves has become an active research direction. Extensive investigations have been devoted to the properties of such waves, leading to the conclusion that the plasma composition is crucial to their emergence and propagation. Plasmas are in general composed of ions and electrons and, in the presence of positive and negative ions, they are referred as electronegative plasmas (ENPs) [14–16] that can be created in plasma processing reactors [17] and low-temperature laboratory experiments [18,19]. In the framework of the Korteweg-de Vies (KdV) equation [12], when only positive ions are considered, nonlinear terms are positive, leading to compressive solitary waves. This changes when both positive and negative ions are included, which considerably affects the nonlinearity of the system and consequently the characteristics of IA waves [20–22]. In fact, negative ions in plasma mainly modify the charge neutrality condition, and cause the number of electron to decrease. This otherwise implies that various phenomena might emerge due to the negative ions themselves as

* Corresponding author at: Laboratoire de Biophysique, Département de Physique, Faculté des Sciences, Université de Yaoundé I, B.P. 812 Yaoundé, Cameroun.
E-mail addresses: cherifps@yahoo.fr (C.S. Panguetna), conrad@aims.ac.za (C.B. Tabi), tckofane@yahoo.com (T.C. Kofané).

http://dx.doi.org/10.1016/j.cnsns.2017.07.014
1007-5704/

well as by the lack of electrons [19], as actually confirmed by a broad range of studies devoted to KdV [23,24] and modified KdV (mKdV) solitons [25], including compressive and rarefractive large amplitude structures. Based on the laboratory experiments of Ghim and Hershkowitz [26], Mamun et al. [27] recently paid attention to the existence of IA and dust-acoustic waves in an electronegative plasma made of Boltzmann negative ions, Boltzmann electrons and cold mobile positive ions. This was followed by the investigation on other aspects and characteristics of such plasmas waves, related to their response to external magnetic fields, in one or more dimension [28,29], in the vicinity of the KdV equations obtained from the reductive perturbation approximation. However, the hydrodynamics equations can also be reduced to nonlinear Schrödinger (NLS) equations, whose exact solutions are known as envelope solitons. In this work, we mean to address comprehensively the response of such waves to the effects of the negative ion parameters, especially the negative ion concentration ratio and the electron-to-negative ion temperature ratio. We also show that under certain conditions, new classes of waves may emerge with complex profiles and characteristics. One of the direct mechanisms leading to the formation of modulated IA waves is modulational instability (MI), a consequence of the interplay between nonlinear and dispersive effects [7,30–32].

The rest of the paper is structured as follows: in Section 2, we present the electronegative plasma model, followed by the derivation of the NLS equation, whose signs of the coefficients are discussed with respect to negative ion parameters. In Section 3, exact solutions are derived. They are identified as bright envelopes and kink-wave solitons, and their features are shown to change with the negative ion concentration and electron-to-negative ion temperature. In Section 4, we investigate the occurrence of MI and its relationship with the emergence of envelope-type IA solitary waves. A comprehensive parametric analysis of the instability growth rate is also performed, while some concluding remarks are given in Section 5.

2. Mathematical model and asymptotic expansion

We consider a homogeneous, collisionless and unmagnetized plasma made of Maxwellian electrons and negative ion plus cold mobile positive ions. The associated nonlinear dynamics of the IA waves is described by the set of following normalized fluid equations [27,33,34]:

$$\frac{\partial n_i}{\partial t}+\frac{\partial n_i u_i}{\partial x}=0, \tag{1a}$$

$$\frac{\partial u_i}{\partial t}+u_i\frac{\partial u_i}{\partial x}+\frac{\partial \phi}{\partial x}=0, \tag{1b}$$

$$\frac{\partial^2 \phi}{\partial x^2}=\mu_e \exp\phi+\mu_n \exp\sigma_n\phi-n_i, \tag{1c}$$

with n_i and u_i being the number density of positive ions and the ion fluid velocity, respectively. They are respectively normalized by the unperturbed ion number density n_0 and the ion-acoustic speed $C_{si}=\sqrt{Zk_BT_e/m}$, with T_e denoting the electron temperature, k_B the Boltzmann constant and Z the charged dust state. ϕ is the electric potential normalized by the thermal potential k_BT_e/e, with e being the magnitude of the electron charge. Time and space variables are respectively normalized by the ion Debye length $\lambda_{Di}=\sqrt{k_BT_e/4\pi e^2 n_i^{(0)}}$ and the ion plasma period $\omega_{pi}^{-1}=(\sqrt{4\pi e^2 n_i^{(0)}/m_i})^{-1}$, with m_i being the ion mass and k_B the Boltzmann constant. $\sigma_n=T_e/T_n$ is the electron-to-negative ion temperature ratio. The other parameters are given by $\mu_e=n_e^{(0)}/n_i^{(0)}$ and $\mu_n=n_n^{(0)}/n_i^{(0)}$, with $n_i^{(0)}$, $n_n^{(0)}$ and $n_e^{(0)}$ being the equilibrium densities of positive ions, negatives ions and electrons, respectively. Additionally, at equilibrium, the plasma neutrality condition is satisfied, i.e., $\mu_e+\mu_n=1$. The negative ion concentration ratio, $\alpha=n_n^{(0)}/n_e^{(0)}$, can then be introduced so that $\mu_e=1/(1+\alpha)$ and $\mu_e=\alpha/(1+\alpha)$. We further consider excitations not too far from equilibrium and expand the Poisson's equation in a Taylor's series, i.e.,

$$\frac{\partial^2 \phi}{\partial^2 x}=1+a_1\phi+a_2\phi^2+a_3\phi^3-n_i, \tag{2}$$

with the expansion coefficients being

$$a_1=\mu_e+\mu_n\sigma_n,\quad a_2=\frac{\mu_e+\mu_n\sigma_n^2}{2},\quad a_3=\frac{\mu_e+\mu_n\sigma_n^3}{6} \tag{3}$$

Eqs. (1a), (1b) and (2) include nonlinear and dispersive terms whose effects can be preserved by using the reductive perturbation expansion technique. The method implies the introduction of the spatial and temporal stretched variables, $\xi=\epsilon(x-v_gt)$ and $\tau=\epsilon^2 t$, where v_g is the group velocity and ϵ, a small parameter that measures the strength of nonlinearity. The dependent physical variables around their equilibrium values are expanded as

$$\begin{pmatrix} n_i(x,t)\\ u_i(x,t)\\ \phi(x,t)\end{pmatrix}=\begin{pmatrix}1\\0\\0\end{pmatrix}+\sum_{p=1}^{\infty}\epsilon^p\sum_{l=-\infty}^{+\infty}\begin{pmatrix} n_l^{(p)}(\xi,\tau)\\ u_l^{(p)}(\xi,\tau)\\ \phi_l^{(p)}(\xi,\tau)\end{pmatrix}A^l(n,t) \tag{4}$$

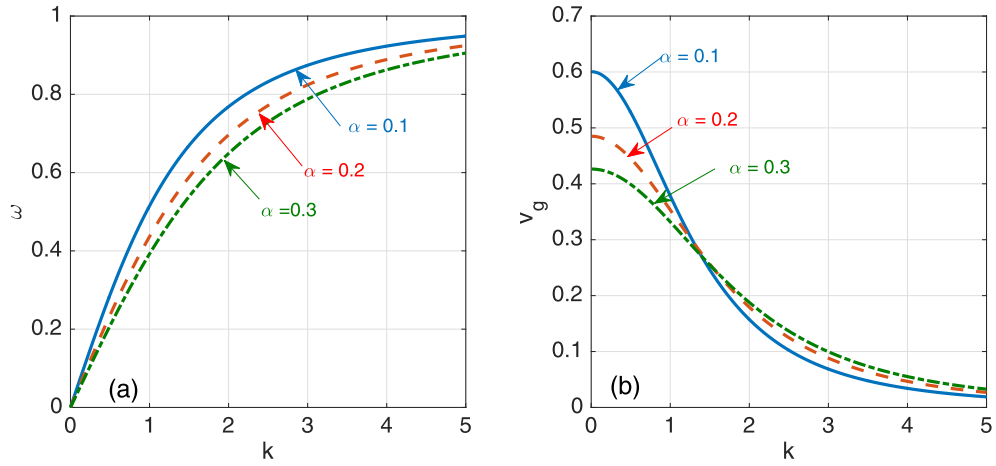

Fig. 1. The angular wave frequency ω and the group velocity v_g are plotted against the wavenumber k in panels (a) and (b), respectively. The influence of the negative ion concentration ratio α is studied in both cases for σ_n=17.5.

It is obvious that the above series contains all overtones $A^l(n,t) = \exp[il(kx - \Omega t)]$ up to order p. These are due to nonlinear terms with the corresponding coefficients being of maximum order ϵ^p, along with the relations $(n_l^{(p)})^* = n_{-l}^{(p)}$, $(u_l^{(p)})^* = u_{-l}^{(p)}$, and $(\phi_l^{(p)})^* = \phi_{-l}^{(p)}$, where $()^*$ denotes the complex conjugate of the corresponding quantity. Substituting (4) into (1a), (1b) and (2), the first-order harmonics are obtained in the form

$$n_1^{(1)} = (k^2 + a_1)\phi_1^{(1)}, \quad \text{and} \quad u_1^{(1)} = \frac{\omega}{k}(k^2 + a_1)\phi_1^{(1)}, \tag{5}$$

given that the dispersion relation

$$\omega^2 = \frac{k^2}{k^2 + a_1} \tag{6}$$

is satisfied. The later obviously depends on plasma parameters as shown in Fig. 1(a), where it is plotted versus the wavenumber k for different values of the negative ion concentration ratio α. The frequency here is found to be an increasing function of the later. For the second order, with $n = 2$ and $l = 0$, we obtain

$$\phi_0^{(2)} = \beta_\phi |\phi_1^{(1)}|^2, \quad n_0^{(2)} = \beta_n |\phi_1^{(1)}|^2, \quad \text{and} \quad u_0^{(2)} = \beta_u \left|\phi_1^{(1)}\right|^2, \tag{7}$$

with $\beta_\phi = \frac{-2a_2 v_g^2 + (k^2 - 3a_1)}{a_1 v_g^2 - 1}$, $\beta_n = a_1\beta_\phi + 2a_2$, and $\beta_u = \frac{-2\omega}{(k^2+a_1)^2} + v_g\beta_n$. At the same order, for $l = 1$, solutions $\phi_1^{(2)}$, $n_1^{(2)}$ and $u_1^{(2)}$ exist under the compatibility condition

$$v_g = a_1 \frac{\omega^3}{k^3}, \tag{8}$$

which is in fact the group velocity of the IA waves. As ω, v_g is shown in Fig. 1(b) to strongly depend on plasma parameters, especially α. For $l = 2$, the components of the second harmonic mode are obtained as

$$\phi_2^{(2)} = \alpha_\phi (\phi_1^{(1)})^2, \quad n_2^{(2)} = \alpha_n (\phi_1^{(1)})^2, \quad u_2^{(2)} = \alpha_u (\phi_1^{(1)})^2, \tag{9}$$

where

$$\alpha_\phi = \frac{(k^2 + a_1)^2}{2k^2} - \frac{a_2}{3k^2}, \quad \alpha_n = (a_1 + 4k^2)\alpha_\phi + a_2, \quad \alpha_u = \frac{\omega}{k}(\alpha_n - (k^2 + a_1)^2).$$

By making use of all the previous steps, canceling the third-order equations, with $n = 3$ and $l = 1$, and letting $\phi_1^{(1)} = \psi$, we finally get the NLS equation for IA envelope waves in the form

$$i\frac{\partial \psi}{\partial \tau} + P\frac{\partial^2 \psi}{\partial \xi^2} + Q|\psi|^2\psi = 0, \tag{10}$$

where the coefficients P and Q are given by:

$$\begin{aligned} P &= \frac{\omega^3}{2k^2}\left[-\frac{2k}{\omega}(k^2 + a_1)(\alpha_u + \beta_u) - (k^2 + a_1)(\alpha_n + \beta_n) + 2a_2(\alpha_\phi + \beta_\phi) - 3a_3\right] \\ Q &= -\frac{3a_1\omega^5}{2k^4}. \end{aligned} \tag{11}$$

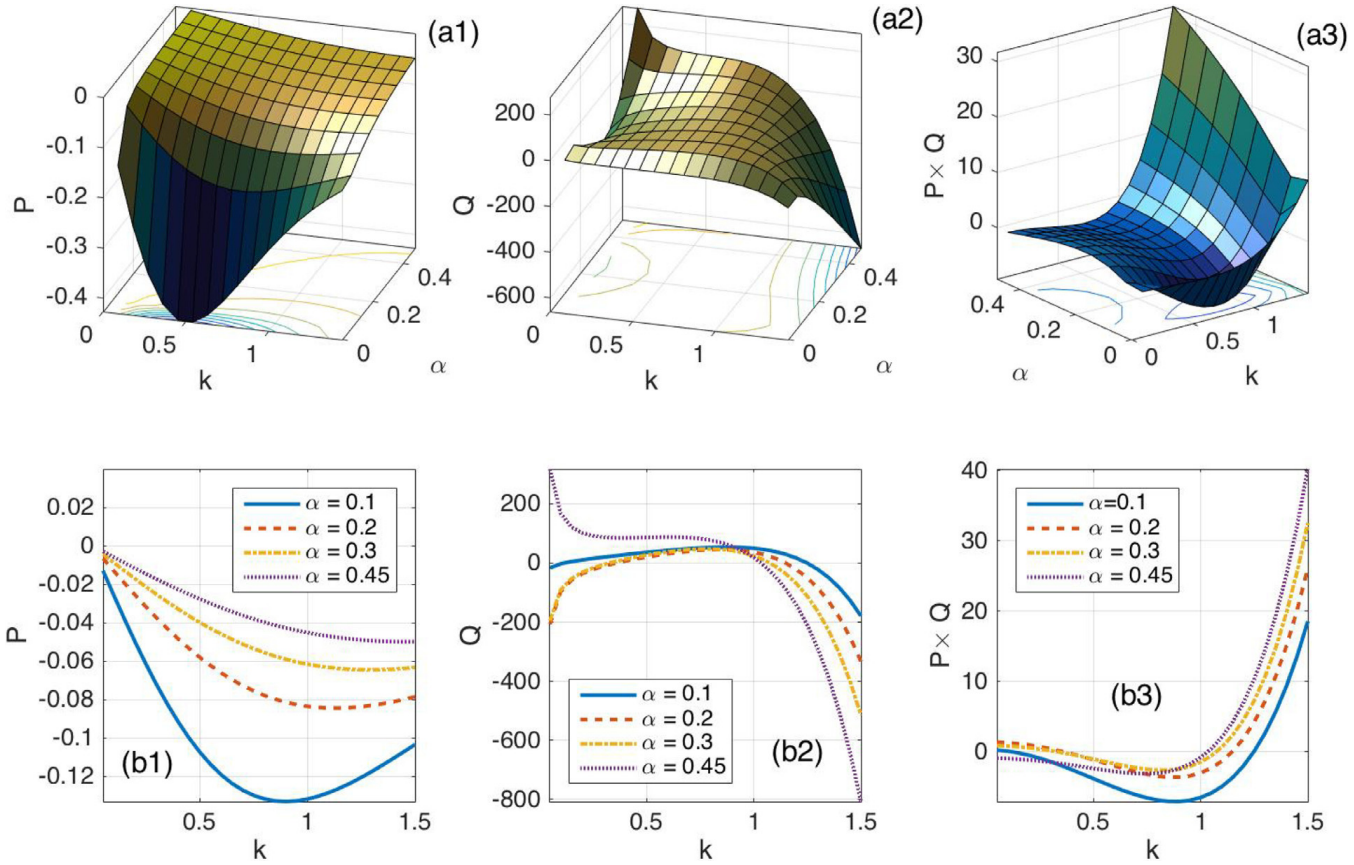

Fig. 2. Panels $(aj)_{j=1,2}$ show plots of the parameters P and Q, along with their product $P \times Q$, versus the wavenumber k and the negative ion density ratio α. The dispersion coefficient P is as a whole negative and the nonlinearity coefficient is positive in some intervals, and higher than P. This gives interesting features from their product which, depending on the value of alpha, admits one or two positive intervals. This is clearly illustrated in panels $(bj)_{j=1,2,3}$, where the parameters and their product are plotted versus the wavenumber k. For $\alpha = 0.1$, 0.2 and 0.3, Q has two negative intervals and remains positive for $k_{cr,\,1} < k < k_{cr,\,2}$. For higher values of α, Q is positive the interval $0 < k < k_{cr,\,2}$. In panels (b3) then, one observes two regions where $P \times Q$ is positive, and one region where it is negative, corresponding to regions where $Q > 0$. We have fixed $\sigma_n = 17.5$.

P and Q are the dispersion and the nonlinear coefficients, respectively. In Figs. 2(a1) and (a2), they are plotted versus k and α. In general P is negative, but Q is negative in some intervals of k and the negative ion concentration ration α. This is explicitly shown in Figs. 2(b1) and (b2), where the negative intervals of Q (versus k) depend on the value of α. For small values of the later, there are two regions where $Q < 0$, i.e., $k < k_{cr,\,1}$ and $k > k_{cr,\,2}$, and one region where $Q > 0$, $k_{cr,\,1} < k < k_{cr,\,2}$. The same calculations are repeated in Fig. 3(a1), (a2) ,(b1) and (b2), where the effect of the electron-to-negative ion temperature ratio σ_n is studied. Its effect is contrary to what is observed for α, i.e., increasing its value rather gives rise to two intervals where $Q < 0$ (see Fig. 3(b2)). It is also obvious that Q is 10^3 times higher than P, which suggests that the appearance of nonlinear waves will mostly depend on the sign of Q as developed below.

3. Envelope excitations

The NLS equation has solutions, which include envelope solitons, breather-type localized structures. In this work, we are interested in envelope solitons whose importance has been discussed in a broad range of areas including biophysics [35–38], plasma physics [39], nonlinear optics and metamaterials [40], just to name a few. As a whole, finding some kinds of solutions for Eq. (10) requires the study of the sign of the product $P \times Q$, which, when positive leads to the bright-envelope IA solitons. For a complete analysis in this regard, we have represented PQ versus k and α in Fig. 2(a3), and only versus k in Fig. 2(b3) with changing α. From the parametric analysis of the previous section on the signs of P and Q, one could predict the occurrence of the two positive intervals of the product PQ with increasing α. This is indeed obvious in Fig. 2(b3), where the two regions $k < k_{cr,\,1}$ and $k > k_{cr,\,2}$ clearly appear. Moreover, with in mind the results of Fig. 3(a1), (a2), (b1) and (b2), it would be more interesting to also explore the effect of σ_n on the formation of modulated IA waves. This is performed in Panels (a3) and (b3) of Fig. 3, where PQ is respectively plotted in the plane (k, σ_n) and versus k, respectively. In the later, the change in σ_n importantly affects the positive region of PQ, but the effect is contrary to that observed for α. The two positive zones exist and get reduced with increasing σ_n. Also, in the two cases, depending on negative parameter values, there exists one region where PQ is positive, i.e., $k > k_{cr,\,2}$. Although we are not quite sure of their values, one may also state that there are two critical values of k, $k_{cr,\,1}$ and $k_{cr,\,2}$ so that bright envelope solitons may be found for $k < k_{cr,\,1}$ and

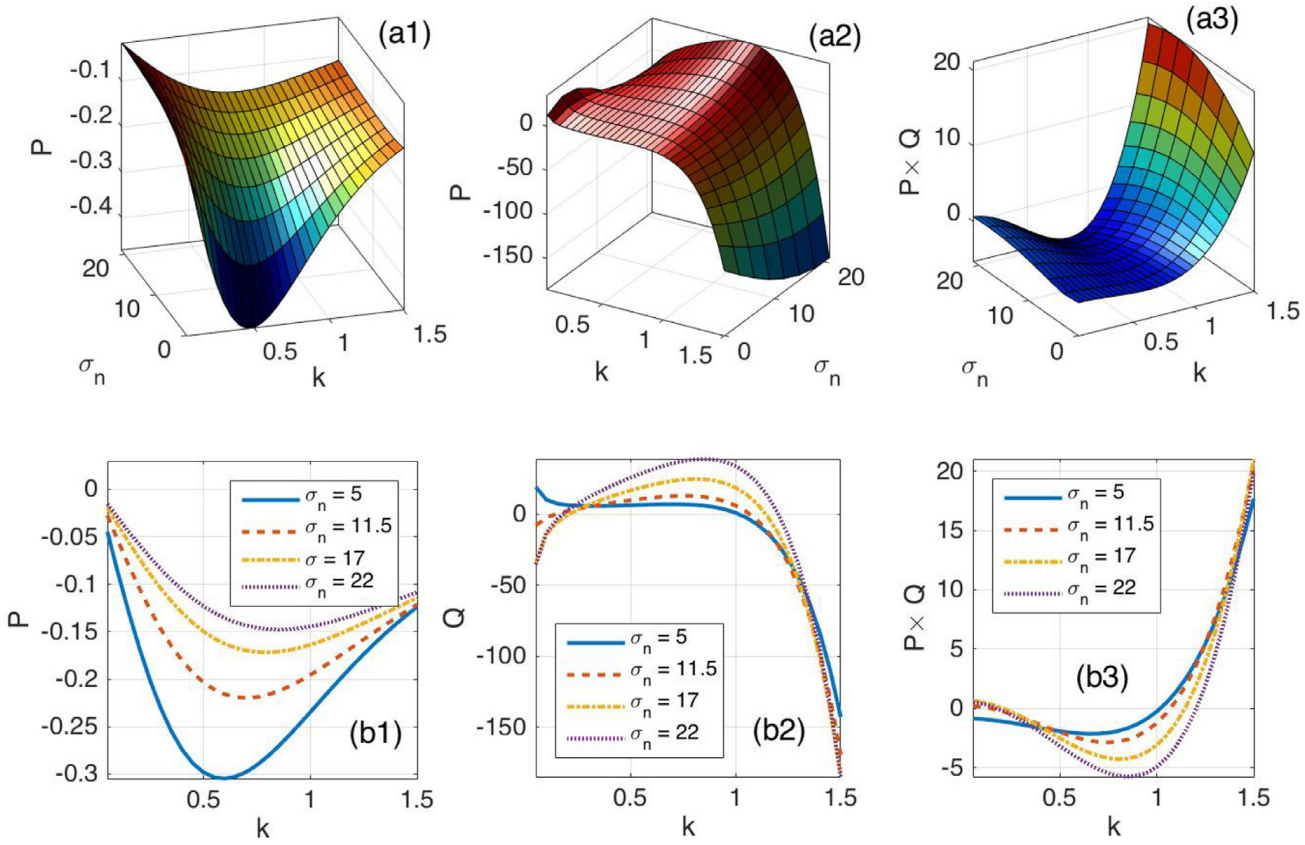

Fig. 3. Panels $(aj)_{j=1,2}$ show plots of the parameters P and Q, along with their product $P \times Q$, versus the wavenumber k and the electron-to-negative ion temperature ratio σ. The dispersion coefficient P remains negative for any k and σ_n. However, for small values of σ_n, there is only one region where Q is negative. With increasing σ_n, there are two intervals like in Fig. 2. Equally, the product $P \times Q$, for small values of σ_n has one positive interval for k, while two positive regions appear for $\sigma_n \geq 11.5$. All the panels have been plotted for $\alpha = 0.1$.

$k > k_{cr,2}$. Otherwise, when parameters are picked from intervals where $PQ < 0$, solutions for (10) will be of envelope dark-type [39,41,42]. However, the general envelope-type solution is written in the form

$$\psi(\xi, \tau) = \psi_0(\xi, \tau) e^{i\Theta(\xi,\tau)} + c.c., \tag{12}$$

where the slowly varying amplitude ψ_0 and the phase correction Θ are real quantities and obtained by plugging solution (12) into Eq. (10). In this section, we study two cases based on the previous discussion on the sign of the product $P \times Q$.

(i) The bright-type envelope solutions

These solutions arise in regions of parameters where $PQ > 0$. Making use of trial solution (12), the bright soliton solutions for Eq. (10) are given by Fedele and Schamel [41], Fedele [42].

$$\psi_0 = \rho_0 \mathrm{sech}\left(\frac{\xi - v_e \tau}{L}\right), \quad \text{and} \quad \Theta = \frac{1}{2P}\left\{v_e \xi - \left(PQ\rho_0^2 + \frac{1}{2}v_e^2\right)\tau\right\}, \tag{13}$$

where v_e is the velocity of the envelope and L, the envelope spatial width related to the amplitude ρ_0 by $L\rho_0 = \sqrt{2P/Q}$. The global solution $\phi(x, t)$ describing the electric potential may be obtained by considering the different steps of Section 2. The corresponding solutions are shown in Fig. 4 for different values of the wavenumber k. For any value of k, the bright soliton profile remains constant as it propagates, but the phase which slowly depends on space and time, experiences small deformation of the wave packet internal structure during propagation. Equally, the plasma negative ion parameters such as α and σ_n are also supposed to influence their structures. This is for example summarized in Fig. 5, where the effect of the negative ion concentration ratio, α, is to reduce the spatial expansion of the obtained solution. For $\alpha = 0.3$, for example, one indeed get more spatially localized structures. The parameter α indeed gives an idea on the suitable concentration of the negative ions and its consequences on the formation of bright-envelope IA waves. For instance, localized modulated IA wave packets have been observed in the earth's magnetosphere, where they are related to localized field and density variations [43,44].

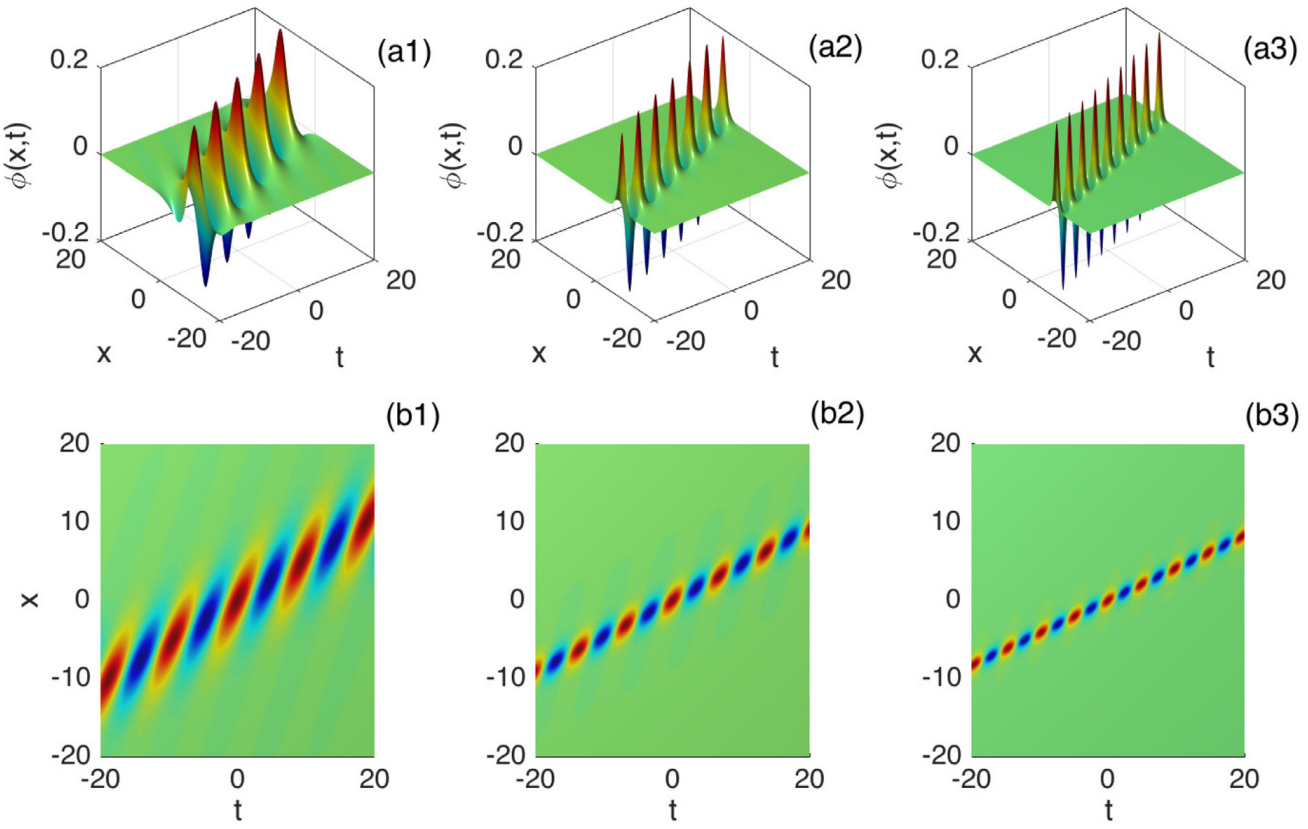

Fig. 4. Spatiotemporal evolution of solutions (13), with their corresponding density plots, for different values of the wavenumber k: (a1)–(b1) $k = 1.2$, (a2)–(b2) $k = 1.3$ and (a3)–(b3) $k = 1.8$, with $\alpha = 0.3$ and $\sigma_n = 17.5$.

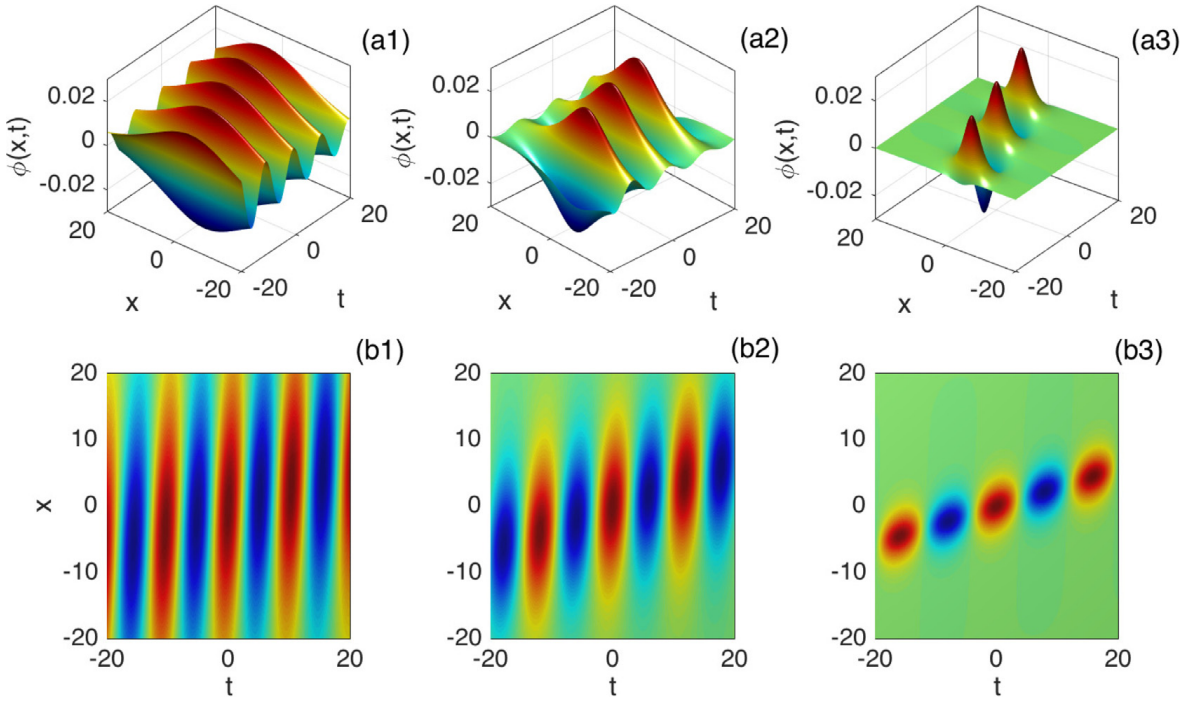

Fig. 5. Space-time evolution of solutions (13), along with their corresponding density plots, under the effect of the negative ion concentration ratio α: $\alpha = 0.1$, $\alpha = 0.2$ and $\alpha = 0.3$, with $\sigma_n = 17.5$ and $k = 0.22$.

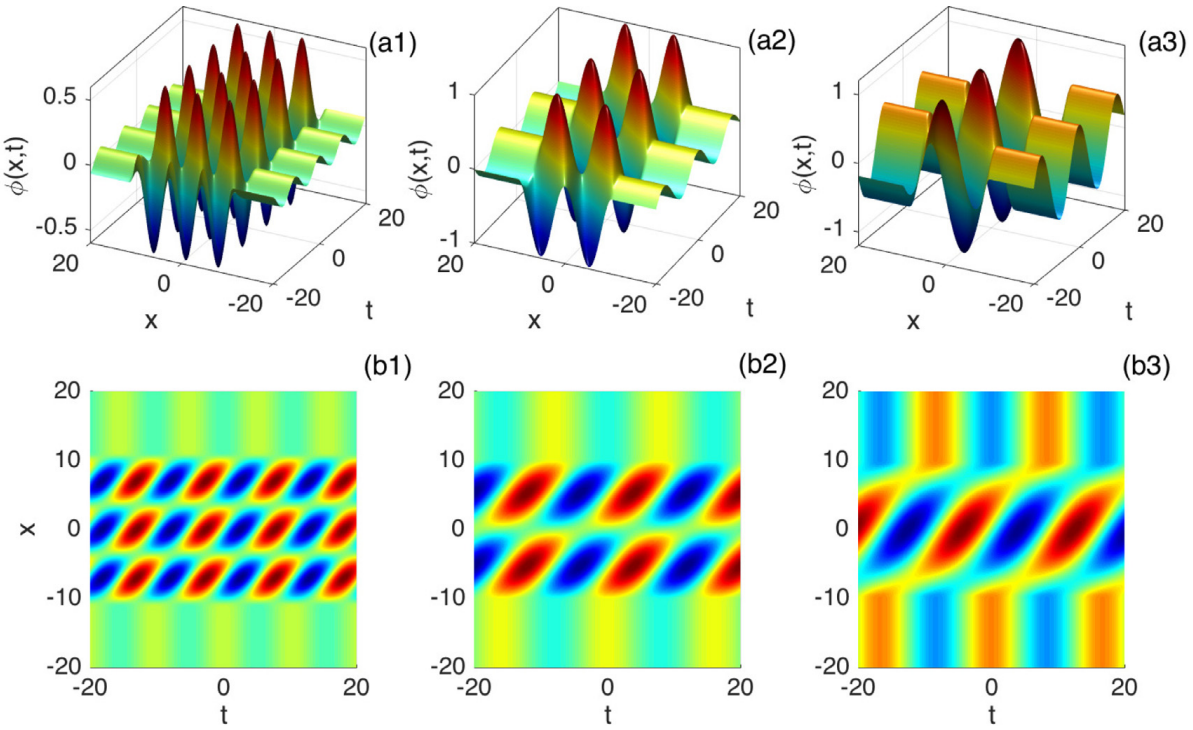

Fig. 6. The panels show space-time evolution of the dark envelope solutions (14), with their corresponding density plots, for different values of the negative ion concentration ratio α: $\alpha = 0.1$, $\alpha = 0.2$ and $\alpha = 0.3$, with $\sigma_n = 17.5$ and $k = 0.65$.

(ii) The dark-type envelope solutions

Such solutions are usually obtained in regions of parameters where $P \times Q < 0$ and may propagate as dark envelope wavepackets. Their general expression writes [41,42]

$$\psi_0 = \rho_0 \left| \tanh\left(\frac{\xi - v_e \tau}{L'} \right) \right|, \quad \text{and} \quad \Theta = \frac{1}{2P} \left\{ v_e \xi - \left(PQ\rho_0^2 + \frac{v_e^2}{2} \right) \tau \right\}, \tag{14}$$

where $L'\rho_0 = \sqrt{2|P/Q|}$. The corresponding solutions are represented in Fig. 6 for different values of α. In particular, the localized part is enclosed between temporally oscillating structures, but spatially, there are jumps between the dark breathers which characterize the kink-antikink origin of these structures. Such effects are more ostensible in Fig. 6 (a3)–(b3), where $\alpha = 0.3$. Also, one clearly remarks that the number of oscillating structures between kink profiles reduces with increasing α, which still confirms the important effect of negative ions on the electric potential in the plasma. This introduces a new class of soliton which we call here the "kink-wave" soliton. In order to better picture some specific features of the kink-wave soliton, it has been plotted in space for different values of α (see Fig. 7). In panels $(\text{aj})_{j=1,2,3}$, we have imposed $\alpha = 0.1$ and $\phi(x, t)$ has been plotted at different instant to picture the time frame. One clearly sees the oscillating features inside the two states of the kink, main characteristic of the kink-wave IA soliton. With increasing α, we obtain the features of Fig 7$(\text{bj})_{j=1,2,3}$, where the frequency of oscillations drops, leading to some multi-humped features of the solution. Finally, for $\alpha = 0.3$, the signature of the electric potential is displayed in Fig. 7$(\text{cj})_{j=1,2,3}$. Once again, the frequency of the oscillating part has dropped. To get these results, we have considered $\sigma_n = 17.5$. With increasing α, the concentration of negative ions increases and this affects the electron-to-negative ion temperature, whose effects may be seen by changing the value of σ_n as depicted in Fig. 8. It is clear from there that the frequency of the oscillating part of the solution increases with σ_n, leading to more obvious features of the kink form. This straightforwardly corroborates what was already predicted in Figs. 2 and 3, where the effect of σ_n on the coefficients was contrary to that of α.

4. Modulational instability

MI is related to the apparition of solitons in system where there are competitive effects between nonlinearity and dispersion. In general nonlinear modulated waves share the same regions of parameter with solitons solutions. Nonlinear equations admit plane wave solutions that may be stable or unstable, depending on the system parameters. For example, solutions for Eq. (10) can be assumed to be in the form $\psi = \psi_0(\xi) \exp(iQ\psi^2\tau)$ where ψ_0 is a constant (real) amplitude of the pump carrier wave. The stability of any solution is investigated under small perturbations in phase, in amplitude or in both. Since we are interested here in amplitude modulation, the corresponding perturbed solution then writes $\psi = (\psi_0 + \delta\psi) \exp(iQ\psi^2\tau)$, where $\xi = (K\zeta - \Omega\tau)$ is the modulation phase with $K \ll k$ and $\Omega \ll \omega$ are respectively the wave number and the frequency of the modulation; $\delta\psi \ll \psi_0$ is the small amplitude perturbation, which is introduced in the form $\delta\psi = U + iV$, where

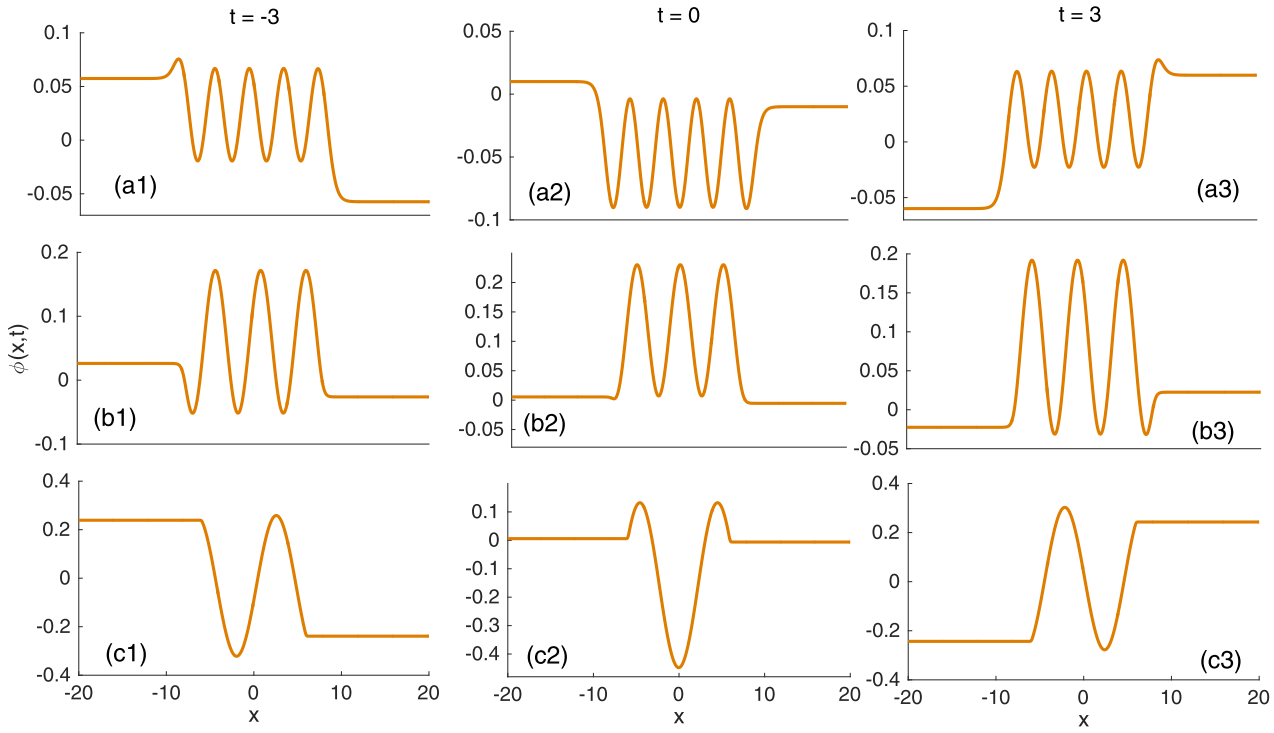

Fig. 7. The panels show spacial features of the dark envelope solutions (14), under the effect of the negative ion concentration ratio α. Panels $(\mathrm{aj})_{j=1,2,3}$ are plotted for $\alpha = 0.1$, $(\mathrm{bj})_{j=1,2,3}$ for $\alpha = 0.2$ and $(\mathrm{cj})_{j=1,2,3}$ for $\alpha = 0.3$, with $\sigma_n = 17.5$.

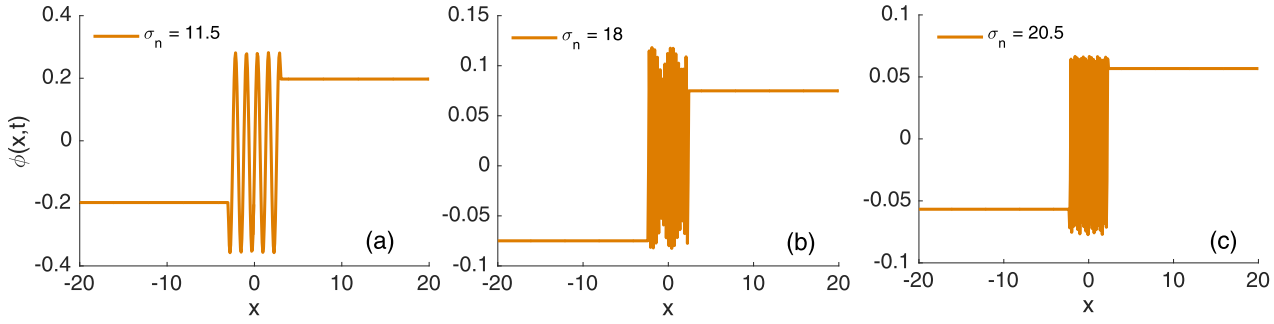

Fig. 8. The panels show spacial evolution of the dark envelope solutions (14) for different values of the electron-to-negative ion temperature ratio σ_n, where panel(a) corresponds to: $\sigma_n = 20$, (b) $\sigma_n = 21$ and (c) $\sigma_n = 20.5$, with $\alpha = 0.1$.

$U = U_0 \exp[i(K\zeta - \Omega\tau)]$ and $V = V_0 \exp[i(K\zeta - \Omega\tau)]$. After substituting all these into Eq. (10) and linearizing around the unperturbed plane wave solution, one finally obtains the nonlinear dispersion relation

$$\Omega^2 = (PK^2)^2\left(1 - \frac{2Q\psi_0^2}{PK^2}\right). \tag{15}$$

For the plane wave solution to be unstable, the frequency Ω should be complex, i.e., $\Omega^2 < 0$. Obviously, this highly depends on the sign of Q/P. When Q/P is negative, it is clear that Ω will be real and for $Q/P > 0$, it is likely that the perturbation frequency be negative. This is straightforwardly related to the results obtained in the previous section and confirms that soliton and nonlinear waves due to MI share the same parameter regions. In general, the instability is a purely growing mode for $Q/P > 0$, which is materialized by the MI growth rate

$$\Gamma = \sqrt{-\Omega^2} = |PK|\sqrt{2\frac{Q\psi_0^2}{P} - K^2}. \tag{16}$$

In the previous section, we detected regions of positive PQ, depending on the value of α and σ_n. In Fig. 9, where the growth rate is represented versus the perturbation wavenumber K, we have for example consider the case where there are two regions, i.e., $k < k_{cr,\,1}$ and $k > k_{cr,\,2}$, respectively. In the first case, Γ is a decreasing function of k (see Fig. 9(a)), while in the second case, Γ increases with k. We should however stress that we have fixed the value of α to 0.2, which to some extend might not give all the information related to the onset of instability. In fact, two parameters, α and σ_n, are considered to have strong impact on the emergence of nonlinear patterns of the electric potential ϕ. This is also confirmed by the plots

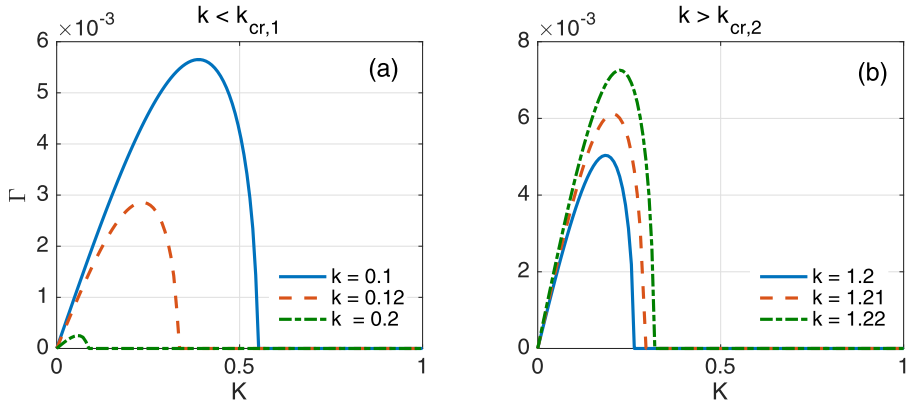

Fig. 9. The panels show the growth rate of instability versus the perturbation wavenumber K. In panel (a), small values of the initial wavenumber k are considered, while in panel (b) high values of k introduced. Below $k_{cr,1}$, Γ is a decreasing function of k, and above $k_{cr,2}$, it increases with increasing k. We have considered $\alpha = 0.1$ and $\sigma = 11.5$.

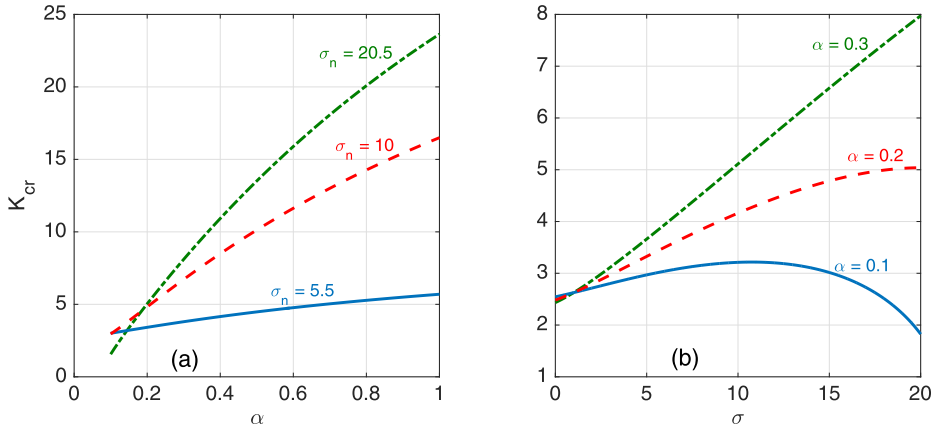

Fig. 10. The panels show the critical wavenumber K_c versus (a) the negative ion concentration ratio, α, and (b) the electro-to-negative ion temperature ratio, σ_n. In each of the case one respectively changes σ_n and α, with $k = 0.2$ and $\psi_0 = 0.2$.

of Fig. 10, where the critical wavenumber $K_c = \psi_0\sqrt{|2Q/P|}$ is strongly modified by the negative ion parameters. In Fig. 10(a), K_c is plotted versus the negative ion concentration ratio α and its dependence on the electron-to-negative ion temperature ratio σ_n is illustrated. Inversely, in Fig. 10(b), K_c is shown versus σ_n and different values of α are used. It then appears that K_c is an increasing function of both α and σ_n, and therefore may affect importantly the instability growth rate Γ, and consequently the formation of modulated IA waves. It might then be of importance to study the behaviors of such parameters when one considers small and high regions of the unperturbed wavenumber k. In Fig. 11, for example, we have plotted the growth rate versus K and α (Fig. 11(aj)$_{j=1,2,3}$), and its corresponding stability/instability diagrams (Fig. 11(bj)$_{j=1,2,3}$), for different values of $k < k_{cr,1}$. The features of MI are described by a breast of instability, which gets reduced with increasing k. On the other side, in Fig. 12, the same calculations are performed for $k > k_{cr,2}$, and Γ is an increasing function of k. The results of Figs. 11 and 12 therefore confirm our prediction of Fig. 9. Beyond the effects of the unperturbed wavenumber k, one may also notice that for $k < k_{cr,1}$, only values of α between 0.1 and 0.3 are supposed to give rise to localized structures. Intervals for K also get reduced and for $k = 0.2$, the instability region is well inside small K and small α (see Fig. 11(b3)). The contrary is observed in Fig. 12, where high values of both α and K are expected to give rise to trains of modulated waves. To complete our analysis, we have also plotted the MI growth rate versus the ratio σ_n, still for the two different intervals of positive PQ. For $k < k_{1,cr}$, results are summarized in Fig. 13, where unstable wave patterns are expected for values of σ_n higher than 15. However, with increasing k in that interval, the instability region get reduced as previously. Interestingly, the region of instability gets expanded with increasing k within the interval $k > k_{cr,2}$. Here, unstable wave patterns are expected for all σ_n, but the corresponding interval of K gets expanded with increasing k as shown in Fig. 14. To be more explicit, the two regions of k display different behaviors and the increase, or decrease, of the growth rate Γ, both in the $(K,\alpha)-$ and $(K,\sigma_n)-$planes is strongly affected by the wavenumber k. This also give an idea on the concentration of negative ions that may lead to the formation of modulated IA waves under the activation of MI. In, the process, the nonlinearity of the plasma system is importantly modified, and this conditions the formation and emergence of any kind of envelope trains of wave, given that parameters are picked from regions of instability, while the initial plane wave may propagate unperturbedly where such regions disappear.

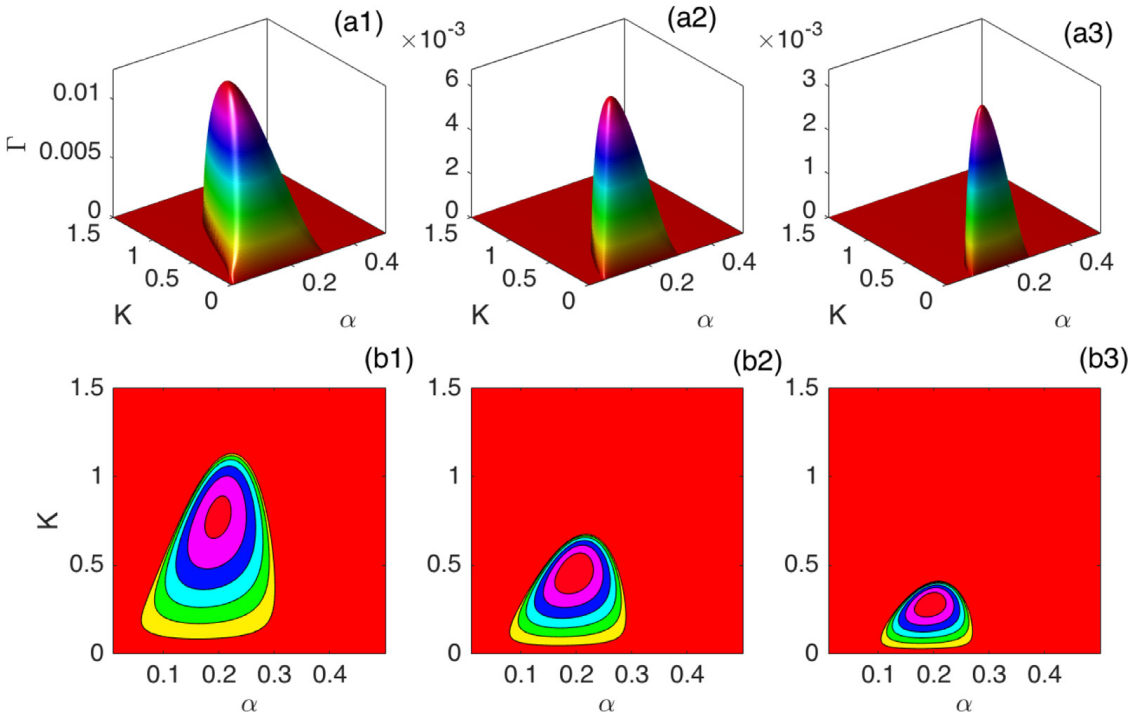

Fig. 11. The GR of MI is plotted versus the wavenumber K and the negative ion concentration ratio. The small $k-$regime has been considered and different values of the initial wavenumber are taken to be: (a1)–(b1) $k = 0.1$, (a2)–(b2) $k = 0.15$ and (a3)–(b3) $k = 0.2$, with $\sigma_n = 17.5$ and $\psi_0 = 0.2$.

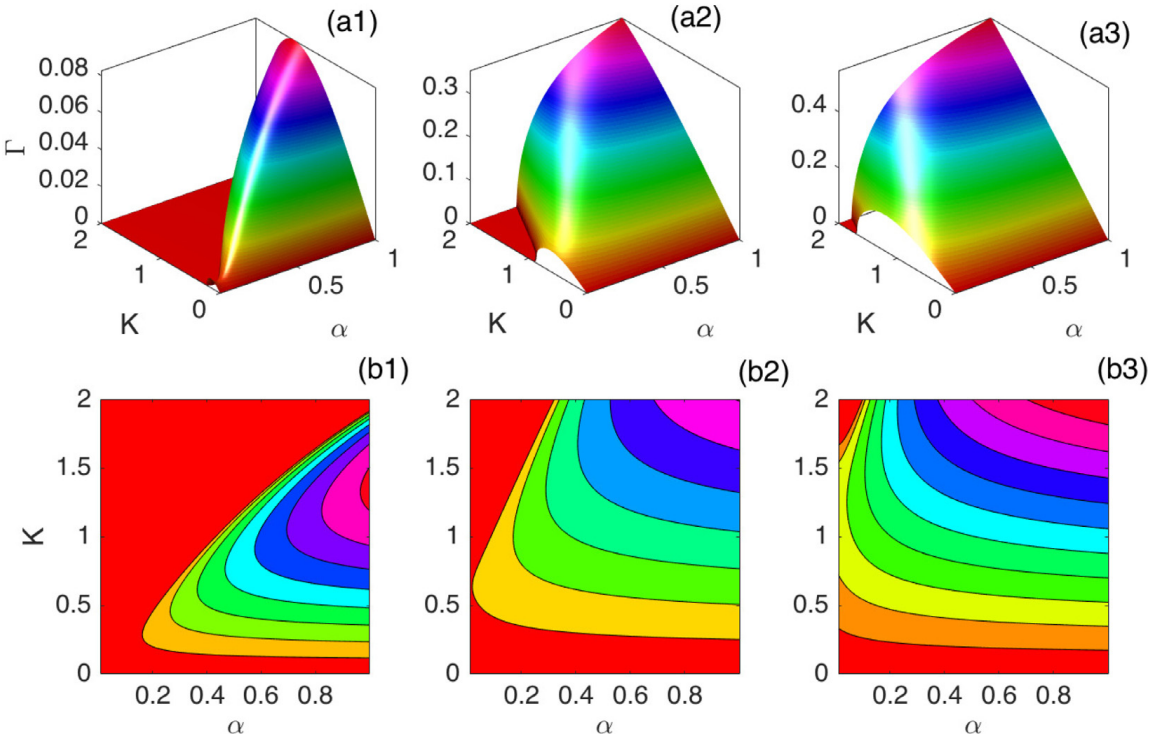

Fig. 12. The GR of MI is plotted versus the wavenumber K and the negative ion concentration ratio. The high $k-$regime has been considered and different values of the initial wavenumber are taken to be: (a1)–(b1) $k = 1.2$, (a2)–(b2) $k = 1.25$ and (a3)–(b3) $k = 1.5$, with $\sigma_n = 17.5$ and $\psi_0 = 0.2$.

5. Conclusion

In the present contribution, we have addressed the formation of modulated IA waves in an electronegative plasma composed of Boltzmann negative ions, Boltzmann electrons and cold mobile positive ions. The reductive perturbation method has been employed to reduce the whole dynamics to a NLS equation, with coefficients depending on the negative ions parameters of the plasma. Exact solutions have been found in the form of bright and "kink-wave" envelopes, and their

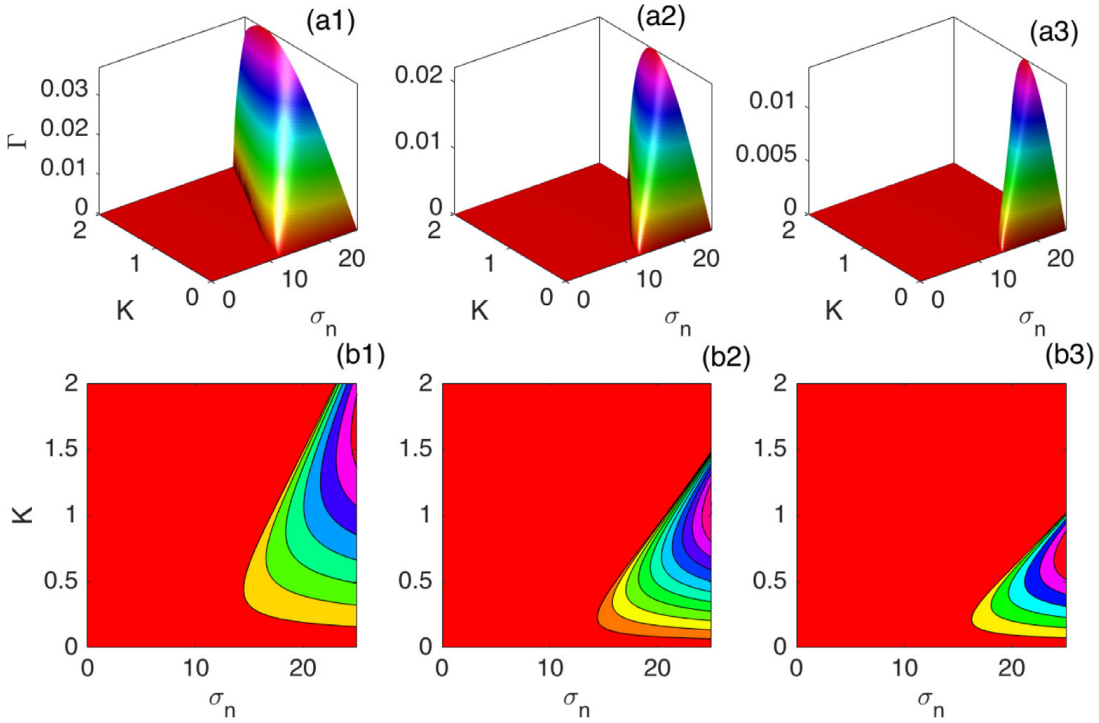

Fig. 13. The growth rate of MI is plotted versus the wavenumber K and the electron-to-negative ion temperature ratio σ_n. The case $k < k_{1,cr}$ has been considered and different values of the initial wavenumber are taken to be: (a1)–(b1) $k = 0.1$, (a2)–(b2) $k = 0.15$ and (a3)–(b3) $k = 0.2$, with $\alpha_n = 0.3$ and $\psi_0 = 0.2$.

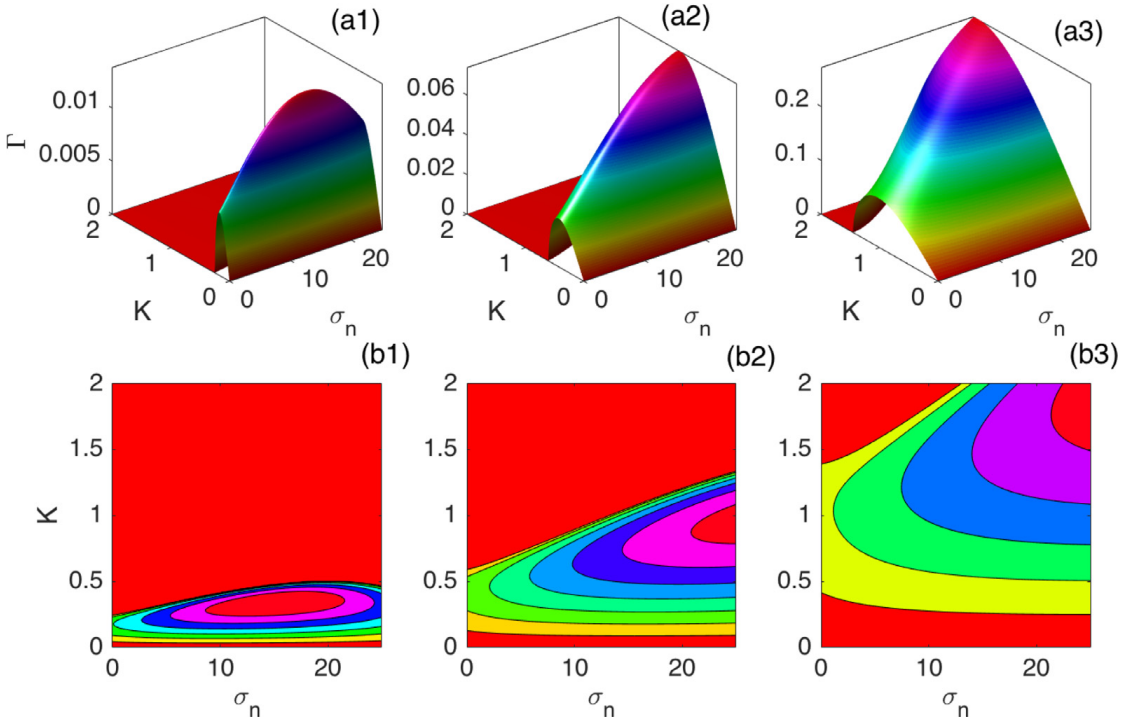

Fig. 14. The GR of MI is plotted versus the wavenumber K and the electron-to-negative ion temperature ratio. The case $k > k_{2,cr}$ has been considered and different values of the initial wavenumber are taken to be: (a1)–(b1) $k = 1.2$, (a2)–(b2) $k = 1.25$ and (a3)–(b3) $k = 1.5$, with $\alpha = 0.3$ and $\psi_0 = 0.2$.

response to the negative ion concentration ratio (α) and the electron-to-negative ion temperature ratio (σ_n) has been discussed. Mainly, we have observed that α and σ_n had divergent effects on the kink-wave solution. The same feature have also been observed in the study of MI, where the occurrence of modulated IA waves has been discussed with respect to some two detected positive intervals of the product PQ. Indeed, negative ions modify the features of the found plasma waves because of their strong effect on the nonlinearity of the system. Albeit the interesting results obtained here, it remains important to address this analysis to more suitable plasma environments with more that one negative ion species, both in the non-relativistic and the relativistic context. Investigations in that direction are being carried out and will be submitted elsewhere for publication.

References

[1] Kodama Y, Hasegawa A. Opt Lett 1992;17:31.
[2] Afanasjev VV. Opt Lett 1993;18:790.
[3] Mohamadou A, Ayissi BE, Kofané TC. Phys Rev E 2006;74:046604.
[4] Maïna I, Tabi CB, Mohamadou A, Ekobena HPF, Kofané TC. Chaos 2015;25:043118.
[5] Etémé AS, Tabi CB, Mohamadou A. Commun Nonl Sci Num Simul 2017;43:211.
[6] Tabi CB, Ondoua RY, Ekobena HP, Mohamadou A, Kofané TC. Phys Lett A 2016a;380:2374.
[7] Mefire GRY, Tabi CB, Mohamadou A, Ekobena HPF, Kofané TC. Chaos 2013;23:033128.
[8] Wamba E, Mohamadou A, Kofané TC. Phys Rev E 2008;77:046216.
[9] Andreev PA, Kuzmenkov LS. Phys Rev A 2008;78:053624.
[10] Becker C, Stellmer S, Soltan-Panahi1 P, Dörscher S, Baumert M, Richter E-M, et al. Nat Phys 2008;4:496.
[11] Zabusky NJ, Kruskal MD. Phys Rev Lett 1965;15:240.
[12] Ikezi H, Taylor R, Baker D. Phys Rev Lett 1970;25:11.
[13] Taylor R, MacKenzie KR, Ikezi H. Rev Sci Instrum 1972;43:1675.
[14] Kimura T, Imagaki K, Ohe K. J Phys D 1998;31:2295.
[15] Rahman O, Mamun AA, Ashrafi KS. Astrophys Space Sci 2001;335:425.
[16] Berezhnoj SV, Shin CB, Buddemeir U, Kaganovich I. Appl Phys Lett 2000;77:800.
[17] Gottscho RA, Gaebe CE. IEEE Trans Plasma Sci 1986;14:92.
[18] Jacquinot J, McVey BD, Scharer JE. Phys Rev Lett 1977;39:88.
[19] Ichiki R, Yoshimura S, Watanabe T, Nakamura Y, et al. Phys Plasmas 2002;9:4481.
[20] Hussain S, Shan SA, Akhtar N, Masud MM. Astrophys Space Sci 2014;352:605.
[21] Shan SA, Akhtar N. Astrophys Space Sci 2013;346:367.
[22] Das GC, Nag A. Assam Univ J Sci Technol 2010;5:169.
[23] Washimi H, Taniuti T. Phys Rev Lett 1966;17:996.
[24] Mehdipoor M. Astrophys Space Sci 2013;348:115.
[25] Nakamura Y, Tsukabayashi I. Phys Rev Lett 1984;52:2356.
[26] Ghim YK, Hershkowitz N. Appl Phys Lett 2009;94:151503.
[27] Mamun AA, Shukla PK, Eliasson B. Phys Rev E 2009;80:046406.
[28] Anowar MG, Ashrafi KS, Mamun AA. J Plasma Phys 2011;77:133.
[29] Duha SS, Rahman MS, Mamun AA, Anowar GM. J Plasma Phys 2012;78:279.
[30] Tabi CB, Maïna I, Mohamadou A, Ekobena HPF, Kofané TC. EPL 2014;106:18005.
[31] Mimshe JCF, Tabi CB, Edongue H, Ekobena HPF, Kofané TC. Phys Scr 2013;87:025801.
[32] Tabi CB, Etémé AS, Mohamdou A. Physica A 2017;474:186.
[33] Tsytovich VN, Vladimirov SV, Morfill GE, Goree J. Phys Rev E 2001;63:056609.
[34] Zheng X, Chen Y, Hu H, Wang G, Huang F, Dong C, et al. Phys Plasmas 2009;16:023701.
[35] Tabi CB, Mohamadou A, Kofané TC. Eur Phys J D 2008;50:307.
[36] Tabi CB, Mohamadou A, Kofané TC. Int J Biomath 2009;2:405.
[37] Tabi CB, Dang AK, Oumarou RD, Ekobena HPF, Kofané TC. Physica A 2016b;442:498.
[38] Tabi CB, Ekobena HPF, Mohamadou A, Kofané TC. Phys Scr 2011;83:035802.
[39] Kourakis I, Shukla PK. Nonl Proc Geophys 2005;12:407.
[40] Mohamadou A, Tatsing PH, Latchio CGT, Tabi CB, Kofané TC. J Mod Opt 2014;61:1670.
[41] Fedele R, Schamel H. Eur Phys J B 2002;27:313.
[42] Fedele R. Phys Scr 2002;65:502.
[43] Alpert Y. Phys Rep 2001;339:323.
[44] Pottelette R, Ergun RE, Treumann RA, Berthomier M, Carlson CW, McFadden JP, et al. Geophys Res Lett 1999;26:2629.

Two-dimensional modulated ion-acoustic excitations in electronegative plasmas

Chérif S. Panguetna, Conrad B. Tabi, and Timoléon C. Kofané

Citation: Physics of Plasmas **24**, 092114 (2017); doi: 10.1063/1.5001725
View online: http://dx.doi.org/10.1063/1.5001725
View Table of Contents: http://aip.scitation.org/toc/php/24/9
Published by the American Institute of Physics

Two-dimensional modulated ion-acoustic excitations in electronegative plasmas

Chérif S. Panguetna,[1,a)] Conrad B. Tabi,[2,3,b)] and Timoléon C. Kofané[1,c)]
[1]*Laboratoire de Mécanique, Département de Physique, Faculté des Sciences, Université de Yaoundé I, B.P. 812 Yaoundé, Cameroun*
[2]*Laboratoire de Biophysique, Département de Physique, Faculté des Sciences, Université de Yaoundé I, B.P. 812 Yaoundé, Cameroun*
[3]*Botswana International University of Science and Technology, Private Bag 16, Palapye, Botswana*

(Received 4 May 2017; accepted 21 August 2017; published online 11 September 2017)

Two-dimensional modulated ion-acoustic waves are investigated in an electronegative plasma. Through the reductive perturbation expansion, the governing hydrodynamic equations are reduced to a Davey-Stewartson system with two-space variables. The latter is used to study the modulational instability of ion-acoustic waves along with the effect of plasma parameters, namely, the negative ion concentration ratio (α) and the electron-to-negative ion temperature ratio (σ_n). A parametric analysis of modulational instability is carried out, where regions of plasma parameters responsible for the emergence of modulated ion-acoustic waves are discussed, with emphasis on the behavior of the instability growth rate. Numerically, using perturbed plane waves as initial conditions, parameters from the instability regions give rise to series of dromion solitons under the activation of modulational instability. The sensitivity of the numerical solutions to plasma parameters is discussed. Some exact solutions in the form one- and two-dromion solutions are derived and their response to the effect of varying α and σ_n is discussed as well. *Published by AIP Publishing.*
[http://dx.doi.org/10.1063/1.5001725]

I. INTRODUCTION

Solitonic structures have long been an attractive topic in nonlinear physics since they arise in nonlinear optics,[1] Bose-Einstein condensates,[2] biophysics,[3–6] and plasma physics,[7–9] just to cite a few. They are in general the results of the interplay between nonlinear and dispersive effects, and can propagate over long distance, keeping their shape and characteristics unchanged. In plasma physics, nonlinear excitations have been intensively investigated as solutions of the nonlinear Schrödinger (NLS) and the Korteweg-de Vries (KdV) equations.[8–12] Plasmas are usually composed of negative ions, positive ions, and electrons, and in the presence of a significant number of negative ions, they are qualified as electronegative plasmas (ENPs).[13–15] The presence of negative ions in a plasma modifies its basic nature and importantly affects wave propagation of various kinds as well as their characteristics. For example, it was reported by Mamun *et al.*[16,17] that negative ions in a plasma modify the nonlinearity of the system and consequently affect the interplay between nonlinear and dispersive effects which are the main conditions for the emergence of ion-acoustics waves (IAWs). The charge neutrality condition gets modified in that context, leading to the increase in the negative ion density, and to the decrease in the number density of electrons. This means that the shielding effect produced by the electrons decreases and the behavior of the plasma consequently changes. Also, it was predicted that negative ions in such plasmas are in Boltzmann equilibrium[19,20] and that was confirmed via some experiments by Ghim and Hershkowitz.[18] A limited number of contributions have been devoted to nonlinear excitations in ENPs,[21–25] and most of the works, to the best of our knowledge, have been limited to one-dimensional plasma systems. Some seminal works on two- and three-dimensional models include the Zakarov-Kuznetsov (ZK) equation,[26,27] the Kadomtsev-Petviashvili (KP) equation,[28,29] and Davey-Stewartson (DS) equations.[30,31] Duha *et al.*[17] studied IAWs in magnetized dusty plasmas via the KP equation and showed that negative ion parameters may importantly affect the characteristics and stability of IAWs. Bedi and Gill[32] successfully derived the DS equation in a plasma in the presence of kappa-distributed hot electrons and established the strong relationship between the nonlinear Schrödinger (NLS) equation and the DS ones. They reinforced the idea of Nishinari *et al.*[33,34] that the DS system is a higher-dimensional generalization of the NLS equation, since it includes transverse scale length and dynamics in the transverse direction. More importantly, the latter might bring about additional nonlinear features compared to the NLS equation and may support very rich behaviors under the activation of multi-dimensional modulational instability (MI) and the subsequent plasma modes. It remains open for us to investigate the behaviors of such modes in ENPs. In the present paper, we propose a comprehensive analysis of MI in the aforementioned vein and show that there is a correlation between the emergence of two-dimensional (2D) modulated IAWs and dromion solitons. Notably, using the Hirota bilinear method, we derive exact one- and two-dromion solutions and we analyze their response to some plasma parameters, especially the negative ion concentration ratio and the

[a)]cherifps@yahoo.fr
[b)]Author to whom correspondence should be addressed: conrad@aims.ac.za. Tel.: +237-6788-735-50.
[c)]tckofane@yahoo.com

electron-to-negative ion temperature ratio. For this purpose, the rest of the paper is outlined as follows: in Sec. II, we introduce the two-dimensional model of ENPs and we use the reductive perturbation expansion to reduce the whole hydrodynamic equations to a set of DS equations. In Sec. III, the two-dimensional MI is addressed, where the response of the MI growth rate to the effect of the negative ion parameters is comprehensively studied, including a comparison between analytical predictions and numerical results. In Sec. IV, one- and two-dromion solitons solutions are presented and their features under the negative ion effect are studied. In that framework, we study different kinds of head-on collisions and discuss the robustness of the dromion structures under wave interaction. Some concluding remarks are given in Sec. V.

II. MODEL EQUATIONS

We consider a three species plasma system composed of Maxwellian electrons and light negative ions, having Boltzmann distribution, in addition to cold mobile positive ions.[35,36] In plasma systems, the charge neutrality condition, i.e., $n_e = n_p - n_n$, gets modified by the presence of negative ions, with n_e, n_p, and n_n being, respectively, the electron, positive, and negative ions densities. The inertia of electrons and negative ions can be neglected because the phase velocity of the IAWs is higher than the positive ion thermal speed and lower than the electron and negative ion thermal speeds.[24,25,37] The formulation of the corresponding model in one-dimension is given in Ref. 37, and we generalize it here to get the following normalized 2D-space equations

$$\frac{\partial n_i}{\partial t} + \mathrm{div}(n_i \vec{v}) = 0, \tag{1a}$$

$$\frac{\partial \vec{v}}{\partial t} + \left(\vec{v} \cdot \overrightarrow{\mathrm{grad}}\right)\vec{v} = -\overrightarrow{\mathrm{grad}}\,\phi, \tag{1b}$$

$$\Delta\phi = \mu_e \exp\phi + \mu_n \exp\sigma_n\phi - n_i, \tag{1c}$$

where n_i is the number density of positive ion, normalized by the unperturbed value n_{i0}. $\vec{v} = u\vec{i} + v\vec{j}$ with u and v being the velocity of charged dusts (with mass m_i) in x and y directions, respectively. Overall charge neutrality at equilibrium is $n_i^{(0)} = n_e^{(0)} + n_n^{(0)}$. The variables appearing in Eqs. (1a) and (1c) have been appropriately normalized. $\vec{v}$ is normalized by the dust-acoustic (DA) speed $c = \sqrt{Zk_BT_e/m_i}$ with T_e denoting the electron temperature, k_B, the Boltzmann constant, and Z, the charged dust state, i.e., the number of electrons per ions residing on the dust-grain surface. ϕ is the electrostatic wave potential normalized by k_BT_e/e, where e is the magnitude of the electron charge. The time and space variables are normalized by the ion Debye length $\lambda_D = (k_BTe/4\pi e^2 n_i)^{1/2}$ and the ion plasma period $\omega^{-1} = (4\pi e^2 n_{i0}/m_i)^{-1/2}$, respectively. Here, $\sigma_n = T_e/T_n$ is the electrons-to-negative ion temperature ratio, $\mu_e = n_{e0}/n_{i0}$ and $\mu_n = n_{n0}/n_{i0}$ where n_{i0}, n_{n0}, and n_{e0} are the unperturbed densities of the positive ions, negative ions, and electrons, respectively. At equilibrium, the neutrality condition of the plasma is $\mu_e + \mu_n = 1$, where $\mu_e = n_{e0}/n_{i0} = 1/(1+\alpha)$, where $\alpha = n_{n0}/n_{e0}$ is the negative ion concentration ratio. Using the power series expansion of the exponential terms in (1c) around zero, it becomes

$$\frac{\partial^2\phi}{\partial^2 x} + \frac{\partial^2\phi}{\partial^2 y} = 1 + a_1\phi + a_2\phi^2 + a_3\phi^3 - n_i, \tag{2}$$

where, $a_1 = \mu_e + \mu_n\sigma_n$, $a_2 = \frac{\mu_e + \mu_n\sigma_n^2}{2}$ and $a_3 = \frac{\mu_e + \mu_n\sigma_n^3}{6}$.

In order to investigate the propagation of IAWs and derive the set of DS equations, we employ the standard reductive perturbation expansion. The stretched variables in space and time may be introduced as $\xi = \epsilon(x - v_g t)$, $\eta = \epsilon y$ and $\tau = \epsilon^2 t$, where v_g is the group velocity that will be found later by the solvability condition of equations (1). ϵ is a small parameter that measures the strength of nonlinearity. The dependent physical variables around their equilibrium values are expanded as follows:

$$\begin{pmatrix} n_i(x,y,t) \\ u_i(x,y,t) \\ v_i(x,y,t) \\ \phi(x,y,t) \end{pmatrix} = \begin{pmatrix} 1 \\ 0 \\ 0 \\ 0 \end{pmatrix} + \sum_{p=1}^{\infty}\epsilon^p \sum_{l=-\infty}^{+\infty} \begin{pmatrix} n_l^{(p)}(\xi,\eta,\tau) \\ u_l^{(p)}(\xi,\eta,\tau) \\ v_l^{(p)}(\xi,\eta,\tau) \\ \phi_l^{(p)}(\xi,\eta,\tau) \end{pmatrix} A^l(n,t). \tag{3}$$

Obviously, the above series includes all overtones $A^l(x,t) = \exp[il(kx - \Omega t)]$ up to order p. These are due to some nonlinear terms, which implies that the corresponding coefficients are of maximum order ϵ^p, along with the relations $(n_{il}^{(p)})^* = n_{i-l}^{(p)}$, $(u_l^{(p)})^* = u_{-l}^{(p)}$, $(v_l^{(p)})^* = v_{-l}^{(p)}$ and $(\phi_l^{(p)})^* = \phi_{-l}^{(p)}$. The asterisk denotes the complex conjugate. We substitute solutions (3) into Eqs. (1a), (1b), and (2), and we equate each coefficient in powers of ϵ to zero. We obtain, at order $O(\epsilon^1)$, for $l = 1$, the solutions

$$\phi_1^{(1)} = \frac{1}{k^2 + a_1} n_{i1}^{(1)}, \quad u_1^{(1)} = \frac{\omega}{k} n_{i1}^{(1)}, \quad v_1^1 = 0, \tag{4}$$

which exist only if the dispersion relation

$$\omega^2 = \frac{k^2}{k^2 + a_1}, \tag{5}$$

is satisfied. At the same order, but for $l = 0$, we obtain $n_{i0}^{(1)} = u_0^{(1)} = v_0^{(1)} = \phi_0^{(1)} = 0$. The coefficients of the second harmonic, at order $O(\epsilon^2)$, may be found using the same procedure. This leads for example to the equation

$$a_1\phi_0^{(2)} - n_{i0}^{(2)} - 2a_2|\phi_1^{(1)}|^2 = 0, \tag{6}$$

for $l = 0$, and the set of equations

$$\begin{aligned} &-v_g\frac{\partial n_{i1}^{(1)}}{\partial\xi} - i\omega n_{i1}^{(2)} + iku_1^{(2)} + \frac{\partial u_1^{(1)}}{\partial\xi} = 0, \\ &-i\omega v_1^{(2)} = -\frac{\partial\phi_1^{(1)}}{\partial\eta} - v_g\frac{\partial u_1^{(1)}}{\partial\xi} - i\omega u_1^{(2)} + ik\phi_1^{(2)} = -\frac{\partial\phi_1^{(1)}}{\partial\xi}, \\ &(k^2 + a_1)\phi_1^{(2)} - n_{i1}^{(2)} = 2ik\frac{\partial\phi_1^{(1)}}{\partial\xi}, \end{aligned} \tag{7}$$

for $l = 1$, from which the solvability condition

$$v_g = a_1 \frac{\omega^3}{k^3}, \tag{8}$$

is obtained, along with the solutions

$$v_1^{(2)} = \frac{-i}{\omega(k^2+a_1)}\frac{\partial n_1^{(1)}}{\partial \eta}, \quad \phi_1^{(2)} = \frac{n_1^{(2)}}{(k^2+a_1)} + \frac{2ik}{(k^2+a_1)^2}\frac{\partial n_1^{(1)}}{\partial \xi},$$
$$u_1^{(2)} = \frac{ik}{(k^2+a_1)^{3/2}}\frac{\partial n_1^{(1)}}{\partial \xi} + \frac{\omega}{k} n_1^{(2)}. \tag{9}$$

For $l=2$, we extract the set of equations

$$\begin{aligned} &-2i\omega n_{i2}^{(2)} + 2iku_2^{(2)} + 2ikn_{i1}^{(1)}u_1^{(1)} = 0,\\ &-2i\omega u_2^{(2)} + ik(u_1^{(1)})^2 + 2ikn_{i1}^{(1)}u_1^{(1)} = 0,\\ &(4k^2+a_1)\phi_2^{(2)} - n_{i2}^{(2)} + a_2(\phi_1^{(1)})^2 = 0 \quad \text{and} \quad -2i\omega v_2^{(2)} = 0, \end{aligned} \tag{10}$$

which admits the solutions

$$\phi_2^{(2)} = \alpha_\phi (n_{i1}^{(1)})^2, \quad n_{i2}^{(2)} = \alpha_n (n_{i1}^{(1)})^2, \quad u_2^{(2)} = \alpha_u (n_{i1}^{(1)})^2,$$
$$v_2^{(2)} = 0, \tag{11}$$

with

$$\alpha_\phi = \frac{1}{2k^2} - \frac{a_2}{3k^2(k^2+a_1)^2},$$
$$\alpha_n = (a_1+4k^2)\alpha_\phi + \frac{a_2}{(k^2+a_1)^2}, \quad \alpha_u = \frac{\omega}{k}(\alpha_n - 1). \tag{12}$$

The zeroth harmonic mode also appears due to the self-interaction of the modulated carrier wave. Its expression cannot be determined completely within the second order, and we will have to consider the third-order equations. Thus, the set of equations corresponding to the $(l=0)-$ components of the third-order part of the reduced equations is given by

$$\begin{aligned} &-v_g\frac{\partial n_{i0}^{(2)}}{\partial \xi} + \frac{\partial u_0^{(2)}}{\partial \xi} + \frac{\partial v_0^{(2)}}{\partial \eta} + \frac{2}{(k^2+a_1)^{1/2}}\frac{\partial |n_{i1}^{(1)}|^2}{\partial \xi} = 0,\\ &-v_g\frac{\partial u_0^{(2)}}{\partial \xi} + \frac{\partial \phi_0^{(2)}}{\partial \xi} + \frac{1}{k^2+a_1}\frac{\partial |n_{i1}^{(1)}|^2}{\partial \xi} = 0,\\ &-v_g\frac{\partial v_0^{(2)}}{\partial \xi} + \frac{\partial \phi_0^{(2)}}{\partial \eta} + \frac{1}{k^2+a_1}\frac{\partial |n_{i1}^{(1)}|^2}{\partial \eta} = 0, \end{aligned} \tag{13}$$

to which we have added Eq. (6) from the order $(\epsilon^2, l=0)$. This leads to

$$\delta_1\frac{\partial^2\phi_0^2}{\partial \xi^2} - \frac{\partial^2\phi_0^2}{\partial \eta^2} - \delta_2\frac{\partial^2|n_{i1}^{(1)}|^2}{\partial \xi^2} - \delta_3\frac{\partial^2|n_{i1}^{(1)}|^2}{\partial \eta^2} = 0, \tag{14}$$

with

$$\delta_1 = v_g^2 a_1 - 1, \quad \delta_2 = \frac{2v_g}{(k^2+a_1)^{1/2}} + \frac{1}{k^2+a_1} - \frac{2a_2v_g^2}{(k^2+a_1)^2},$$
$$\delta_3 = \frac{1}{k^2+a_1}. \tag{15}$$

The various expressions found in the above calculations are then introduced into the $(l=1)$-component of the third-order part of the equations. One then finds the following amplitude equation

$$i\frac{\partial n_{i1}^{(1)}}{\partial \tau} + \gamma_1\frac{\partial^2 n_{i1}^{(1)}}{\partial \xi^2} + \gamma_2\frac{\partial^2 n_{i1}^{(1)}}{\partial \eta^2} + \gamma_3|n_{i1}^{(1)}|^2 n_{i1}^{(1)} + \gamma_4\phi_0^{(2)}n_{i1}^{(1)} = 0, \tag{16}$$

with the coefficients

$$\gamma_1 = \frac{3ka_1}{2(k^2+a_1)^{5/2}}, \gamma_2 = \frac{a_1}{2k(k^2+a_1)^{3/2}},$$
$$\gamma_3 = -\frac{k}{2(k^2+a_1)^{1/2}}\left[6 + \frac{2k^2}{a_1} + \frac{3a_1}{2k^2} - \frac{4a_2}{3k^2(k^2+1)} - \frac{2a_2}{3k^2} + \frac{2a_2}{(k^2+a_1)^2} + \frac{2a_2^2}{3k^2(k^2+a_1)^3} - \frac{3a_3}{(k^2+a_1)^3}\right],$$
$$\gamma_4 = -\frac{k(k^2+a_1)^{3/2}}{a_1} - \frac{ka_1}{2(k^2+a_1)^{1/2}} + \frac{ka_2}{(k^2+a_1)^{3/2}}. \tag{17}$$

Further introducing the notations $F = n_{i1}^{(1)}$ and $G = \phi_0^{(2)}$, Eqs. (16) and (14) become

$$i\frac{\partial F}{\partial \tau} + \gamma_1\frac{\partial^2 F}{\partial \xi^2} + \gamma_2\frac{\partial^2 F}{\partial \eta^2} + \gamma_3|F|^2F + \gamma_4 GF = 0, \tag{18a}$$

$$\delta_1\frac{\partial^2 G}{\partial \xi^2} - \frac{\partial^2 G}{\partial \eta^2} - \delta_2\frac{\partial^2|F|^2}{\partial \xi^2} - \delta_3\frac{\partial^2|F|^2}{\partial \eta^2} = 0. \tag{18b}$$

Equation (18) are the well-known DS equations in two-space that was initially derived by Davey and Stewartson to describe modulated waves packets in water of finite depth.[38] Thereafter, it was shown to admit soliton-like solutions via the inverse scattering transform.[39] A rigorous derivation of the DS equations was proposed in Ref. 40 in the context of nonlinear propagation of gravity-capillary surface waves under tension. One may also cite many contributions devoted to multi-dimensional classical plasma systems.[30,32–34,41] Specifically, DS equations were shown to arise in multi-dimensional plasmas under the assumption that ion waves were parallel to the magnetic field.[34] In the previous case, the electronegative character of the plasma was ignored leading to the simplified case $a_1 = 1$, i.e., $\omega^2 = \frac{k^2}{k^2+1}$, therefore giving rise to the modification in the group velocity as clearly pictured in Fig. 1. For the frequency, in the presence of negative ions, the upper cut-off value drops, while for the group velocity, the lower cut-off value drops and its upper cut-off value increases. This clearly shows that the presence of negative ions may bring about important features in the formation 2D IAWs. Also, we clearly see that the coefficients (15) and (17) of the DS system depend on the negative ion parameters, which in turn affect their sign and consequently the MI of plane wave solutions as supported by Sec. III.

III. MODULATIONAL INSTABILITY

The DS equations govern the MI of 2D IAWs, and we look for the stability/instability conditions for the emergence

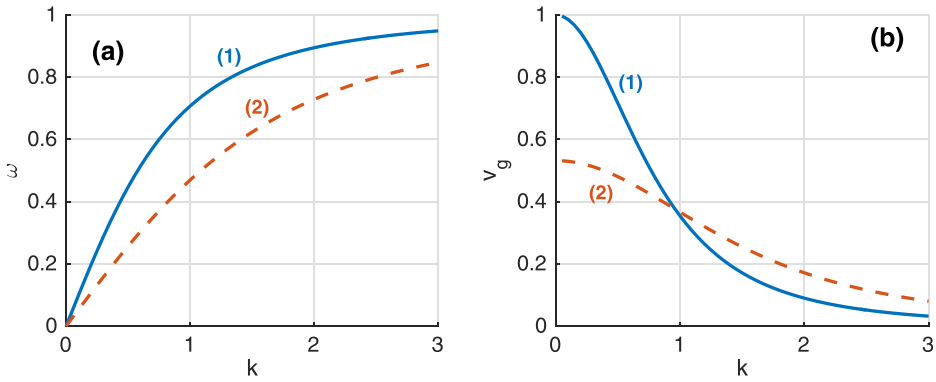

FIG. 1. The panels show (a), the frequency and (b), the group velocity versus the wavenumber k. The curves labelled by (1) and (2) correspond, respectively, to the simple plasma, with only one ion species, and to the electronegative plasma.

of modulated waves in ENPs. Similar procedure was adopted in Refs. 30, 33, and 34 on a simplified 2D model, i.e., by considering only one ion type. Homogeneous solutions for the DS system are usually considered in the form $F = F_0 \exp i(\alpha_1\xi + \alpha_2\eta - \Omega\tau + \varphi)$, $G = G_0$, where $F_0, G_0, \alpha_1, \alpha_2$ and ϕ are real constants. The above trial solutions may propagate in the system under the condition that the dispersion relation $\Omega = \gamma_1\alpha_1^2 + \gamma_2\alpha_2^2 - \gamma_3 F_0^2 - \gamma_4 G_0$ be satisfied. Small perturbations are usually introduced into such solutions in order to test their stability and robustness. We therefore consider the perturbed solutions

$$F = (F_0 + \Delta F)e^{i(\alpha_1\xi+\alpha_2\eta-\Omega\tau+\varphi+\Delta\varphi)}, \quad G = G_0 + \Delta G, \quad (19)$$

where the perturbations ΔF, ΔG, and $\Delta\varphi$ are assumed in the form

$$\begin{pmatrix}\Delta F\\ \Delta G\\ \Delta\varphi\end{pmatrix} = \begin{pmatrix}\delta F\\ \delta G\\ \delta\varphi\end{pmatrix}\mathrm{Re}\{e^{i(\mu_1\xi+\mu_2\eta-\nu\tau)}\}. \quad (20)$$

Making use of the above and linearizing around the unperturbed plane waves lead to a homogeneous system in δF, δG, and $\delta\varphi$, which admits non-trivial solutions if its determinant is zero. This yields the nonlinear dispersion relation

$$\nu_1^2 = (\mu_1^2\gamma_1 + \mu_2^2\gamma_2)\Big(\mu_1^2\gamma_1 + \mu_2^2\gamma_2 - 2\gamma_3 F_0^2 + 2\gamma_4 F_0^2\frac{\mu_1^2\delta_2 + \mu_2^2\delta_3}{\mu_2^2 - \mu_1^2\beta_1}\Big), \quad (21)$$

where $\nu_1 = (\nu - 2\gamma_1\mu_1\alpha_1 - 2\gamma_2\mu_2\alpha_2)$. The plane wave will then be said to be unstable under modulation if $\nu_1^2 < 0$, i.e.,

$$(\mu_1^2\gamma_1 + \mu_2^2\gamma_2)^2 \times\left\{1 - 2F_0^2\left(\frac{\gamma_3(\mu_2^2 - \mu_1^2\beta_1) - \gamma_4(\mu_1^2\delta_2 + \mu_2^2\delta_3)}{(\mu_2^2 - \mu_1^2\beta_1)(\mu_1^2\gamma_1 + \mu_2^2\gamma_2)}\right)\right\} < 0. \quad (22)$$

Obviously, the stability/instability condition only depends on the term in brackets, which also give the threshold amplitude

$$F_{0,cr}^2 = \frac{1}{2}\frac{(\mu_2^2 - \mu_1^2\beta_1)(\mu_1^2\gamma_1 + \mu_2^2\gamma_2)}{\gamma_3(\mu_2^2 - \mu_1^2\beta_1) - \gamma_4(\mu_1^2\delta_2 + \mu_2^2\delta_3)}, \quad (23)$$

above which modulated IAWs may be observed. Beforehand, it was shown in Refs. 37 and 42 that some values of α and σ_n do not support the formation of nonlinear waves in ENPs. In order to verify this for the rest of the calculations, we have first plotted the growth rate of MI versus the negative ion concentration ratio α, for different values of σ_n, with fixed perturbation wavenumbers μ_1 and μ_2. The growth rate plotted in Fig. 2 is in general given by $\Gamma = \sqrt{-\nu_1^2}$. For unstable patterns to be observed, the growth rate of instability should be positive. Indeed, the results presented in Fig. 2 confirm the fact that not all the values of the plasma parameters will lead to solitonic structures in the studied plasma system. In the first case, for $k = 0.8$, there are clearly two regions where $\Gamma > 0$, with one belonging to the interval $\alpha < 0.16$ and the other appearing in the interval

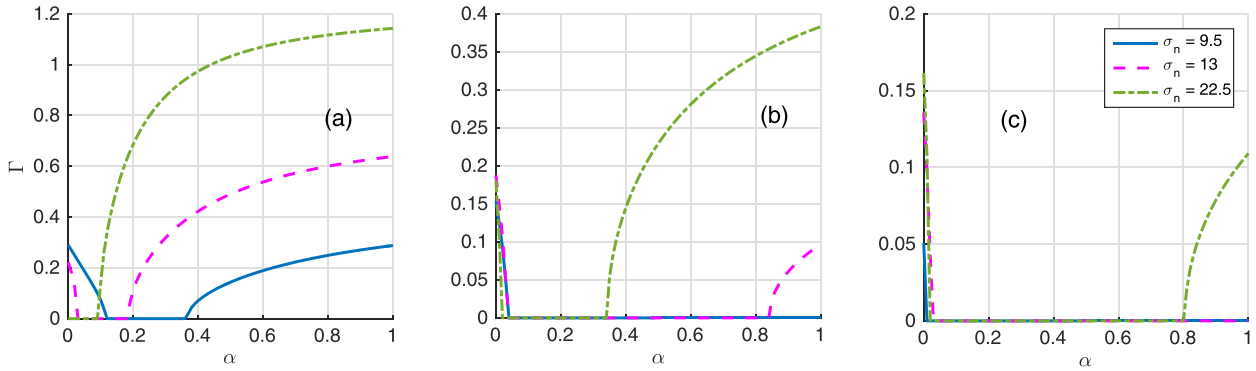

FIG. 2. Instability growth rate versus α, the negative ion concentration ratio. Instability features are obtained for different values of σ_n. Panel (a) corresponds to $k = 0.8$, panels (b) and (c) to $k = 1.2$ and 1.5, respectively. The intervals of α that may lead to unstable IAWs are those corresponding to $\Gamma > 0$. The rest of parameter values are as follows: $\alpha_1 = \alpha_2 = 1.8$, $F_0 = 0.25$, $G_0 = 0.03$, and $\mu_1 = \mu_2 = 1.25$.

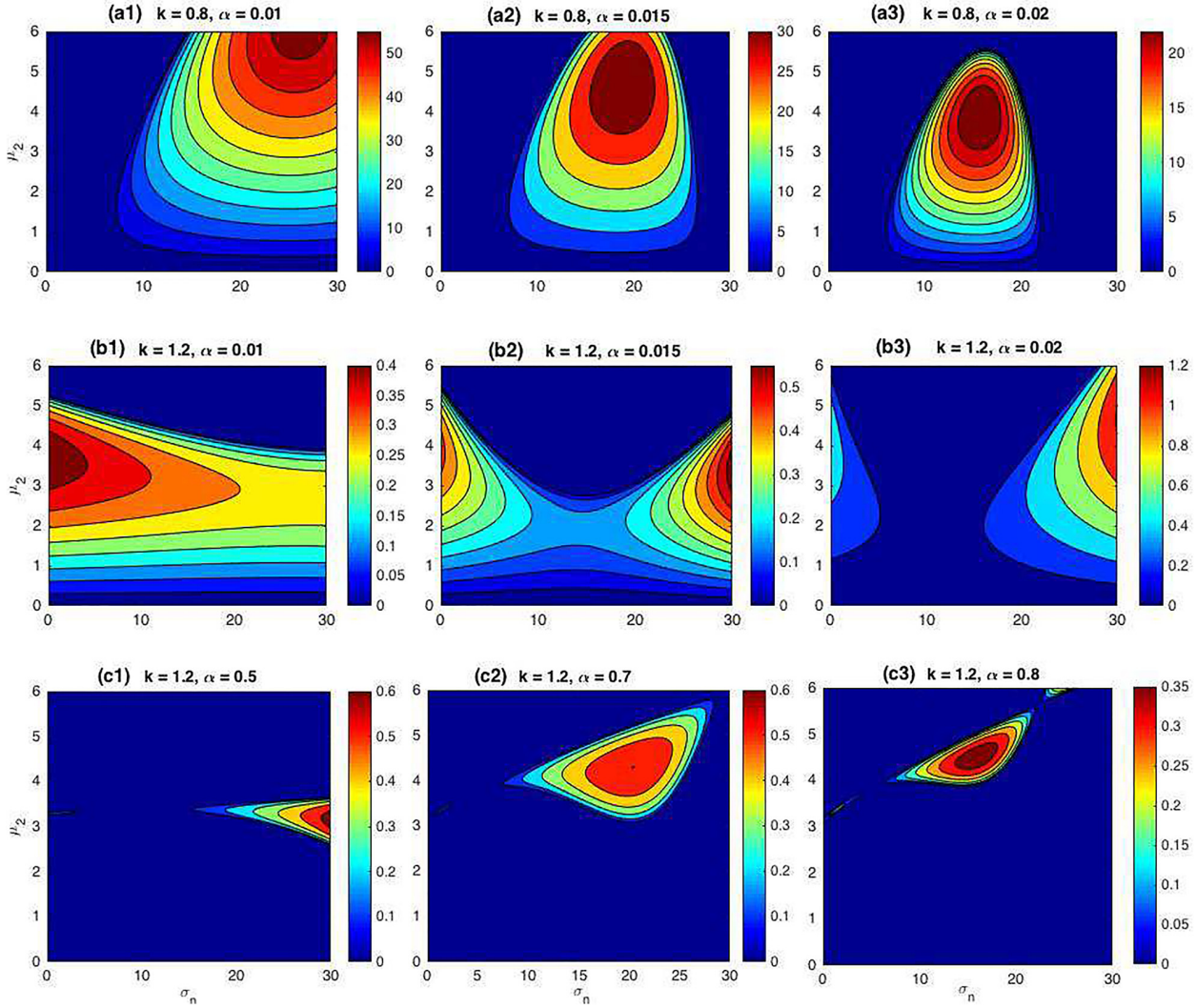

FIG. 3. The instability growth rate is plotted in the $(\sigma_n, \mu_2)-$ plane in agreement with the intervals of α found in Fig. 2. In panels $(\text{aj})_{j=1,2,3}$, we have fixed $k = 0.8$ and: (a1) $\alpha = 0.01$, (a2) $\alpha = 0.015$, and (a3) $\alpha = 0.02$. In panels $(\text{bj})_{j=1,2,3}$, we consider $k = 1.2$, while α takes the respective values as in panels (aj). Panels $(\text{bj})_{j=1,2,3}$ are plotted for $k = 1.2$, but α takes the respective values 0.5, 0.7, and 0.8, which corresponds to the respective panels (c1), (c2), and (c3). We have also fixed $\alpha_1 = \alpha_2 = 1.8$, $F_0 = 0.25$, $G_0 = 0.03$, and $\mu_1 = 1.25$.

$\alpha > 0.38$. The second interval expands with increasing σ_n, while the first tends to disappear for high values of the negative-ion temperature ratio σ_n. Fixing $k = 1.2$, the same behavior persists, except that for $\sigma_n = 9.5$, only the interval of the small α appears, while the interval for high α latter appears when σ_n increases. One may also notice the behavior in Fig. 2(c) of Γ, where additional unstable regions appear for higher σ_n and $k = 1.5$.

Using these intervals of α, we have illustrated some features of the instability spectrum in Fig. 3 in the $(\sigma_n, \mu_2)-$ plane for α picked respectively from small and high regions of Fig. 2, with different values of k and $\mu_1 = 1.25$. Note that regions with contour lines indicate where unstable wave patterns are expected to develop, while the plane wave is supposed to remain stable in the remaining blue regions. In Fig. $3(\text{aj})_{j=1,2,3}$, we have for example fixed $k = 0.8$, when α takes the respective values 0.01 [Fig. 3(a1)], 0.015 [Fig. 3(a2)], and 0.02 [Fig. 3(a3)]. Obviously, with increasing the negative ion concentration ratio, the region of instability gets more and more reduced and the highest value of the growth rate delocalizes. To plot Fig. $3(\text{bj})_{j=1,2,3}$, we have considered $k = 1.2$, α keeping the respective values as previously. Interestingly, the single region of instability observed here progressively splits into two regions with increasing α. Also, the left region of instability tends to disappear in favor of the right one, therefore leading almost to the case of Fig. 3(a1). The last case, i.e., Fig. $3(\text{cj})_{j=1,2,3}$, has been obtained for $k = 1.2$, but with α taking high values, i.e., 0.5 [Fig. 3(c1)], 0.7 [Fig. 3(c2)], and 0.8 [Fig. 3(c3)]. The features of instability are different in this case, and the instability region delocalizes as α increases. Also, for the particular case of Fig. 3(c2), the region where IAWs are expected is quite large compared to the other two cases. We also confirm that the case of Fig. 3(c3) is included in Fig. 3(c2).

To remind, when parameters are picked from regions of instability, nonlinear modulated IAWs are expected to evolve in the system. This is confirmed to be fully sensitive to the electronegative character of the plasma studied here, which implies that the criterion (22) gives more exotic behaviors of the instability of IAWs than the one-

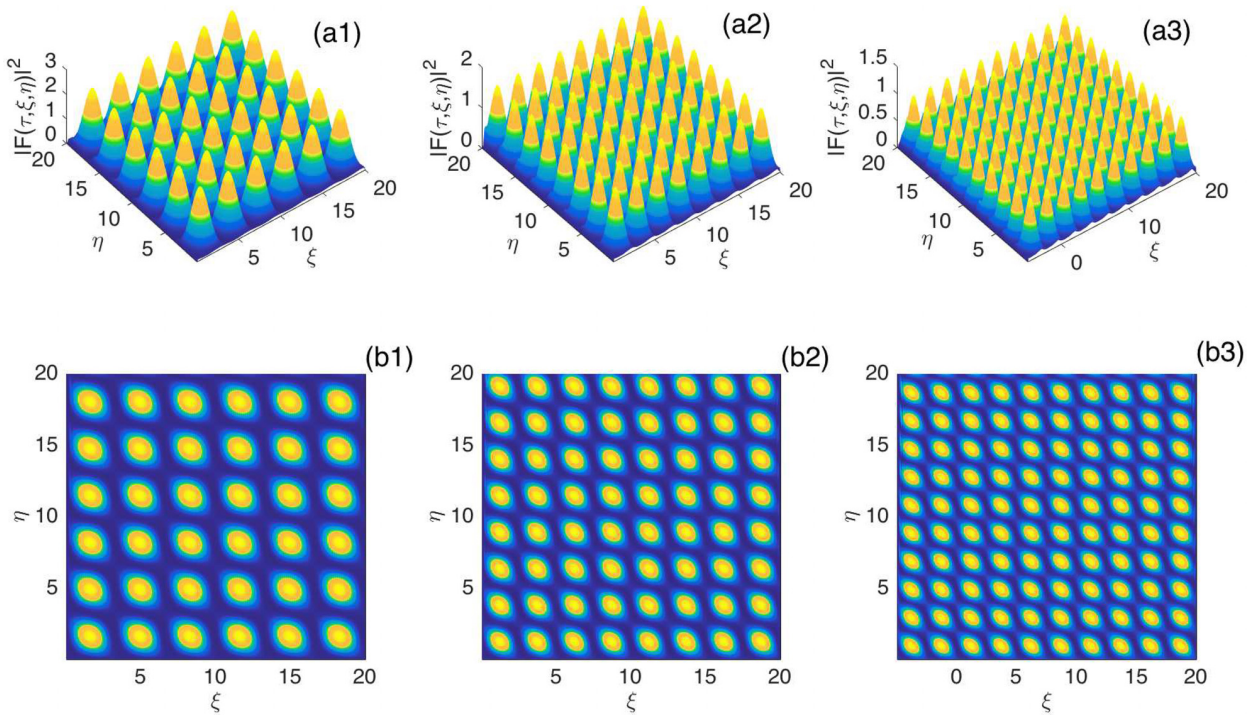

FIG. 4. The panels show wave patterns due to MI in the DS model (18), using Eq. (19) as initial conditions. Numerical solutions are obtained at time $\tau = 200$. Panels (a1)–(b1) have been plotted for $(\alpha = 0.01; \sigma_n = 12.5)$, panels (a2)–(b2) for $(\alpha = 0.02; \sigma_n = 12.5)$ and panels (a3)–(b3) $(\alpha = 0.9; \sigma_n = 22.5)$, with the other parameter values being: $\alpha_1 = \alpha_2 = 1.8$, $F_0 = 0.25$, $G_0 = 0.03$, and $\mu_1 = \mu_2 = 1.25$ and $k = 1.2$.

dimensional case, and particularly the case that does not specifically include the presence of negative ions among other species. Nevertheless, the linear stability analysis gives only information about the regions of parameters where the trains of waves and soliton-like structures may be expected. It does not say anything about the long-time evolution of the investigated waves. Appropriate numerical results, via direct numerical simulation of the DS equation (18), using Eq. (19) as initial conditions, are consequently depicted in Fig. 4. Parameters have mainly been picked from the theoretically predicted instability regions of Fig. 3, which confirms the accuracy of our stability analysis of the plane wave solution. We should stress that unstable regions of parameters are those where the plane wave solution breaks into solitonic trains as the result of the competition between nonlinearity and dispersion. Here obviously, we spontaneously get dromion-lattice structures, significant excitations that are localized in all directions of the plasma with constant period. Figure 4(aj)$_{j=1,2,3}$ show the amplitude of $F(\tau, \xi, \eta)$ and Fig. 4(bj)$_{j=1,2,3}$ show their corresponding density plots at time $\tau = 200$. Most importantly, it is clearly visible that the frequency of the obtained patterns is very sensitive to the variation of the electronegative parameters α and σ_n. For the case of Figs. 4(a1)–(b1) and 4(a2)–(b2), for example, we have, respectively, fixed $(\alpha = 0.02; \sigma_n = 12.5)$ and $(\alpha = 0.08; \sigma_n = 12.5)$. With increasing the value of α, with σ_n constant, there is an increase in the frequency of the dromion-lattices. This was already pointed out by El-Tantawy *et al.*[43] in the case of the breather solutions of the one-dimensional model. We should stress that values for α and σ_n to illustrate these two cases were picked from Fig. 3(a3). In Figs. 4(a3)–4(b3), we have rather considered the couple of parameters $(\alpha = 0.9; \sigma_n = 22.5)$, which corresponds to the region of instability detected in Fig. 3(c2). For these regions, one notices a significant increase in the frequency of the dromions, which shows that α and σ_n cause the explosion of unstable wave patterns. Moreover, one might notice the decrease in the wave amplitude when α and σ_n increase. In the recent years, dromion solitons have been found to be exact solutions for the DS-I equation. The fact that they are obtained here under the activation of MI is a clear sign that when the values of parameters are suitably chosen, the set of Eq. (18) may adopt the DS-I equation comportment and exact dromion solutions may therefore be derived as proposed in Sec. IV.

IV. ONE- AND TWO-DROMION STRUCTURES

The DS equations are divided into two types, the DS-I and DS-II equations, depending on the sign and values of parameters, and the physical systems studied.[44,45] Here, obviously, from the results of Sec. III, one may obtain the two types of systems. However, the dromion soliton solutions obtained numerically in Fig. 4 are solutions of the DS-I system. It has been shown that the system of Eq. (18) may display DS-I behaviors if the conditions[46]

$$\gamma_1/\gamma_2 > 0 \quad \text{and} \quad \gamma_3 > 0, \tag{24}$$

are satisfied. These might then be the necessary conditions to find dromion solutions. The regions of parameters where this is possible are displayed in Fig. 5, where γ_1/γ_2 and γ_3 are plotted versus the wavenumber k, for different values of the

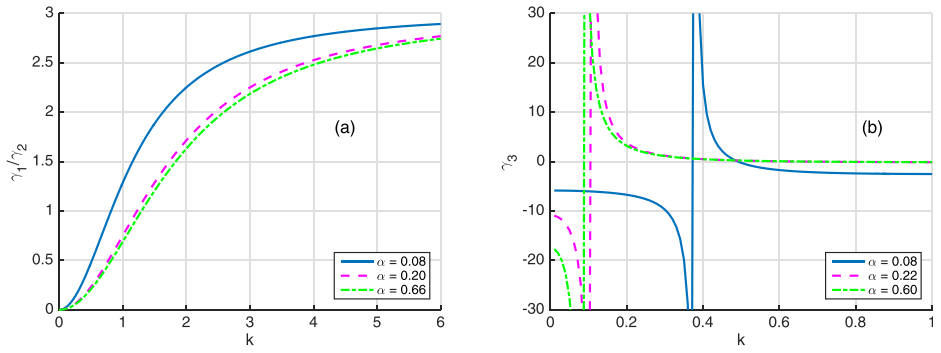

FIG. 5. (a) γ_1/γ_2 is plotted versus the wave number k for $\sigma_n = 12.5$, with different values of α_n picked from the diagrams of Fig. 2. (b) γ_3 is plotted versus k under the same conditions, using the same values of parameters. For any $k>0$, γ_1/γ_2 is positive, while γ_3 presents positive and negative regions.

negative ion concentration ratio α. In Fig. 5(a), the first condition is exclusively fulfilled, given that γ_1/γ_2 is always positive for any $k>0$. Obviously, the condition on γ_3 is the only one that influences the form of Eq. (18) [see Fig. 5(b)]. It should be noticed that the intervals of k, where $\gamma_3>0$, changes with α and there Eq. (18) will take the DS-I form. Otherwise, when $\gamma_3<0$, Eq. (18) will turn into the DS-II form. In the particular case of Fig. 5, the region where $\gamma_3>0$ gets expanded with increasing α. Here, we have fixed $\sigma_n = 12.5$. In order to complete this analysis, we have increased σ_n to 22.5 to plot γ_3 as given by Fig. 6. Contrarily to what is observed in Fig. 5, the region where $\gamma_3>0$ gets reduced when α increases. It is important to precise that together with the wavenumber k, the plasma parameters α and σ_n have been shown to importantly influence the occurrence of MI and in turn, some of the regions where γ_3 is positive are those detected in the study of MI, principally in Fig. 2. Such values will also be used in the rest of the paper in order to bring out the relationship between MI and solitons in the studied plasma system. Using this, finding solutions for Eq. (18) might require the dependent and independent variables to be rescaled so that

$$Q=\gamma_3|F|^2+\gamma_4 G,\quad \xi'=\frac{1}{\sqrt{\delta_1\gamma_3+\delta_2\gamma_4}}\xi,\quad \eta'=\frac{1}{\sqrt{\gamma_3-\delta_3\gamma_4}}\eta. \tag{25}$$

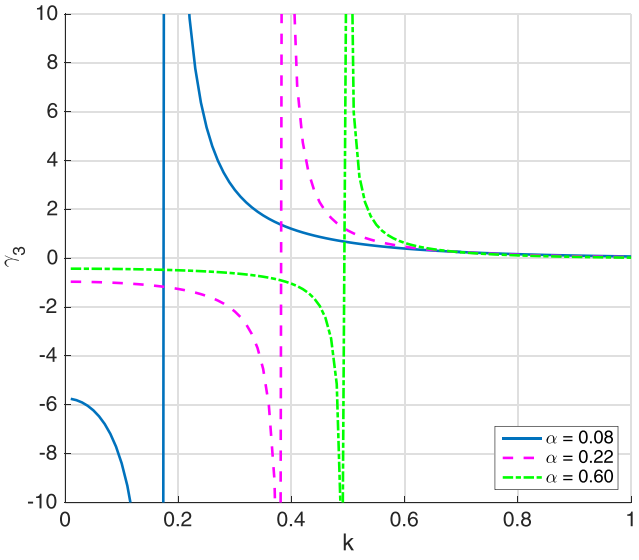

FIG. 6. γ_3 is plotted versus the wavenumber k for $\sigma_n = 22.5$, with α taking different values as predicted in the diagrams of Fig. 2. For any $k>0$, γ_3 presents positive and negative regions, which correspond to the DS-I domain.

We also rotate the coordinate axes by 45°, and we introduce the following new independent variables:

$$X=\frac{1}{\sqrt{2}}(\xi'+\eta'),\qquad Y=\frac{1}{\sqrt{2}}(\xi'-\eta'). \tag{26}$$

Substituting the above into Eq. (18) leads to the following idealized form of the DS-I system

$$iF_\tau + a(F_{XX}+F_{YY}) + bF_{XY} + FQ = 0; \tag{27a}$$

$$a'(Q_{XX}+Q_{YY}) + b'Q_{XY} + 2(|F|)^2_{XY} = 0, \tag{27b}$$

where a, a', b and b' are constants given by

$$\begin{aligned} a &= \frac{\gamma_1}{2(\delta_1\gamma_3+\delta_2\gamma_4)}+\frac{\gamma_2}{2(\gamma_2-\delta_3\gamma_4)},\\ b &= \frac{\gamma_1}{2(\delta_1\gamma_3+\delta_2\gamma_4)}-\frac{\gamma_2}{2(\gamma_2-\delta_3\gamma_4)},\\ a' &= \frac{\delta_1}{2(\delta_1\gamma_3+\delta_2\gamma_4)}-\frac{1}{2(\gamma_2-\delta_3\gamma_4)},\\ b' &= \frac{\delta_1}{2(\delta_1\gamma_3+\delta_2\gamma_4)}+\frac{1}{2(\gamma_2-\delta_3\gamma_4)}. \end{aligned} \tag{28}$$

It is obvious that even after the different transformations, the above set of equations still depends on the plasma parameters, especially α and σ_n.

In order to solve Eq. (27), they can be transformed into the bilinear forms

$$D_{XY}f.f = m(g\cdot g^*) \text{ and } (iD_\tau + a(D_{XX}+D_{YY}) + bD_{XY})g\cdot f = 0, \tag{29}$$

through the variable transformation

$$F=\frac{g}{f}\quad\text{and}\quad Q=c(\ln f)_{XY}, \tag{30}$$

where the Hirota bilinear $D-$ operator is defined by

$$D_x^n g\cdot f = (\partial_{x_1}-\partial_{x_2})^n f(x_1)g(x_2)|_{x_2=x_1=x}. \tag{31}$$

The functions f and g can be expanded in the form of power series as $f = 1+\delta^2 f_2+\delta^4 f_4$ and $g=\delta g_1+\delta^3 g_3$, where δ is an arbitrary parameter. The different solutions are found by

replacing f and g into (29) and collecting terms with the same power in δ. The remaining calculations are made to find g_1, g_3, f_2, and f_4. However, a general expression for g_1 is given by

$$g_1 = \sum_{j=1}^{N} \exp\theta_j, \quad \text{with } \theta_j = k_j X + l_j Y - i\omega_j t + \alpha_j, \tag{32}$$

where k_j, l_j, and α_j are complex constants. For the rest, the Hirota method is straightforward and well-documented nowadays. The one- and two-dromion solutions have been proposed in Ref. 46. In what follows, we exploit those results in order to discuss the features of such waves in the model under our study.

A. The one-dromion soliton

The generalized form of the one-soliton solution is given by

$$F_{1D} = \frac{g_{1D}}{f_{1D}} = \frac{\rho \exp(\theta_1 + \theta_2)}{1 + \alpha \exp(\theta_1 + \theta_1^*) + \beta \exp(\theta_2 + \theta_2^*) + \gamma \exp(\theta_1 + \theta_1^* + \theta_2 + \theta_2^*)}, \tag{33}$$

where $|\rho|^2 = (p_1 + p_1^*)(p_2 + p_2^*)(\gamma - \zeta\beta)$, $\theta_1 = p_1 X + \omega_1 t + \alpha_1$ and $\theta_2 = p_2 Y + \omega_2 t + \alpha_2$, with ζ, β, and γ being real positive constants, $\omega_1 = iap_1^2$ and $\omega_2 = iap_2^2$. It should be noticed that the relative sign of the real parts of p_1 and p_2 determines whether γ should be larger or smaller than $\zeta\beta$. Using suitable values of parameters, especially the couple (α, k), we obtain the one-dromion solition shown in Figs. 7(a)–7(d), where upper panels show plots of the dromion solution and the lower panels display their density plots. From solution (33), $\phi_1^{(1)}(X, Y, t) = (k^2 + a1)F_{1D}$ has been represented at different instants, and one clearly sees how its shape and amplitude are conserved. However, these characteristics are sensitive to the plasma parameters as shown in Figs. 7(e) and 7(f). We have fixed $\alpha = 0.25$ and, as a whole, for $\sigma_n < 10$, the amplitude is a decreasing function of σ_n as shown in Fig. 7(e). Contrarily, Fig. 7(f) shows that the amplitude of the dromion increases with $\sigma_n > 10$. Importantly, the width of the solution gets expanded when σ_n increases in both cases.

B. The two-dromion soliton

One can proceed in a similar way and find the two-dromion solution in the form

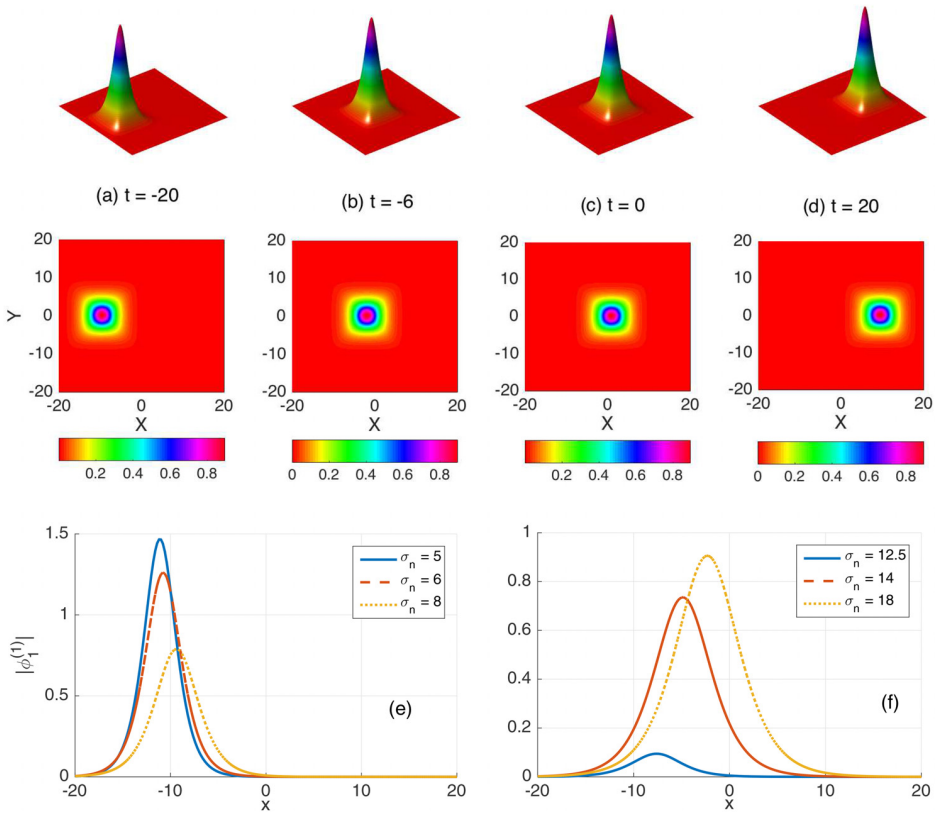

FIG. 7. Panels (a)–(d) show the surface and corresponding density plots of the one-dromion solution (33) in the $(X, Y)-$ space at different instants. (e) and (f) show the effect of the ENP parameters, α and σ_n, on the amplitude and width of the one-dromion solution. For (a)–(d) parameters are fixed as $k = 0.15$, $\alpha = 0.2$, and $\sigma_n = 5.5$. For (e) and (f), we have used the values for α and k with changing σ_n.

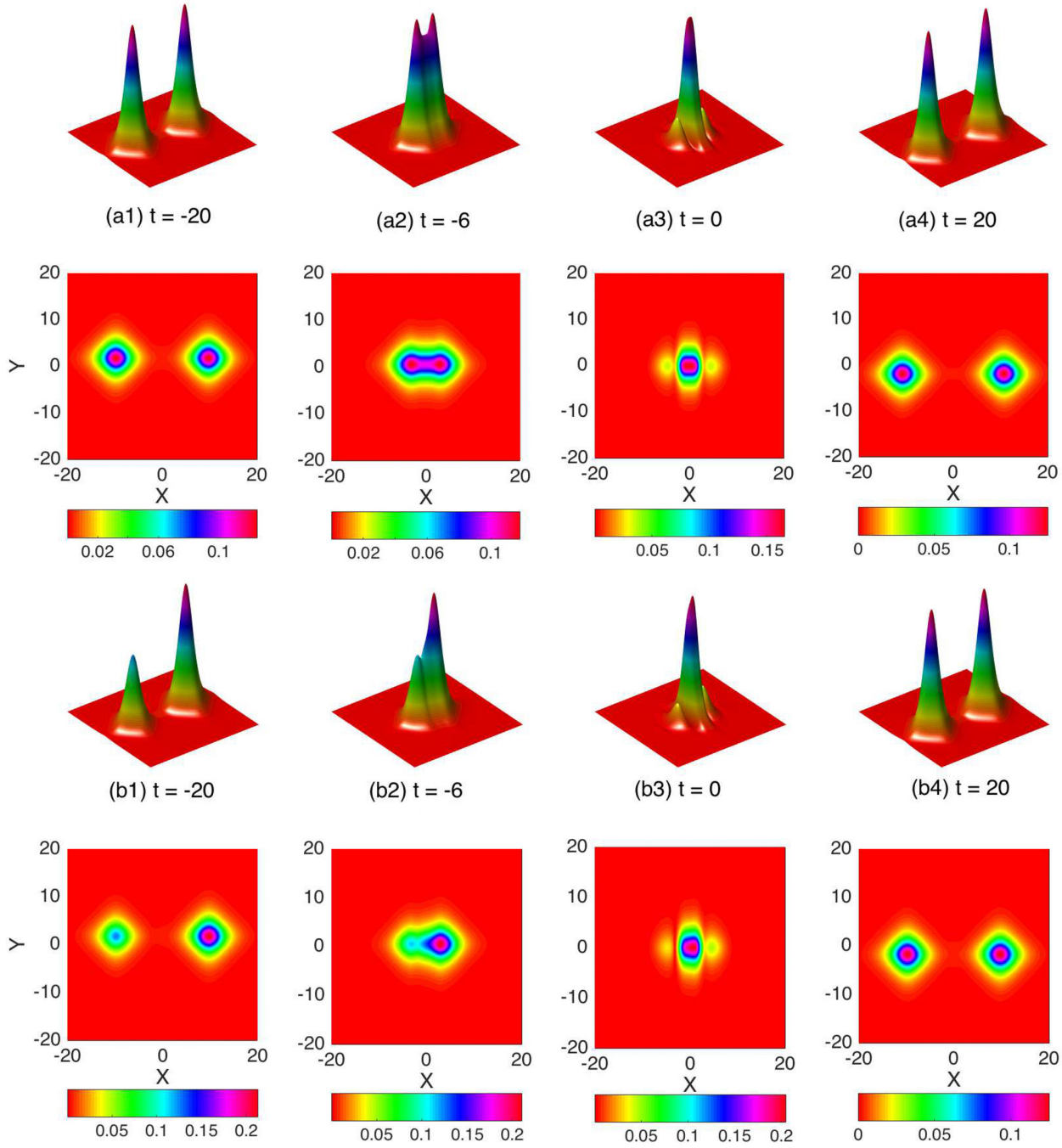

FIG. 8. The panels show the elastic collision of the two-dromion solution (34) in the $(X, Y)-$ space at different instants. In $(\mathrm{aj})_{j=1,2,3}$, two dromions of the same amplitude interact and keep their individual characteristics after collision. In panels $(\mathrm{bj})_{j=1,2,3}$, a small dromion and a highly localized one interact and there is an equipartition of energy after collision, leading to two identical waves, with the same characteristics. Parameters are $k = 0.15$, $\alpha = 0.2$, and $\sigma_n = 5.5$.

$$F_{2D} = \frac{\left\{\begin{array}{l}\rho_{11}\exp(\theta_1+\theta_3)+\rho_{12}\exp(\theta_2+\theta_3)\\ +\rho_{21}\exp(\theta_1+\theta_1^*+\theta_2+\theta_3)+\rho_{22}\exp(\theta_1+\theta_2+\theta_2^*+\theta_3)\end{array}\right\}}{\left\{\begin{array}{l}1+A\exp(\theta_1+\theta_1^*)+B\exp(\theta_2+\theta_2^*)+C\exp(\theta_3+\theta_3^*)+D(\exp(\theta_1+\theta_2^*)\\ +\exp(\theta_2+\theta_1^*))+E(\exp(\theta_1+\theta_2^*+\theta_3+\theta_3^*)+\exp(\theta_2+\theta_1^*+\theta_3+\theta_3^*))\\ +F\exp(\theta_1+\theta_1^*+\theta_2+\theta_2^*)+G\exp(\theta_2+\theta_2^*+\theta_3+\theta_3^*)\\ +H\exp(\theta_1+\theta_1^*+\theta_3+\theta_3^*)+I\exp(\theta_1+\theta_1^*+\theta_2+\theta_2^*+\theta_3+\theta_3^*)\end{array}\right\}}, \tag{34}$$

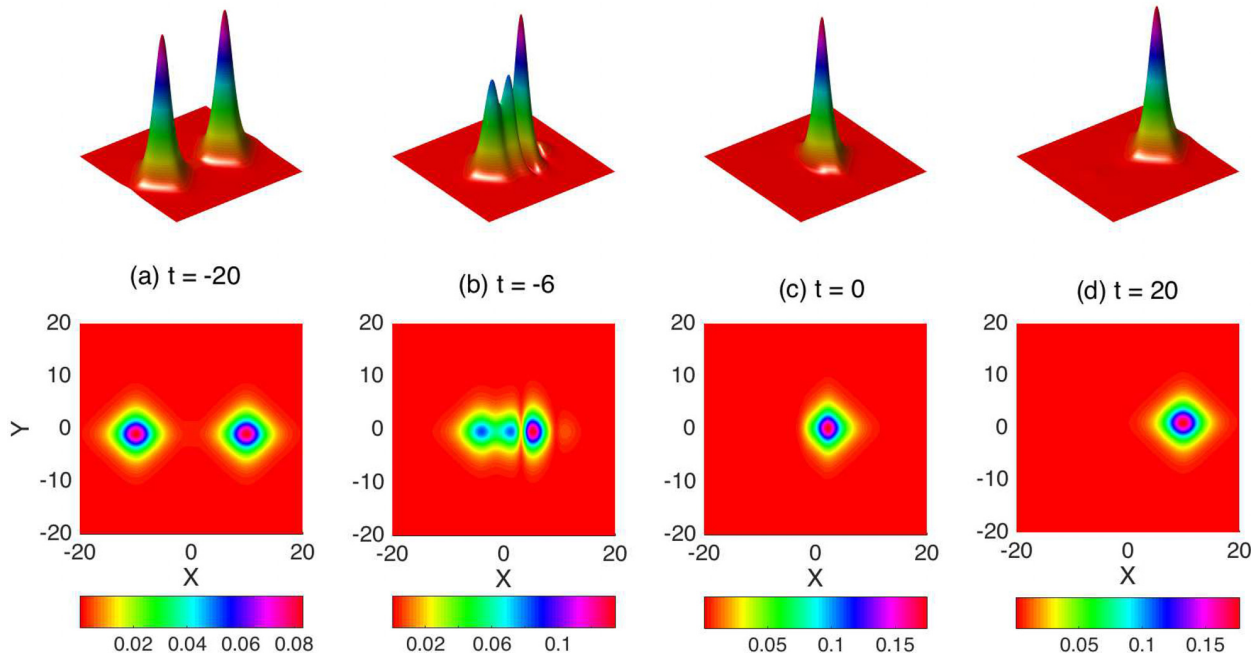

FIG. 9. The panels show inelastic collision time frame of two identical dromions in the $(X, Y)-$ space at different instants. After collision, the two waves merge into one, which carries the sum of the energies brought by each of the dromions. Parameters are as follows: $k = 0.15$, $\alpha = 0.2$, and $\sigma_n = 5.5$.

where A, B, C, D, E, F, G, H, and I are real, positive constants. θ_1, θ_2, and θ_2 are assumed to be in the forms $\theta_1 = p_1X + \omega_1 t + \beta_1$, $\theta_2 = p_2X + \omega_2 t + \beta_2, \theta_3 = p_3Y + \omega_3 t + \beta_3$, with the conditions $\omega_1 = iap_1^2, \omega_2 = iap_2^2$, and $\omega_3 = iap_3^2$. Commonly, solitonic structures undergo elastic and inelastic collisions where they exchange or share energy.[47] During elastic collisions, the two waves conserve their respective characteristics before and after interacting as shown in Fig. 8(aj)$_{j=1,2,3,4}$ at different instants. Another scenario, which may arise during elastic collisions is energy equipartition. This is for example depicted in Fig. 8(bj)$_{j=1,2,3,4}$. When two dromions with different amplitudes and width interact, the one with the highest amplitude may transfer some energy to the small one, the whole process leading to two identical dromions of equal amplitude and width. In Fig. 9, a different spectrum of behaviors is obtained, where the two dromions initially having the same amplitude interact and merge into one. This is not surprising, as the phenomenon of inelastic collision is inherent to multi-component plasmas, which may include electrons, positive, and negative ions.[48,49] This is one of the main mechanisms leading to the production of plasma particles, via energy recombination among the available dynamical modes.[48,49] Experiments on plasmas have shown the existence of interacting solitons, as it was the case in a monolayer strongly coupled complex (dusty) plasma.[50] One may also notice the contribution by Mandal and Sharma[51,52] who reported interacting solitons in the electron-acoustic regime of collisionless plasmas. Using a one-dimensional ENP model, the interaction between positive and negative solitons was studied with the emphasis on the coupled effects of α and σ_n.[42] However, in the latest context, dromion solutions have not been reported in the literature, including their response to strong concentration of negative ions and the subsequent plasma temperature.

V. CONCLUDING REMARKS

We have considered a two-dimensional ENP model to study the propagation of modulated IAWs and some subsequent exact solutions. Using the reductive perturbation method, we have shown that IAWs may be described using the DS equations with coefficients strongly dependent on negative ion parameters, i.e., the electron-to-negative ion temperature ratio (σ_n) and the negative ion concentration ratio (α). The MI of planar waves has been addressed based on such parameters, which were found to importantly affect the features of instability. A parametric analysis of MI has been performed to that effect, where some values of α and σ_n have been found to be against the emergence of modulated IAWs. Analytical investigations of MI have been confirmed numerically, where the activation of MI in the DS equation (18) has led to series of dromion-like structures, very sensitive to plasma parameters. Knowing that dromions are intrinsic solutions of the DS-I equations, the Bilinear Hirota method has been used to find their exact expressions. The impact of the plasma parameters on their shape and characteristics has been discussed, along with some collision scenarios. We have shown that when parameters are suitably fixed, such dromion solutions may undergo elastic and inelastic interactions. The next step to this study would be a generalization of the studied model to its three-dimensional version in a magnetized ENP.

[1]A. Mohamadou, B. E. Ayissi, and T. C. Kofané, Phys. Rev. E **74**, 046604 (2006).
[2]E. Wamba, A. Mohamadou, and T. C. Kofané, Phys. Rev. E **77**, 046216 (2008).
[3]I. Maïna, C. B. Tabi, A. Mohamadou, H. P. F. Ekobena, and T. C. Kofané, Chaos **25**, 043118 (2015).
[4]A. S. Etémé, C. B. Tabi, and A. Mohamadou, Commun. Nonlinear Sci. Numer. Simul. **43**, 211 (2017).

[5]C. B. Tabi, R. Y. Ondoua, H. P. Ekobena, A. Mohamadou, and T. C. Kofané, Phys. Lett. A **380**, 2374 (2016).
[6]G. R. Y. Mefire, C. B. Tabi, A. Mohamadou, H. P. F. Ekobena, and T. C. Kofané, Chaos **23**, 033128 (2013).
[7]E. A. Kuznetsov, A. M. Rubenchik, and V. E. Zakharov, Phys. Rep. **142**, 103 (1986).
[8]I. Kourakis and P. K. Shukla, Nonlinear Proc. Geophys. **12**, 407 (2005).
[9]J. Borhanian, I. Kourakis, and S. Sobhanian, Phys. Lett. A **373**, 3667 (2009).
[10]A.-u. Rahman, M. McKerr, W. F. El-Taibany, I. Kourakis, and A. Qamar, Phys. Plasmas **22**, 022305 (2015).
[11]H. Washimi and T. Taniuti, Phys. Rev. Lett. **17**, 996 (1966).
[12]H. Ikezi, R. Taylor, and D. Baker, Phys. Rev. Lett. **25**, 11 (1970).
[13]T. Kimura, K. Imagaki, and K. Ohe, J. Phys. D: Appl. Phys. **31**, 2295 (1998).
[14]O. Rahman, A. A. Mamun, and K. S. Ashrafi, Astrophys. Space Sci. **335**, 425 (2011).
[15]S. V. Berezhnoj, C. B. Shin, U. Buddemeir, and I. Kaganovich, Appl. Phys. Lett. **77**, 800 (2000).
[16]M. G. Anowar, K. S. Ashrafi, and A. A. Mamun, J. Plasma Phys. **77**, 133 (2011).
[17]S. S. Duha, M. S. Rahman, A. A. Mamun, and G. M. Anowar, J. Plasma Phys. **78**, 279 (2012).
[18]Y. K. Ghim and N. Hershkowitz, Appl. Phys. Lett. **94**, 151503 (2009).
[19]R. N. Franklin and J. Snell, J. Plasma Phys. **64**, 131 (2000).
[20]A. J. Lichtenberg, I. J. Kouznetsov, Y. T. Lee, M. A. Lieberman, I. D. Kaganovich, and L. D. Tsendin, Plasma Sources Sci. Technol. **6**, 437 (1997).
[21]A. S. Bains, B. Li, and M. Tribeche, Phys. Plasmas **20**, 092119 (2013).
[22]S. A. El-Tantawy and W. M. Moslem, Astrophys. Space Sci. **337**, 209 (2012).
[23]S. Guo, L. Mei, and Z. Zhang, Phys. Plasmas **22**, 052306 (2015).
[24]A. Mannan, A. A. Mamun, and P. K. Shukla, Phys. Scr. **85**, 065501 (2012).
[25]S. K. El-Labany, W. M. Moslem, K. A. Shnishin, S. A. El-Tantawy, and P. K. Shukla, Phys. Plasmas **18**, 042306 (2011).
[26]M. A. Allen and G. Rowlands, J. Plasma Phys. **50**, 413 (1993).
[27]S. Munro and E. J. Parkes, J. Plasma Phys. **62**, 305 (1999).
[28]W. S. Duan, Chaos, Solitons Fractals **14**, 503 (2002).
[29]X. N. Chen and S. D. Sharma, J. Fluid Mech. **291**, 263 (1995).
[30]J.-K. Xue, Phys. Lett. A **330**, 390 (2004).
[31]W. S. Duan, Phys. Plasmas **10**, 3022 (2003).
[32]C. Bedi and T. S. Gill, Phys. Plasmas **19**, 062109 (2012).
[33]K. Nishinari, K. Abe, and J. Satsuma, J. Phys. Soc. Jpn. **62**, 2021 (1993).
[34]K. Nishinari, K. Abe, and J. Satsuma, Phys. Plasmas **1**, 2559 (1994).
[35]B.-X. Gan, Y.-H. Chen, and M. Y. Yu, J. Appl. Phys. **101**, 113310 (2007).
[36]X. Zheng, Y. Chen, H. Hu, G. Wang, F. Huang, C. Dong, and M. Y. Yu, Phys. Plasmas **16**, 023701 (2009).
[37]A. A. Mamun, P. K. Shukla, and B. Eliasson, Phys. Rev. E **80**, 046406 (2009).
[38]A. Davey and K. Stewartson, Proc. R. Soc. London, Ser. A **338**, 101 (1974).
[39]C. Sulem and P. L. Sulem, *The Nonlinear Schrödinger Equation* (Springer-Verlag, 1999).
[40]W. Craig, U. Schanz, and C. Sulem, Ann. I. H. P. Sec. C **14**, 615 (1977).
[41]P. Carbonaro, Chaos, Solitons Fractals **45**, 959 (2012).
[42]S. A. El-Tantawy, Chaos, Solitons Fractals **93**, 162 (2016).
[43]S. A. El-Tantawy, A. M. Wazwaz, and S. A. Shan, Phys. Plasmas **24**, 022105 (2017).
[44]M. J. Ablowitz and H. Segur, *Solitons and the Inverse Scattering Transform* (SIAM, Philadelphia, 1981).
[45]R. Radha and M. Lakshmanan, J. Phys. A: Math. Gen. **30**, 3229 (1997).
[46]S. S. Ghosh, A. Sen, and G. S. Lakhina, Nonlinear Processes Geophys. **9**, 463 (2002).
[47]M. A. Moghanjoughi, Phys. Plasmas **17**, 092304 (2010).
[48]H. P. Le and J.-L. Cambier, Phys. Plasmas **23**, 063505 (2016).
[49]J. Vranjes, M. Kono, D. Petrovic, S. Poedts, A. Okamoto, S. Yoshimura, and M. Y. Tanaka, Plasma Sources Sci. Technol. **15**, S1 (2006).
[50]S. K. Sharma, A. Boruah, and H. Bailung, Phys. Rev. E **89**, 013110 (2014).
[51]D. Mandal and D. Sharma, Phys. Plasmas **21**, 102107 (2014).
[52]D. Mandal and D. Sharma, Phys. Plasmas **23**, 022108 (2016).

Accepted Manuscript

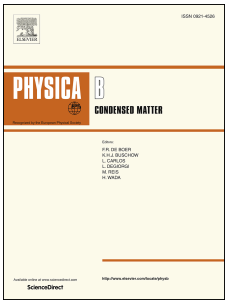

Electronegative (3+1)-dimensional modulated excitations in plasmas

Conrad B. Tabi, Chérif S. Panguetna, Timoléon C. Kofané

PII: S0921-4526(18)30432-0

DOI: 10.1016/j.physb.2018.06.032

Reference: PHYSB 310940

To appear in: *Physica B: Physics of Condensed Matter*

Received Date: 7 April 2018

Revised Date: 3 May 2018

Accepted Date: 25 June 2018

Please cite this article as: C.B. Tabi, Ché.S. Panguetna, Timolé.C. Kofané, Electronegative (3+1)-dimensional modulated excitations in plasmas, *Physica B: Physics of Condensed Matter* (2018), doi: 10.1016/j.physb.2018.06.032.

Electronegative (3+1)-dimensional Modulated Excitations in Plasmas

Conrad B. Tabi[1,2*], Chérif S. Panguetna[3†] and Timoléon C. Kofané[3‡]

[1]Botswana International University of Science and Technology, Private Bag 16 Palapye, Botswana
[2]Laboratoire de Biophysique, Département de Physique, Faculté des Sciences, Université de Yaoundé I, B.P. 812 Yaoundé, Cameroun
[3]Laboratoire de Mécanique, Département de Physique, Faculté des Sciences, Université de Yaoundé I, B.P. 812 Yaoundé, Cameroun

June 26, 2018

Highlights

- Modulated envelope waves are studied in three-dimensional electronegative plasmas.
- The modulation angle and the plasma parameters are found to affect the stability of the plane wave solutions.
- Oblique, parallel and transverse modulations are discussed.
- Parallel and transverse modulations are detected in opposite plasma parameter regions.

*Corresponding author: conrad@aims.ac.za or tabic@biust.ac.bw (C. B. Tabi)
†cherifps@yahoo.fr(C. S. Panguetna)
‡tckofane@yahoo.com (T. C. Kofané)

Abstract

A three-dimensional electronegative plasma model is studied. Modulated ion-acoustic waves are investigated via the activation of modulational instability in the Davey-Stewartson equations, with three space variables. The contributions of the modulation angle (θ) and electronegative plasma parameters are discussed to that effect, including some particular cases such as the parallel and transverse modulations. The parametric linear stability analysis that is proposed shows that the growth rate of instability displays opposite regions of instability for parallel and transverse modulations when the negative ion concentration ratio (α) and the electron-to-negative ion temperature ratio (σ_n) change.

Keywords: Electronegative Plasmas; Modulational Instability; Modulation angle.

---

1 Introduction

In the last twenty years, solitonic structures have been studied in a broad range physical systems, especially in nonlinear optics [1, 2, 3, 4], biophysics [5, 6, 7, 8] and in Bose-Einstein condensates [9, 10]. They originate from the competition between nonlinear and dispersive effects, and can move over long distances, with unaltered characteristics. The physics of dusty plasmas has significantly been related to linear and nonlinear waves, usually observed in space and laboratory plasmas. For example, ion-acoustic solitons have been the object of intense investigations, both theoretically and experimentally in plasmas comprising electrons and positive ions [11, 13, 14, 15, 16, 17]. In electronegative plasmas (ENPs), one finds both negative and positive ion species, as well as electrons. Negative ion plasmas may be obtained as a result of basic processes, such as dissociative or non-dissociative electron attachment to neutrals, especially when electronegative gases are injected into an electrical gas discharge or injected from an external source [11, 12, 18]. In ENPs, there should be a critical concentration of negative ions for compressive soliton propagation to be possible. Indubitably, this is straightforwardly related to the critical negative ion density, which for some values beyond that critical one, may support the emergence of rarefractive solitons [19]. Nevertheless, if at the critical density, the interplay between dispersive and nonlinear effects is lost and consequently the usual Korteweg-de Vries (KdV) theory will no more be suitable for studying soliton propagation [20, 21]. However, a

time-dependent perturbation may lead to a modified KdV (mKdV) equation, only in the presence of higher-order nonlinearity [22]. More recently, experimental observations of Peregrine solitons in nonlinear optical fibers [23, 24], water tank experiment [25, 26] and in plasmas [27, 28] have opened a new route to study their characteristics more deeply. Along the same lines, Ion acoustic waves (IAWs) are found to be modulationally unstable when the plasma contains a critical amount of negative ions and described by the nonlinear Schrödinger (NLS) equation. Mamun et al. [11], based on laboratory experiments, have recently paid attention to the existence of IA and DIA waves in an electronegative plasma made of Boltzmann negative ions, Boltzmann electrons and cold mobile positive ions. Also, we have highlighted, in our previous works, the impact of the negative ion concentration ratio and the electron-to-negative ion temperature ratio on the modulational instability (MI) both in one- and two dimensional contexts [29, 30]. In fact, the MI of nonlinear excitations in plasmas is a well-known phenomenon leading to energy localization, the main consequence being the formation of bright envelope solitons. This means that, in the absence of instability, dark solitons are the most probable excitations to emerge in such systems. MI therefore originates from the fact that a small plane wave perturbation grows exponentially and the resulting sidebands get amplified, to finally display trains of oscillations. In general, the subsequent bright solitons are solutions of the NLS equation, which can be derived from generic hydrodynamic plasma equations using appropriate expansion methods such as the reductive perturbative method [16, 17], the derivative expansion method [31], the Kryslov-Bogoliubov method [32, 33], to name just a few. In more recent contributions, particular attention has been paid to the multi-dimensional versions of such methods, leading to more upgraded amplitude equations such as the Davey-Stewartson (DS) equation and the multi-dimensional NLS equation, with at least two space variables. The MI and soliton solutions of the 2D-DS equations have been recently addressed, with emphasis on the effects of the ENP parameters. Periodic solutions and MI of the DS were also proposed by Tajiri et al. [34]. Gill and co-workers [35] also studied 2D envelope electron acoustic waves in the presence of Cairns non-thermal distribution of hot electrons. Bedi and Gill [15] studied envelope electron acoustic waves subjected to transverse perturbations, in the presence of $\kappa-$distributed hot electrons. In three dimensions, Carbonaro [14] derived DS equations from a plasma system consisting of cold electrons, hot electrons and steady background of ions, and further supported the idea of Kourakis and Shukla [13] that in higher dimensions the MI phenomenon is mostly controlled by the modulation angle, leading to parallel, transverse and oblique modulations. The concept is also introduced in the present work and applied to ENPs. We study the dynamical outcomes of the interplay between ENP parameters and the angle of modulation using the

MI technique. The 3D-DS equations are first derived via the reductive perturbation method, followed by a comprehensive parametric linear stability analysis of plane wave solutions. Some particular cases such as the parallel and transverse modulations are discussed. Some concluding remarks ends the paper.

2 Mathematical Model

We consider an unmagnetized electronegative plasma system composed of Maxwellian electrons and negative ions in addition to cold mobile positive ions [11, 29, 36]. The nonlinear features of the IAWs may be described by the following set of coupled normalized ion-fluid equations in three-space dimension:

$$\frac{\partial n_i}{\partial t} + \mathrm{div}\left(n_i \overrightarrow{V}\right) = 0, \tag{1a}$$

$$\frac{\partial \overrightarrow{V}}{\partial t} + \left(\overrightarrow{V} \cdot \overrightarrow{\mathrm{grad}}\right) \overrightarrow{V} = -\overrightarrow{\mathrm{grad}}\phi, \tag{1b}$$

$$\Delta\phi = \mu_e \exp\phi + \mu_n \exp\sigma_n\phi - n_i, \tag{1c}$$

where n_i is the number density of positive ions, which is normalized by the unperturbed value n_{i0}. $\overrightarrow{V} = u\overrightarrow{e_x} + v\overrightarrow{e_y} + w\overrightarrow{e_z}$, where u, v and w are the velocities of charged dusts (with mass m_i) in x, y and z directions, respectively. The overall charge neutrality at equilibrium is $n_i^{(0)} = n_e^{(0)} + n_n^{(0)}$. The different variables that appear in Eqs. (1a)-(1c) have also been adequatly normalized: n_i is normalized by the unperturbed ion density n_{i0}; $\overrightarrow{V}$ is normalized by the dust-acoustic (DA) speed $c = \sqrt{Zk_BT_e/m_i}$, with T_e denoting the electron temperature, k_B the Boltzmann constant and Z the charged dust state, i.e., the number of electrons per ion found on the dust-grain surface. ϕ represents the electrostatic wave potential and is normalized by k_BT_e/e, where e is the magnitude of the electron charge. The time and space variables are normalized by the ion-Debye length $\lambda_D = (k_BTe/4\pi e^2 n_i)^{1/2}$ and the ion plasma period $\omega^{-1} = (4\pi e^2 n_{i0}/m_i)^{-1/2}$, respectively. $\sigma_n = T_e/T_n$ is the electrons-to-negative ion temperature ratio, $\mu_e = n_{e0}/n_{i0}$ and $\mu_n = n_{n0}/n_{i0}$, where n_{i0} , n_{n0} and n_{e0}, are the unperturbed densities of the positive ions, negative ions and electrons, respectively. At equilibrium, the neutrality condition of the plasma reads $\mu_e + \mu_n = 1$, where $\mu_e = n_{e0}/n_{i0} = 1/(1+\alpha)$, with $\alpha = n_{n0}/n_{e0}$. Using the power series expansion of the exponential functions around zero, Eq. (1c) becomes

$$\frac{\partial^2\phi}{\partial x^2} + \frac{\partial^2\phi}{\partial y^2} + \frac{\partial^2\phi}{\partial z^2} = 1 + a_1\phi + a_2\phi^2 + a_3\phi^3 - n_i, \tag{2}$$

where, $a_1 = \mu_e + \mu_n\sigma_n$, $a_2 = \frac{\mu_e + \mu_n\sigma_n^2}{2}$ and $a_3 = \frac{\mu_e + \mu_n\sigma_n^3}{6}$.

In order to investigate the propagation of IAWs and derive the amplitude equations for the above-described plasma system, we employ the standard reductive-perturbation technique. We introduce the stretched variables in space and time as, $\xi = \epsilon(x - v_g t)$, $\eta = \epsilon y$, $\zeta = \epsilon z$ and $\tau = \epsilon^2 t$, where the group velocity v_g will be determined later by the solvability condition of Eqs. (1). The dependent physical variables around their equilibrium values are given by the trial expressions

$$n = 1 + \sum_{p=1}^{\infty} \epsilon^p \sum_{l=-\infty}^{+\infty} n_{il}^{(p)}(\xi, \eta, \zeta, \tau) A^l(x, t) \tag{3a}$$

$$\phi = \sum_{p=1}^{\infty} \epsilon^p \sum_{l=-\infty}^{+\infty} \phi_{l}^{(p)}(\xi, \eta, \zeta, \tau) A^l(x, t) \tag{3b}$$

$$\overrightarrow{V} = \sum_{p=1}^{\infty} \epsilon^p \sum_{l=-\infty}^{+\infty} \begin{pmatrix} u_l^{(p)}(\xi, \eta, \zeta, \tau) \\ v_l^{(p)}(\xi, \eta, \zeta, \tau) \\ w_l^{(p)}(\xi, \eta, \zeta, \tau) \end{pmatrix} A^l(x, t). \tag{3c}$$

We Note that the above series include all overtones $A^l(x,t) = \exp[il(kx - \omega t)]$ up to order p, generated by the nonlinear terms, i.e., the corresponding coefficients are of maximum order ϵ^p. The reality condition of physical variables requires the relations $\left(n_{il}^{(p)}\right)^* = n_{i-l}^{(p)}$, $\left(u_l^{(p)}\right)^* = u_{-l}^{(p)}$, $\left(v_l^{(p)}\right)^* = v_{-l}^{(p)}$, $\left(w_l^{(p)}\right)^* = w_{-l}^{(p)}$ and $\left(\phi_l^{(p)}\right)^* = \phi_{-l}^{(p)}$ to be satisfied. The asterisk denotes the complex conjugation. Substituting trial solutions (3a)-(3c) into the basic Eqs. (1a), (1b) and (2), and equating the quantities with equal power of ϵ, we obtain at ϵ^1 order, for $l = 1$, the following solutions corresponding to the first harmonic of perturbation

$$\phi_1^{(1)} = \frac{1}{k^2 + a_1} n_{i1}^{(1)}, \; u_1^{(1)} = \frac{\omega}{k} n_{i1}^{(1)}, \; v_1^1 = 0, \; w_1^1 = 0, \tag{4}$$

given that the dispersion relation

$$\omega^2 = \frac{k^2}{k^2 + a_1} \tag{5}$$

be satisfied. We process the same way and obtain the second-order terms, namely the amplitudes of the second harmonics and constant terms as well as the non vanishing contributions to the first harmonics. We obtain the following equations at $O(\epsilon^2)-$order, for $l = 0$,

$$a_1 \phi_0^{(2)} - n_{i0}^{(2)} - 2a_2 |\phi_1^{(1)}|^2, \tag{6}$$

and

$$\begin{aligned} &-v_g \frac{\partial n_{i1}^{(1)}}{\partial \xi} - i\omega n_{i1}^{(2)} + iku_1^{(2)} + \frac{\partial u_1^{(1)}}{\partial \xi} = 0; \quad -v_g \frac{\partial u_1^{(1)}}{\partial \xi} - i\omega u_1^{(2)} + ik\phi_1^{(2)} = -\frac{\partial \phi_1^{(1)}}{\partial \xi} = 0; \\ &-i\omega v_1^{(2)} = -\frac{\partial \phi_1^{(1)}}{\partial \eta}, \quad -i\omega w_1^{(2)} = -\frac{\partial \phi_1^{(1)}}{\partial \zeta}; \quad (k^2 + a_1)\phi_1^{(2)} - n_{i1}^{(2)} = 2ik\frac{\partial \phi_1^{(1)}}{\partial \xi} \end{aligned} \tag{7}$$

for $l=1$. For $l=2$, the system reduces to

$$\begin{aligned} &-2i\omega n_{i2}^{(2)}+2iku_2^{(2)}+2ikn_{i1}^{(1)}u_1^{(1)}=0;\quad -2i\omega u_2^{(2)}+ik(u_1^{(1)})^2+2ikn_{i1}^{(1)}u_1^{(1)}=0;\\ &(4k^2+a_1)\phi_2^{(2)}-n_{i2}^{(2)}+a_2(\phi_1^{(1)})^2=0;\quad -2i\omega v_2^{(2)}=0,\quad -2i\omega w_2^{(2)}=0, \end{aligned} \tag{8}$$

which provides the compatibility condition

$$v_g=a_1\frac{\omega^3}{k^3}. \tag{9}$$

By solving equation (8), we find the second harmonic quantities $n_{2i}^{(2)}$, $u_2^{(2)}$ and $\phi_2^{(2)}$ in term of $\phi_1^{(1)}$ in the form

$$\phi_2^{(2)}=\alpha_\phi\left(n_{i1}^{(1)}\right)^2,\quad n_{i2}^{(2)}=\alpha_n\left(n_{i1}^{(1)}\right)^2,\quad u_2^{(2)}=\alpha_u\left(n_{i1}^{(1)}\right)^2,\quad v_2^{(2)}=w_2^{(2)}=0, \tag{10}$$

with

$$\alpha_\phi=\frac{1}{2k^2}-\frac{a_2}{3k^2(k^2+a_1)^2},\quad \alpha_n=(a_1+4k^2)\alpha_\phi+\frac{a_2}{(k^2+a_1)^2},\quad \alpha_u=\frac{\omega}{k}(\alpha_n-1). \tag{11}$$

Moreover, the expression for the zeroth harmonic mode cannot be determined completely within the second order, so we will have to consider the third-order equations. Therefore, the set of equations given by the $(l=0)-$components of the third-order part of the reduced equations is given by

$$\begin{aligned} &-v_g\frac{\partial n_{i0}^{(2)}}{\partial\xi}+\frac{\partial u_0^{(2)}}{\partial\xi}+\frac{\partial v_0^{(2)}}{\partial\eta}+\frac{\partial w_0^{(2)}}{\partial\zeta}+\frac{2\omega}{k}\frac{\partial|n_{i1}^{(1)}|^2}{\partial\xi}=0;\quad -v_g\frac{\partial v_0^{(2)}}{\partial\xi}+\frac{\partial\phi_0^{(2)}}{\partial\zeta}+\frac{\omega^2}{k^2}\frac{\partial|n_{i1}^{(1)}|^2}{\partial\zeta}=0;\\ &-v_g\frac{\partial u_0^{(2)}}{\partial\xi}+\frac{\partial\phi_0^{(2)}}{\partial\xi}+\frac{\omega^2}{k^2}\frac{\partial|n_{i1}^{(1)}|^2}{\partial\xi}=0;\quad -v_g\frac{\partial v_0^{(2)}}{\partial\xi}+\frac{\partial\phi_0^{(2)}}{\partial\eta}+\frac{\omega^2}{k^2}\frac{\partial|n_{i1}^{(1)}|^2}{\partial\eta}=0, \end{aligned} \tag{12}$$

to which we add Eq. (6) from $O(\epsilon^2)$, for $l=0$. From Eqs. (12), we get

$$\delta_1\frac{\partial^2\phi_0^2}{\partial\xi^2}-\left(\frac{\partial^2\phi_0^2}{\partial\eta^2}+\frac{\partial^2\phi_0^2}{\partial\zeta^2}\right)-\delta_2\frac{\partial^2|n_{i1}^{(1)}|^2}{\partial\xi^2}-\delta_3\left(\frac{\partial^2|n_{i1}^{(1)}|^2}{\partial\eta^2}-\frac{\partial^2|n_{i1}^{(1)}|^2}{\partial\zeta^2}\right)=0, \tag{13}$$

with

$$\delta_1=v_g^2a_1-1,\delta_2=\frac{2v_g\omega}{k}+\frac{\omega^2}{k^2}-\frac{2a_2v_g^2\omega^4}{k^4},\delta_3=\frac{\omega^2}{k^2}. \tag{14}$$

The various expressions found in the above calculations are then introduced into the $(l=1)-$component of the third-order part of the equations. This leads to the following amplitude equation

$$i\frac{\partial n_{i1}^{(1)}}{\partial\tau}+\gamma_1\frac{\partial^2n_{i1}^{(1)}}{\partial\xi^2}+\gamma_2\left(\frac{\partial^2n_{i1}^{(1)}}{\partial\eta^2}+\frac{\partial^2n_{i1}^{(1)}}{\partial\zeta^2}\right)+\gamma_3|n_{i1}^{(1)}|^2n_{i1}^{(1)}+\gamma_4\phi_0^{(2)}n_{i1}^{(1)}=0, \tag{15}$$

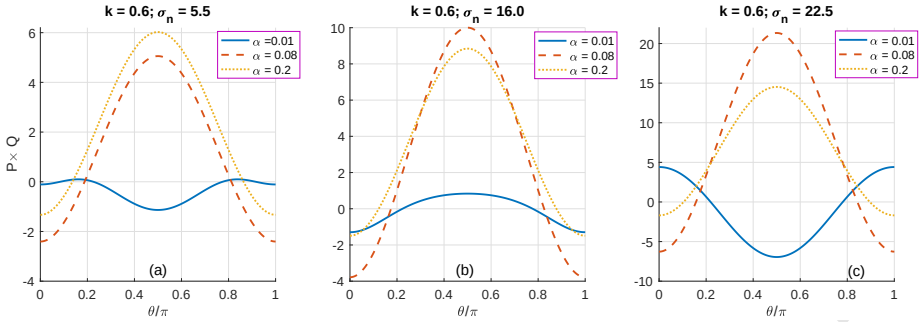

Figure 1: The panels show the plots of the product $P \times Q$ versus the modulation angle θ, under the influence of the plasma parameters σ_n and α. Each panel corresponds to a value of σ_n submitted to the increasing effect of α.

where

$$\gamma_1 = \frac{-3ka_1}{2(k^2+a_1)^5/2}, \quad \gamma_2 = \frac{a_1}{2k(k^2+a_1)^3/2},$$
$$\gamma_3 = -\frac{k}{2(k^2+a_1)^{1/2}}\left[6 + \frac{2k^2}{a_1} + \frac{3a_1}{2k^2} - \frac{4a_2}{3k^2(k^2+1)} - \frac{2a_2}{3k^2} + \frac{2a_2}{(k^2+a_1)^2} + \frac{2a_2^2}{3k^2(k^2+a_1)^3} - \frac{3a_3}{(k^2+a_1)^3}\right],$$
$$\gamma_4 = -\frac{k(k^2+a_1)^{3/2}}{a_1} - \frac{ka_1}{2(k^2+a_1)^{1/2}} + \frac{ka_2}{(k^2+a_1)^{3/2}}. \tag{16}$$

Further introducing the notations $F = n_{i1}^{(1)}$ and $G = \phi_0^{(2)}$, the coupled equations (13) and (15) become

$$i\frac{\partial F}{\partial \tau} + \gamma_1 \frac{\partial^2 F}{\partial \xi^2} + \gamma_2 \left(\frac{\partial^2 F}{\partial \eta^2} + \frac{\partial^2 F}{\partial \zeta^2}\right) + \gamma_3 |F|^2 F + \gamma_4 GF = 0, \tag{17a}$$

$$\delta_1 \frac{\partial^2 G}{\partial \xi^2} - \left(\frac{\partial^2 G}{\partial \eta^2} + \frac{\partial^2 G}{\partial \zeta^2}\right) - \delta_2 \frac{\partial^2 |F|^2}{\partial \xi^2} - \delta_3 \left(\frac{\partial^2 |F|^2}{\partial \eta^2} + \frac{\partial^2 |F|^2}{\partial \zeta^2}\right) = 0. \tag{17b}$$

The above system (17) represents the DS equations that were initially derived to describe modulated waves packets in water of finite depth [37]. Their soliton solutions were then investigated via the inverse scattering transform [38]. Dromion solutions in the 2D context were also derived recently with emphasis on their interaction and energy exchange [30].

3 Modulational instability

The DS Eqs. (17) admit the trivial homogeneous solutions $F = F_0 e^{i\gamma_3 F_0^2 \tau}$ and $G = 0$, where F_0 is a real constant that represents the amplitude of carrier wave. MI of IAWs is investigated under small perturbations in phase, in amplitude or in both. Since we are interested in amplitude modulation, the corresponding perturbed solutions then write $F = (F_0 + \delta F(\xi, \eta, \zeta, \tau))e^{i\gamma_3 F_0^2 \tau}$ and $G = \delta G(\xi, \eta, \zeta, \tau))$ with $\delta F \ll F_0$. After linearizing Eqs. (17) around the unperturbed

plane wave solutions, we obtain the governing equations for the small perturbations δF and δG in the form

$$i\frac{\partial \delta F}{\partial \tau}+\gamma_1\frac{\partial^2 \delta F}{\partial \xi^2}+\gamma_2\left(\frac{\partial^2 \delta F}{\partial \eta^2}+\frac{\partial^2 \delta F}{\partial \zeta^2}\right)+\gamma_3 F_0^2(\delta F+\delta F^*)+\gamma_4 \delta G F_0=0, \tag{18a}$$

$$\begin{aligned}\delta_1\frac{\partial^2 \delta G}{\partial \xi^2}-\left(\frac{\partial^2 \delta G}{\partial \eta^2}+\frac{\partial^2 \delta G}{\partial \zeta^2}\right)-\delta_2 F_0\frac{\partial^2(\delta F+\delta F^*)}{\partial \xi^2}\\ -\delta_3 F_0\left(\frac{\partial^2(\delta F+\delta F^*)}{\partial \eta^2}+\frac{\partial^2(\delta F+\delta F^*)}{\partial \zeta^2}\right)=0.\end{aligned} \tag{18b}$$

We make use of the transformation $\delta F = a + ib$ and $\delta G = c + id$, with

$$(a,b,c,d)=(a_0,b_0,c_0,d_0)e^{i(\mu_1\xi+\mu_2\eta+\mu_3\zeta-\Omega\tau)},$$

and obtain the nonlinear dispersion relation

$$\Omega^2=\left[\gamma_1\mu_1^2+\gamma_2(\mu_2^2+\mu_3^2)\right]^2\left[1+\frac{2F_0^2}{(\gamma_1\mu_1^2+\gamma_2(\mu_2^2+\mu_3^2))}\left(\frac{\delta_2\gamma_4\mu_1^2+\delta_3\gamma_4(\mu_2^2+\mu_3^2)}{-\delta_1\mu_1^2+\mu_2^2+\mu_3^2}-\gamma_3\right)\right]. \tag{19}$$

The perturbation wavenumber vector can be expressed using spherical coordinates, i.e., $(\mu_1,\mu_2,\mu_3) = (K\cos\theta, K\sin\theta\cos\varphi, K\sin\theta\sin\varphi)$. Eq. (19) then reduces to

$$\Omega^2=K^2P^2\left(K^2-2F_0^2\frac{Q}{P}\right), \tag{20}$$

where

$$P=\gamma_1\cos^2\theta+\gamma_2\sin^2\theta \quad \text{and} \quad Q=\gamma_3+\gamma_4\frac{\delta_2\cos^2\theta+\delta_3\sin^2\theta}{\delta_1\cos^2\theta-\sin^2\theta}. \tag{21}$$

There will be instability if the frequency Ω is complex, i.e., $\Omega^2 < 0$. According to expression (20), this mainly depends on the product $P \times Q$ and the value of the perturbation wavenumber which is such that $K < K_{cr} = F_0\sqrt{\frac{2Q}{P}}$. Although we obtain a result similar to the one in Ref. [13], we remark here that the instability condition depends of the angle θ which may lead to different instability scenarios as shown in Fig. 1, where $P \times Q$ is plotted versus the modulation angle θ, additionally to the effects of the plasma parameters. In Fig. 1(a), for example, $\sigma_n = 5.5$ and one observes two lateral regions of instability for $\alpha = 0.01$, especially in the intervals $0.1\pi \leq \theta \leq 0.23\pi$ and $0.75\pi \leq \theta \leq 0.88\pi$. However, with $\alpha = 0.08$ and 0.2, one observes a central region of instability which excludes the lateral ones observed previously. This later behavior persists for $\sigma_n = 16$ as the central instability interval of θ gets expanded as α increases (see Fig. 1(b)). More interestingly, lateral regions of instability appear once more for $\sigma_n = 22.5$, with $\alpha = 0.01$, in the intervals $0 < \theta \leq 0.22\pi$ and $0.78\pi \leq \theta \leq \pi$ (see Fig. 1(c)).

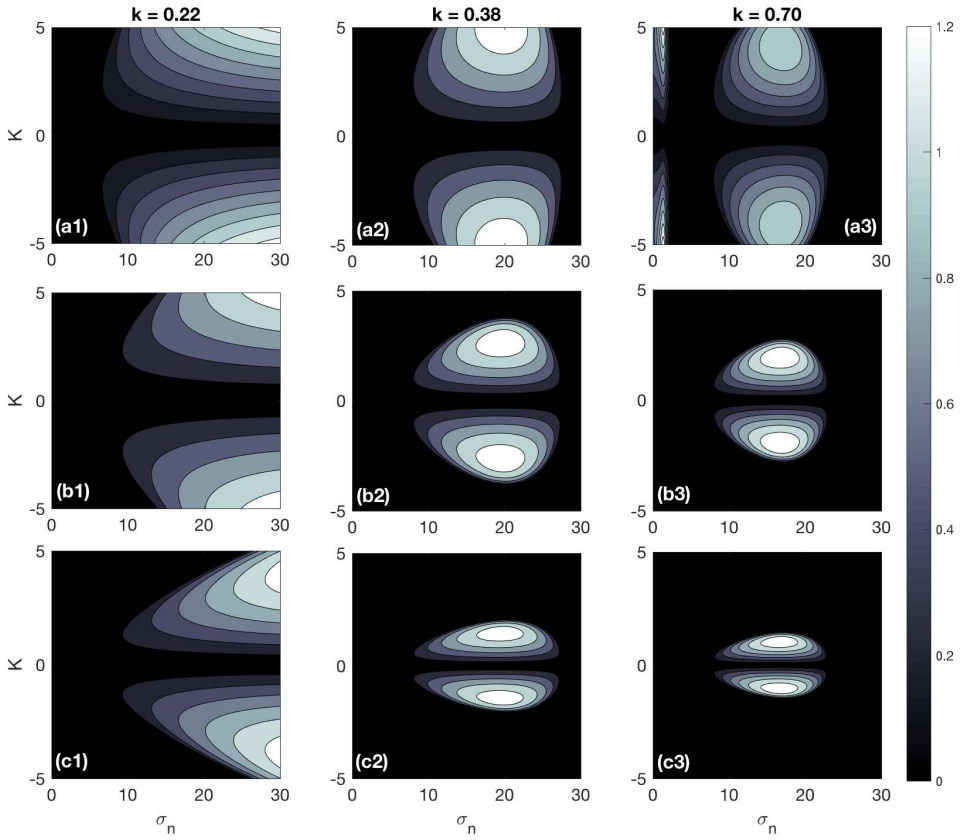

Figure 2: The growth rate of MI is plotted versus the wavenumber K and the electron-to-negative ion temperature ratio σ_n in the generalized case, i.e., $\theta \neq 0$. Panels $(\mathrm{aj})_{j=1,2,3}$ corresponds to to $\theta = \pi/10$, panels $(\mathrm{bj})_{j=1,2,3}$, gives results for $\theta = \pi/5$ and panels $(\mathrm{cj})_{j=1,2,3}$ have been recorded for $\theta = \pi/3$. The three columns correspond to different values of the wavenumber k, with $\alpha = 0.8$.

With increasing α, the previous central region where $P \times Q > 0$ appears again, and tends to expand. In general, MI is characterized by its growth rate given by the expression

$$\Gamma = \sqrt{-\Omega^2} = |PK|\sqrt{2\frac{QF_0^2}{P} - K^2}. \tag{22}$$

Fig. 2 is a good illustration of the above growth rate of instability which has been plotted versus the perturbation wavenumber K and the electron-to-negative ion temperature ratio σ_n. We have in fact considered different values of the modulation angle θ to clearly illustrate what is discussed in Fig. 1. Panels $(\mathrm{aj})_{j=1,2,3}$ have been plotted for $\theta = \pi/10$, a value that gives rise to instability domains. Especially, for $k = 0.70$, one notices the coexistence of two regions of instability both for very small and high σ_n, that disappear with increasing θ as shown in

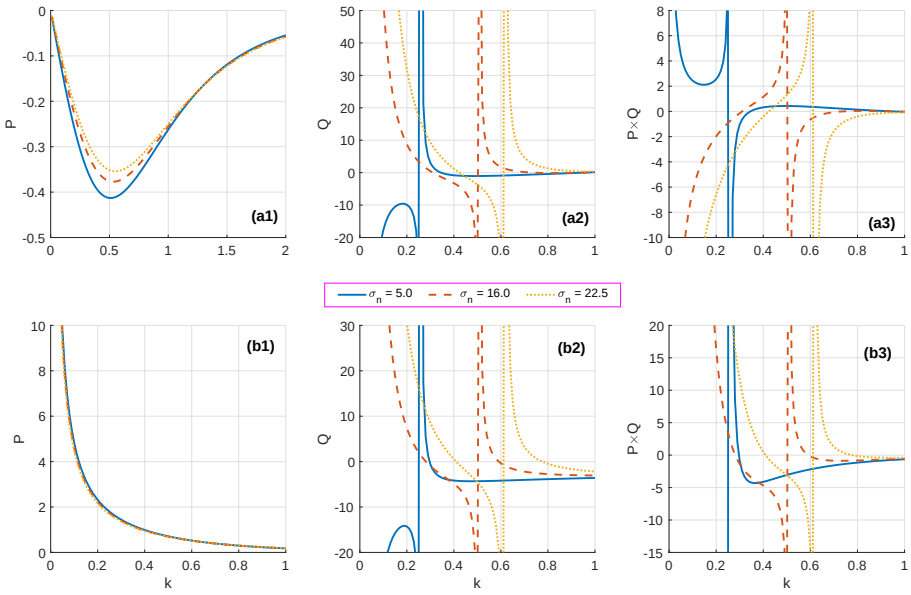

Figure 3: The dispersion coefficient P, the nonlinearity coefficient Q and the product $P \times Q$ are depicted versus the wavenumber k for different values of the electron-to-negative ion temperature ratio σ_n. Panels $(\text{aj})_{j=1,2,3}$ correspond to the parallel modulation, i.e., $\theta = 0$, while panels $(\text{bj})_{j=1,2,3}$ stand for the perpendicular modulation, i.e., $\theta = \pi/2$. The solid blue line corresponds to $\sigma_n = 5$, the dashed-red line corresponds to $\sigma_n = 16.0$ and the dotted-yellow line corresponds to $\sigma_n = 22.5$, with $\alpha = 0$.

Fig. 2(b3). For the rest, θ and k have the effect of reducing the instability domain expansion. Those regions are where modulated IAWs are expected, depending on the right choice of both the wave and plasma parameters.

In what follows, depending on the value of θ, we address two main cases known as the parallel and the transverse modulations [13].

A) Parallel modulation

Parallel modulation is obtained for $\theta = 0$, which reduces the coefficients P and Q to the simplified expressions

$$P = \gamma_1 \quad \text{and} \quad Q = \gamma_3 + \frac{\gamma_4 \delta_2}{\delta_1} \tag{23}$$

Interestingly, the above two coefficients still depend of the wavenumber k as clearly depicted by Fig. 3 (a1) and (a2). In this case, the sign of P remains negative with changing the value of the electron-to-negative ion temperature ratio σ_n. However, due to the later, there are regions of k

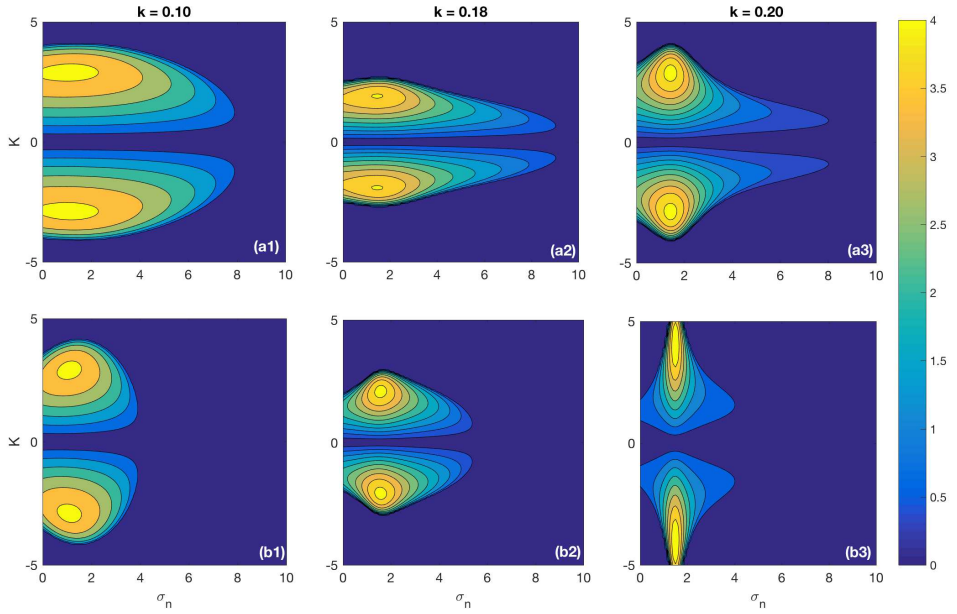

Figure 4: The growth rate of MI is plotted versus the wavenumber K and the electron-to-negative ion temperature ratio σ_n for the parallel modulation ($\theta = 0$). The columns, from left to right correspond respectively to $k = 0.1$, 0.18 and 0.20. The upper line, i.e., panels $(\mathrm{aj})_{j=1,2,3}$ corresponds to to $\alpha = 0.1$ and the lower line, made of panels $(\mathrm{bj})_{j=1,2,3}$, gives results for $\alpha = 0.5$.

where the nonlinearity coefficient Q is positive or negative. This brings about some instability regions as shown in Fig. 3(a3), where we have plotted the product $P \times Q$. Specifically, for $\sigma_n = 5$, $P \times Q$ presents two positive regions, i.e., $0 < k < 0.25$ and $0.32 < k < 0.85$. For the rest, only one region of instability exist for $\sigma_n = 16$ and 22.5, which are respectively $0.3 < k < 0.5$ and $0.42 < k < 0.6$. Using these values of the wavenumber k, we have also plotted the MI growth rate in Fig. 4 versus the perturbation wavenumber K and σ_n. While the different panels $(\mathrm{aj})_{j=1,2,3}$ correspond to different values of the wavenumber k, they have been plotted when the negative ion concentration ratio takes the value $\alpha = 0.1$. There, regions of instability are detected and one sees how sensitive they are to the values of k. Along the same line, still considering the previous values of k, the MI growth rate has been plotted for $\alpha = 0.5$ and the corresponding results are recorded in Fig. 4$(\mathrm{bj})_{j=1,2,3}$. Compared to the case in panels $(\mathrm{aj})_{j=1,2,3}$, regions of instability are restricted to small values of the electron-to-negative ion temperature ratio σ_n.

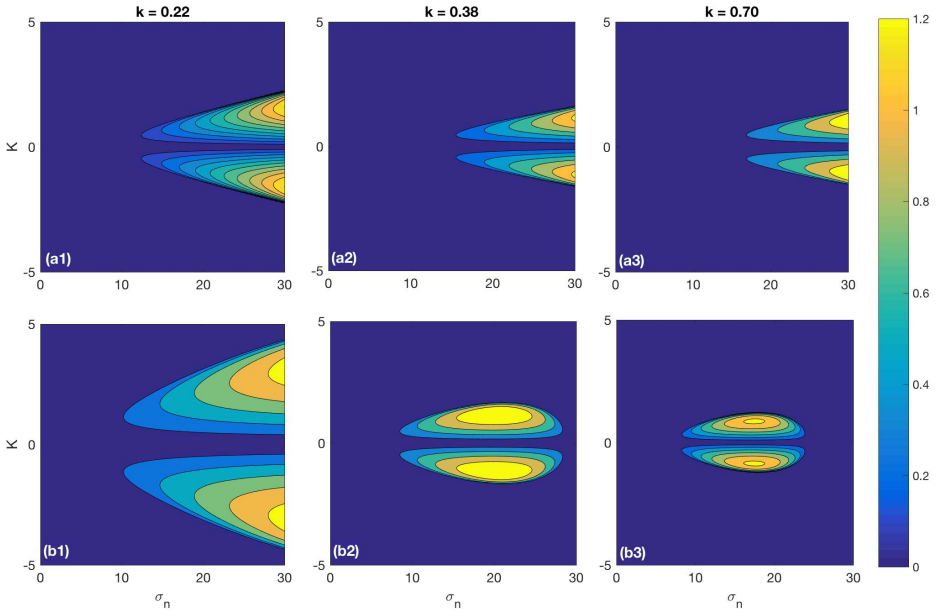

Figure 5: The growth rate of MI is plotted versus the wavenumber K and the electron-to-negative ion temperature ratio σ_n for the perpendicular modulation ($\theta = \pi/2$). The columns, from left to right correspond respectively to $k = 0.22$, 0.38 and 0.70. The upper line, i.e., panels $(\mathrm{aj})_{j=1,2,3}$ corresponds to to $\alpha = 0.1$ and the lower line, made of panels $(\mathrm{bj})_{j=1,2,3}$, gives results for $\alpha = 0.5$.

B) Transverse modulation

The transverse modulation is obtained for $\theta = \pi/2$, which reduces P and Q to

$$P = \gamma_2 \quad \text{and} \quad Q = \gamma_3 - \gamma_4\delta_3. \tag{24}$$

They are plotted in Figs. 3 (b1) and (b2). Contrarily to the case $\theta = 0$, the dispersion parameter P remains positive with changing σ_n, while the value of Q is very sensitive to such a change. Also in this case, there are regions of instability, i.e., where $P \times Q > 0$, as shown in Fig. 3(b3). Obviously, regions of k where MI is expected are the opposite of what has been obtained in Fig. 3(a3). If only very limited values of k can give rise to instability for $\sigma_n = 5$, regions of instability are more obvious for $\sigma_n = 16$ and 22.5. For each of the later cases, there are two regions of instability $0.23 < k < 0.5$ and $0.5 < k < 0.55$ for $\sigma_n = 16$; $0.45 < k < 0.6$ and $0.6 < k < 0.75$ for $\sigma_n = 22.5$. The detected regions of k may indeed give rise to unstable patterns as shown in contour plot of the MI growth rate of Fig. 5. In Figs. 5$(\mathrm{aj})_{j=1,2,3}$, we have considered $\alpha = 0.1$ as in Fig. 4, except that here, one notices a delocalization of the instability domain in the $(\sigma_n, K)-$plane. To remind, for the case of the parallel modulation, instability

has been detected in regions of small σ_n, i.e., values that belong to the interval $0 < \sigma_n < 10$. In this case, i.e., the transverse modulation, modulated IAWs may mainly be found in regions belonging to the interval $10 \leq \sigma_n \leq 30$. In Fig. 5(bj)$_{j=1,2,3}$, we have fixed $\alpha = 0.5$. Compared to Fig. 4(a1), the regions of K giving rise to instability are larger in Fig. 5(b1). There is indeed instability delocalization for $k = 0.38$, where regions of instability belong to the interval $9.8 \leq \sigma_n \leq 28.5$ (see Fig. 5(b2)). The detected region gets more reduced both in the $K-$ and σ_n-directions when $k = 0.70$ as depicted in Fig. 5(b3).

4 Conclusion

In the present paper, we have addressed the MI of IAWs in a 3D unmagnetized electronegative plasma model. Using the reductive-perturbation approach, we have shown that the model equations can be reduced to a set of DS equations in three dimensions, whose coefficients have been found to be dependent on the plasma parameters. Under the activation of MI, we have detected various dynamical modes, this because of the presence of the modulation angle θ. In that respect, a comprehensive parametric analysis of wave instability has been conducted, where regions of instability/stability have been revealed to be very sensitive to θ, σ_n and α. Two main cases have finally been addressed, the longitudinal ($\theta = 0$) and the transverse ($\theta = \pi/2$) modulations. It has in general been found that the two regimes do not belong to the same intervals of the electron-to-negative ion temperature ratio (σ_n) and the wavenumber k. This indeed shows that they have different dynamical features mainly under the activation of MI. The later can support a broad range of excitations depending on the values of the original parameter like α and σ_n. When the used parameters fall well inside the instability regions, ion acoustic solitons may be expected to emerge and display coherent spatiotemporal behaviors. Also, the strong relationship between IAWs and MI has been discussed intensively, including the emergence of exotic solitons like dromions and rogue waves. In the proposed model, finding such exact solutions remains an opened problem which is actually under investigation, especially in the presence of magnetic and relativistic effects.

Acknowledgements

The work by CBT is supported by the Botswana International University of Science and Technology under the grant **DVC/RDI/2/1/16I (25)**.

References

[1] D. Mihalache, D. Mazilu, F. Lederer, Y. V. Kartashov, L-C. Crasovan, L. Torner, and B. A. Malomed, Phys. Rev. Lett. **97** (2006) 073904

[2] D. D. E. Temgoua and T. C. Kofané, Phys. Rev. E **93** (2016) 062223.

[3] M. Djoko and T. C. Kofané, Opt. Commun. **416** (2018) 198.

[4] A. Mohamadou, B. E. Ayissi and T. C. Kofané, Phys. Rev. E **74** (2006) 046604.

[5] I. Maïna, C. B. Tabi, A. Mohamadou, H. P. F. Ekobena and T. C. Kofané, Chaos **25** (2015) 043118.

[6] A. S. Etémé, C. B. Tabi and A. Mohamadou, Commun. Nonl. Sci. Num. Simul. **43** (2017) 211.

[7] C. B. Tabi, R.Y. Ondoua, H. P. Ekobena, A. Mohamadou and T. C. Kofané, Phys. Lett. A **380** (2016) 2374.

[8] G. R. Y. Mefire, C. B. Tabi, A. Mohamadou, H. P. F. Ekobena and T. C. Kofané, Chaos **23** (2013) 033128.

[9] A.-X. Zhang and J.-K. Xue, Phys. Rev. A **75** (2007) 013624.

[10] E. Wamba, A. Mohamadou, T. C. Kofané, Phys. Rev. E **77** (2008) 046216.

[11] A. A. Mamun, P. K. Shukla and B. Eliasson, Phys. Rev. E **80** (2009) 046406.

[12] P. K. Shukla and A. A. Mamun, New J. Phys. **5** (2003) 17

[13] I. Kourakis and P. K. Shukla, Phys. Rev. E **69** (2004) 036411.

[14] P. Carbonaro, Chaos Solit. Fract. **45** (2012) 959.

[15] C. Bedi and T. S. Gill, Phys. Plasmas **19** (2012) 062109.

[16] K. Nishinari, K. Abe and J. Satsuma, J. Phys. Soc. Jpn. **62** (1993) 2021.

[17] K. Nishinari, K. Abe and J. Satsuma, Phys. Plasmas **1** (1994) 2559.

[18] S. V. Vladimirov, K. Ostrikov and G. E. Morfill, Phys. Rev. E **67** (2003) 036406.

[19] H. Ikezi, R. Taylor and D. Baker, Phys. Rev. Lett. **25** (1970) 11.

[20] M. Mehdipoor, Astrophys. Space Sci. **348** (2013) 115 .

[21] H. Washimi and T. Taniuti, Phys. Rev. Lett. **17** (1966) 996.

[22] Y. Nakamura and I. Tsukabayashi, Phys. Rev. Lett. **52** (1984) 2356 .

[23] J. M. Dudley, G. Genty and B. J. Eggleton, Optics Exp. **16** (2008) 3644.

[24] B. Kibler, J. Fatome, C. Finot, G. Millot, F. Dias, G. Genty, N. Akhmediev and J. M. Dudley, Nat. Phys. **6** (2010) 790.

[25] A. Chabchoub, N. Hoffmann, M. Onorato and N. Akhmediev, Phys. Rev. X **2** (2012) 011015.

[26] A. Chabchoub, N. Hoffmann, M. Onorato, A. Slunyaev, A. Sergeeva, E. Pelinovsky and N. Akhmediev, Phys. Rev. E **86** (2012) 056601.

[27] H. Bailung, S. K. Sharma and Y. Nakamura, Phys. Rev. Lett. **107** (2011) 255005.

[28] S. K. Sharma and H. Bailung, J. Geophys. Res. Space Phys. **118** (2013) 919.

[29] C. S. Panguetna, C. B. Tabi and T. C. Kofané, Commun. Nonlinear Sci. Numer. Simul. **55** (2018) 326.

[30] C. S. Panguetna, C. B. Tabi and T. C. Kofané, Phys Plasmas **24** (2017) 092114.

[31] R. Sabry, W. M. Moslem and P. K. Shukla, Astrophys. Space Sci. **333** (2011) 203.

[32] N. Jehan, M. Salahuddin, H. Saleem, and A. M. Mirza, Phys. Plasmas 15, 092301 (2008).

[33] N. Jehan, M. Salahuddin, and A. M. Mirza, Phys. Plasmas 16, 062305 (2009).

[34] M. Tajiri, H. Miura and T. Arai, Phys. Rev. E **66** (2002) 067601.

[35] T. S. Gill, C. Bedi and A. S. Bains, Phys. Plasmas **16** (2009) 032111.

[36] A. E. Mowafy and W. M. Moslem, J. King Saud Univ.-Sci. **24** (2012) 343.

[37] A. Davey and K. Stewartson, Proc. R. Soc. London Ser. A **338** (1974) 101.

[38] C. Sulem and P. L. Sulem, "The nonlinear Schrödinger equation", (Springer-Verlag, 1999)

Journal of Theoretical and Applied Physics
https://doi.org/10.1007/s40094-019-00342-8

RESEARCH

Low relativistic effects on the modulational instability of rogue waves in electronegative plasmas

Chérif S. Panguetna[1] · Conrad B. Tabi[2,3] · Timoléon C. Kofané[1,3]

Received: 7 May 2019 / Accepted: 2 August 2019

Abstract
Relativistic ion-acoustic waves are investigated in an electronegative plasma. The use of the reductive perturbation method summarizes the hydrodynamic model to a nonlinear Schrödinger equation which supports the occurrence of modulational instability (MI). From the MI criterion, we derive a critical value for the relativistic parameter α_1, below which MI may develop in the system. The MI analysis is then conducted considering the presence and absence of negative ions, coupled to effects of relativistic parameter and the electron-to-negative ion temperature ratio. Under high values of the latter, additional regions of instability are detected, and their spatial expansion is very sensitive to the change in α_1 and may support the appearance of rogue waves whose behaviors are discussed. The parametric analysis of super-rogue wave amplitude is performed, where its enhancement is debated relatively to changes in α_1, in the presence and absence of negative ions.

Keywords Relativistic electronegative plasma · Rogue waves · Modulational instability

Introduction

Envelope solitons, generic solutions of the nonlinear Schrödinger (NLS) equation, have been extensively studied during the past 30 years, due to their fundamental importance in nonlinear physics. Based on their localization properties, breather solitons have been used as models of rogue waves (RWs) whose behaviors and characteristics are not yet fully unmasked, mainly because they may appear suddenly, propagate within short times, destroy everything on their way and disappear without any trace [1, 2]. For instance, it has been well established that they may appear in physical systems as the consequence of the interplay between nonlinear and dispersive effects, under the activation of the so-called MI phenomenon [3–8]. Recently, interest in studying RWs has gone beyond oceanography and hydrodynamics [9, 10] to reach some other areas related to optics and photonics [11–14], Bose–Einstein condensation [15–17], biophysics [18–21], plasma physics [22, 23], just to name a few. Particularly, ion-acoustic super-RWs were found in an ultra-cold neutral plasma in the presence of ion-fluid and nonextensive electron distribution [24]. In the same direction, magnetosonic RWs, of first and second order, were investigated numerically in a magnetized plasma [25]. The occurrence of fundamental and second-order RWs was also investigated in a relativistically degenerate plasma using the NLS equation [23]. Comparison between experimental and theoretical occurrences of RWs was proposed recently and applied to multicomponent plasmas with negative ions [26]. A comprehensive analysis by El-Tantawy et al. [27] once more brought out the close relationship between the existence of ion-acoustic RWs and MI in electronegative plasmas (ENPs) in the presence of Maxwellian negative ions, where the dynamical behaviors of the Akhmediev breather (AB), Kuznetsov–Ma (KM) breather and super-RWs were compared.

✉ Conrad B. Tabi
conrad@aims.ac.za; tabic@biust.ac.bw

Chérif S. Panguetna
cherifps@yahoo.fr

Timoléon C. Kofané
tckofane@yahoo.com

[1] Laboratoire de Mécanique, Département de Physique, Faculté des Sciences, Université de Yaoundé I, B.P. 812, Yaoundé, Cameroun

[2] Laboratoire de Biophysique, Département de Physique, Faculté des Sciences, Université de Yaoundé I, B.P. 812, Yaoundé, Cameroun

[3] Botswana International University of Science and Technology, Private Bag 16, Palapye, Botswana

Published online: 16 August 2019

ENPs and their applications have become an active research direction, mainly due to their particular properties related to the simultaneous presence of positive and negative ions, and electrons. Many different processes have been used to experimentally produce ENPs, including plasma processing reactors [28] and low-temperature experiments [29, 30]. Obviously, from recent contributions, when only positive ions are taken into consideration, the nonlinear terms of the Korteweg–de Vries (KdV) equation are positive, and one may obtain only compressive solitary waves [31], whereas in the presence of both positive and negative ions, soliton characteristics considerably change, due to the nonlinear response of the system to the presence of negative ions [32, 33]. This is indubitably related to the charge neutrality condition which changes, leading to a decrease in the number of electrons and a decrease in their subsequent shielding effect. Quite a limited number of works have been devoted to ENPs, including the contributions by Ghim and Hershkowitz [34] and Mamun et al. [35], where the existence of ion-acoustic waves (IAWs) and dust-acoustic waves (DAWs) was addressed in ENPs containing Boltzmann negative ions, Boltzmann electrons and cold mobile positive ions. The response of such waves, solutions of the KdV equation, to external magnetic fields was also studied [32, 33]. Panguetna et al. [36] proposed a comprehensive study of IAWs and their dependence to electronegative parameters such as the negative ion concentration ratio (α) and the electron-to-negative ion temperature ratio (σ_n). In two-space dimensions, beyond the study of MI, dromion solutions and their collision scenario were also studied [37]. More recently, the ENP model was extended to its three-dimensional version, giving Tabi et al. [38] the room to study the effect of the modulation angle on the onset of MI, with application to the three-dimensional Davey–Stewartson equations. Obviously, none of the above-cited works includes relativistic effects which should be considered in the emergence of IAWs when the speed a plasma particle approaches that of light. The nonlinear behaviors of plasma waves may importantly be modified by relativistic effects and lead to fascinating spectra of results, exploitable in the laboratory and in the space. IAWs in weakly relativistic plasmas were studied by Das et al. [39, 40], via the KdV equation, and applied to both nonisothermal and isothermal plasmas. El-Labany [41] reported on the existence of modulated weakly relativistic IAWs in a collisionless, unmagnetized, warm plasma with nonthermal electrons using a NLS equation. The latter was also derived recently by Abdikian [42], in three dimensions, to study the emergence of IAWs, under the activation of MI, in a magnetoplasma with pressure of relativistic electrons. Further confirmation was given on the effect of relativistic parameter to bring about new instability and dynamical regimes in the generation mechanism of modulated IAWs via MI.

The main purpose of the present work is to investigate IAWs properties in an ENP, under weak relativistic effects, in one dimension. One of our main results suggests that there is a critical value, $\alpha_{1,\mathrm{cr}}$, of the relativistic parameter below which MI and its subsequent nonlinear regime (RWs) may appear in the system.

The layout of the paper goes as follows. In Sect. 2, the relativistic ENP model is presented and a reductive perturbation method (RPM) is employed to derive a NLS equation which describes the evolution of modulated wave packets. In Sect. 3, the criterion for MI is derived, from which we find a critical expression for the relativistic parameter. Importance is then given to the effect of negative ions on such instabilities. The response from RWs solutions to relativistic effects is investigated in the same context, followed by a parametric analysis of the super-RW maximum amplitude when ENP and relativistic parameters are varied. The paper ends with concluding remarks in Sect. 4.

Model and amplitude equation

In its original formulation, the model for ENPs is composed of Maxwellian electron and negative ions in addition to cold mobile positive ions [35–38, 43]. In the presence of weak relativistic effects, the dynamics of IAWs is governed by the following set of normalized fluid equations:

$$\frac{\partial n_i}{\partial t} + \frac{\partial n_i u_i}{\partial x} = 0, \tag{1a}$$

$$\frac{\partial(\gamma u_i)}{\partial t} + u_i \frac{\partial(\gamma u_i)}{\partial x} + \frac{\partial \phi}{\partial x} = 0, \tag{1b}$$

$$\frac{\partial^2 \phi}{\partial x^2} = \mu_n \exp \sigma_n \phi + \mu_e \exp \phi - n_i. \tag{1c}$$

The relativistic character of the studied plasma system relies on the factor

$$\gamma = \frac{1}{\sqrt{1 - \alpha_1 u_i^2}} \simeq 1 + \frac{\alpha_1}{2} u_i^2, \tag{2}$$

which is the result of Lorentz transformations. The parameter α_1 incorporates the relativistic effect, here manifested in terms of the plasma density, by the relationship $\alpha_1 = c_s^2/c^2$. n_i and u_i are, respectively, the number density positive ions (normalized by the unperturbed value n_0) and the ion-fluid velocity (normalized by the IA speed $c_s = \sqrt{k_B T_e/m}$). ϕ is the electrostatic wave potential normalized by mc_s^2/e,

where e is the magnitude of the electron charge. The time and space variables are normalized by the ion Debye length $\lambda_D = \sqrt{k_B T_e/4\pi e^2 n}$ and the ion plasma period $\omega^{-1} = 1/\sqrt{4\pi e^2 n_0/m}$, respectively. Here, $\sigma_n = T_e/T_n$ is the electrons-to-negative ion temperature ratio, $\mu_e = n_{e0}/n_0$ and $\mu_n = n_{n0}/n_0$, where n_0 , n_{n0} and n_{e0}, are the unperturbed densities of the positive ions, negative ions and electrons, respectively. At equilibrium, the neutrality condition of the plasma reads $\mu_e + \mu_n = 1$, where $\mu_e = n_{e0}/n_0 = 1/(1+\alpha)$, with $\alpha = n_{n0}/n_{e0}$. Using the power series expansion of the exponential function around zero, Eq. (1c) becomes

$$\frac{\partial^2 \phi}{\partial x^2} = 1 + a_1\phi + a_2\phi^2 + a_3\phi^3 - n_i, \tag{3}$$

where $a_1 = \mu_e + \mu_n\sigma_n$, $a_2 = \frac{\mu_e+\mu_n\sigma_n^2}{2}$ and $a_3 = \frac{\mu_e+\mu_n\sigma_n^3}{6}$. Modulated IAWs appear in physical systems as the consequence of the interplay between nonlinearity and dispersion. Therefore, to explicitly include such effects, the RPM is commonly used [22, 24, 36, 37], which results in equations describing the development of the modulation of the amplitude in the lowest order of an asymptotic expansion. To start, we introduce the stretched variables in space and time as $\xi = \epsilon(x - v_g t)$ and $\tau = \epsilon^2 t$, where the group velocity v_g will be determined later by the solvability condition of Eq. (1). ϵ is a small real parameter ($\epsilon << 1$) that measures the strength of the perturbation. The dependent physical variables around their equilibrium values are assumed as

$$\begin{pmatrix} n_i(x,t) \\ u_i(x,t) \\ \phi(x,t) \end{pmatrix} = \begin{pmatrix} 1 \\ 0 \\ 0 \end{pmatrix} + \sum_{p=1}^{\infty} \epsilon^p \sum_{l=-\infty}^{+\infty} \begin{pmatrix} n_l^{(p)}(\xi,\tau) \\ u_l^{(p)}(\xi,\tau) \\ \phi_l^{(p)}(\xi,\tau) \end{pmatrix} A^l(n,t). \tag{4}$$

We note that the above series includes all overtones $A^l(n,t) = \exp[il(kx - \Omega t)]$, up to order p. These are generated by the nonlinear terms, which means that the corresponding coefficients are of maximum order ϵ^p. Then, the relations $n_l^{(p)*} = n_{-l}^{(p)}$, $u_l^{(p)*} = u_{-l}^{(p)}$ and $\phi_l^{(p)*} = \phi_{-l}^{(p)}$ should be satisfied because of reality condition of physical variables. The asterisk denotes the complex conjugate. Substituting the trial solutions (4) into basic Eqs. (1a), (1b) and (3) and equating the quantities with equal power of ϵ, one obtains several coupled equations in different orders of ϵ.

At (ϵ^1)-order, we have the set of equations

$$\begin{aligned} &-i\omega n_1^{(1)} + iku_1^{(1)} = 0, \quad -i\omega u_1^{(1)} + ik\phi_1^{(1)} = 0, \\ &(k^2 + a_1)\phi_1^{(1)} - n_1^1 = 0, \end{aligned} \tag{5}$$

which is solvable under the condition that the dispersion relation $\omega^2 = \frac{k^2}{k^2+a_1}$ be verified, leading to the first harmonic of perturbation

$$n_1^{(1)} = \frac{k^2}{\omega^2}\phi_1^{(1)}, \quad \text{and} \quad v_1^{(1)} = \frac{k}{\omega}\phi_1^{(1)}. \tag{6}$$

We process the same way to obtain the second-order terms, namely the amplitudes of the second harmonics and constant terms as well as the nonvanishing contribution to the first harmonics. We obtain the following equation for $p = 2$ and $l = 0$:

$$a_1\phi_0^{(2)} - n_0^{(2)} + 2a_2|\phi_1^{(1)}|^2 = 0. \tag{7}$$

The $(p = 2, l = 1)$-order provides the compatibility condition in terms of group velocity, $v_g = a_1\frac{\omega^3}{k^3}$. For $l = 2$, the components of the second harmonic mode $n_2^{(2)}$, $v_2^{(2)}$ and $\phi_2^{(2)}$ are obtained in terms of $\phi_1^{(1)}$ as

$$\begin{aligned} &\phi_2^{(2)} = \alpha_\phi\left(\phi_1^{(1)}\right)^2, \quad n_2^{(2)} = \alpha_n\left(\phi_1^{(1)}\right)^2, \\ &v_2^{(2)} = \alpha_v\left(\phi_1^{(1)}\right)^2, \end{aligned} \tag{8}$$

with

$$\begin{aligned} &\alpha_\phi = \frac{k^2}{2\omega^2} - \frac{a_2}{3k^2}, \quad \alpha_n = (a_1 + 4k^2)\alpha_\phi + a_2, \\ &\alpha_u = \frac{\omega}{k}\alpha_n - \frac{k^3}{\omega^3}. \end{aligned}$$

The zeroth harmonic mode also appears due to the self-interaction of the modulated carrier wave. Its expression cannot be completely expressed using the second order. We will have to consider the third-order equations. Therefore, the set of equations given by the $(l = 0)$-components of the third-order part are given by

$$\begin{aligned} &-v_g n_0^{(2)} + v_0^{(2)} = -\frac{2k^3}{\omega^3}|\phi_1^{(1)}|^2, \\ &-v_g u_0^{(2)} + \phi_0^{(2)} = -\frac{k^2}{\omega^2}|\phi_1^{(1)}|^2, \end{aligned} \tag{9}$$

to which we have added Eq. (7) from $(n = 2, l = 0)$. Along the same line, the following second-order quantities in the zeroth harmonic are found:

$$\begin{aligned} &\phi_0^{(2)} = \beta_\phi|\phi_1^{(1)}|^2, \quad n_0^{(2)} = \beta_n|\phi_1^{(1)}|^2, \\ &v_0^{(2)} = \beta_v|\phi_1^{(1)}|^2, \end{aligned} \tag{10}$$

with

$$\begin{aligned} &\beta_\phi = \frac{-2a_2v_g^2 + (k^2 - 3a_1)}{a_1v_g^2 - 1}, \quad \beta_n = a_1\beta_\phi + 2a_2, \\ &\beta_v = \frac{-2\omega}{(k^2 + a_1)^2} + v_g\beta_n. \end{aligned}$$

Finally, substituting the above derived expressions into the $(n = 3, l = 1)$-components, we obtain the following nonlinear Schrödinger equation:

$$i\frac{\partial\psi}{\partial\tau} + P\frac{\partial^2\psi}{\partial\xi^2} + Q|\psi|^2\psi = 0, \tag{11}$$

for the slow evolution of the first-order amplitude of the plasma perturbation potential $\phi_1^{(1)} = \psi$. P and Q are the dispersion and nonlinearity coefficients, respectively, and their expressions are given by

$$\begin{aligned} P =& \frac{\omega^3}{2k^2}\left[\frac{3\alpha_1 k^4}{2\omega^2} - \frac{2k}{\omega}(k^2 + a_1)(\alpha_u + \beta_u)\right. \\ & \left. -(k^2 + a_1)(\alpha_n + \beta_n) + 2a_2(\alpha_\phi + \beta_\phi) - 3a_3\right], \\ Q =& -\frac{3a_1\omega^5}{2k^4}. \end{aligned} \tag{12}$$

The nonlinear Schrödinger (NLS) equation provides a canonical description for the envelope dynamics of a quasi-monochromatic plane wave propagating in a weakly nonlinear dispersive medium when dissipative processes are negligible [44]. Later, it was found that NLS equation had applications in different subjects. In quantum mechanics, it is obtained in localizing the potential of the Hartree equation [45]. In chemistry, it appears as a continuous-limit model for mesoscopic molecular structures [46]. In protein folding and bending, in the propagation of Davydov's solitons, it is responsible for energy transport and storage along α-helix proteins [8, 47, 48], bubble propagation and energy localization for specific molecular processes such as DNA transcription and replication [49, 50]. In laser propagation, the NLS equation describes the propagation of a laser beam in a medium whose index of reflection is sensitive to the wave amplitude [51–53]. In hydrodynamics, it describes the interaction between short-wave and long-wave gravitational disturbances in the atmosphere [54–56]. Other applications appear in water waves at the free surface of an ideal fluid and in plasma physics (interaction between Langmuir and ion-acoustic waves [22, 23, 27, 36, 42]). Applications of the NLS equation in fiber optics have stimulated further studies in optical communications [57–60]. NLS equation also appears in the description of the Bose–Einstein condensate (BEC), a context where it is often called the Gross–Pitaevskii equation [61–64]. Despite the NLS equation support for spatially localized envelope solitons such as the bright- and dark-type solitons, there is a hierarchy of freak (rational) solutions to the self-focusing NLS equation. In the present work, these solutions represent excitations due to the MI of plasma and known as the RWs [66, 67]. They have been described as waves which appear from nowhere and disappear without a trace. There is also an extensive literature studying various types of solitons on finite background (SFB) consisting of a localized nonlinear structure evolving upon a nonzero background plane wave. In fact, Akhmediev et al. [65, 68, 69], based on the fact the simplest solution of the NLS equation could be a plane wave $\psi \sim e^{i\phi}$, proposed that the emergence of SFB solitons may be a consequence of the instability of the plane wave, through a perturbed solution $\psi \sim \left(1 + \sum_{j=1}^{n} a_j(\xi)\cos j\zeta(\tau - \tau_{0j})\right)$, where $a_j(\xi)$ are Fourier coefficients of the periodic perturbation, ζ is the external modulation frequency, n is the number of harmonics of the fundamental frequency and τ_{0j} is the initial phase of the jth harmonic. This, after linearizing around the unperturbed wave, leads to coefficients a_j of the form $a_j(\xi) = A_j e^{(i\alpha_j + \delta_i\xi)} + B_j e^{(-i\alpha_j - \delta_i\xi)}$, where $\tan\alpha_j = 2\delta_j/(j\zeta)^2$, with $\delta_j = j\zeta\sqrt{1 - j^2\zeta^2/4}$ being the growth rate of the jth harmonic of the perturbation which remains positive for frequencies in the range $0 < j\zeta < 2$. For the first harmonic case, the MI is established and the instability growth rate has a maximum at $\zeta = \sqrt{2}$. However, for arbitrary values of ζ, different cases of RWs were proposed and extensively studied, among which the generalized form [12, 13, 27, 69–71]

$$\begin{aligned} \psi(\xi,\tau) =& \sqrt{\frac{2P}{Q}} \\ & \times\left\{\frac{(1-4a)\cosh(2bP\tau) + \sqrt{2a}\cos(c\xi) + i\sinh(2bP\tau)}{\sqrt{2a}\cos(c\xi) - \cosh(2bP\tau)}\right\} \\ & \times\exp(2iP\tau), \end{aligned} \tag{13}$$

obtained for $\zeta = 2/\sqrt{5}$. Here, the single governing parameter a determines the physical behavior of the solution through the function arguments $b = \sqrt{8a(1-2a)}$ and $c = \frac{2\pi}{L} = 2\sqrt{1-2a}$, with L being the periodicity length of the solution [69, 70]. We should stress that solution (13) can describe three different kinds of breather solutions, depending on the value of a. The super-RW solutions of the focusing NLS equation (11) are localized in both time and space. There are, in fact, two such solutions, the Peregrine soliton and the second-order rogue wave soliton, which are obtained from the general theory of Akhmediev et al. [68, 69] when $\zeta \to 0$

$$\begin{aligned} \psi_j(\xi,\tau) =& \sqrt{\frac{2P}{Q}} \\ & \times\left\{(-1)^j + \frac{G_j(\xi,\bar{\tau}) + 2iP\tau H_j(\xi,\bar{\tau})}{F_j(\xi,\bar{\tau})}\right\}\exp(2iP\tau), \end{aligned} \tag{14}$$

where j is the order of the solution and $\bar{\tau} = 2P\tau$. The functions $G_j(\xi,\bar{\tau})$, $H_j(\xi,\bar{\tau})$ and $F_j(\xi,\bar{\tau})$ are polynomials in variables of $\bar{\tau}$ and ξ, with $F_j(\xi,\bar{\tau})$ not having no real zero. We should, however, stress that the Peregrine RW can be derived as a limiting case of the KM breather, especially

when $a \to 1/2$ [72]. In order to get the two solutions, we will restrict our study to the cases $j \leq 2$.

Modulational instability and rogue waves

The relative sign of P and Q determines the stability of plane-wave solutions to small periodic perturbations. This also implies that any solution whose amplitude is governed by Eq. (11) depends on the sign of PQ, which, in most of plasma systems, depends on system parameters. To this effect, let us assume plane solutions for Eq. (11) to be of the form $\psi(\xi,\tau) = \psi_0(\xi)e^{iQ\psi_0^2\tau}$ that is subjected to a small perturbation $\delta\psi(\xi,\tau) = (U_0 + iV_0)e^{i(K\zeta-\Omega\tau)}$, with K and Ω being, respectively, the wave number and frequency of the perturbation. Following the standard calculations of MI, one obtains the nonlinear dispersion relation

$$\Omega^2 = (K^2P)^2\left(1 - \frac{K_{\rm cr}^2}{K^2}\right), \tag{15}$$

with the critical wave number of the perturbation being $K_{\rm cr} = \psi_0\sqrt{\frac{2Q}{P}}$. For the plane wave to be unstable under modulation, the condition $\Omega^2 < 0$ should be satisfied, i.e.,

$$K < K_{\rm cr} = \psi_0\sqrt{\frac{2Q}{P}}, \tag{16}$$

which clearly shows that for $PQ > 0$, the amplitude-modulated envelope is unstable. This includes several factors related to the ENP system, including the electron-to-negative ion temperature ratio, the negative ion concentration ratio and the newly introduced relativistic parameter α_1.

The relativistic character of the studied plasma system clearly appears in the expression of the dispersion coefficient P, which can be rewritten in the form

$$P = P_{\rm rel} + P_0, \tag{17}$$

P_0 being the nonrelativistic expression that was obtained in Ref. [36] in the form

$$\begin{aligned} P_0 =& \frac{\omega^3}{2k^2}\Big[-\frac{2k}{\omega}(k^2 + a_1)(\alpha_u + \beta_u) \\ & -(k^2 + a_1)(\alpha_n + \beta_n) + 2a_2(\alpha_\phi + \beta_\phi) - 3a_3\Big]. \end{aligned} \tag{18}$$

The above expression was found to be negative, so that the analysis of MI was found to be controlled by the expression of Q that was positive or negative for some values of the wave number k. We should stress that coefficient of nonlinearity in the present study keeps the same expression and therefore keeps the same features as in Ref. [36]. For its part, the relativistic contribution in the expression of P is such that

$$P_{\rm rel} = \frac{3k^2\omega}{4}\alpha_1, \tag{19}$$

and the MI criterion $PQ > 0$ is given by $(P_{\rm rel} + P_0) \times Q > 0$. Indeed, this criterion can be expanded to get

$$P_0Q > \frac{9\alpha_1\omega^6 a_1}{8k^2}, \tag{20}$$

where the right-hand side is what was obtained for the nonrelativistic electronegative model. Therefore, the relativistic contribution is a perturbation to the case of Ref. [36], which, to the best of our knowledge, has not been discussed extensively. In the meantime, knowing P_0Q, it is possible to find the range of α_1 that gives rise to MI through the inequality

$$\alpha_1 < \frac{8k^2}{9\omega^6 a_1}P_0Q = \alpha_{1,\rm cr}. \tag{21}$$

Obviously, the critical value of the relativistic parameter depends on the plasma parameter, and its value is sensitive to the change of the negative ion concentration ratio, for example, as shown in Fig. 1. We should stress that in any of the cases, α_1 should remain positive for MI to occur. Figure 1a is plotted for $\sigma_n = 11.5$ and displays the response of α_1 to the absence of negative ions ($\alpha = 0$) and its comportment when the plasma contains negative ions ($\alpha = 0.1$). In the first case, there are two regions where α_1 is positive, and such regions, labeled MI, are likely to support the formation of envelope bright solitons, this in the presence of negative ions. However, the absence of negative ions is characterized with only one region where α_1 is positive or region of MI. In Fig. 1b, the value of the electron-to-negative ion ratio is increased to 21. One observes that in the absence of negative ions, there is still one region where α_1 is positive, but the two regions brought by the presence of negative ions in Fig. 1a merge to form only one large region. Therefore, the electron-to-negative ion temperature ratio enlarges the domain of k and α_1 that may lead to the formation of bright, or NLS, envelope solitons as the consequence of MI. One should remember that for intervals of k where $\alpha_1 < 0$, no MI should be expected. Such regions in Fig. 1 are indicated by the label (MS). Some of the values of α_1 appearing in those areas have been chosen to plot the product PQ in Fig. 2. Figure 2a is obtained for the value $\sigma_n = 5$ of the electron-to-negative ion temperature ratio. There, the instability domain is very sensitive to the change in α_1, and there exists only one region of instability for a value $k > k_{\rm cr}$ of the wave number. However, the region of stability expands with increasing α_1.

In Fig. 2b, there is only one interval of instability for the nonrelativistic case, while for $\alpha_1 = 5$, two regions of instability appear. However, when $\sigma_n = 10$, the emerging small region of instability disappears. This behavior becomes more

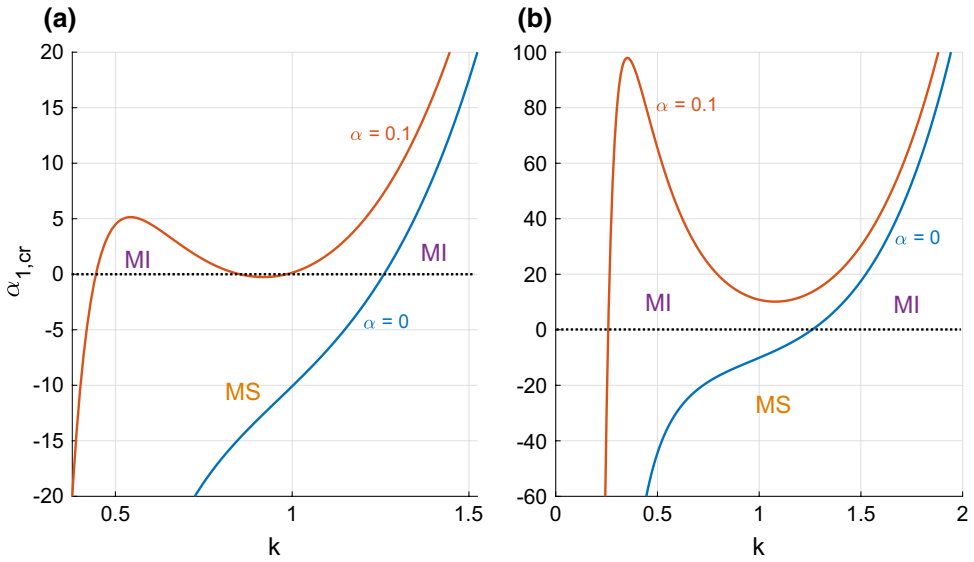

Fig. 1 The panels show plots of the critical value of the relativistic parameter α_1, versus the wave number k, for different values of the electron-to-negative ion temperature ratio. The blue corresponds to $\alpha = 0$ and the red line corresponds to $\alpha = 0.1$, with: **a** $\sigma_n = 11.5$ and **b** $\sigma_n = 21$. Regions of modulational instability are denoted by MI, while regions of modulational stability are indicated as MS

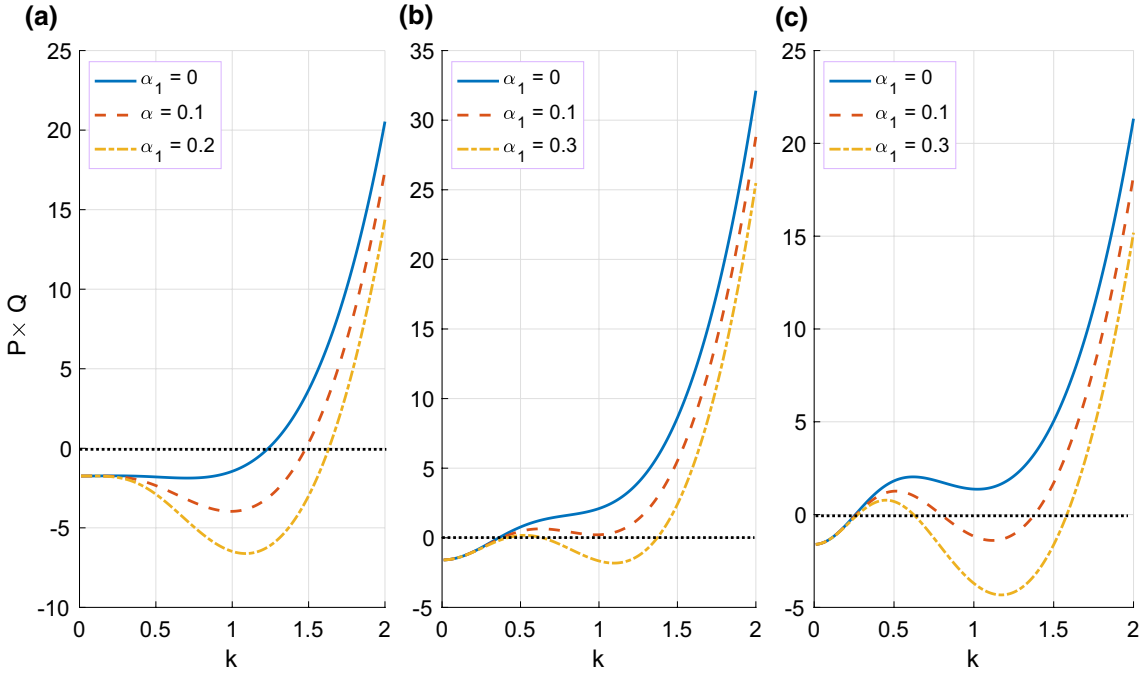

Fig. 2 Panels show how the product PQ responds to the change in α_1. **a** corresponds to $\sigma_n = 5$, **b** to $\sigma_n = 11.5$ and **c** to $\sigma_n = 21$. The blue line corresponds to the nonrelativistic case, while the red and color lines picture the correction brought by the relativistic parameter α_1, with $\alpha = 0.3$

obvious in Fig. 2c, where $\sigma_n = 21$. For $\alpha_1 = 0$, the nonrelativistic system presents one large region of instability, which breaks into two regions under relativistic effects.

Based on all the above calculations, it is clear that critical wave number of perturbation given by Eq. (16) can also be rewritten in a way we perceive clearly the relativistic contribution in the form

$$K_{\rm cr} = \frac{K_{\rm cr,0}}{\sqrt{1 + \frac{P_{\rm rel}}{P_0}}}, \tag{22}$$

where $K_{\rm cr,0} = \psi_0\sqrt{2Q/P}$ is the critical value of K obtained for the nonrelativistic case [36]. Equation (22) suggests that if $P_0 \to \infty$, the nonrelativistic problem will be retried. Otherwise, relativistic effects will be present in the system and

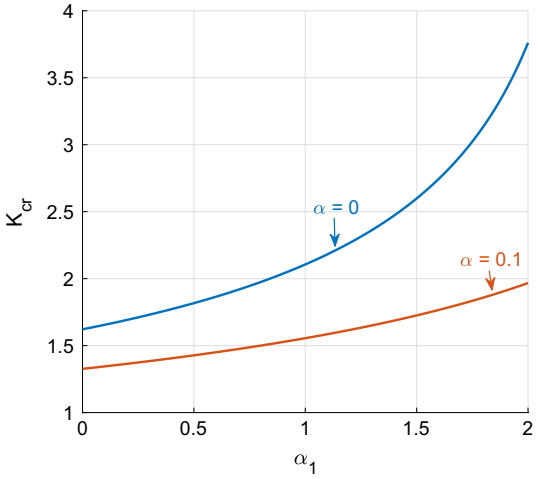

Fig. 3 Panel shows plots of the critical K_{cr} versus the relativistic parameter α_1, in the absence ($\alpha = 0$) and presence ($\alpha = 0.1$) of negative ions, with $\sigma_n = 21$

influence the features of K_{cr} as shown in Fig. 3, where the two curves give information both in the absence and presence of negative ions. In general, K_{cr} is an increasing function of α_1, but the range for instability to occur is larger when negative ions are absent. In such intervals, one may expect the appearance of RWs.

The growth of periodic perturbations on a plane-wave background arising in many nonlinear dispersive systems is the consequence of the fundamental property of MI, this in the narrow band approximation. Beyond this context, the nonlinear stage of MI is described by the exact breather solution of the NLS equation, which has been considered as prototypes of RWs [73–76], that can be analytically studied under the conditions that allow MI to emerge in the NLS equation. For example, Figs. 4 and 5 give plots of the Akhmediev breather (AB) [69] and the Kuznetsov–Ma breather (KMB) [74, 77], respectively. The AB from solution (13) is obtained for $0 < a < 1/2$, and the largest modulation occurs for $\tau = 0$, with the maximum of the envelope at $\xi = 0$. For its part, the KMB is obtained for $1/2 < a < \infty$. Its explicit expression has been proposed in the form [74, 77]

$$\psi_{KM}(\xi,\tau) = \sqrt{\frac{2P}{Q}} \times \left\{ 1 + \frac{2(1-2a)\cos(2b_1 P\tau) - ib_1 \sin(2b_1 P\tau)}{\sqrt{2a}\cosh(c_1\xi) - \cos(2b_1 P\tau)} \right\} \times \exp(2iP\tau), \tag{23}$$

where $b_1 = -ib = \sqrt{8a(2a-1)}$ and $c_1 = -ic = \sqrt{4(2a-1)}$. This waveform is localized in space, but periodic in time. Interestingly, one can recover the Peregrine solution in the limit of infinite temporal period. It was reported recently by Tantawy et al. [27] that these breather solutions are very sensitive to the change in ENP parameters such as α and σ_n. However, the MI in the improved model has also shown big changes in the features of MI due the presence of the relativistic parameter α_1. This is also ostensible in the panels of Fig. 4, where the time and spatial expansion of the breather get modified with increasing α_1; this because it appears in the exponential growth rate of the MI through $P = P_0 + P_{rel}$. For the KMB, the relativistic parameter has the effect of increasing the temporal separation between the adjoining solitonic objects and decreasing their amplitude, which

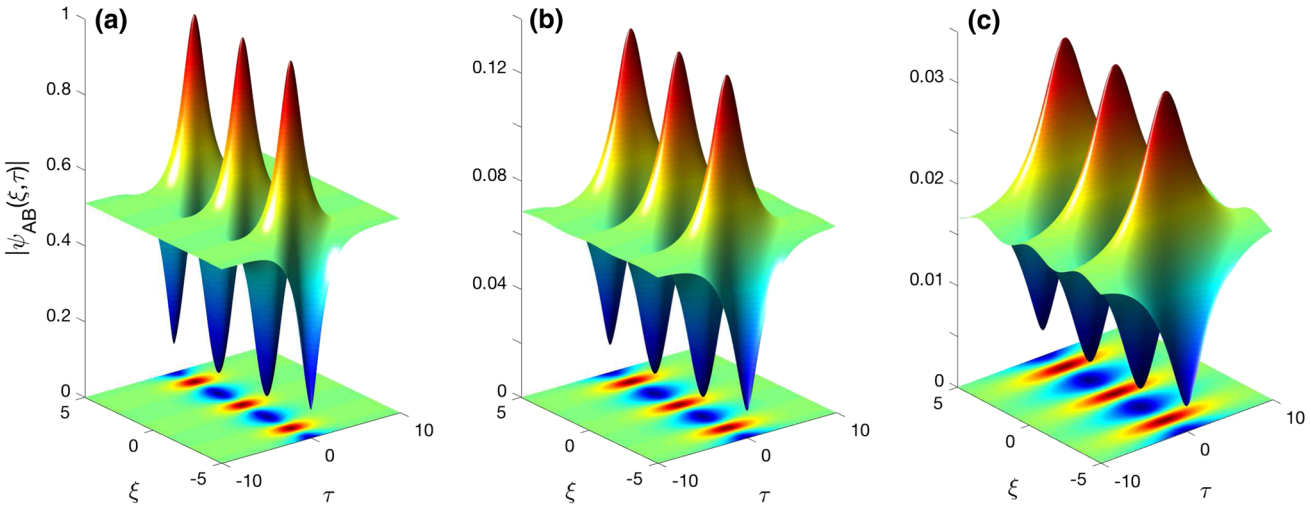

Fig. 4 The panels show the surface and contour plots of the Akhmediev breather, with their corresponding density plots, for different values of the relativistic parameter: **a** $\alpha_1 = 0.1$, **b** $\alpha_1 = 0.2$ and **c** $\alpha_1 = 0.3$. Values for the rest of parameters are $\alpha = 0.1$, $\sigma_n = 11.5$ and $k = 1.8$

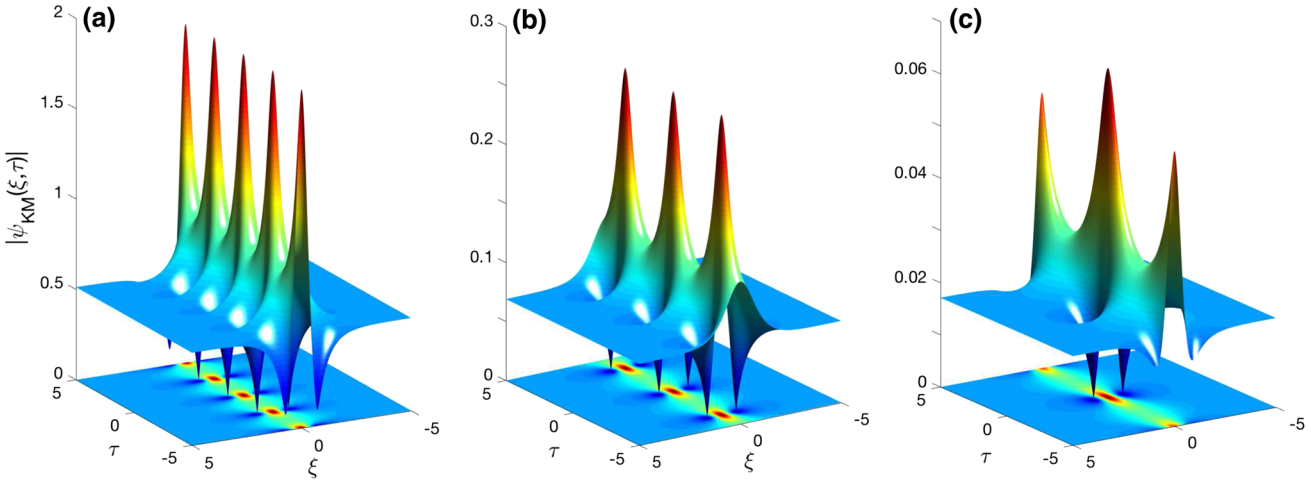

Fig. 5 The panels show the evolution and contour plots of the Kuznetsov–Ma breathers, for different values of the relativistic parameter: **a** $\alpha_1 = 0.1$, **b** $\alpha_1 = 0.2$ and **c** $\alpha_1 = 0.3$. Values for the rest of parameters are $\alpha = 0.1$, $\sigma_n = 11.5$ and $k = 1$

implies reduction in nonlinear effects, causing energy loss and wave amplitude drop. The observed effects, discussed by El-Tanatawy et al. [27], have also been highlighted by Sun et al. [13], this in the absence of relativistic effects.

From Eq. (14), the Peregrine soliton is obtained for $j = 1$, with the polynomials H_1, G_1 and F_1 being such that $H_1(\xi,\bar{\tau}) = 2G_1(\xi,\bar{\tau}) = 8$ and $F_1(\xi,\bar{\tau}) = 1 + 4\xi^2 + 16(P\tau)^2$. The corresponding solution is written in the form [72, 78, 79]

$$\psi_P(\xi,\tau) = \sqrt{\frac{2P}{Q}}\left\{1 - \frac{4(1+4iP\tau)}{1+4\xi^2+16(P\tau)^2}\right\} \times \exp(2iP\tau). \tag{24}$$

It should be noted that it is also the limiting case of the Akhmediev solution when the spatial period tends to infinity. This solution has the form of a single-peaked structure that decays to a plane-wave asymptotic background at either large ξ or τ, but exhibits non-trivial behaviors over a small region in (ξ,τ) as shown in Fig. 6, within the MI region. The second-order/super-RW is obtained from Eq. (14) if $j = 2$, and the polynomials that build the corresponding solution are given by

$$\begin{aligned} G =& \frac{3}{8} - 3\xi^2 - 2\xi^4 - 9\hat{\tau}^2 - 10\hat{\tau}^4 - 12\xi^2\hat{\tau}^2, \\ H =& \frac{15}{4} + 6\xi^2 - 4\xi^4 - 2\hat{\tau}^2 - 4\hat{\tau}^4 - 8\xi^2\hat{\tau}^2, \\ D =& \frac{3}{24} + \frac{9}{8}\xi^2 + \frac{1}{2}\xi^4 + \frac{2}{3}\xi^6 + \frac{33}{8}\hat{\tau}^2 + \frac{9}{2}\hat{\tau}^4 \\ &+ \frac{2}{3}\hat{\tau}^6 - 3\xi^2\hat{\tau}^2 + 2\xi^4\hat{\tau}^2 + 2\xi^2\hat{\tau}^4, \end{aligned} \tag{25}$$

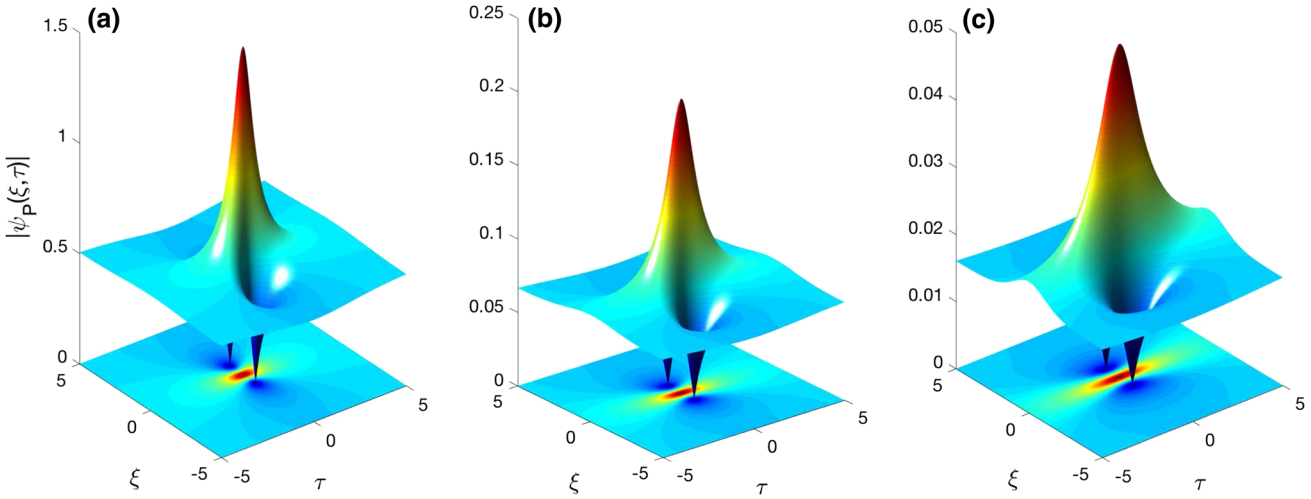

Fig. 6 The panels show the evolution and the corresponding contour plots of the fundamental/Peregrine soliton for different values of the relativistic parameter: **a** $\alpha_1 = 0.1$, **b** $\alpha_1 = 0.2$ and **c** $\alpha_1 = 0.3$. Values for the rest of parameters are $\alpha = 0.1$, $\sigma_n = 10$ and $k = 1.2$

with $\hat{\tau} = 2P\tau$. This leads to the simplified expression

$$\psi_2(\xi,\tau) = \sqrt{\frac{2P}{Q}}\left\{1 + \frac{G + 2iP\tau H}{D}\right\}\exp(2i|P|\tau), \tag{26}$$

which is in fact a nonlinear superposition of simple solutions. This implies that two or more Peregrine solitons can be combined into a more complicated doubly localized structures with a higher amplitude. One of the interesting features of such solutions is that the higher-order excitations are of higher amplitudes and more focused ones compared to the principal solution; i.e., their maximum amplitude can reach many times that of the background level. The corresponding solutions are shown in Fig. 7. The two solutions are very sensitive to the change in the relativistic parameter α_1. Their amplitude decreases with increasing the latter, as already seen in the previous cases, i.e., for the breather solutions. For example, Abdelwahed et al. [80] studied the effects of superthermal electron on the features of nonlinear acoustic waves in unmagnetized collisionless ion pair plasma with superthermal electrons with application to electronegative plasmas. They found that the relativistic parameter and the wave number have the same effect of causing the amplitude to decrease for ion pairs (H^+, H^-), which implies lowering the dispersion, and nonlinearity with strong impact on the amount of rogue energy.

Experimental observation of second-order RWs has been reported recently by Pathak et al. [23] in a multicomponent plasma containing negative ions, where it was reported that super-RWs were more possible to observe experimentally than ordinary RWs. They considered different cases, including plasmas in the presence and absence of negative ions. As already discussed here, the presence of negative ions can indeed modify the instability features and disturb the appearance of coherent structures in plasma. Coupled with relativistic effects, new behaviors may appear, either in the amplitude or in the width, or in both, of the emerging RWs.

More interestingly, such waves appear in regions of parameters where modulated IAWs are expected as the result of the interplay between nonlinear and dispersive effects; this because they have in common the term $\sqrt{\frac{2P}{Q}}$ which should be positive. It is for example shown in Fig. 8 that the negative ion concentration ratio α has influence on the RW amplitude, where the different panels correspond, respectively, to $\alpha = 0.1$, 0.5 and 0.85. Depending on such values, the regions of instability, related to the RW appearance, display different features. For $\alpha = 0$, it is obvious from Fig. 8a that the RW solutions exist in regions of high σ_n, i.e., $25 \le \sigma_n \le 50$, where the highest $|\psi_{S,\max}| = |\psi_S(0,0)| = 4\sqrt{\frac{2P}{Q}}$ belongs to $k = 2$, while high-amplitude RWs are expected for $k = 1.8$ in the case of $\alpha = 0.5$ as depicted in Fig. 8b. Of course, $\alpha = 0$ corresponds to the case where there are no negative ions. The result is therefore not surprising because Fig. 1 reveals the appearance of modulated waves even in the absence of negative ions, where $0 < \alpha_1 < \alpha_{1,\mathrm{cr}}$. Comparing these two cases, one clearly sees that the wave amplitude in Fig. 8b has decreased and the zone of instability gets delocalized, with the highest MI growth rate appearing in the interval $30 \le \sigma_n \le 45$. For $\alpha = 0.85$, $|\psi_{S,\max}|$ is shown in Fig. 8c. Obviously, $|\psi_{S,\max}|$ has increased and regions of instability are expanded, compared to what is observed in Fig. 8b. It should be noted that the calculations of Fig. 8 have been made for a relativistic parameter $\alpha_1 = 0.1$. The same calculations are repeated in Fig. 9, but for $\alpha_1 = 0.3$, with α

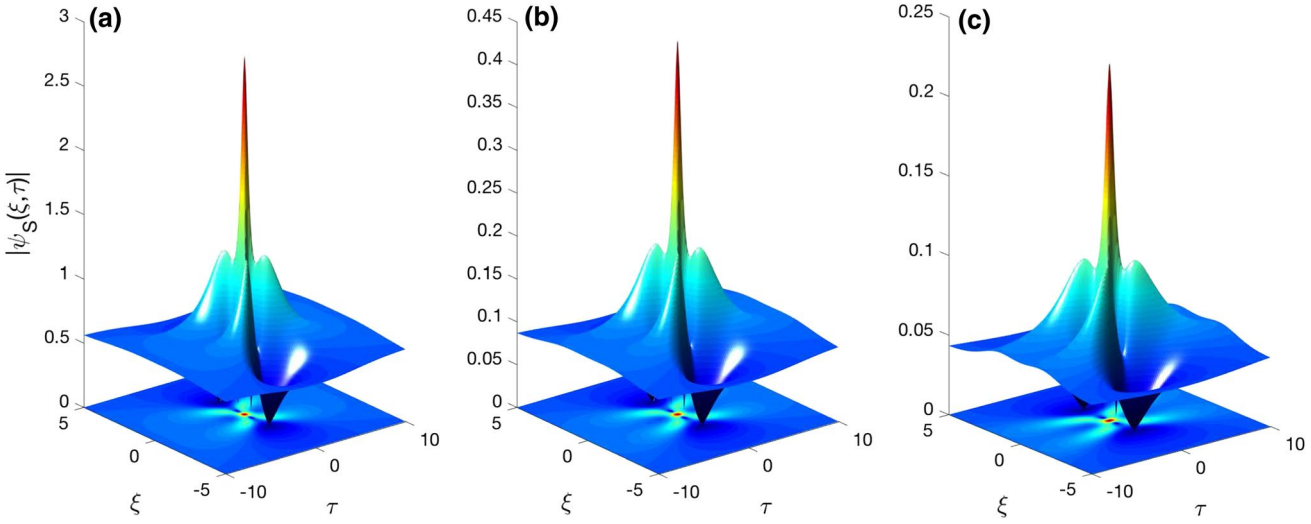

Fig. 7 The panels show the evolution of the second-order super-rogue waves for different values of the relativistic parameter: **a** $\alpha_1 = 0.1$, **b** $\alpha_1 = 0.2$ and **c** $\alpha_1 = 0.3$. Values for the rest of parameters are $\alpha = 0.1$, $\sigma_n = 10$ and $k = 1.2$

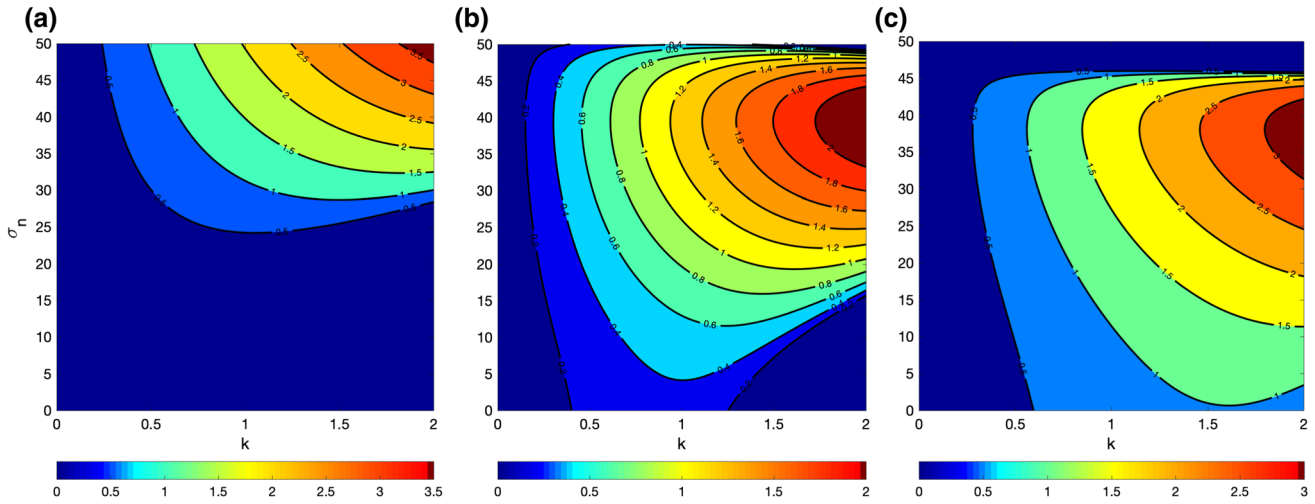

Fig. 8 The panels show the maximum RW amplitude $|\psi_{S,\max}|$ versus k and σ_n, for $\alpha_1 = 0.1$ and **a** $\alpha = 0$, **b** $\alpha = 0.5$ and **c** $\alpha = 0.85$. The lines delimitate areas of parameters where $P/Q > 0$, while the dark-blue region is where $P/Q < 0$

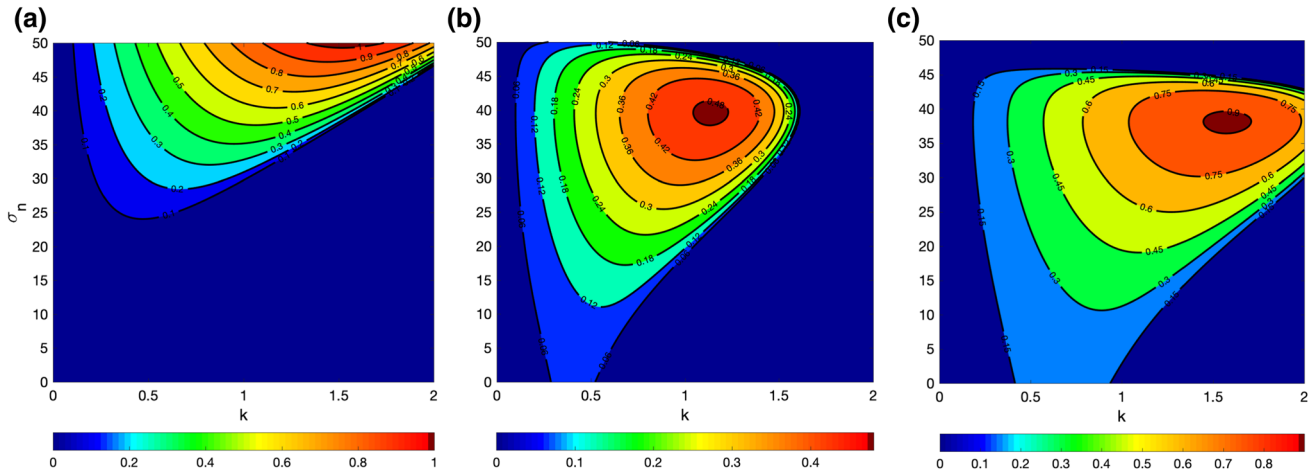

Fig. 9 The panels show the maximum RW amplitude $|\psi_{S,\max}|$ versus k and σ_n, for $\alpha_1 = 0.3$ and **a** $\alpha = 0$, **b** $\alpha = 0.5$ and **c** $\alpha = 0.85$. The lines delimitate areas of parameters where $P/Q > 0$, while the dark-blue region is where $P/Q < 0$

keeping the same values as previously. Although the detected regions of instability display the same behaviors as in Fig. 8, it is nevertheless obvious that the wave amplitude is lower which shows that against α_1, α can influence the appearance and formation of RW in the studied weakly relativistic plasma system. The dynamical behaviors of RWs were discussed in the nonrelativistic model of ENPs, and a critical value for α was proposed [25], below which the wave amplitude decreases or increases, depending on the other plasma parameter values. However, in our context, it is highly ostensible that the relativistic character of the studied system contributes to change such behaviors, therefore leading to much richer comportments.

Concluding remarks

In conclusion, a weakly relativistic model of ENP has been proposed in this work, and we have addressed the dynamics of ion-acoustic waves. In fact, after reducing the proposed model to a NLS equation, we have studied the MI, through its growth rate, and its response to plasma parameters such as α, σ_n and α_1. One of the main results was the determination of the critical value of the relativistic parameter α_1 under which MI may take place. Based on this, we have characterized the appearance of MI both in the presence ($\alpha \neq 0$) and absence ($\alpha = 0$) of negative

ions. The influence of the electron-to-negative ion temperature ratio on MI has also been discussed, where additional regions of instability have been detected due to the interplay between α_1 and σ_n. Moreover, the link between instability and the appearance of RWs has been discussed along with their response to both negative ion concentration and relativistic effects. The parametric analysis of the RW amplitude has been performed, showing that it may be enhanced or reduced, depending on the balance between ENP parameters and the introduced relativistic effects.

Acknowledgements This work is supported by the Botswana International University of Science and Technology under the Grant No. DVC/RDI/2/1/16I (25). CBT thanks the Kavli Institute for Theoretical Physics (KITP), University of California Santa Barbara (USA), where this work was supported in part by the National Science Foundation Grant No. NSF PHY-1748958 and NIH Grant No. R25GM067110.

References

1. Akhmediev, N., Ankiewicz, A., Taki, M.: Waves that appear from nowhere and disappear without a trace. Phys. Lett. A **373**, 675 (2009)
2. Akhmediev, N., Soto-Crespo, J.M., Ankiewicz, A.: Extreme waves that appear from nowhere: on the nature of rogue waves. Phys. Lett. A **373**, 2137 (2009)
3. Maïna, I., Tabi, C.B., Mohamadou, A., Ekobena, H.P.F., Kofané, T.C.: Discrete impulses in ephaptically coupled nerve fibers. Chaos **25**, 043118 (2015)
4. Tabi, C.B., Maïna, I., Mohamadou, A., Ekobena, H.P.F., Kofané, T.C.: Long-range intercellular Ca^{2+} wave patterns. Physica A **435**, 1 (2015)
5. Etémé, A.S., Tabi, C.B., Mohamadou, A.: Long-range patterns in Hindmarsh–Rose networks. Commun. Nonlinear Sci. Numer. Simul. **43**, 211 (2017)
6. Tabi, C.B., Ondoua, R.Y., Ekobena, H.P., Mohamadou, A., Kofané, T.C.: Energy patterns in coupled α-helix protein chains with diagonal and off-diagonal couplings. Phys. Lett. A **380**, 2374 (2016)
7. Mefire, G.R.Y., Tabi, C.B., Mohamadou, A., Ekobena, H.P.F., Kofané, T.C.: Modulated pressure waves in large elastic tubes. Chaos **23**, 033128 (2013)
8. Madiba, S.E., Tabi, C.B., Ekobena, H.P.F., Kofané, T.C.: Long-range energy modes in α-helix lattices with inter-spine coupling. Physica A **514**, 298 (2019)
9. Kharif, C., Pelinovsky, E., Slunyaev, A.: Rogue Waves in the Ocean. Springer, Heidelberg (2009)
10. Chabchoub, A., Hoffmann, N., Onorato, M., Slunyaev, A., Sergeeva, A., Pelinovsky, E., Akhmediev, N.: Observation of a hierarchy of up to fifth-order rogue waves in a water tank. Phys. Rev. E **86**, 056601 (2012)
11. Dudley, J.M., Genty, G., Dias, F., Kibler, B., Akhmediev, N.: Modulation instability, Akhmediev Breathers and continuous wave supercontinuum generation. Opt. Express **17**, 21497 (2009)
12. Kibler, B., Fatome, J., Finot, C., Millot, G., Genty, G., Wetzel, B., Akhmediev, N., Dias, F., Dudley, J.M.: Observation of Kuznetsov–Ma soliton dynamics in optical fibre. Sci. Rep. **2**, 463 (2012)
13. Sun, W.-R., Tian, B., Sun, Y., Chai, J., Jiang, Y.: Akhmediev breathers, Kuznetsov–Ma solitons and rogue waves in a dispersion varying optical fiber. Laser Phys. **26**, 035402 (2016)
14. Frisquet, B., Kibler, B., Millot, G.: Collision of Akhmediev breathers in nonlinear fiber optics. Phys. Rev. X **3**, 041032 (2013)
15. Li, S., Prinari, B., Biondini, G.: Solitons and rogue waves in spinor Bose–Einstein condensates. Phys. Rev. E **97**, 022221 (2018)
16. Li, L., Yu, F.: Non-autonomous multi-rogue waves for spin-1 coupled nonlinear Gross–Pitaevskii equation and management by external potentials. Sci. Rep. **7**, 10638 (2017)
17. Bludov, Y.V., Konotop, V.V., Akhmediev, N.: Vector rogue waves in binary mixtures of Bose–Einstein condensates. Eur. Phys. J. Spec. Top. **185**, 169 (2010)
18. Tabi, C.B.: Fractional unstable patterns of energy in α-helix proteins with long-range interactions. Chaos Solitons Fract. **116**, 092114 (2018)
19. Tchinang, J.D.T., Togueu, A.B.M., Tchawoua, C.: Biological multi-rogue waves in discrete nonlinear Schrödinger equation with saturable nonlinearities. Phys. Lett. A **380**, 3057 (2016)
20. Jia, H.-X., Liu, Y.-J., Wang, Y.-N.: Rogue-wave interaction of a nonlinear Schrödinger model for the alpha-helical protein. Z. Naturforsch. A **27**, 71 (2015)
21. Du, Z., Tian, B., Qu, Q.-X., Chai, H.-P., Wu, X.-Y.: Semirational rogue waves for the three-coupled fourth-order nonlinear Schrödinger equations in an alpha helical protein. Superlattice Microstrust. **112**, 362 (2017)
22. Sultana, S., Islam, S., Mamun, A.A., Schlickeiser, R.: Modulated heavy nucleus-acoustic waves and associated rogue waves in a degenerate relativistic quantum plasma system. Phys. Plasmas **25**, 012113 (2018)
23. Pathak, P., Sharma, S.K., Nakamura, Y., Bailung, H.: Observation of second order ion acoustic Peregrine breather in multicomponent plasma with negative ions. Phys. Plasmas **23**, 022107 (2016)
24. El-Tantawy, S.A., El-Bedwehy, N.A., Moslem, W.M.: Super rogue waves in ultracold neutral nonextensive plasmas. J. Plasma Phys. **79**, 1049 (2013)
25. El-Tantawy, S.A., El-Bedwehy, N.A., El-Labany, S.K.: Ion-acoustic super rogue waves in ultracold neutral plasmas with nonthermal electrons. Phys. Plasmas **20**, 072102 (2013)
26. Bailung, H., Sharma, S.K., Nakamura, Y.: Observation of Peregrine solitons in a multicomponent plasma with negative ions. Phys. Rev. Lett. **107**, 255005 (2011)
27. El-Tantawy, S.A., Wazwaz, A.M., Ali Shan, S.: On the nonlinear dynamics of breathers waves in electronegative plasmas with Maxwellian negative ions. Phys. Plasmas **24**, 022105 (2017)
28. Gottscho, R.A., Gaebe, C.E.: Negative ion kinetics in RF glow discharges. IEEE Trans. Plasma Sci. **14**, 92 (1986)
29. Jacquinot, J., McVey, B.D., Scharer, J.E.: Mode conversion of the fast magnetosonic wave in a deuterium-hydrogen tokamak plasma. Phys. Rev. Lett. **39**, 88 (1977)
30. Ichiki, R., Yoshimura, S., Watanabe, T., Nakamura, Y., Kawai, Y.: Experimental observation of dominant propagation of the ion-acoustic slow mode in a negative ion plasma and its application. Phys. Plasmas **9**, 4481 (2002)
31. Ikezi, H., Taylor, R., Baker, D.: Formation and interaction of ion-acoustic solitions. Phys. Rev. Lett. **25**, 11 (1970)
32. Anowar, M.G., Ashrafi, K.S., Mamun, A.A.: Dust ion-acoustic solitary waves in a magnetized dusty electronegative plasma. J. Plasma Phys. **77**, 133 (2011)

33. Duha, S.S., Rahman, M.S., Mamun, A.A., Anowar, G.M.: Multidimensional instability of dust ion-acoustic solitary waves in a magnetized dusty electronegative plasma. J. Plasma Phys. **78**, 279 (2012)
34. Ghim, Y.K., Hershkowitz, N.: Experimental verification of Boltzmann equilibrium for negative ions in weakly collisional electronegative plasmas. Appl. Phys. Lett. **94**, 151503 (2009)
35. Mamun, A.A., Shukla, P.K., Eliasson, B.: Solitary waves and double layers in a dusty electronegative plasma. Phys. Rev. E **80**, 046406 (2009)
36. Panguetna, C.S., Tabi, C.B., Kofané, T.C.: Electronegative nonlinear oscillating modes in plasmas. Commun. Nonlinear Sci. Numer. Simul. **55**, 326 (2018)
37. Panguetna, C.S., Tabi, C.B., Kofané, T.C.: Two-dimensional modulated ion-acoustic excitations in electronegative plasmas. Phys. Plasmas **24**, 092114 (2017)
38. Tabi, C.B., Panguetna, C.S., Kofané, T.C.: Electronegative (3+1)-dimensional modulated excitations in plasmas. Physica B **545**, 70 (2018)
39. Das, G.C., Paul, S.N.: Ion?acoustic solitary waves in relativistic plasmas. Phys. Fluids **28**, 823 (1985)
40. Das, G.C., Karmakar, B., Paul, S.: Propagation of solitary waves in relativistic plasmas. IEEE Trans. Plasma Sci. **16**, 22 (1988)
41. El-Labany, S., Krim, M.A., El-Warraki, S., El-Taibany, W.: Modulational instability of a weakly relativistic ion acoustic wave in a warm plasma with nonthermal electrons. Chin. Phys. **12**, 759 (2003)
42. Abdikian, A.: Modulational instability of ion-acoustic waves in magnetoplasma with pressure of relativistic electrons. Phys. Plasmas **24**, 052123 (2017)
43. Zheng, X., Chen, Y., Hu, H., Wang, G., Huang, F., Dong, C., Yu, M.Y.: Dust voids in collision-dominated plasmas with negative ions. Phys. Plasmas **16**, 023701 (2009)
44. Sulem, C., Sulem, P.-L.: The Nonlinear Schrödinger Equation: Self-Focusing and Wave Collapse. Springer, New York (1999)
45. Pitaevskii, L.P.: Vortex lines in an imperfect bose gas. Sov. Phys. JETP **13**, 451 (1961)
46. Gaididei, Y.B., Rasmussen, K.O., Christiansen, P.L.: Nonlinear excitations in two-dimensional molecular structures with impurities. Phys. Rev. E **52**, 2951 (1995)
47. Ondoua, R.Y., Tabi, C.B., Ekobena, H.P., Mohamadou, A., Kofané, T.C.: Discrete energy transport in the perturbed Ablowitz–Ladik equation for Davydov model of α-helix proteins. Eur. Phys. J. B **86**, 374 (2012)
48. Ekobena, H.P.F., Tabi, C.B., Mohamadou, A., Kofané, T.C.: Intramolecular vibrations and noise effects on pattern formation in a molecular helix. J. Phys. Condens. Matter **23**, 375104 (2011)
49. Tabi, C.B., Mimshe, J.C.F., Ekobena, H.P.F., Mohamadou, A., Kofané, T.C.: Nonlinear wave trains in three-strand α-helical protein models. Eur. Phys. J. B **86**, 374 (2013)
50. Mimshe, J.C.F., Tabi, C.B., Edongue, H., Ekobena, H.P.F., Mohamadou, A., Kofané, T.C.: Wave patterns in α-helix proteins with interspine coupling. Phys. Scr. **87**, 025801 (2013)
51. Chin, S.L., Hosseini, S.A., Liu, W., Luo, Q., Théberge, F., Aközbek, N., Becker, A., Kandidov, V.P., Kosareva, O.G., Schroeder, H.: The propagation of powerful femtosecond laser pulses in opticalmedia: physics, applications, and new challenges. Can. J. Phys. **83**, 863 (2005)
52. Sprangle, P., Penano, J.R., Hafizi, B.: Propagation of intense short laser pulse in the atmosphere, propagation of intense short laser pulses in the atmosphere. Phys. Rev. E **66**, 046418 (2002)
53. Shim, B., Schrauth, S.E., Gaeta, A.L.: Filamentation in air with ultrashort mid-infrared pulses. Opt. Express **19**, 9118 (2001)
54. Long, R.R.: Solitary waves in the westerlies. J. Atmos. Sci. **21**, 197 (1964)
55. Benny, D.J.: Long nonlinear waves in fluid flows. Appl. Math. **45**, 52 (1966)
56. Ruvinski, K.D., Feldstein, F.I., Freidman, G.I.: Effect of nonlinear damping due to the generation of capillary-gravity ripples on the stability of short wind waves and their modulation by an internal-wave train. Izv. Atmos. Ocean. Phys. **22**, 219 (1986)
57. Franken, P., Hill, A.E., Peters, C.W., Weinrich, G.: Generation of optical harmonics. Phys. Rev. Lett. **7**, 118 (1961)
58. Kapron, F.P., Maurer, R.D., Teter, M.P.: Theory of backscattering effects in waveguides. Appl. Opt. **11**, 1352 (1972)
59. Miya, T., Hanawa, F., Chida, K., Ohmori, Y.: Dispersion-free VAD single-mode fibers in the 1.5-μm wavelength region. Appl. Opt. **22**, 372 (1983)
60. Agrawal, G.P.: Nonlinear Fiber Optics, Optics and Photonics, 5th edn. Academic Press, Cambridge (2013)
61. Wamba, E., Mohamadou, A., Kofané, T.C.: Modulational instability of a trapped Bose–Einstein condensate with two- and three-body interactions. Phys. Rev. E **77**, 046216 (2008)
62. Tamilthiruvalluvar, R., Wamba, E., Subramaniyan, S., Porsezian, K.: Impact of higher-order nonlinearity on modulational instability in two-component Bose–Einstein condensates. Phys. Rev. E **99**, 032202 (2019)
63. Belobo Belobo, D., Ben-Bolie, G.H., Kofané, T.C.: Dynamics of matter-wave condensates with time-dependent two- and three-body interactions trapped by a linear potential in the presence of atom gain or loss. Phys. Rev. E **89**, 042913 (2014)
64. Belobo Belobo, D., Ben-Bolie, G.H., Kofané, T.C.: Dynamics of kink, antikink, bright, generalized Jacobi elliptic function solutions of matter-wave condensates with time-dependent two- and three-body interactions. Phys. Rev. E **91**, 042902 (2015)
65. Hsu, H.C., Kharif, C., Abid, M., Chen, Y.Y.: A nonlinear Schrödinger equation for gravity? Capillary water waves on arbitrary depth with constant vorticity. Part 1. J. Fluid Mech. **854**, 146 (2018)
66. Toenger, S., Godin, T., Billet, C., Dias, F., Erkintalo, M., Genty, G., Dudley, J.M.: Emergent rogue wave structures and statistics in spontaneous modulation instability. Sci. Rep. **5**, 10380 (2015)
67. Sun, W.R., Wang, L.: Vector rogue waves, rogue wave-to-soliton conversions and modulation instability of the higher-order matrix nonlinear Schrödinger equation. Eur. Phys. J. Plus **133**, 495 (2018)
68. Akhmediev, N.N., Eleonskii, V.M., Kulagin, N.E.: Generation of periodic trains of picoseconld pulses in an optical fiber: exact solutions. Sov. Phys. JETP **62**, 894 (1985)
69. Akhmediev, N.N., Korneev, V.I.: Modulation instability and periodic solutions of the nonlinear Schrödinger equation. Teor. Mat. Fiz. **69**, 189 (1986)
70. Wang, L.H., Porsezian, K., He, J.S.: Breather and rogue wave solutions of a generalized nonlinear Schrödinger equation. Phys. Rev. E **87**, 053202 (2013)
71. Abdikian, A., Ismaeel, S.: Ion-acoustic rogue waves and breathers in relativistically degenerate electron-positron plasmas. Eur. Phys. J. Plus **132**, 368 (2017)
72. Ankiewicz, A., Clarkson, P.A., Akhmediev, N.: Rogue waves, rational solutions, the patterns of their zeros and integral relations. J. Phys. A Math. Theor. **43**, 122002 (2010)
73. Akhmediev, N., Eleonskii, V., Kulagin, N.: Exact first-order solutions of the nonlinear Schrödinger equation. Theor. Math. Phys. **72**, 809 (1987)
74. Kuznetsov, E.: Solitons in a parametrically unstable plasma. Akad. Nauk SSSR Dokl. **236**, 575 (1977)
75. Dysthe, K.B., Trulsen, K.: Note on breather type solutions of the NLS as models for freak-waves. Phys. Scr. **T82**, 48 (1999)
76. Osborne, A., Onorato, M., Serio, M.: The nonlinear dynamics of rogue waves and holes in deep-water gravity wave trains. Phys. Lett. A **275**, 386 (2000)

77. Ma, Y.C.: The perturbed plane? Wave solutions of the cubic Schrödinger equation. Stud. Appl. Math. **60**, 43 (1979)
78. Peregrine, D.H.: Water waves, nonlinear Schrödinger equations and their solutions. J. Aust. Math. Soc. Ser. B Appl. Math. **25**, 16 (1983)
79. Ankiewicz, A., Devine, N., Akhmediev, N.: Are rogue waves robust against perturbations? Phys. Lett. A **373**, 3997 (2009)
80. Abdelwahed, H.G., El-Shewy, E.K., Zahran, M.A., Elwakil, S.A.: On the rogue wave propagation in ion pair superthermal plasma. Phys. Plasmas **23**, 022102 (2016)

IOP Publishing Physica Scripta
Phys. Scr. 95 (2020) 075211 (17pp) https://doi.org/10.1088/1402-4896/ab8f40

Modulational instability of coupled waves in electronegative plasmas

C B Tabi[1,4], C S Panguetna[2], T G Motsumi[3] and T C Kofané[1,2]

[1] Botswana International University of Science and Technology, Private Bag 16 Palapye, Botswana
[2] Laboratoire de Mécanique, Département de Physique, Faculté des Sciences, Université de Yaoundé I, B.P. 812 Yaoundé, Cameroon
[3] Department of Mathematics, University of Botswana, Private Mail Bag 22 Gaborone, Botswana

E-mail: conrad@aims.ac.za, tabic@biust.ac.bw, cherifps@yahoo.fr, teko@aims.ac.za and tckofane@yahoo.com

Received 21 February 2020, revised 21 April 2020
Accepted for publication 1 May 2020
Published 13 May 2020

Abstract

The dynamics of coupled ion-acoustic waves is investigated in an electronegative plasma made of Boltzmann negative ions, cold mobile positive ions and Boltzmann electrons. Using the reductive perturbation method, it is shown that the system can fully be described by a set of two coupled nonlinear Schrödinger equations. The parametric analysis of modulational instability reveals the existence of regions of instability that are sensitive to changes in plasma parameters such as the negative ion concentration ratio and the electron-to-negative ion temperature ratio. The analytical results are confronted to numerical simulations, where we examine the long-time dynamics of modulated waves in the electronegative plasma. One obtains the generation of nonlinear modulated waves that are sensitive to the negative-ion concentration ratio. Exact solutions for individual modes are discussed and one finally derives the coupled solution. The response of the latter to the plasma parameter variations is also addressed.

Keywords: electronegative plasmas, modulational instability, counter-propagating waves, solitons

(Some figures may appear in colour only in the online journal)

1. Introduction

During the last two decades, the study of plasma systems is significantly growing, this because of their broad range of applications in microwave transmission [1, 2], space plasmas [3–5], fusion plasmas [6–8] and so on. A plasma that contains a high density of negative ions is known as an electronegative plasma (ENP), generated experimentally via many different methods. ENPs are commonly found in several space observations, including ($H^+ - H^-$) and ($H^+ - O_2^-$), and in the D− and F− areas of the Earth ionosphere [9, 10]. High altitude Titan's upper atmosphere is a good example of places where heavy ions chemistry takes place [11]. According to Coates *et al* [11], the high density of negative ions in such areas may play important roles in the formation of thiolins and many other organic-rich aerosols that eventually fall, via the atmosphere, to the surface [12]. When negative ions are considered in a plasma, the charge neutrality condition gets modified and, obviously, the increase in the negative ion density reduces the electron number density and drastically affects their shielding effect. This has a straightforward effect on the nonlinear properties of the plasma environment, and the subsequent ion-acoustic wave (IAW) characteristics. Several contributions have pointed out the importance of the balance between nonlinearity and dispersion in the formation of IAWs in ENPs [13–15]. Especially, their modulational instability (MI) has been addressed by a few authors, with interest in the way some plasma parameters, such as the electron-to-negative ion temperature ratio and the negative ion concentration ratio, may affect the formation of modulated IAWs [16, 17, 18–20]. Among the partial differential equations that support the propagation of such waves, the nonlinear Schrödinger (NLS) equation remains the most famous, as it has been extensively derived from different

[4] Author to whom any correspondence should be addressed.

plasma models [18–20].Its generalized version such as the Davey-Stewartson equations were also derived, and their solutions discussed [21, 22]. Recent developments have also addressed Rogue wave solutions of the NLS equation, both in one and two dimensions. [20, 21].

Soliton collision and interaction are interesting and fundamental nonlinear phenomena which take place when solitary waves propagate in nonlinear media such as optical fiber communications [23], the spinor Bose–Einstein condensates [24], and plasma physics [21, 25, 26]. First predicted by Zabusky and Kruskal [27], soliton interaction has been observed in the laboratory in shallow water wave experiments [28] and in plasma experiments [29–32]. During such a process, two solitary entities approach each another and interact, with some energy and position exchanges, and continue to travel individually, keeping their waveform and characteristics. Most of the works devoted to the study of this phenomenon have been done for small amplitude plasma waves supported by the Korteweg–de Vries (KdV) equation. For example, the interaction of two counter-propagating solitons of equal amplitude in complex plasmas was studied experimentally and numerically by Harvey *et al* [33] who found that the solitary wave with temporal delay results from collisions. Tagare *et al* [34] found that rarefactive solitons could be produced by small amplitude electron-acoustic (EA) soliton interaction in magnetized plasmas containing cold electron beam, background plasma electrons, and two-temperature ions. New types of EA solitons were produced by the head-on collision of solitary waves in electron beam plasma system with isothermal hot electrons by Berthomier *et al* [35]. Verheest *et al* [36] studied head-on collisions of electrostatic solitons in nonthermal plasmas using the KdV and the modified KdV equations. El-Tantawy [25] recently made use of the extended Poincaré-Lighthill-Kuo (PLK) reductive perturbation method and studied the collisions of weakly nonlinear structures in an ENP consisting of Boltzmann electrons, Boltzmann negative ions, and cold mobile positive ions. Besides, many authors studied the nonlinear structures in ENPs having one type of negative ions [37–39]. Moreover, the propagation and the head-on collisions of nonplanar ion-acoustic (IA) solitons in ENPs containing two different types of negative ions were also addressed. Other contributions have also shown that the system of equations governing the physics of plasmas can be reduced to a pair of coupled NLS equations. Remarkably, the coupled NLS equations that admit soliton solutions are also well-known to support MI, with new wave-coupling phenomena compared with the ordinary process of MI. In that context, Gupta *et al* [40] studied the MI of electromagnetic waves when relativistic effects are taken into account via a pair of coupled NLS equations combining transverse and longitudinal waves. The MI of plane waves was addressed by Wright [41] using an integrable defocusing set of coupled NLS, with a trigonal spectral curve. The MI of two nonlinearly coupled upper-hybrid waves in plasmas was studied by Kourakis *et al* [42] using coupled NLS equations whose analytical solutions were also reviewed in the form of Bright-bright and Bright-dark coupled envelope solitons. Nevertheless, from the different studies conducted on the emergence and interaction of solitary waves in ENPs, only a few, if none, highlights MI arising from the interaction of two wave packets in the context of coupled NLS equations. In this paper, we embark in such an analysis and establish the strong link between interacting bright envelope solitons and the emergence of MI, and its dependence to relevant physical ENP parameters, namely the electrons-to-negative ion temperature ratio and the negative-ion concentration ratio.

The work is layed out as follows: section 2 introduces the hydrodynamic model equations from which the coupled NLS equations are derived using the multiple-scale perturbation method. In section 3, we undertake the analytical study of the linear stability analysis and MI of plane wave solutions of the coupled NLS equations. A comprehensive parametric analysis of MI phenomenon is carried out with insistence on the effect of negative ion parameters. This is followed by some computational applications of MI. The formation of single and coupled bright envelope soliton excitations is discussed in section 4, where explicit coupled soliton profiles are presented along with their response to negative-ion parameter changes during the head-on collisions. The results are finally summarized in the concluding section 5.

2. Mathematical Model and coupled NLS equations

2.1. Model

Let us consider a three-component collisionless plasma consisting of Maxwellian electrons and negative ions in addition to cold mobile positive ions. In this system, the electron and negative ions inertia are neglected due to the fact that IAWs propagate at phase speed. The later is much higher than the positive ion thermal speed which, in turn, is much lower than the electron and negative ion thermal speeds. The self-consistent electric field acting on a plasma retards the most mobile charged particles, which usually leads to a Boltzmann distribution of electrons. In the case of weak attachment (when the self-diffusion of negative ions prevails over the bulk processes), the Boltzmann distribution is realized for both electrons and negative ions. In all cases of interest, this situation takes place for a small role of attachment in comparison to the ambipolar diffusion of negative ions [43, 44]. The dynamics of IAWs in such plasmas can be described by the following set of normalized hydrodynamic equations [21, 22, 45]:

$$\frac{\partial n_i}{\partial t} + \frac{\partial n_i u}{\partial x} = 0, \tag{1a}$$

$$\frac{\partial u}{\partial t} + u\frac{\partial u}{\partial x} + \frac{\partial \phi}{\partial x} = 0, \tag{1b}$$

$$\frac{\partial^2 \phi}{\partial^2 x} = \Lambda(\phi) - n_i, \tag{1c}$$

where $\Lambda(\phi) = \mu_e \exp(\phi) + \mu_n \exp(\sigma_n \phi) \approx 1 + a_1\phi + a_2\phi^2 + a_3\phi^3 - n$, with $a_1 = \mu_e + \mu_n\sigma_n$, $a_2 = \frac{\mu_e + \mu_n\sigma_n^2}{2}$ and $a_3 = \frac{\mu_e + \mu_n\sigma_n^3}{6}$. In the above set of equations, n_i and u are respectively, the number density and velocity of charged dusts (with mass m), normalized by the unperturbed value n_0 and the dust-acoustic (DA) speed $c_s = \sqrt{Zk_BT_e/m}$, with T_e denoting the electron temperature, k_B the Boltzmann constant and Z the charged dust state, i.e., the number of electrons per ions residing on the dust-grain surface. ϕ is the electrostatic wave potential normalized by k_BT_e/e, where e is the magnitude of the electron charge. The time and space variables are normalized by the ion Debye length $\lambda_D = (k_BTe/4\pi e^2 n_0)^{1/2}$ and the ion plasma period $\omega^{-1} = (4\pi e^2 n_0/m)^{-1/2}$, respectively. In equation (1*c*), $\sigma_n = T_e/T_n$ is the electron-to-negative ion temperature ratio, where $\mu_e = n_{e0}/n_0$ and $\mu_n = n_{n0}/n_0$, with n_0, n_{n0}, and n_{e0} being the unperturbed densities of the positive ions, negative ions, and electrons, respectively. At equilibrium, the neutrality condition of the plasma reads $\mu_e + \mu_n = 1$, where $\mu_e = n_{e0}/n_0 = 1/(1+\alpha)$, with $\alpha = n_{n0}/n_{e0}$ being the negative-ion concentration ratio.

2.2. The coupled NLS equations

In order to investigate the interaction of IAWs and derive the amplitude equations for the plasma system considered here, we make use of the multiple-scale expansion method [46, 47]. In doing so, we introduce the stretched variables in space and time as $x_n = \epsilon^n x$ and $t_n = \epsilon^n t$. This gives the differential relations $\frac{\partial}{\partial x} = \sum_{n=0}^{N} \epsilon^n \frac{\partial}{\partial x_n}$ and $\frac{\partial}{\partial t} = \sum_{n=0}^{N} \epsilon^n \frac{\partial}{\partial t_n}$. The dependent physical variables around their equilibrium values are expanded as

$$\begin{pmatrix} n_i(x,t) \\ u_i(x,t) \\ \phi(x,t) \end{pmatrix} = \begin{pmatrix} 1 \\ 0 \\ 0 \end{pmatrix} + \sum_{p=1}^{\infty} \epsilon^p \begin{pmatrix} n_p(x_0, x_1, x_2, \ldots; t_0, t_1, t_2, \ldots) \\ u_p(x_0, x_1, x_2, \ldots; t_0, t_1, t_2, \ldots) \\ \phi_p(x_0, x_1, x_2, \ldots; t_0, t_1, t_2, \ldots) \end{pmatrix} \tag{2}$$

Substituting equation (2) into equations (1), equating the quantities with equal power of ϵ and keeping up to the cubic-order terms in the perturbation expansion, we obtain the following sets of differential equations:

(i) At order $O(\epsilon^1)$,

$$\frac{\partial n_1}{\partial t_0} + \frac{\partial u_1}{\partial x_0} = 0, \quad \frac{\partial u_1}{\partial t_0} + \frac{\partial \phi_1}{\partial x_0} = 0, \quad \frac{\partial^2 \phi_1}{\partial x_0^2} = a_1\phi_1 - n_1. \tag{3}$$

(ii) At order $O(\epsilon^2)$,

$$\begin{aligned} &\frac{\partial n_2}{\partial t_0} + \frac{\partial n_1}{\partial t_1} + \frac{\partial u_2}{\partial x_0} + \frac{\partial u_1}{\partial x_1} + n_1\frac{\partial u_1}{\partial x_0} + u_1\frac{\partial n_1}{\partial x_0} = 0, \\ &\frac{\partial u_2}{\partial t_0} + \frac{\partial u_1}{\partial t_1} + u_1\frac{\partial u_1}{\partial x_0} + \frac{\partial \phi_2}{\partial x_0} + \frac{\partial \phi_1}{\partial x_1} = 0, \\ &\frac{\partial^2 \phi_2}{\partial x_0^2} + 2\frac{\partial^2 \phi_1}{\partial x_0 x_1} = a_1\phi_2 + a_2(\phi_1)^2 - n_2. \end{aligned} \tag{4}$$

(iii) At order $O(\epsilon^3)$,

$$\begin{aligned} &\frac{\partial n_3}{\partial t_0} + \frac{\partial n_2}{\partial t_1} + \frac{\partial n_1}{\partial t_2} + \frac{\partial u_3}{\partial x_0} \\ &\quad + \frac{\partial u_2}{\partial x_1} + \frac{\partial u_1}{\partial x_2} + n_2\frac{\partial u_1}{\partial x_0} + n_1\frac{\partial u_2}{\partial x_0} + n_1\frac{\partial u_1}{\partial x_1} + u_2\frac{\partial n_1}{\partial x_0} \\ &\quad + u_1\frac{\partial n_2}{\partial x_0} + u_1\frac{\partial n_1}{\partial x_1} = 0, \\ &\frac{\partial u_3}{\partial t_0} + \frac{\partial u_2}{\partial t_1} + \frac{\partial u_1}{\partial t_2} + u_2\frac{\partial u_1}{\partial x_0} \\ &\quad + u_1\frac{\partial u_1}{\partial x_1} + \frac{\partial \phi_3}{\partial x_0} + \frac{\partial \phi_2}{\partial x_1} + \frac{\partial \phi_1}{\partial x_2} = 0, \\ &\frac{\partial^2 \phi_3}{\partial x_0^2} + \frac{\partial^2 \phi_1}{\partial x_1^2} + 2\frac{\partial^2 \phi_1}{\partial x_0 x_2} + 2\frac{\partial^2 \phi_2}{\partial x_0 x_1} \\ &\quad = a_1\phi_3 + 2a_2\phi_1\phi_2 + a_3(\phi_1)^3 - n_3, \end{aligned} \tag{5}$$

In order to derive the coupled NLS equations, solutions for the field equations (3)–(5) should be found. Therefore, for the order $O(\epsilon^1)$, solutions for the set of differential equations (3) are suggested as

$$\begin{aligned} n_1 &= N\exp(i\theta) + N'\exp(i\theta') + c.c., \\ u_1 &= u_1^{(1)}\exp(i\theta) + u_1'^{(1)}\exp(i\theta') + c.c., \\ \phi_1 &= \phi_1^{(1)}\exp(i\theta) + \phi_1'^{(1)}\exp(i\theta') + c.c., \end{aligned} \tag{6}$$

where N, N', $u_1^{(1)}$, $u_1'^{(1)}$, $\phi_1^{(1)}$ and $\phi_1'^{(1)}$ are unknown complex amplitudes to be determined from the solution of the field equations. θ and θ' are the phases defined by $\theta = \omega t_0 - kx_0$ and $\theta' = \omega' t_0 - k' x_0$, with ω and k (ω' and k') being, respectively, the angular frequency and the wavenumber of the progressive (regressive) wave. Introducing equations (6) into equations (3), the following solutions are obtained

$$\begin{aligned} u_1^{(1)} &= \frac{\omega}{k}N, \qquad \phi_1^{(1)} = \frac{\omega^2}{k^2}N = \frac{1}{k^2 + a_1}N, \\ u_1'^{(1)} &= -\frac{\omega'}{k'}N', \qquad \phi_1'^{(1)} = \frac{\omega'^2}{k'^2}N' = \frac{1}{k'^2 + a_1}N', \end{aligned} \tag{7}$$

provided that the dispersion relations $\omega^2 = \frac{k^2}{k^2+a_1}$, and $\omega'^2 = \frac{k'^2}{k'^2+a_1}$ are satisfied.

For $O(\epsilon^2)$ order equation, we first introduce equations (6) and (7) into (4) to obtain the set of equations

$$\begin{aligned}\frac{\partial n_2}{\partial t_0} + \frac{\partial u_2}{\partial x_0} &= -\left(\frac{\partial N}{\partial t_1} + \frac{\omega}{k}\frac{\partial N}{\partial x_1}\right)e^{i\theta} \\ &+ \left(\frac{\partial N'}{\partial t_1} - \frac{\omega'}{k'}\frac{\partial N'}{\partial x_1}\right)e^{i\theta'} + 2i\omega N^2 e^{2i\theta} \\ &+ 2i\omega' N'^2 e^{2i\theta'} + i\left((\omega+\omega') + \frac{k'\omega}{k} + \frac{k\omega'}{k'}\right)NN'e^{i(\theta+\theta')} \\ &+ i\left((\omega-\omega') + \frac{k'\omega}{k} - \frac{k\omega'}{k'}\right)NN'^{*}e^{i(\theta-\theta')} + c.c\,., \end{aligned} \tag{8a}$$

$$\begin{aligned}\frac{\partial u_2}{\partial t_0} + \frac{\partial \phi_2}{\partial x_0} &= -\left(\frac{\omega}{k}\frac{\partial N}{\partial t_1} + \frac{\omega^2}{k^2}\frac{\partial N}{\partial x_1}\right)e^{i\theta} \\ &+ \left(\frac{\omega'}{k'}\frac{\partial N'}{\partial t_1} + \frac{\omega'^2}{k'^2}\frac{\partial N'}{\partial x_1}\right)e^{i\theta'} \\ &+ i\frac{\omega^2}{k}N^2 e^{2i\theta} + i\frac{\omega'^2}{k'}N'^2\exp(2i\theta') \\ &+ i\omega\omega'\left(\frac{1}{k}+\frac{1}{k'}\right)NN'e^{i(\theta+\theta')} \\ &+ i\omega\omega'\left(\frac{1}{k'}-\frac{1}{k'}\right)NN'^{*}e^{i(\theta-\theta')} + c.c\,., \end{aligned} \tag{8b}$$

$$\begin{aligned}\frac{\partial^2\phi_2}{\partial x_0^2} &+ n_2 - a_1\phi_2 \\ &= +2i\frac{\omega^2}{k}\frac{\partial N}{\partial x_1}e^{i\theta} - 2i\frac{\omega'^2}{k'}\frac{\partial N'}{\partial x_1}e^{i\theta'} + a_2\frac{\omega^4}{k^4}N^2e^{2i\theta} \\ &+ a_2\frac{\omega'^4}{k'^4}N'^2\exp(2i\theta') + 2a_2\frac{\omega^2\omega'^2}{k^2k'^2}NN'e^{i(\theta+\theta')} \\ &+ 2a_2\frac{\omega^2\omega'^2}{k^2k'^2}NN'e^{i(\theta-\theta')} \\ &+ a_2\frac{\omega^4}{k^4}|N|^2 + a_2\frac{\omega'^4}{k'^4}|N'|^2 + c.c\,.., \end{aligned} \tag{8c}$$

where, N^* is the complex conjugate of N. The differential Eqs (8) suggests us to seek for solutions n_2, u_2 and ϕ_2 as

$$\begin{aligned} n_2 &= \hat{N}_2^{(0)} + N_2^{(1)}e^{i\theta} + N'^{(1)}_2 e^{i\theta'} + N_2^{(2)}e^{2i\theta} + N'^{(2)}_2 e^{2i\theta'} \\ &\quad + N_2^{(+)}e^{i(\theta+\theta')} + N_2^{(-)}e^{i(\theta-\theta')} + c.c\,., \\ u_2 &= \hat{u}_2^{(0)} + u_2^{(1)}e^{i\theta} + u'^{(1)}_2 e^{i\theta'} + u_2^{(2)}e^{2i\theta} + u'^{(2)}_2 e^{2i\theta'} \\ &\quad + u_2^{(+)}e^{i(\theta+\theta')} + u_2^{(-)}e^{i(\theta-\theta')} + c.c\,., \\ \phi_2 &= \hat{\phi}_2^{(0)} + \phi_2^{(1)}e^{i\theta} + \phi'^{(1)}_2 e^{i\theta'} + \phi_2^{(1)}e^{2i\theta} \\ &\quad + \phi'^{(1)}_2 e^{2i\theta'} + \phi_2^{(+)}e^{i(\theta+\theta')} + \phi_2^{(-)}e^{i(\theta-\theta')} + c.c\,., \end{aligned} \tag{9}$$

where $\hat{N}_2^{(0)}$, $u_2^{(1)}$... $p_2^{(0)}$ are some functions of slow variables. Introducing these solutions into equations (8) leads to the set of equations

$$\hat{N}_2^{(0)} = a_1\hat{\phi}_2^{(0)} + a_2\frac{\omega^4}{k^4}|N|^2 + a_2\frac{\omega^4}{k^4}|N'|^2, \tag{10a}$$

$$\begin{aligned} i\omega N_2^{(1)} - iku_2^{(1)} &= -\left(\frac{\partial N}{\partial t_1} + \frac{\omega}{k}\frac{\partial N}{\partial x_1}\right), \\ i\omega u_2^{(1)} - ik\phi_2^{(1)} &= -\left(\frac{\omega}{k}\frac{\partial N}{\partial t_1} + \frac{\omega^2}{k^2}\frac{\partial N}{\partial x_1}\right), \\ N_2^{(1)} &= (a_1+k^2)\phi_2^{(1)} + 2i\frac{\omega^2}{k}\frac{\partial N}{\partial x_1}, \\ i\omega N'^{(1)}_2 - ik'u'^{(1)}_2 &= -\left(\frac{\partial N'}{\partial t_1} + \frac{\omega'}{k'}\frac{\partial N'}{\partial x_1}\right), \\ i\omega u'^{(1)}_2 - ik'\phi'^{(1)}_2 &= -\left(\frac{\omega'}{k'}\frac{\partial N'}{\partial t_1} + \frac{\omega'^2}{k'^2}\frac{\partial N'}{\partial x_1}\right), \\ N'^{(1)}_2 &= (a_1+k'^2)\phi'^{(1)}_2 + 2i\frac{\omega'^2}{k'}\frac{\partial N'}{\partial x_1}, \end{aligned} \tag{10b}$$

$$\begin{aligned} &\omega N_2^{(2)} - ku_2^{(2)} = \omega N^2, \quad 2\omega u_2^{(2)} - 2k\phi_2^{(2)} = \frac{\omega^2}{k}N^2, \\ &N_2^{(2)} = (4k^2+a_1)\phi_2^{(2)} + a_2\frac{\omega^4}{k^4}N^2, \\ &\omega N'^{(2)}_2 - k'u'^{(2)}_2 = \omega' N'^2, \\ &2\omega' u'^{(2)}_2 - 2k'\phi'^{(2)}_2 = \frac{\omega'^2}{k'}N'^2, \\ &N'^{(2)}_2 = (4k'^2+a_1)\phi'^{(2)}_2 + a_2\frac{\omega'^4}{k'^4}N'^2. \end{aligned} \tag{10c}$$

The expressions of the following functions of slow variables are also carried out:

$$\begin{aligned} &n_2^{(-)} = A_n^{(-)}NN', \quad u_2^{(-)} = A_u^{(-)}NN', \quad \phi_2^{(-)} = A_\phi^{(-)}NN', \\ &n_2^{(+)} = A_n^{(+)}NN'^{*}, \quad u_2^{(+)} = A_u^{(+)}NN'^{*}, \quad \phi_2^{(+)} = A_\phi^{(+)}NN'^{*}, \end{aligned} \tag{11}$$

with

$$\begin{aligned} A_n^{(\pm)} &= \frac{\alpha^{(\pm)}}{\beta^{(\pm)}}, \quad A_\phi^{(\pm)} = \frac{(\omega\pm\omega')^2}{(k\pm k')^2}A_n^{(\pm)} - \delta^{\pm}, \\ A_u^{(\pm)} &= \frac{\omega\pm\omega'}{k\pm k'}A_n^{(\pm)} - \left\{\frac{\omega}{k}+\frac{\omega'}{k'}\right\}, \\ \alpha^{(\pm)} &= 1 - \frac{(\omega\pm\omega')^2}{(k\pm k')^2}\{(k\pm k')^2 + a_1\}, \\ \beta^{(\pm)} &= 2a_2\frac{\omega^2\omega'^2}{k^2k'^2} - \delta^{\pm}\{(k\pm k')^2 + a_1\}, \\ \delta^{(\pm)} &= \frac{2\omega\omega'}{kk'} + \frac{\omega^2k' \pm \omega'^2k}{kk'(k\pm k')}. \end{aligned}$$

Solving equations (10*a*) for $u_2^{(1)}$ and $\phi_2^{(1)}$, we have

$$\begin{aligned} u_2^{(1)} &= \frac{\omega}{k}N_2^{(1)} - \frac{i}{k}\left\{\frac{\partial N}{\partial t_1} + \frac{\omega}{k}\frac{\partial N}{\partial x_1}\right\}, \\ \phi_2^{(1)} &= \frac{\omega^2}{k^2}N_2^{(1)} - \frac{2i\omega}{k^2}\left\{\frac{\partial N}{\partial t_1} + \frac{\omega}{k}\frac{\partial N}{\partial x_1}\right\}. \end{aligned} \tag{12}$$

Comparing equations (12) to equations (10*b*) and taking into account the dispersion relation, we obtain

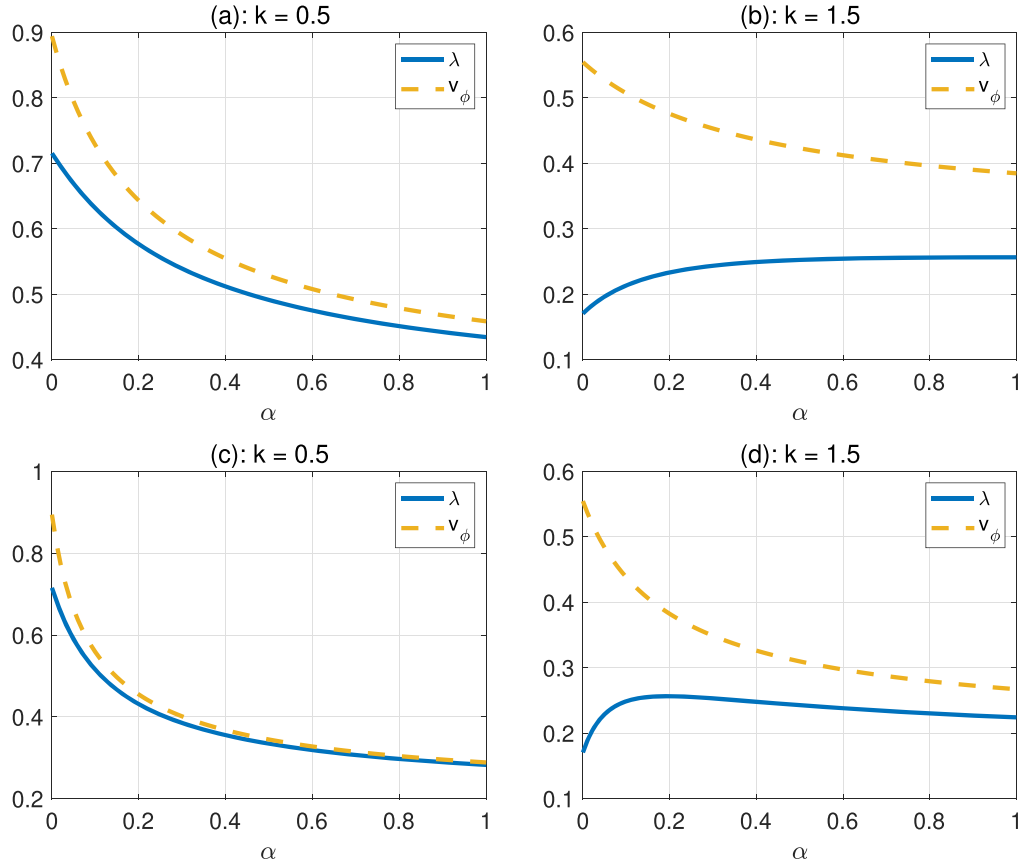

Figure 1. The panels show the group speed $\lambda = \frac{\partial \omega}{\partial k}$ and the phase speed $v_\phi = \frac{\omega}{k}$ versus the negative-ion concentration ratio α. Panels (a) and (b) are plotted for $\sigma_n = 12$, while panels (c) and (d) correspond to $\sigma_n = 22.5$. Values for λ and v_ϕ are recorded for two values of the wavenumber $k = 0.5$ and $k = 1.5$.

$$a_1 \frac{\omega^3}{k^3} \frac{\partial N}{\partial x_1} + \frac{\partial N}{\partial t_1} = 0. \tag{13}$$

From equations (13), the nonzero solution for N must be in the form $N = N(\xi, t_2, \ldots, x_2, \ldots)$, where $\xi = x_1 - \lambda t_1$, with λ being the group speed of the progressive wave and given by $\lambda = a_1 \frac{\omega^3}{k^3}$. We should, however, stress that the group speed can also be derived from the dispersion relation along with the phase speed. These two quantities, related to the model under study, are represented in figure 1 versus the negative-ion concentration ratio α for two values of the electron-to-negative ion temperature ratio σ_n and the wavenumber k. In general, the phase speed is higher than the group speed, especially when $k = 1.5$. However, for $k = 0.5$ and $\sigma_n = 22.5$, one clearly sees in figure 1(c), when $\alpha \to 1$, that $v_\phi \simeq \lambda$, which is similar to a non-dispersive plasma system, while for the rest of the cases, $v_\phi > \lambda$, meaning that the plasma medium is dispersive, which is common in the D− and F− areas of the Earth ionosphere [9, 10, 48].

The solutions for $u_2^{(1)}$ and $\phi_2^{(1)}$ from (12) become

$$\begin{aligned}
u_2^{(1)} &= \frac{\omega}{k} N_2^{(1)} - \frac{i}{k}\left(\frac{\omega}{k} - \lambda\right)\frac{\partial N}{\partial \xi}, \\
\phi_2^{(1)} &= \frac{\omega^2}{k^2} N_2^{(1)} - \frac{2i\omega}{k^2}\left(\frac{\omega}{k} - \lambda\right)\frac{\partial N}{\partial \xi}, \\
u'^{(1)}_2 &= \frac{\omega'}{k'} N'^{(1)}_2 - \frac{i}{k'}\left(\frac{\omega'}{k'} - \lambda'\right)\frac{\partial N'}{\partial \xi'}, \\
\phi'^{(1)}_2 &= \frac{\omega'^2}{k'^2} N'^{(1)}_2 - \frac{2i\omega'}{k'^2}\left(\frac{\omega'}{k'} - \lambda'\right)\frac{\partial N'}{\partial \xi'}.
\end{aligned} \tag{14}$$

Here, one can note that $N' = N'(\xi', t_2, \ldots, x_2, \ldots)$ and $\xi' = x_1 - \lambda' t_1$. These suggest that the group speed λ' of the regressive wave is given by $\lambda' = a_1 \frac{\omega'^3}{k'^3}$. The set given in equations (10*c*) leads to the following solutions:

$$\begin{aligned}
&N_2^{(2)} = \alpha_n N^2, \quad u_2^{(2)} = \alpha_u N^2, \quad \phi_2^{(2)} = \alpha_\phi N^2. \\
&N'^{(2)}_2 = \alpha'_n N'^2, \quad u'^{(2)}_2 = \alpha'_u N'^2, \quad \phi'^{(2)}_2 = \alpha'_\phi N'^2,
\end{aligned} \tag{15}$$

where

$$\alpha_n = \frac{4k^2 + a_1}{2k^2} - \frac{a_2\omega^2}{3k^4},$$
$$\alpha_u = \frac{\omega}{k}(\alpha_n - 1), \qquad \alpha_\phi = \frac{\omega^2}{k^2}\left(\alpha_n - \frac{3}{2}\right),$$
$$\alpha'_n = \frac{4k'^2 + a_1}{2k'^2} - \frac{a_2\omega'^2}{3k'^4},$$
$$\alpha'_u = \frac{\omega'}{k'}(\alpha'_n - 1), \qquad \alpha'_\phi = \frac{\omega'^2}{k'^2}\left(\alpha'_n - \frac{3}{2}\right).$$

We should however stress that the solution cannot be determined completely within the second order equation. We therefore need the equations governing $\hat{N}_2^{(0)}$, $\hat{n}_2^{(0)}$, $\hat{\phi}_2^{(0)}$, $N_3^{(1)}$, $N'^{(1)}_3$, $u_3^{(1)}$, $u'^{(1)}_3$, $\phi_3^{(1)}$, $\phi'^{(1)}_3$. Introducing (10*a*) into the second-order equation(8) yields

$$\frac{\partial \hat{N}_2^{(0)}}{\partial t_1} + \frac{\partial \hat{u}_2^{(0)}}{\partial x_1} + \frac{\omega}{k}\frac{\partial |N|^2}{\partial x_1} + \frac{\omega'}{k'}\frac{\partial |N'|^2}{\partial x_1} = 0$$
$$\frac{\partial \hat{u}_2^{(0)}}{\partial t_1} + \frac{\partial \hat{\phi}_2^{(0)}}{\partial x_1} + \frac{\omega^2}{2k^2}\frac{\partial |N|^2}{\partial x_1} + \frac{\omega'^2}{2k'^2}\frac{\partial |N'|^2}{\partial x_1} = 0 \qquad (16)$$

to which we add equation (10*a*). Keeping in mind that N and N' depend, respectively, on ξ and ξ', equations (16) suggest that $\hat{N}_2^{(0)}$, $\hat{n}_2^{(0)}$ and $\hat{\phi}_2^{(0)}$ can be decomposed as $\hat{N}_2^{(0)} = N_2^{(0)}(\xi,\ldots) + N'^{(0)}_2(\xi',\ldots)$, $\hat{u}_2^{(0)} = u_2^{(0)}(\xi,\ldots) + u'^{(0)}_2(\xi',\ldots)$ and $\hat{\phi}_2^{(0)} = \phi_2^{(0)}(\xi,\ldots) + \phi'^{(0)}_2(\xi',\ldots)$, so that equations (16) become

$$-\lambda\frac{\partial N_2^{(0)}}{\partial \xi} + \frac{\partial \hat{u}_2^{(0)}}{\partial \xi} + \frac{\omega}{k}\frac{\partial |N|^2}{\partial \xi} = 0,$$
$$-\lambda\frac{\partial u_2^{(0)}}{\partial \xi} + \frac{\partial \phi_2^{(0)}}{\partial \xi} + \frac{\omega^2}{2k^2}\frac{\partial |N|^2}{\partial \xi} = 0,$$
$$\hat{N}_2^{(0)} = a_1\hat{\phi}_2^{(0)} + a_2\frac{\omega^4}{k^4}|N|^2, \qquad (17)$$

whose solutions are obtained as

$$N_2^{(0)} = \beta_n|N|^2, \qquad u_2^{(0)} = \beta_u|N|^2, \qquad \phi_2^{(0)} = \beta_\phi|N|^2, \qquad (18)$$

where $\beta_\phi = \frac{2\lambda^2 a_2\omega^4 - 2k^3\lambda\omega - k^2\omega^2}{2k^4(1-\lambda^2 a_1)}$, $\beta_u = \lambda a_1\beta_\phi + \lambda$, $a_2\frac{\omega^4}{k^4} - \frac{\omega}{k}$, and $\beta_n = a_1\beta_\phi + a_2\frac{\omega^4}{k^4}$.

From equations (14) and (16), similar expressions are obtained for $N'^{(0)}_2$, $u'^{(0)}_2$ and $\phi'^{(0)}_2$ provided that the unprimed quantities are replaced by the primed ones. In order to complete the multiple-scale procedure, we need the equations governing $N_3^{(1)}$, $N'^{(1)}_3$, $u_3^{(1)}$, $u'^{(1)}_3$, $\phi_3^{(1)}$, $\phi'^{(1)}_3$. In this framework, by equating the terms in $\exp(\theta)$ on one hand, and those in $\exp(\theta')$ on the other, we obtain the following set of equations for the order $O(\epsilon^3)$:

$$i\omega N_3^{(1)} - iku_3^{(1)} = -\frac{\partial N_2^{(1)}}{\partial t_1} - \frac{\partial N}{\partial t_2} - \frac{\partial u_2^{(1)}}{\partial x_1} - \frac{\omega}{k}\frac{\partial N}{\partial x_2} - 2i(k\hat{u}_2^{(0)} + \omega\hat{n}_2^{(0)})N + i(ku_2^{(2)} + \omega n_2^{(2)})N^* + i\frac{k}{k'}(k'u_2^{(+)} + \omega' n_2^{(+)})N'^* + i\frac{k}{k'}(k'u_2^{(-)} + \omega' n_2^{(-)})N',$$

$$i\omega u_3^{(1)} - ik\phi_3^{(1)} = -\frac{\partial u_2^{(1)}}{\partial t_1} - \frac{\omega}{k}\frac{\partial N}{\partial t_2} - \frac{\partial \phi_2^{(1)}}{\partial x_1} - \frac{\omega^2}{k^2}\frac{\partial N}{\partial x_2} + 2i\omega\hat{u}_2^{(0)}N + i\omega u_2^{(2)}N^* + i\omega'\frac{k}{k'}u_2^{(+)}N'^* + i\omega'\frac{k}{k'}u_2^{(-)}N',$$

$$n_3^{(1)} - (k^2 + a_1)\phi_3^{(1)} = 2ik\frac{\partial \phi_2^{(1)}}{\partial x_1} + 2i\frac{\omega^2}{k}\frac{\partial N}{\partial x_2} - \frac{\omega^2}{k^2}\frac{\partial^2 N}{\partial x_1^2} + 4a_2\frac{\omega^2}{k^2}\hat{\phi}_2^{(0)}N + 2a_2\frac{\omega^2}{k^2}\phi_2^{(2)}N^* + 2a_2\frac{\omega'^2}{k'^2}\phi_2^{(+)}N'^* + 2a_2\frac{\omega'^2}{k'^2}\phi_2^{(-)}N' + 2a_3\frac{\omega^6}{k^6}|N|^2N + 2a_3\frac{\omega^2\omega'^4}{k^2k'^4}|N'|^2N, \qquad (19)$$

$$i\omega' N'^{(1)}_3 - ik'u'^{(1)}_3 = -\frac{\partial N'^{(1)}_2}{\partial t_1} - \frac{\partial N'}{\partial t_2} - \frac{\partial u'^{(1)}_2}{\partial x_1} - \frac{\omega'}{k'}\frac{\partial N'}{\partial x_2} - 2i(k'\hat{u}_2^{(0)} + \omega'\hat{n}_2^{(0)})N' + i(k'u'^{(2)}_2 + \omega' n'^{(2)}_2)N'^* + i\frac{k}{k'}(k'u_2^{(+)} + \omega' n_2^{(+)})N'^* + i\frac{k}{k'}(k'u_2^{(-)} + \omega' n_2^{(-)})N',$$

$$i\omega' u'^{(1)}_3 - ik'\phi'^{(1)}_3 = -\frac{\partial u'^{(1)}_2}{\partial t_1} - \frac{\omega'}{k'}\frac{\partial N'}{\partial t_2} - \frac{\partial \phi'^{(1)}_2}{\partial x_1} - \frac{\omega'^2}{k'^2}\frac{\partial N'}{\partial x_2} + 2i\omega'\hat{u}_2^{(0)}N' + i\omega' u'^{(2)}_2 N'^* + i\omega\frac{k'}{k}u_2^{(+)}N^* + i\omega\frac{k'}{k}u_2^{(-)}N,$$

$$n'^{(1)}_3 - (k'^2 + a_1)\phi'^{(1)}_3 = 2ik'\frac{\partial \phi'^{(1)}_2}{\partial x_1} + 2i\frac{\omega'^2}{k'}\frac{\partial N'}{\partial x_2} - \frac{\omega'^2}{k'^2}\frac{\partial^2 N'}{\partial x_1^2} + 4a_2\frac{\omega'^2}{k'^2}\hat{\phi}_2^{(0)}N' + 2a_2\frac{\omega'^2}{k'^2}\phi'^{(2)}_2 N'^* + 2a_2\frac{\omega^2}{k^2}\phi_2^{(+)}N^* + 2a_2\frac{\omega^2}{k^2}\phi_2^{(-)}N + 2a_3\frac{\omega'^6}{k'^6}|N'|^2N' + 2a_3\frac{\omega'^2\omega^4}{k'^2k^4}|N|^2N'. \qquad (20)$$

Eliminating $N_3^{(1)}$, $u_3^{(1)}$ and $\phi_3^{(1)}$ from equations (19) leads to

$$
\begin{aligned}
&2i\omega\left(\frac{\partial N_2^{(1)}}{\partial t_1}+\lambda\frac{\partial N_2^{(1)}}{\partial x_1}\right)+2i\omega\left(\frac{\partial N}{\partial t_2}+\lambda\frac{\partial N}{\partial x_2}\right)\\
&+\left(\lambda^2-4\frac{\omega\lambda}{k}+\frac{2\omega^2}{k^2}-4\frac{\omega^4}{k^2}+\frac{4\lambda\omega^3}{k}\right)\frac{\partial^2 N}{\partial\xi^2}\\
&+\left(-\frac{4a_2\omega^4}{k^2}\beta_\phi+2\omega^2\beta_n+\omega^2\alpha_n\right.\\
&\left.+4k\omega\beta_u+2k\omega\alpha_u-2a_3\frac{\omega^8}{k^6}\right)|N|^2N\\
&+\left(-\frac{4a_2\omega^4}{k^2}\beta'_\phi+2\omega^2\beta'_n+\omega\omega'\frac{k}{k'}(A_n^{(+)}+A_n^{(-)})\right.\\
&\quad+k^2\left(\frac{\omega}{k}+\frac{\omega'}{k'}\right)(A_u^{(+)}+A_u^{(-)})\\
&+4k\omega B'_u-2a_2\frac{\omega^4}{k^2}\alpha_\phi\\
&\left.-2a_2\frac{\omega^2\omega'^2}{k'^2}(A_\phi^{(+)}+A_\phi^{(-)})\right)|N'|^2N=0. \qquad (21)
\end{aligned}
$$

Additionally, we introduce a new variable τ as $t_2=\tau$ and $x_2=\epsilon\xi+\lambda\tau$ [46, 47], and we obtain the following NLS equation:

$$
i\frac{\partial N}{\partial\tau}+\alpha_1\frac{\partial^2 N}{\partial\xi^2}+\alpha_2|N|^2N+\alpha_3|N'|^2N=0, \qquad (22)
$$

where the coefficients α_1, α_2 and α_3 are given by

$$
\begin{aligned}
\alpha_1&=\frac{\lambda^2}{2\omega}-\frac{2\lambda}{k}-2\frac{\omega^3}{k^2}+\frac{2\lambda\omega^2}{k},\\
\alpha_2&=\frac{\omega}{2}(\alpha_n+2\beta_n)+k(\alpha_u+2\beta_u)-\frac{2a_2\omega^3}{k^2}\beta_\phi-a_3\frac{\omega^7}{k^6},\\
\alpha_3&=\omega\beta'_n+2k\beta'_u-\frac{2a_2\omega^3}{k^2}\beta'_\phi\\
&\quad-\frac{a_2\omega^3}{k^2}\alpha_\phi+\frac{\omega' k}{2k'}(A_n^{(+)}+A_n^{(-)})\\
&\quad+\frac{k^2}{2\omega}\left(\frac{\omega}{k}+\frac{\omega'}{k'}\right)(A_u^{(+)}+A_u^{(-)})\\
&\quad-\frac{a_2\omega\omega'^2}{k'^2}(A_\phi^{(+)}+A_\phi^{(-)}).
\end{aligned} \qquad (23)
$$

Through a similar procedure, applied to Eqs(20), the counterpart of equation (22) is obtained in the form

$$
i\frac{\partial N'}{\partial\tau}+\alpha'_1\frac{\partial^2 N'}{\partial\xi'^2}+\alpha'_2|N'|^2N'+\alpha'_3|N|^2N'=0, \qquad (24)
$$

where α'_1, α'_2 and α'_3 are respectively obtained from α_1, α_2 and α_3 by replacing (ω, k) by (ω', k'). Further introducing the change of variables $\xi'=x_1-\lambda' t_1=\xi-(\lambda-\lambda')t_1$ [46, 49], equations (22) and (24)can then be rewritten in terms of ξ and τ as

$$
i\frac{\partial N}{\partial\tau}+\alpha_1\frac{\partial^2 N}{\partial\xi^2}+\alpha_2|N|^2N+\alpha_3|N'|^2N=0, \qquad (25a)
$$

$$
\begin{aligned}
&i\frac{\partial N'}{\partial\tau}+i\left(\frac{\lambda'-\lambda}{\epsilon}\right)\frac{\partial N'}{\partial\xi}+\alpha'_1\frac{\partial^2 N'}{\partial\xi^2}\\
&+\alpha'_2|N'|^2N'+\alpha'_3|N|^2N'=0.
\end{aligned} \qquad (25b)
$$

In this work, we are interested in the particular case $k'=-k$, i.e., $\omega'=\omega$ and $\lambda'=-\lambda$ which clearly introduces the counter-propagating character of the coupled solution. In addition, we perform the dependent variable transformation $N'=N'\exp\left[-i\left(\frac{\lambda}{\epsilon}\xi+\frac{\lambda^2}{\mu_1}\tau\right)\right]$ to get ride of the terms in $\frac{\partial N'}{\partial\xi}$ from equation (25*b*). One finally obtains the following coupled NLS equations:

$$
i\frac{\partial N}{\partial\tau}+\mu_1\frac{\partial^2 N}{\partial\xi^2}+(\mu_2|N|^2+\mu_3|N'|^2)N=0, \qquad (26a)
$$

$$
i\frac{\partial N'}{\partial\tau}+\mu_1\frac{\partial^2 N'}{\partial\xi^2}+(\mu_2|N'|^2+\mu_3|N|^2)N'=0, \qquad (26b)
$$

where

$$
\begin{aligned}
\mu_1=\alpha_1,\quad \mu_2=\alpha_2,\quad \mu_3=\alpha_3&=\omega\beta_n-2k\beta_u\\
&-\frac{2a_2\omega^3}{k^2}\beta_\phi-\frac{\omega^3}{2k^2}(4k^2+a_1)-\frac{2a_2^2\omega^7}{k^6}.
\end{aligned} \qquad (27)
$$

The study of solitons as solutions of coupled NLS equations have attracted lots of consideration these recent years, this because they appear in a broad range of physical settings and finds applications, for example, in biophysics [50, 51], plasma physics [42], coupled electromagnetic waves [52], electrical lattices [53–56] and Bose–Einstein Condensates [57], just to name a few. Usually, when the appropriate asymptotic method is applied to such generic models, the coefficients of the coupled NLS equations depend on system parameters, as it is the case for μ_1, μ_2 and μ_3 in the system under study. For the specific case of ENPs, such dependence is supported by the plots of figure 2, where the coefficients μ_1, μ_2 and μ_3 are plotted versus the wavenumber k, when ENP parameters change. We note from figure 2(a) that for any value of α, the dispersion coefficients μ_1 remains negative, as already reported in some recent works [16, 17, 18–20]. However, figure 2(b) shows that the coefficient of nonlinearity μ_2 is also negative in some intervals of k, when $\alpha=0.1$ and $\alpha=0.4$, but becomes positive when $k>k_{cr,1}$. Values of μ_2 related to $\alpha=0.3$ and 0.4are exclusively positive. In figure 2(c), it is clearly obvious that for $\alpha=0.1$ and $\alpha=0.2$, the nonlinear coupling coefficients μ_3 is negative. For $\alpha=0.3$ and $\alpha=0.4$, μ_3 is positive in some intervals $k<k_{cr,2}$, and negative for the rest of the values of k. Here, the coefficients of the coupled NLS equations have been plotted for $\sigma_n=22$.

3. Modulational instability

MI, a process by which a plane wave breaks up into filaments at high intensities, is a ubiquitous process that takes place in many areas of physics. Over the years, MI has been identified in a broad range of physical settings, among which hydrodynamics [58, 59], neural networks [60–62], plasma physics

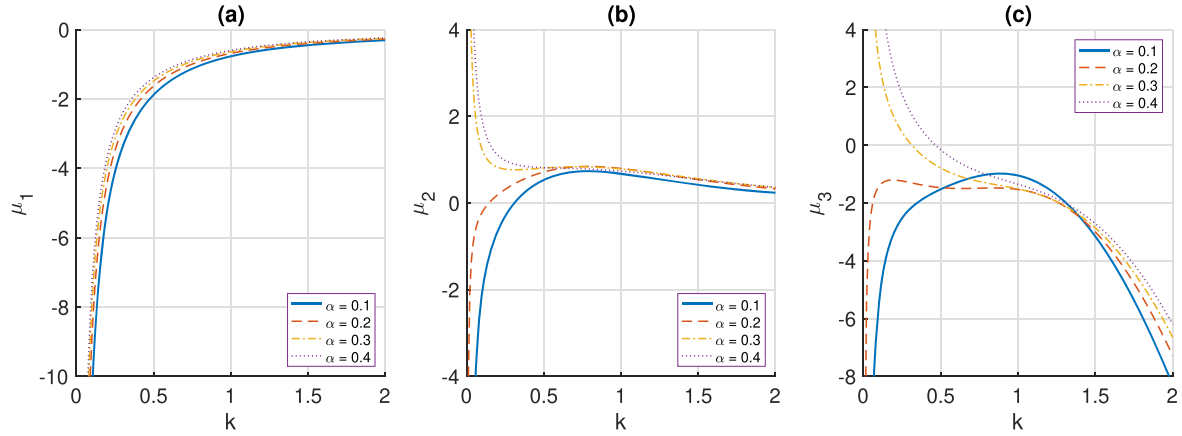

Figure 2. Panels (a), (b) and (c) show plots of the parameters μ_1, μ_2 and μ_3, versus the wave number k and different values of the negative ion density ratio α. The dispersion coefficient μ_1 is always negative while the nonlinearity coefficient μ_2 and the coupling coefficient μ_3 can change signs according to intervals. For $\alpha = 0.1$ and 0.2, μ_2 is negative for $k < k_{cr,1}$ and becomes positive for $k > k_{cr,1}$, while μ_3 is always negative. Conversely, For hight value of α, μ_3 is positive for $k < k_{cr,2}$ and becomes negative for $k > k_{cr,2}$, while μ_2 is always positive. We have fixed $\sigma_n = 17$.

[16, 17, 42, 63–65], molecular biophysics [66–69], nonlinear optics [70–72], and Bose–Einstein condensates [73–75], just to name a few. In order to study the emergence of nonlinear IAWs in the system of equations (26) via the activation of MI, we consider its plane wave solutions to be $N = a_0 e^{i\Omega_n \tau}$ and $N' = a_0' e^{i\Omega_n' \tau}$, given that the real amplitudes a_0 and a_0', and the frequencies Ω_n and Ω_n' satisfy the linear dispersion relation $\Omega_n = \Omega_n' = \mu_2 a_0^2 + \mu_3 a_0'^2$. Small perturbations, $\delta a(\xi, \tau)$ and $\delta a'(\xi, \tau)$, around the above unperturbed states can be introduced as $N = (a_0 + \delta a)e^{i\Omega_n \tau}$ and $N' = (a_0' + \delta a')e^{i\Omega_n \tau}$, leading to the linearized equations

$$\begin{aligned} & i\frac{\partial \delta a}{\partial \tau} + \mu_1 \frac{\partial^2 \delta a}{\partial \xi^2} + \mu_2 a_0^2 (\delta a + \delta a^*) \\ & \quad + \mu_3 a_0 a_0' (\delta a' + \delta a'^*) = 0, \\ & i\frac{\partial \delta a'}{\partial \tau} + \mu_1' \frac{\partial^2 \delta a'}{\partial \xi^2} + \mu_2 a_0'^2 (\delta a' + \delta a'^*) \\ & \quad + \mu_3 a_0' a_0 (\delta a + \delta a^*) = 0. \end{aligned} \tag{28}$$

Finally, assuming solutions for equations (28) to be $\delta a = U e^{i(K\xi - \Omega\tau)} + V e^{-i(K\xi - \Omega^*\tau)}$ and $\delta a' = U' e^{i(K\xi - \Omega\tau)} + V' e^{-i(K\xi - \Omega^*\tau)}$, where K and Ω are respectively the wave number and an arbitrary frequency of the perturbation, we find the following homogeneous set of equations for U, V, U' and V':

$$\begin{pmatrix} M_{11} + \Omega & M_{12} & M_{13} & M_{13} \\ M_{12} & M_{11} - \Omega & M_{13} & M_{13} \\ M_{13} & M_{13} & M_{11} + \Omega & M_{12} \\ M_{13} & M_{13} & M_{12} & M_{11} - \Omega \end{pmatrix} \times \begin{pmatrix} U \\ V \\ U' \\ V' \end{pmatrix} = \begin{pmatrix} 0 \\ 0 \\ 0 \\ 0 \end{pmatrix}, \tag{29}$$

with the matrix elements being $M_{11} = \mu_2 a_0^2 - \mu_1 K^2$, $M_{12} = \mu_2 a_0^2$ and $M_{13} = \mu_3 a_0^2$. System (29) will admit non-trivial solutions if its determinant is zero, which leads to the nonlinear dispersion relation

$$\Omega^4 - A\Omega^2 + B = 0, \tag{30}$$

with $A = 2(\mu_2 a_0^2 - \mu_1 K^2)^2 + 2\mu_3^2 a_0^4$ and $B = (\mu_2 a_0^2 - \mu_1 K^2)^4 + 2\mu_3^2 a_0^4 (\mu_2^2 a_0^4 - (\mu_2 a_0^2 - \mu_1 K^2)^2)$. The plane waves, solutions of system (26), will then be stable if

$$A > 0, \quad B > 0, \quad \text{and} \quad \Delta = A^2 - 4B > 0. \tag{31}$$

In order to verify the above conditions, we have plotted in figure 3 the parameters A, B and Δ versus the perturbation wavenumber K. For the whole analysis, we have fixed $\alpha = 0.3$ and considered $\sigma_n = 16$ for figure 3(aj)$_{j=1,2,3}$, and $\sigma_n = 22$ for figure 3(bj)$_{j=1,2,3}$. Obviously, in all the cases, the parameter A and the discriminant Δ are exclusively positive. The stability of the plane wave solutions then depends only on the sign of the parameter B which, for some values of ENP parameters and the wavenumber k, presents both negative and positive intervals. Additionally, we have plotted in figure 4 the parameters A, B and Δ, which confirms that the coefficient B plays a fundamental role in the stability of the the plane wave solutions. Indeed, in this particular situation, for any value of the electron-to-negative ion temperature ratio σ_n and the wavenumber k, only B is negative for some intervals of α, while A and Δ remain entirely positive. To remind, solutions for equation (30) are in general given by $\Omega_\pm^2 = \frac{1}{2}(A \pm \sqrt{A^2 - 4B})$. If $B < 0$, the solutions Ω_+ of equation (30) are real, while solutions Ω_- are complex. In this case, the growth rate of instability is determined by $\Gamma = \mathrm{Im}\{\sqrt{\Omega_-^2}\}$. Figures 3(a2) and (b2) give information on the regions of K where B is negative. Such regions will be likely to support wave modulation in ENPs. Some other results have also been recorded in figure 3(cj)$_{j=1,2,3}$ for k taking the respective values 0.8, 0.9 and 1. There also, only values of B are responsible for the occurrence of MI. To confirm this, the instability growth rate Γ as function of K, and for different values of k, is plotted in figures 5. We note the existence of a critical value, k_{cr}, of the main wave number k. Thus, for $k < k_{cr}$, Γ is a decreasing function of k (see figure 5(a)), whereas, for $k > k_{cr}$, Γ increases

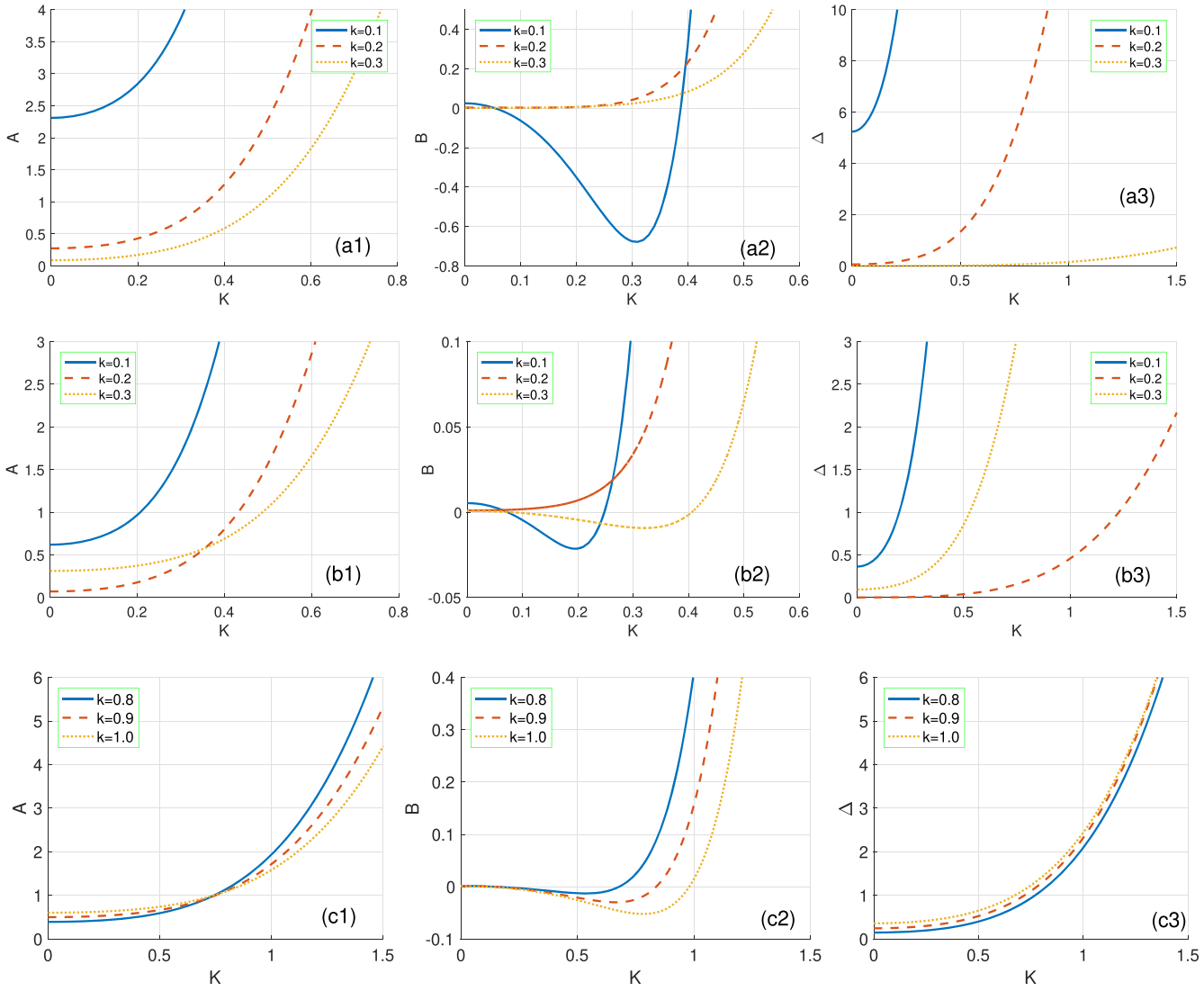

Figure 3. The panels show plots of the parameters A and B of equation (30), and its discriminant $\Delta = A^2 - 4B$, versus the perturbation wavenumber K. For panels (aj)$_{j=1,2,3}$ and (bj)$_{j=1,2,3}$, the wavenumber k takes the values 0.1,0.2 and 0.3. For the upper panels, $\sigma_n = 16$, while for panels (bj)$_{j=1,2,3}$, $\sigma_n = 22$. Panels (cj)$_{j=1,2,3}$ are plotted for different k with values 0.8, 0.9 and 1, with $\sigma_n = 16$. All the curves are obtained for $\alpha = 0.3$ and $a_0 = a_0' = 0.05$.

with k (see figure 5(b)). These results are valid only for the fixed values, $\alpha = 0.5$ and $\sigma_n = 15$, of ENP parameters.

Using the region of k that were detected in figure 5, we further represent the growth rate of instability in figure 6 versus the perturbation wavenumber K and the negative-ion concentration ratio α. For the case $k < k_{cr}$, corresponding to figure 5(a), we have the panels (aj)$_{j=1,2,3}$ of figure 6, where two regions of instability are identified. As k increasingly takes the values 0.1, 0.2 and 0.3, the smallest region of instability tends to expand, while the region situated around the interval $0.5 \leqslant \alpha \leqslant 1$ tends to shrink. However, when $k > k_{cr}$, which corresponds to figure 5(b), we see from figure 6(bj)$_{j=1,2,3}$ that there is only one region of instability which expands to higher values of α when k takes the respective values 0.8, 0.9 and 1, with $\sigma_n = 17$. We repeat the same calculations and plot the growth rate of instability in the $(\sigma_n, K)-$ plane as recorded in figure 7, with $\alpha = 0.8$. Panels (aj)$_{j=1,2,3}$ of figure 7, which corresponds to figure 5(a), show a stretched instability zone along the σ_n- direction, which gets progressively reduced when k takes successively the values 0.1, 0.2 and 0.3. On the other hand, the case $k > k_{cr}$, related to figure 5(b), initially displays two regions of instability for $k = 0.8$. With increasing k, the instability features of the plane waves get affected by the progressive disappearance of the small instability zone, while the larger region located at $\sigma_n > 10$ gets expanded towards small values of the electron-to-negative ion temperature ratio σ_n (see figure 7(bj)$_{j=1,2,3}$). These features clearly show the possibility of obtaining modulated waves in the coupled system, especially when the ENP and wave parameters are suitably chosen to ensure the balance between nonlinear and dispersive effects. In order to confirm such analytical predictions, the results from numerical simulations are shown in figures 8 and 9, where the plane wave is clearly found to disintegrate into

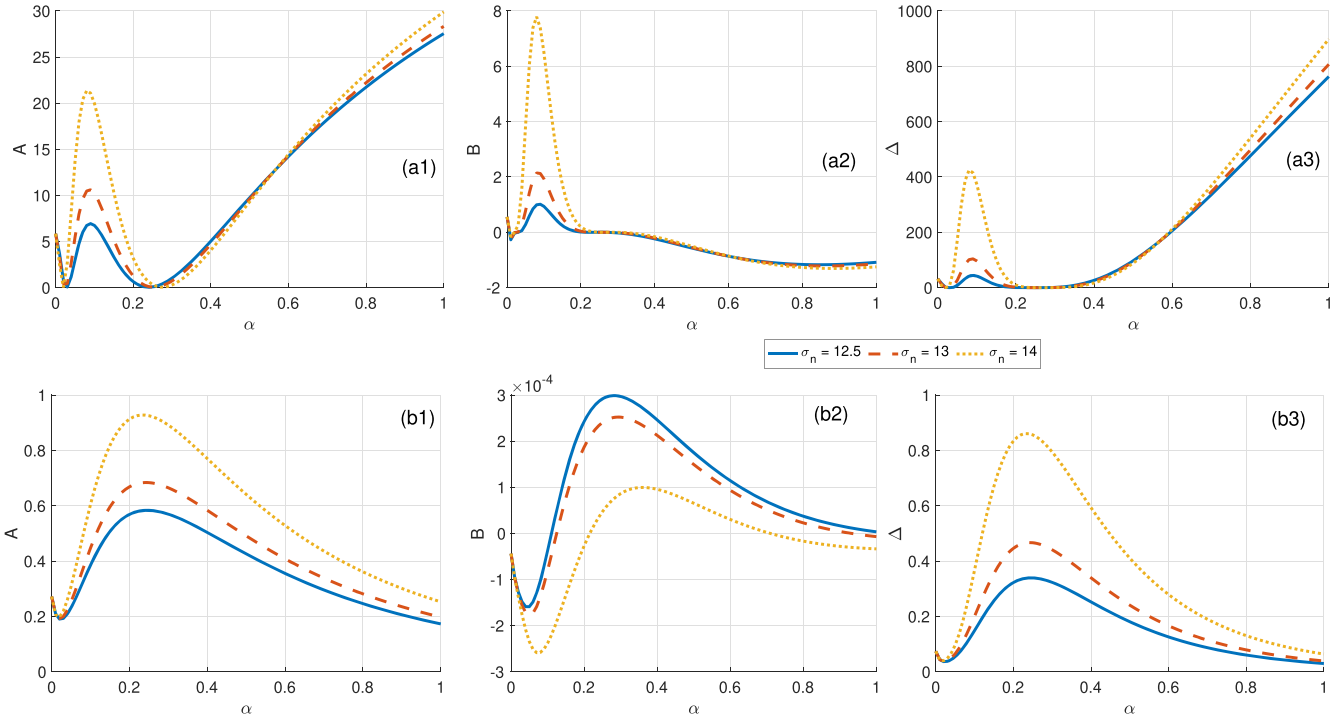

Figure 4. The panels show plots of the parameters A and B of equation (30), and its discriminant $\Delta = A^2 - 4B$, versus the negative-ion concentration ratio α. Panels $(\text{aj})_{j=1,2,3}$ have been plotted for $k = 0.3$, while panels $(\text{bj})_{j=1,2,3}$ have been recorded for $k = 1$. Curves in each of the panels correspond to the respective values 12.5, 13 and 14 of the electron-to-negative ion temperature ratio σ_n, with $a_0 = a_0' = 0.05$.

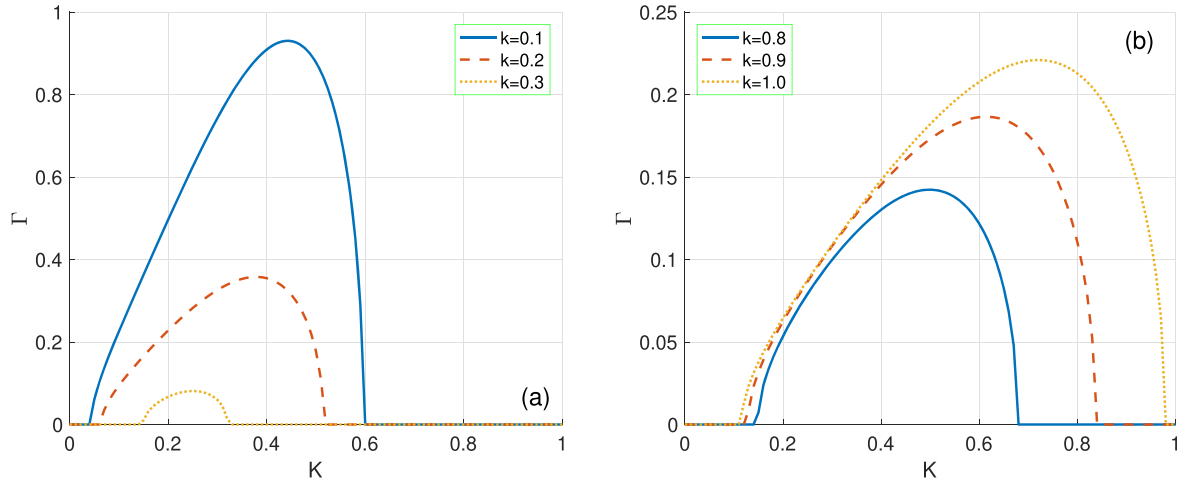

Figure 5. The instability growth rate Γ versus the perturbation wavenumber K. Panel (a) shows the instability intervals of K for small values of k and corresponds to the stability/instability features discussed in figure 3$(\text{bj})_{j=1,2,3}$, while panel (b) displays the growth rate of instability for big K, and corresponds to the results of figure 3$(\text{cj})_{j=1,2,3}$.

soliton-like objects. We should however stress that figures 8 and 9 have been obtained for $\alpha = 0.1$ and $\alpha = 0.3$, respectively. For small values of the negative-ion concentration ratio, the plane wave, at $t = 20$, disintegrate into a train of envelope structures, where that lateral ones grow progressively with time, and one finally gets three identical structures with small lateral radiations at $t = 70$. The oscillation features of the perturbed plane wave are very sensitive to change in α as shown in figure 9 for $\alpha = 0.3$. In fact, at time $t = 20$, the MI gives rise to one breathing mode with two small satellites that tend to grow with time. However, at time $t = 70$ (see figure 9(c)), the phenomenon of MI is characterized by one highly localized soliton, surrounded by two low-amplitude breathers and other satellites. Although the breathing mode is highly modified by the increase in the negative ion concentration, it remains obvious that the coupled-mode in ENPs can support the formation of trains of solitons under the activation of MI. This is a symmetry-breaking instability because of which a small perturbation will experience exponential growth, leading to wave breakup either in space or time. Interestingly, the plane wave

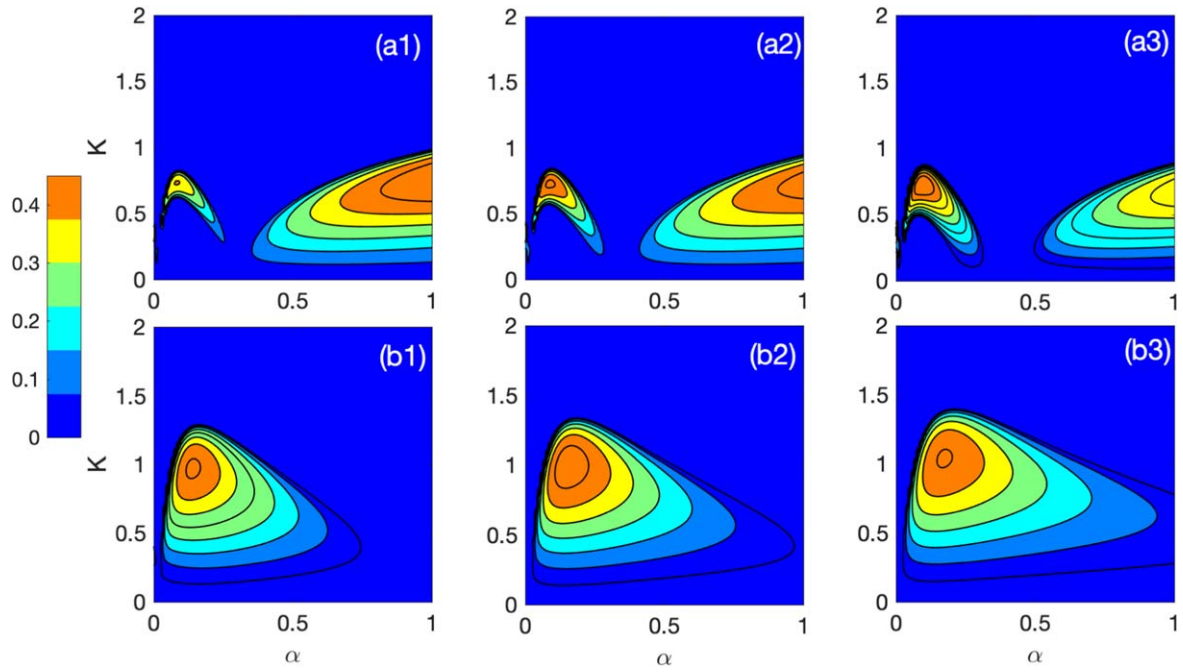

Figure 6. The MI growth rate is represented in the $(\alpha, K)-$ plane in agreement with the predictions in figure 5. Panels $(aj)_{j=1,2,3}$ display results for $k = 0.1$, $k = 0.2$ and $k = 0.3$, while panels $(bj)_{j=1,2,3}$ show the stability/instability features for $k = 0.8$, $k = 0.9$ and $k = 1.0$, with $\sigma_n = 17$ and $a_0 = a_0' = 0.05$.

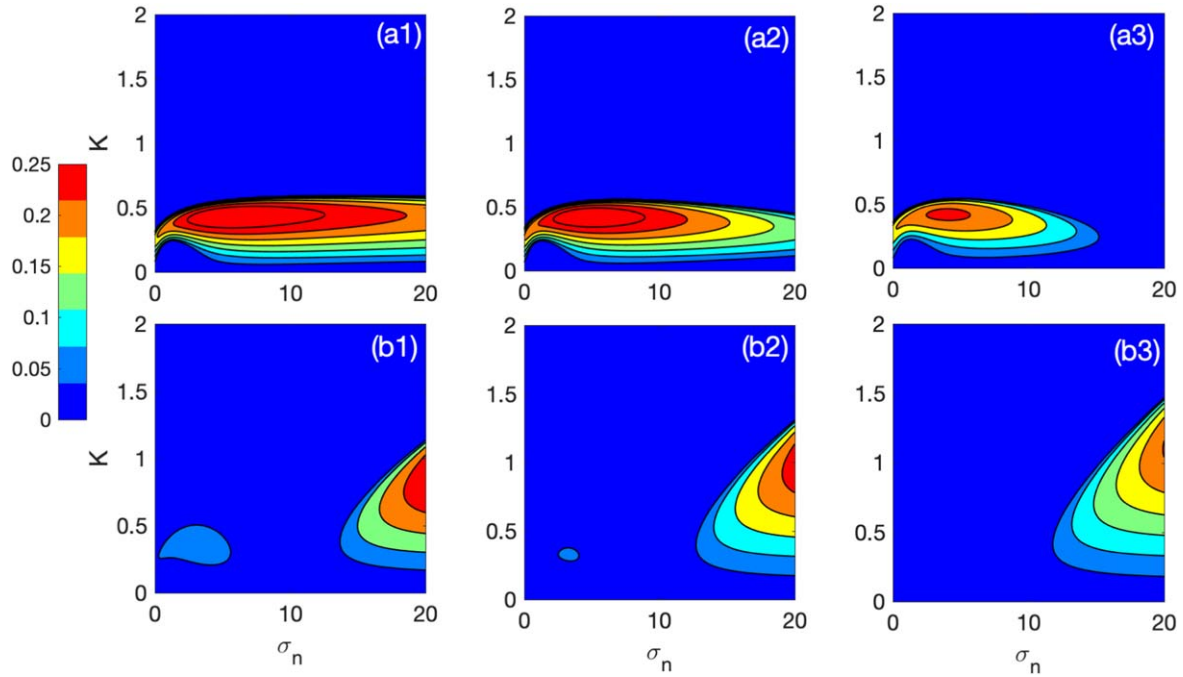

Figure 7. The MI growth rate is represented in the $(\sigma_n, K)-$ plane in agreement with the predictions in figure 5. Panels $(aj)_{j=1,2,3}$ display results for $k = 0.1$, $k = 0.2$ and $k = 0.3$, while panels $(bj)_{j=1,2,3}$ show the stability/instability features for $k = 0.8$, $k = 0.9$ and $k = 1.0$, with $\alpha = 0.1$ and $a_0 = a_0' = 0.05$.

disintegration occurs in the same parameter regions where bright solitons are observed, therefore confirming that MI is responsible for the formation of breathers in plasma systems in general and in ENPs particularly, as extensively discussed parametrically in the literature [16, 17, 42].

4. Nonlinear excitations

According to the previous section, there is a strong relationship between soliton solutions and the occurrence of MI, because, as said so far MI is considered, to some extent, as

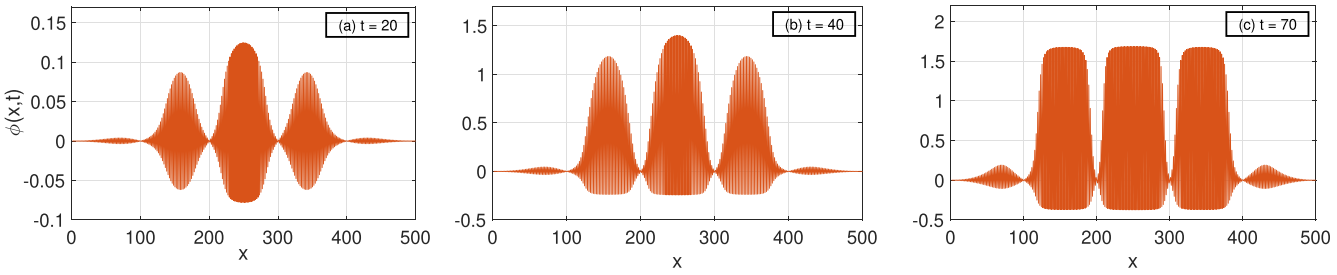

Figure 8. Panels show evolution of the electric potential ϕ resulting from the activation of MI for $\alpha = 0.1$, $\sigma_n = 17$, $k = 0.8$, $a_0 = a_0' = 0.05$, $k' = -k$ and $K = 0.3$, at times: (a) $t = 20$, (b) $t = 40$, (c) $t = 70$ and (d) $t = 100$.

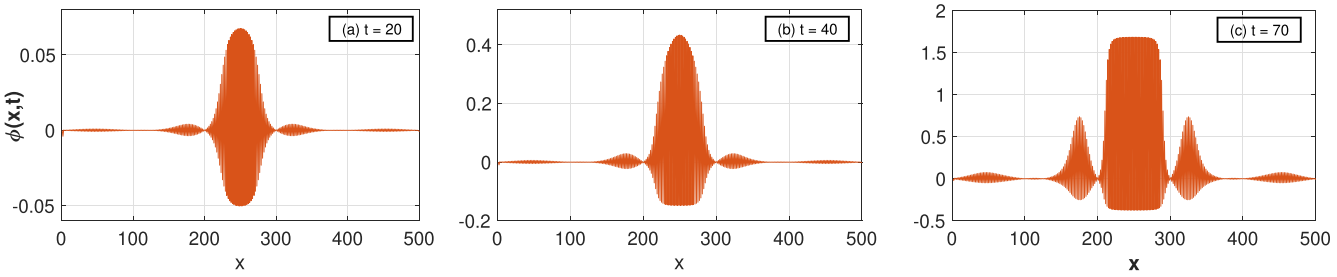

Figure 9. Panels show evolution of the electric potential ϕ resulting from the activation of MI for $\alpha = 0.3$, $\sigma_n = 17$, $k = 0.8$, $a_0 = a_0' = 0.05$, $k' = -k$ and $K = 0.3$, at times: (a) $t = 20$, (b) $t = 40$, (c) $t = 70$ and (d) $t = 100$.

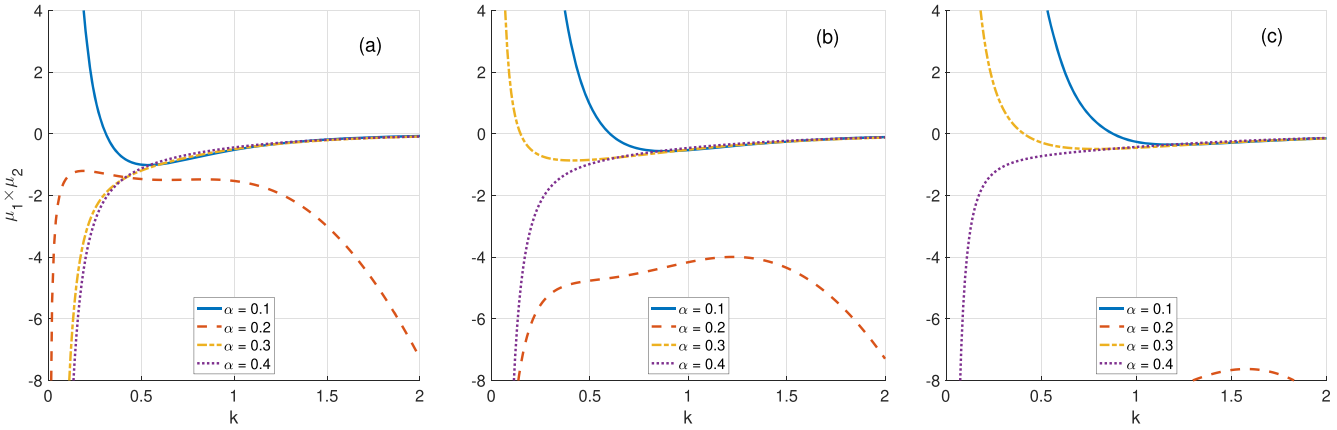

Figure 10. The panels show plots of the product $\mu_1 \times \mu_2$ versus the wavenumber k. (a) correspnds to $\sigma_n = 12$, (b) gives resultrs for $\sigma_n = 17$ and panel (c) is obtained for $\sigma_n = 22$. Each of the panels displays different features of $\mu_1 \times \mu_2$ for different values of the negative ion concentration ratio α.

precursor of the bright soliton formation. Each of the elements obtained in figures 8 and 9 can be found as exact solution of the NLS or the coupled NLS equation.

4.1. Single solutions

In the single mode, the two equations are decoupled by setting one of the components to zero. This reduces the system (26) to single cubic NLS equations with dispersion and nonlinear coefficients being μ_1 and μ_2, respectively. Setting for example $N' = 0$, we obtain the single NLS equation

$$i\frac{\partial N}{\partial \tau} + \mu_1 \frac{\partial^2 N}{\partial \xi^2} + \mu_2 |N|^2 N = 0, \tag{32}$$

whose solutions depend on the sign of the product $\mu_1 \times \mu_2$ depicted in figure 10. We should stress that when this product is positive, bright solitons are obtained, while for $\mu_1 \times \mu_2 < 0$, solutions for the NLS equation (32) are dark solitons. In this work, we are interested in solutions that are related to the occurrence of MI, i.e., bright solitons, explicitly given by

$$N(\xi, \tau) = n_0 \sqrt{\frac{2\mu_1}{\mu_2}}\, \mathrm{sech}(n_0\xi - 2\mu_1 n_0 K_1 \tau) e^{i(K_1\xi - \mu_1(K_1^2 - n_0^2)\tau)}, \tag{33}$$

where n_0 and K_1 are two free parameters. For instance, according to figure 10(a), only the value $\alpha = 0.1$, for $\sigma_n = 12$ can give rise to such solutions. However, when σ_n takes the value 17, it is possible to find intervals of k where $\mu_1 \times \mu_2$ is positive for the two values $\alpha = 0.1$ and $\alpha = 0.2$ (see figure 10(b)). Such regions appear in the intervals

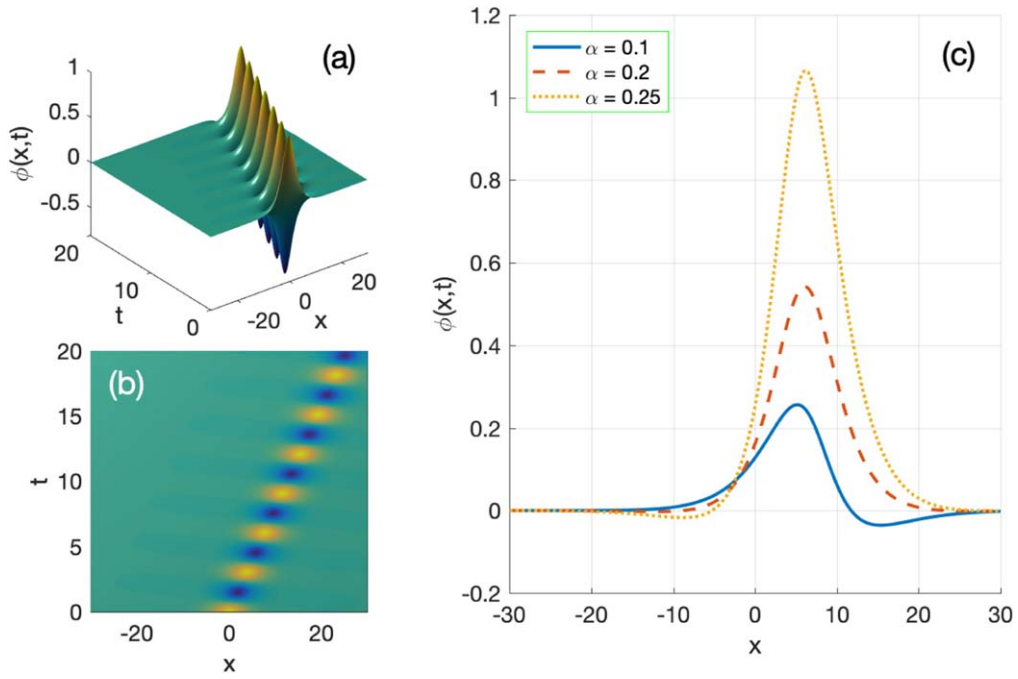

Figure 11. The panels show behaviors of solution (57). The snapshot of the space time evolution is plotted in panels (a) and (b), while panel (c) displays the solution for different values of the negative ion concentration ratio α and time $t = 10$, with $\sigma_n = 17$ and $k = 0.1$.

$0 < k < 0.6$ and $0 < k < 0.25$, respectively for $\alpha = 0.1$ and $\alpha = 0.2$. Finally, the case $\sigma_n = 22$, depicted in figure 10(c), also confirms the values $\alpha = 0.1$ and $\alpha = 0.2$ as the only ones capable of supporting bright-type envelope solitons. Regions corresponding to the two values are found in the intervals $0 < k < 0.9$ and $0 < k < 0.4$, respectively for $\alpha = 0.1$ and $\alpha = 0.2$. From equations (10), one can find the solution in term of ϕ so that the modulated IAWs in this case can be fully described by the solution

$$\phi(x,t) = \frac{2\epsilon n_0}{k^2 + a1}\sqrt{\frac{2\mu_1}{\mu_2}}\,\mathrm{sech}(\epsilon n_0 x + \epsilon n_0(2\epsilon\mu_1 K_1 - \lambda)t) \times \cos\{(\epsilon K_1 - k)x + [\omega - \epsilon(\lambda K_1 + \epsilon\mu_1(K_1^2 - n_0^2))]t\} + O(\epsilon^2). \tag{34}$$

which is represented in figures 11. This shows a bright-envelope soliton which is very sensitive to the change in α. This particular case corresponds to what was already discussed in [16], in a single-mode ENP. Bright envelope has been widely discussed in plasma physics and find applications in different classes of plasmas.

4.2. Coupled solutions

In the case of coupled solutions, the two components N and N' are considered to be different from zero. However, the type of solution will depend on the sign of the coefficient

$$\Delta = \frac{\mu_1\mu_2 - \mu_1\mu_3}{\mu_2^2 - \mu_3^2}, \tag{35}$$

so that when $\Delta > 0$, equations (26) will admit bright soliton solutions. On the contrary, when $\Delta < 0$, dark solitons will be obtained as solutions. In doing so, we have represented Δ in figure 12, where each panel corresponds to a different value of the electron-to-negative ion temperature ratio. Each of the panels of figure 12 also shows the sign of Δ with changing α, the negative-ion concentration ratio. For regions corresponding to $\Delta > 0$, solutions for individual equations (26) are given by

$$N(\xi,\tau) = N_0\,\mathrm{sech}(n_0\xi + 2\mu_1 n_0 K_1\tau)e^{i(K_1\xi - \Omega_1\tau)} \tag{36a}$$

$$N'(\xi,\tau) = N_0'\,\mathrm{sech}(n_0'\xi + 2\mu_1 n_0' K_2\tau)e^{i(K_2\xi - \Omega_2\tau)} \times e^{-i\left(\frac{\lambda}{\epsilon}\xi + \frac{\lambda^2}{\mu_1}\tau\right)}, \tag{36b}$$

where

$$N_0^2 = \frac{2n_0^2\mu_1}{\mu_2 + \mu_3}, \quad N_0'^2 = \frac{2n_0'^2\mu_1}{\mu_2 + \mu_3}, \quad \Omega_1 = -\mu_1(n_0^2 - K_1^2), \quad \Omega_2 = -\mu_1(n_0'^2 - K_2^2), \quad K_2 = K_1.$$

This leads to the coupled solution

$$\phi(x,t) = \frac{2\epsilon N_0}{k^2 + a_1}\,\mathrm{sech}(\epsilon n_0 x + \epsilon n_0(2\epsilon\mu_1 K_1 - \lambda)t) \times \cos\{(\epsilon K_1 - k)x + (\omega - \epsilon K_1 - \epsilon^2\Omega_1)t\} + \frac{2\epsilon N_0'}{k'^2 + a_1}\,\mathrm{sech}(\epsilon n_0' x + \epsilon n_0'(2\epsilon\mu_1 K_2 - \lambda)t) \times \cos\left\{(\lambda + \epsilon K_2 - k')x + \left[\omega' - \lambda^2 + \epsilon\left(\frac{\epsilon\lambda^2}{\mu_1} - \lambda K_2 - \epsilon\Omega_2\right)\right]t\right\} + O(\epsilon^2). \tag{37}$$

The behaviors of the above solution (37) are depicted in figure 13, where the counter-propagating waves collide and

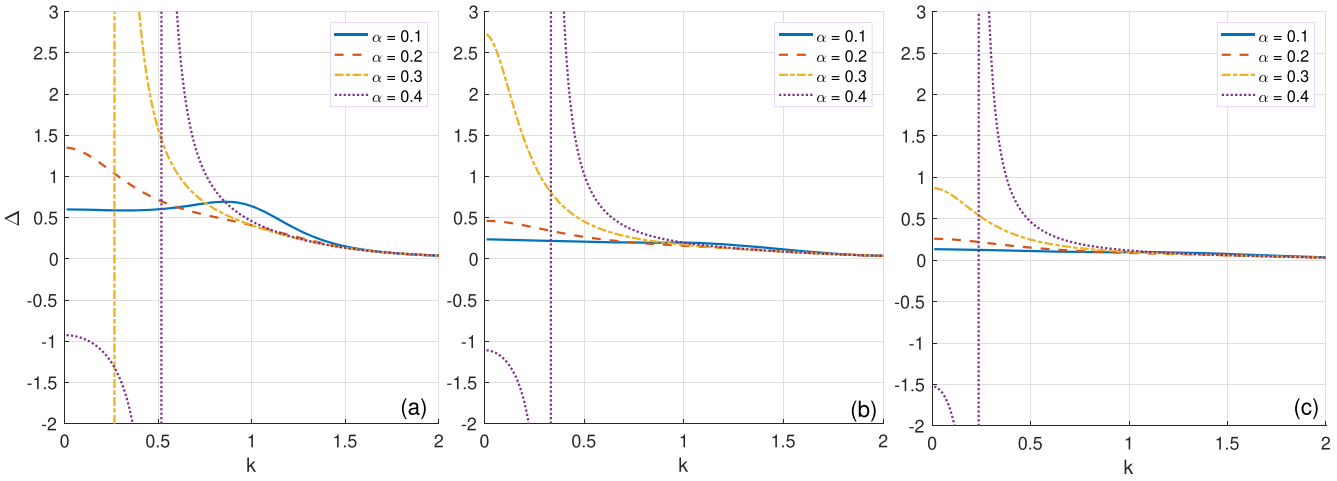

Figure 12. The panels show plots of the quantity $\Delta = \frac{\mu_1\mu_2 - \mu_1\mu_3}{\mu_2^2 - \mu_3^2}$ versus the wavenumber k. Each panel contains results for different values of the negative ion concentration ratio α, and panel (a) corresponds to $\sigma_n = 12$, panel (b) corresponds to $\sigma_n = 17$ and $\sigma_n = 22$.

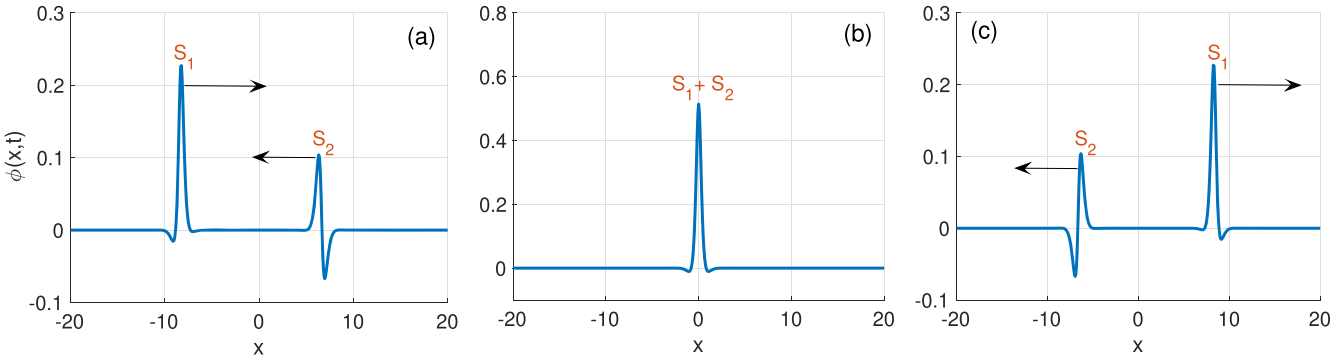

Figure 13. The panels show plots of the coupled solution (43). (a) and (b) show the spatiotemporal behaviors of the coupled soliton solution for the respective values $\alpha = 0.1$ and $\alpha = 0.2$ of the negative-ion concentration ratio. (c)-(d) display the time effect on the solution for $\alpha = 0.1$. All the calculations have been made using the parameter values $\sigma_n = 22$, $n_0 = n_0' = 0.8$, $K_1 = K_2 = 0.05$, $\epsilon = 0.02$, $k = 0.1$ and $k' = -k$.

keep their shape after interaction. The scenario has been recorded at times $t = -20$, 0 and 20. In general, the two colliding waves are asymmetric envelope solitons that are known in many physical setting that support the propagation of solitons. However, from panel (b) of figure 13, the combined wave forms a pulse whose amplitude is obviously the sum of both amplitudes. In order to qualitatively study the impact of the ENP parameters, we have plotted the maximum amplitude of the head-on collision in figure 14 versus α and σ_n. In figure 14(a), the wave amplitude is the highest for values of α close to 1, while the corresponding interval for σ_n varies between 4.9 and 5.3. Here, we have fixed the wavenumber as $k = 0.9$. In general, $\phi_{\max}(0, 0)$ is a decreasing function of both α and σ_n. Otherwise, the amount of energy exchanged between the two solitons is lowered by high values of the negative-ion concentration ratio and the electron-to-negative ion temperature ratio. When $k = 1.2$, the later behaviors remain, but highest values of the wave amplitude are obtained for very small values of σ_n, which corresponds to values of α in the interval $0.4 \leqslant \alpha \leqslant 1$ (see figure 14(b)). In panel (c) of figure 14, the highest amplitude of the head-on collision is also observed at the edge of the diagram, i.e., $\sigma_n = 1.2$, while high energy exchange between the two solitons is expected in the interval $0.3 \leqslant \alpha \leqslant 1$, for $k = 1.9$. In this particular case, energy exchange is likely to vanish for high values of σ_n and α but, interestingly, for their other values, soliton collision takes place. Moreover, figures 14(b) and (c) support the fact that high σ_n and α cannot simultaneously contribute to high energy exchange, which otherwise means that high values of σ_n correspond to small values of α for efficient energy exchange during head-on collision. This agrees with the parametric analysis summarized in figure 12, where positive values of Δ support coupled breather solutions under the competitive effects of nonlinear and dispersive effects.

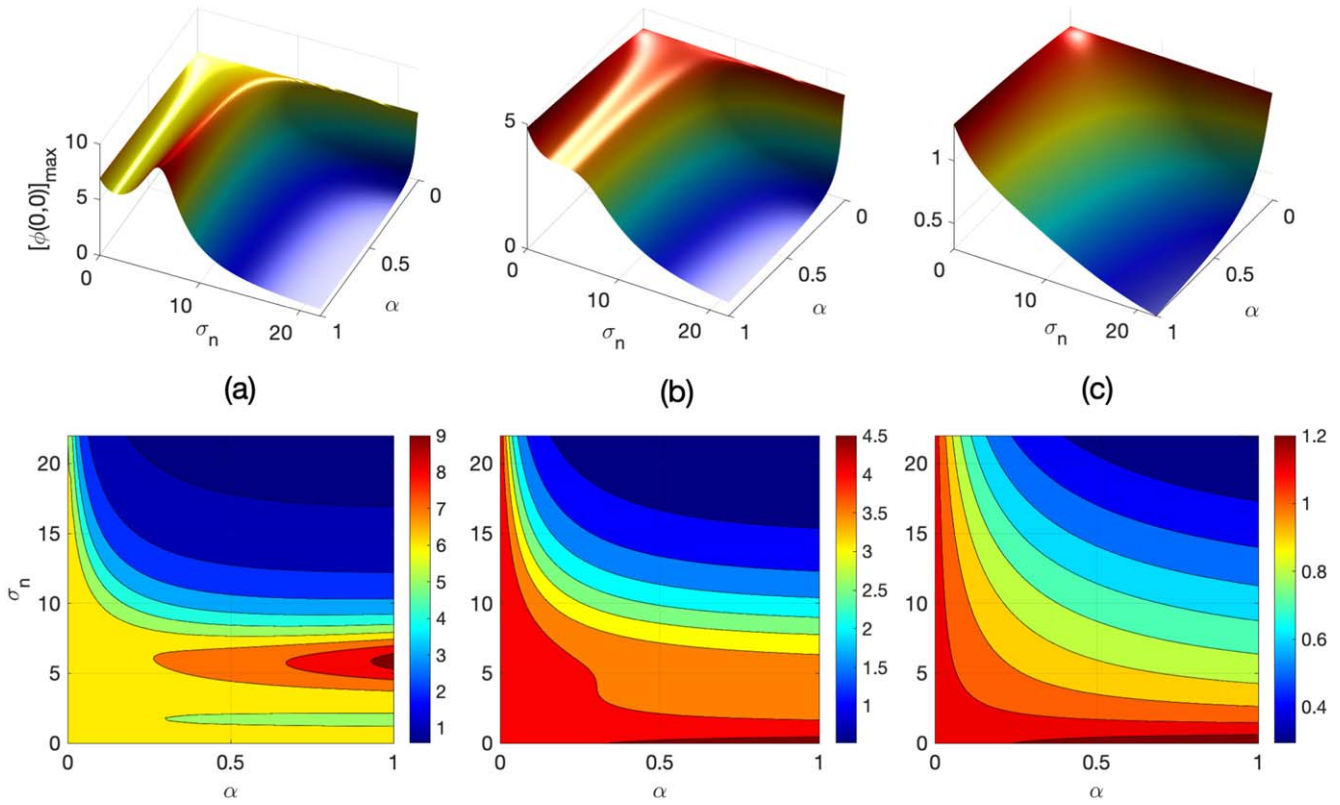

Figure 14. The panels show the maximum amplitude of the head-on collision as a function of the negative-ion concentration ratio α and the electron-to-negative ion temperature ratio σ_n, for different values of the wavenumber k: (a) $k = 0.9$, (b) $k = 1.2$ and (c) $k = 1.9$.

5. Concluding remarks

We have addressed nonlinear counter-propagating waves in an ENP model. Through the multiple-scale expansion method, the plasma evolution equations have been reduced to nonlinearly coupled NLS equations, with coefficients strongly dependent on negative ion parameters, i.e., the electron-to-negative ion temperature ratio (σ_n) and the negative ion concentration ratio (α). The study of MI of plane wave solutions has revealed that such solutions may become unstable under slight perturbations as the result of the interplay between nonlinear and dispersive effects. Some areas of ENP parameters, were this is possible, have been detected in the gain spectrum for small values of the wavenumber k of the progressive wave. The outcomes of the nonlinear development of MI predicted analytically have been identified via numerical simulations. The so-called MI has manifested itself through the formation of localized trains of pulses that are very sensitive to changes in ENP parameters. In the same context, we have also presented single and coupled soliton solutions of the system, including the straightforward relation with the MI phenomenon. A parametric analysis for the maximum amplitude of the head-on collision was performed where we have discussed the effect of wavenumber k on the values of α and σ_n capable of giving rise to efficient energy exchange between colliding breathing IAWs.

When negative ions are considered inertialess and in Boltzmann distribution, as well as electrons, it remains that the dynamics of the system is based on the positive ion behaviors. For this reason, the system is described by a one-fluid model instead of the two-fluid model. This consideration that has been demonstrated in [43, 44] and taken up by Mamun *et al* [45], allows to eliminate the equation of the motion of negative species. Most of the contributions devoted to the study of solitons in plasma systems and its relationship with MI have always been reduced to the study of the linear stability analysis, which somehow just indicates regions of parameters where solitons can be observed, without giving any information on their long-time evolution. Here, we have indeed shown that predictions can be straightforwardly related to pattern formation, in the context where counter-propagating waves are involved in the process of energy transport via soliton head-on collision. Along the same line, we have also shown that there is a strong interdependence between the nonlinearity and dispersion, regulated by the ENP parameters, and the phenomenon of MI. In doing so, we have realized that high values of the electron-to-negative ion temperature ratio and negative-ion concentration ratio could not simultaneously contribute to high energy exchange, which otherwise means that high values of σ_n are related to small values of α for efficient energy exchange during head-on collision.

Acknowledgments

The work by CBT is supported by the Botswana International University of Science and Technology under the grant

DVC/RDI/2/1/16I (**25**). I thank the Kavli Institute for Theoretical Physics (KITP), University of California Santa Barbara (USA), where this work was supported in part by the National Science Foundation Grant no.**NSF PHY-1748958**.

Availability of data

Data sharing is not applicable to this article as no new data were created or analyzed in this study.

ORCID iDs

C B Tabi https://orcid.org/0000-0001-6505-7866

References

[1] Kuo S P and Faith J 1997 *Phys. Rev.* E **56** 2143
[2] Thoma C, Rose D V, Miller L C, Clark R E and Hughes T P 2009 *J. Appl. Phys.* **106** 043301
[3] Nickeler D H and Wiegelmann T 2010 *Ann. Geophys.* **28** 1523
[4] Klimushkin D Y and Mager P N 2012 *Plasma Phys. Control. Fusion* **54** 015006
[5] Souza V M 2015 *Braz. J. Phys.* **45** 510
[6] Bertelli N, Balakin A A, Westerhof E, Garcia O E, Nielsen A H and Naulin V 2010 *J. Phys. Conf. Series* **260** 012002
[7] Abel I G, Plunk G G, Wang E, Barnes M, Cowley S C, Dorland W and Schekochihin A A 2013 *Rep. Prog. Phys.* **76** 116201
[8] Joglekar A S, Thomas A G R, Fox W and Bhattacharjee A 2014 *Phys. Rev. Lett.* **112** 105004
[9] Portnyagin Yu I, Klyuev O F, Shidlovsky A A, Evdokimov A N, Buzdigar T W, Matukhin P G, Pasynkov S G, Shamshev K N, Sokolov V V and Semkin N D 2011 *Adv. Space Res.* **11** 89
[10] Sabry R, Moslem W M and Shukla P K 2009 *Phys. Plasmas* **16** 032302
[11] Coates A J, Crary F J, Lewis G R, Young D T, Waite J H Jr. and Sittler E C Jr. 2007 *Geophys. Res. Lett.* **34** L22103
[12] Chaizy P H *et al* 1991 *Nature* **349** 393
[13] Hussain S, Shan S A, Akhtar N and Masud M M 2014 *Astrophys. Space Sci.* **352** 605
[14] Shan S A and Akhtar N 2013 *Astrophys. Space Sci.* **346** 367
[15] Das G C and Nag A 2010 *Assam Univ. J. Sci. Technol.* **5** 169
[16] Panguetna C S, Tabi C B and Kofané T C 2018 *Commun. Nonl. Sci. Numer. Simulat.* **55** 326
[17] Panguetna C S, Tabi C B and Kofané T C 2019 *J. Theor. Appl. Phys.* **13** 237
[18] Kourakis I and Shukla P K 2005 *Nonl.Proc. Geophys.* **12** 407
[19] Islam S, Sultana S and Mamun A A 2017 *Phys. Plasmas* **24** 092115
[20] El-Tantawy S A, Wazwaz A M and Ali Shan S 2017 *Phys. Plasmas* **24** 022105
[21] Panguetna C S, Tabi C B and Kofané T C 2017 *Phys. Plasmas* **24** 092114
[22] Tabi C B, Panguetna C S and Kofané T C 2018 *Physica* B **545** 70
[23] Peng J and Zeng H 2019 *Commun. Phys.* **2** 34
[24] Wang M, Tian B, Shan W-R, Lü X and Xue Y-S 2012 *Nonl. Dyn.* **69** 1137
[25] El-Tantawy S A 2016 *Chaos Solit. Fract.* **93** 162
[26] Kakad A, Kakad B and Omura Y 2017 *Phys. Plasmas* **24** 060704
[27] Zabusky N J and Kruskal M D 1965 *Phys. Rev. Lett.* **15** 240
[28] Maxworthy T 1980 *J. Fluid Mech.* **96** 47
[29] Ikezi H, Taylor R and Baker D 1970 *Phys. Rev. Lett.* **25** 11
[30] Ze F and Hershkomitz N 1979 *Phys. Rev. Lett.* **42** 1747
[31] Nakamura Y, Bailung H and Lonngren K E 1999 *Phys. Plasmas* **6** 3466
[32] Sharma S K, Boruah A and Bailung H 2014 *Phys. Rev.* E **89** 013110
[33] Harvey P, Durniak C, Samsonov D and Morfill G 2010 *Phys. Rev.* E **81** 057401
[34] Tagare S G, Singh S V, Reddy R V and Lakhina G S 2004 *Nonl. Process. Geophys.* **11** 215
[35] Berthomier M, Pottelette R, Malingre M and Khotyainsev Y 2000 *Phys. Plasmas* **7** 2987
[36] Verheest F, Hellberg M A and Hereman W A 2012 *Phys. Rev.* E **86** 036402
[37] Saleem H and Batool N 2009 *Phys. Plasmas* **16** 022302
[38] Ichiki R, Yoshimura S, Watanabe T, Nakamura Y and Kawai Y 2002 *Phys. Plasmas* **9** 4481
[39] Kolobov V I and Economou D J 1998 *Appl. Phys. Lett.* **72** 656
[40] Gupta M R, Soma B K and Dasgupta B 1981 *J. Plasma Phys.* **25** 499
[41] Wright O C 1995 *Physica* D **82** 1
[42] Kourakis I, Shukla P K and Morfill G 2005 *New J. Phys.* **7** 153
[43] Bogdanov E A and Kudryavtsev A A 2001 *Tech. Phys. Lett.* **27** 905
[44] Franklin R N and Snell J 2000 *J. Plasma Phys.* **64** 131
[45] Mamun A A, Shukla P K and Eliasson B 2009 *Phys. Rev.* E **80** 046406
[46] Bansi C D K, Tabi C B and Mohamadou A 2018 *Chaos Solit. Fract.* **109** 170
[47] Bakirtas I and Demiray H 2004 *Appl. Math. Comput.* **154** 747
[48] Yesil A and Ünal I 2011 Electromagnetic wave propagation in ionospheric plasma *Behaviour of Electromagnetic Waves in Different Media and Structures* ed A Agdagli (London: IntechOpen) (https://intechopen.com/books/behavior-of-electromagnetic-waves-in-different-media-and-structures/electromagnetic-wave-propagation-in-ionospheric-plasma1) (https://doi.org/10.5772/19197)
[49] Akgün G and Demiray H 2001 *Int. J. Eng. Sci.* **39** 563
[50] Tabi C B, Ekobena Fouda H P, Mohamadou A and Kofané T C 2011 *Phys. Scr.* **83** 035802
[51] Tabi C B, Tankou E and Mohamadou A 2017 *Chaos Solit. Fract.* **95** 187
[52] Wabnitz S, Trillo S, Wright E M and Stegeman G I 1991 *J. Opt. Soc. Am.* B **8** 602
[53] Kengne E, Abdourahman and Lakhssassi A 2020 *Chin. J. Phys.* **63** 271
[54] Yemélé D and Kofané T C 2006 *J. Phys.* D **39** 4504
[55] Li X-X, Cheng R-J, Zhang A-X and Xue J-K 2019 *Phys. Rev.* E **100** 032220
[56] Kofané T, Zebaze M and Zibi A 1990 *J. Phys. D: Appl. Phys.* **23** 764
[57] Williams J, Walser R, Cooper J, Cornell E and Holland M 2000 *Phys. Rev.* A **61** 033612
[58] Whitham G B 1965 *Proc. R. Soc. London-Ser.* A **283** 238
[59] Benjamin T B and Feir J E 1967 *J. Fluid Mech.* **27** 417
[60] Maïna I, Tabi C B, Mohamadou A, Ekobena H P F and Kofané T C 2015 *Chaos* **25** 043118
[61] Etémé A S, Tabi C B and Mohamadou A 2017 *Commun. Nonl. Sci. Num. Simul.* **43** 211
[62] Tabi C B, Etémé A S, Mohamadou A and Kofané T C 2019 *Chaos Solit. Fract.* **123** 116
[63] Washimi H and Taniuti T 1966 *Phys. Rev. Lett.* **17** 996

[64] Goswami J, Chandra S and Ghosh B 2018 *Laser Part. Beams* **36** 136
[65] Ghosh B, Chandra S and Paul S N 2011 *Phys. Plasmas* **18** 012106
[66] Tabi C B, Ondoua R Y, Ekobena H P, Mohamadou A and Kofané T C 2016 *Phys. Lett.* A **380** 2374
[67] Ekobena H P F, Tabi C B, Mohamadou A and Kofané T C 2011 *J. Phys.: Condens. Matter* **23** 375104
[68] Tabi C B, Mimshe J C F, Ekobena H P F, Mohamadou A and Kofané T C 2013 *Eur. Phys. J.* B **86** 374
[69] Madiba S E, Tabi C B, Ekobena H P F and Kofané T C 2019 *Physica* A **514** 298
[70] Mohamadou A, Ayissi B E and Kofané T C 2006 *Phys. Rev.* E **74** 046604
[71] Tagwo H, Tiofack C G L, Dafounansou O, Mohamadou A and Kofané T C 2016 *J. Mod. Opt.* **63** 558
[72] Zakeri G-A and Yomba E 2015 *Phys. Rev.* E **91** 062904
[73] Salasnich L, Parola A and Reatto L 2003 *Phys. Rev. Lett.* **91** 080405
[74] Wamba E, Mohamadou A and Kofané T C 2008 *Phys. Rev.* E **77** 046216
[75] Zanga D, Fewo S I, Tabi C B and Kofané T C 2020 *Commun. Nonl. Sci. Num. Simul* **80** 104993